Structural Health Monitoring of Wind Turbine Systems: Data-based Lifetime Models Development for Integration into Control Systems

Von der Fakultät für Ingenieurwissenschaften,
Abteilung Maschinenbau und Verfahrenstechnik
der
Universität Duisburg-Essen
zur Erlangung des akademischen Grades
einer
Doktorin der Ingenieurwissenschaften
Dr.-Ing.
genehmigte Dissertation

von

Nejra Beganović
aus
Sarajevo, Bosnien und Herzegowina

Gutachter: Univ.-Prof. Dr.-Ing. Dirk Söffker
Univ.-Prof. Dr.-Ing. Claus-Peter Fritzen, Universität Siegen
Univ.-Prof. Dr.-Ing. Tamara Nestorović, Ruhr-Universität Bochum

Tag der mündlichen Prüfung: 23. November 2016

Acknowledgements

This thesis and accompanying research work were carried out at the Department of Dynamics and Control of University of Duisburg-Essen during 2013-2016. Concerning long-term time and resource investments of a number of person and institutions, I am grateful to those who supported me directly or indirectly in any way. Without them it would not be possible neither to initiate nor to complete this thesis.

As first, I would like to thank Univ.-Prof. Dr.-Ing. Dirk Söffker for providing an academic and pleasant environment for conducting the research work, necessary resources, as well as for the guidance during these three years, regardless of whether it belongs to a numerous suggestions regarding conceptual and core thesis content or to a discussions about key thesis results. Furthermore, my great thanks go to Univ.-Prof. Dr.-Ing. Claus-Peter Fritzen and Univ.-Prof. Dr.-Ing. Tamara Nestorović for overtaking the role of advisors and giving me helpful hints and independent objective scientific insight in the thesis.

As a scholarship holder of German Academic Exchange Service (Deutscher Akademischer Austausch Dienst - DAAD), I am grateful to DAAD and DAAD staff who made this research possible. Special thanks to my family without whom I would not be what I am and who are always there for me whenever I need them.

I especially wish to thank my colleagues at the University of Duisburg-Essen for personal and moral support, friendship, and all other necessities who made the time spent at University of Duisburg-Essen more interesting and pleasant. I want also to thank Yvonne Vengels, Friederike Kögler, and Adnan Hasanović for their enthusiastic help and finding the solutions for all administrative tasks.

Duisburg, February 2017 Nejra Beganovic

Kurzfassung

Aufgrund unterschiedlicher Lastprofile unterliegen technische Systeme individuellen Änderungen durch die Schadenserhöhung und die Änderungen von Systemparametern über die Einsatzdauer. Diese Änderungen führen zu einer Abnahme der Systemzuverlässigkeit und letztlich zum Funktionsverlust. Da die Alterung eines Systems unvermeidbar ist, sind sowohl die Identifikation von Effekten, die den größten Beitrag zum Funktionsverlust haben als auch die Vorhersage der verbrauchten bzw. verbleibenden Lebensdauer von zentraler Bedeutung zur Einleitung geeigneter Maßnahmen unter Berücksichtigung des momentanen State-of-Health (SoH).

Diese Arbeit befasst sich mit der Entwicklung einer effizienten Strategie zur Bestimmung des SoH und der Lebensdauervorhersage ausgewählter Komponenten rekuperativer und alternativer Energieerzeugungssysteme. Konkret werden die Komponenten von Wind-Turbinen (WT) betrachtet. Elementare Bestandteile sind somit insbesondere die Anpassung von Betriebsbedingungen und die Steigerung der Lebensdauer durch adaptive Regelungsstrategien auf Basis des geschätzten SoH. Zentrales Ziel der Arbeit ist die Modellbildung der Funktionalität technischer Systeme also die Erstellung von Lebensdauermodellen, welches die Grundlage zur Entwicklung einer geeigneten Regelungsstrategie bildet. Der Konzept ist als das Safety and Reliability Control Engineering (SRCE) Konzept genannt und wurde erstmals im Jahr 1996 entwickelt und veröffentlicht. Das eingeführte SRCE-Konzept ermöglicht es, die Systemzuverlässigkeit zu beeinflussen und die Lebensdauer unter Berücksichtigung von Wissen bezüglich des aktuellen SoH zu steigern. Zur Entwicklung eines Lebensdauermodells ist es notwendig, die Zusammenhänge zwischen den Messergebnissen eines Structural Health Monitoring (SHM) Systems und der Zustandsdegradierung zu identifizieren. In diesem Kontext wird ein Schwerpunkt dieser Arbeit auf SHM von Windturbinen Komponenten gelegt, wobei besondere Aufmerksamkeit auf SHM Methoden gerichtet wird, die zur Überwachung von Rotorblättern, Lagern, Getrieben sowie Energiespeichern geeignet sind. In diesem Sinne werden nicht nur einzelne Komponenten in ihrer Gesamtheit berücksichtigt, sondern auch die verschiedenen Einsatzmaterialien (Verbundwerkstoffe, metallische Strukturen).

Anhand eines Simulationsmodells wird die Implementierung einer adaptiven Regelungsstrategie für eine Windturbine diskutiert, welche die Möglichkeit zur gleichzeitigen Verlängerung der Lebensdauer sowie Leistungsregelung illustriert. Gemäß den Voraussetzungen für eine adaptive Regelungsstrategien wird die Ermüdungslast von Windturbinen untersucht und in das Modell integriert. In diesem Fall wird der Reglerentwurf durch Wissen, welches aus der Untersuchung der Ermüdungslast resultiert, und der Restlebensdauervorhersage bedingt. Die in dieser Arbeit vorgeschlagene, zuverlässigkeitsorientierte Regelungsstrategie beeinflusst die Zuverlässigkeit des Systems durch an den aktuellen SoH angepasste Regelungsvorgänge.

Außerdem werden drei neue, im Kontext dieser Arbeit entwickelte Ansätze zur Lebensdauermodellierung präsentiert. Diese greifen auf SHM Daten aus der Überwachung eines tribologischen Systems zurück. Zusätzlich zur Entwicklung der Lebensdauermodelle für das tribologische System werden Untersuchungen bezüglich verschiedener Schädigungsmechanismen und Ansätze zur Lebensdauermodellierung von Lithium-Ionen Batterien (LIBs) anhand experimenteller Daten eines LIB Prüfstand dargestellt und diskutiert.

Der Hauptbeitrag dieser Arbeit liegt in der Entwicklung neuer Ansätze zur Lebensdauermodellierung und dem Nachweis, dass eine adaptive, zuverlässigkeitsorientierte Regelungsstrategie die Vermeidung von vorzeitigem Systemversagen, erhöhten Betriebs- sowie Wartungskosten als auch kritischer Situationen, die zu großen ökonomischen sowie menschlichen Verlusten führen, ermöglicht.

Mit den drei vorgeschlagenen Lebensdauermodellen konnten die vorgegebene oder zufriedenstellende Vorhersagegenauigkeiten erzielt werden. Dabei sind jedoch die Anzahl der Modellparameter, die Modellkomplexität, die Genauigkeit des Models und die Anforderungen an die experimentellen Datensätze unterschiedlich. Diese vier Kriterien werden vor dem Hintergrund der Modellevaluierung und Anwendbarkeit auf reale Systeme diskutiert.

Durch die Messung struktureller Lasten und des Effektes mechanischer Belastung auf die Systemzuverlässigkeit kann gezeigt werden, dass eine adaptive Regelungsstrategie die Reduktion struktureller Lasten, insbesondere der auf die Rotorblätter wirkenden flap-wise Biegemomente, ermöglicht und somit eine Möglichkeit zur Steigerung der Restnutzungsdauer darstellt. Dabei ist die Diskrepanz zwischen gewünschter und tatsächlicher Generatorleistung minimal. Die Ergebnisse zeigen, dass im Fall exzessiver struktureller Lasten am Ende der Lebensdauer die Regelungsziele im Kontext der Energieerzeugung geringfügig geopfert werden. Die dargestellten Ergebnisse wurden mit einem Simulationsmodell einer Windturbine erzielt.

Abstract

Technical systems experience different changes due to damage increase and the change of system parameters over service lifetime. These changes are caused by system exposure to different loading profiles, leading to decreased reliability and ultimately to the loss of functionality. Concerning inevitable aging of the system, it is important to examine effects with highest impact to reducing reliability and to predict the remaining or consumed lifetime of the system so that appropriate actions can be performed in accordance with actual State-of-Health (SoH).

This thesis concerns the establishment of an efficient approach for determining the SoH and lifetime prognosis of particular components of recuperative and alternative power generation systems. Concretely, Wind Turbine (WT) systems are considered. The adaption of operation conditions in accordance to estimated current State-of-Health as well as extension of the lifetime through adapted control strategy is therefore an important part. The main aim of the thesis is modeling of functionality of technical systems through the establishment of lifetime models, which are prerequisite for the development of suitable control strategy. Such control concept is known as Safety and Reliability Control Engineering (SRCE) concept and is firstly introduced and published in 1996. Aforementioned concept enables affecting system's reliability and the extension of the lifetime by integrating the knowledge about current SoH into the control strategy. To establish lifetime model, the measurements from Structural Health Monitoring (SHM) systems and their correlation to the degradation is necessary. In accordance with this, special emphasis in this thesis is given to SHM of wind turbine components, especially those SHM methods applicable to rotor blades, bearings and gearboxes, as well as energy storage devices. In this sense, not only an examination of the component itself but also an examination of its constituent materials, are taken in consideration (composite materials, metallic structures).

Implementation of adapted control strategy illustrating simultaneously the possibilities for lifetime extension and power regulation are discussed using simulation model of wind turbine. In accordance with prerequisites for adapted control strategy implementation, wind turbine fatigue load is examined and integrated into the model. Controller design in this case is conditioned by the knowledge about examined fatigue load and predicted remaining useful lifetime. Reliability-oriented control strategy proposed in the thesis affects system's reliability through adapted control actions in accordance with current SoH.

Additionally, the development of three new lifetime modeling approaches taking in consideration SHM data from tribological system are presented in this thesis. Beside lifetime model establishment concerning tribological system, an examination of damage mechanisms and lifetime modeling approaches related to Lithium-Ion Batteries (LIBs) using experimental data from LIB test rig is illustrated and discussed.

Main contribution of this thesis lies in the development of new lifetime modeling approaches and in proved possibility of adapted reliability-oriented control strategy to avoid premature failures of the system, increased operation and maintenance costs, as well as critical events leading to high economical and human resource losses.

Obtained results concerning proposed lifetime models with regards to prediction accuracy are satisfying for all three proposed models. The number of model parameters, model complexity, prediction accuracy, and requirements set on experimental data sets used for model training vary. These four criterion are discussed in terms of model evaluation and determination of model applicability to real systems.

By tracking structural loads and effect of induced mechanical stresses on system's reliability, it is illustrated that structural loads, primarily flap-wise bending moments of rotor blades, are decreased through adapted control strategy providing extension of remaining useful lifetime. The discrepancy between desired and obtained generator power is held as less as possible. According to the results, control objectives related to power generation are slightly sacrificed, but only when the level of structural load is excessive and the system is close to its end of life. Presented results are obtained using simulation model of wind turbine.

Contents

List of Figures

List of Tables

Nomenclature

SHM	Structural Health Monitoring
WT	Wind Turbine
O&M	Operation and Maintenance
NREL	National Renewable Energy Laboratory
SRCE	Safety and Reliability Control Engineering
MTBF	Mean Time Between Failures
MTTF	Mean Time to Failure
MDT	Mean Downtime
MTTR	Mean Time to Repair
SCADA	Supervisory Control and Data Acquisition
DOE/MSU	Department of Energy, Montana State University
FACT	Fatigue of Composites for Wind Turbines
CREW	Continuous Reliability Enhancement for Wind
WMEP	Scientific Measurement and Evaluation Programme
OWMEP	Offshore Scientific Measurement and Evaluation Programme
RELIAWIND	Reliability focused research on optimizing wind energy systems design, operation and maintenance
DOWEC	Dutch Offshore Wind Energy Converter
LWK	Landwirtschaftskammer
VTT	State Technical Research Center
AE	Acoustic Emission
RUL	Remaining Useful Lifetime
ANN	Artificial Neural Network
HMM	Hidden Markov Models
HRM	Hazard Rate Model
PHRM	Proportional Hazard Rate Model
GPM	General Path Model
PoF	Physics of Failure
UKF	Unscented Kalman Filter
EKF	Extended Kalman Filter
CDKF	Central Difference Kalman Filter
FBG	Fibre Bragg Gratings
OSHM	Online Structural Health Monitoring
CSHM	Condition-based Structural Health Monitoring
RSHM	Reliability-based Strctural Health Monitoring
SPM	Shock Pulse Method
CT	Computed Tomography
CFRP	Carbon Fiber Reinforced Polymer
FFT	Fast Fourier Transform
STFT	Short Time Fourier Transform

CWT	Continuous Wavelet Transform
DWT	Discrete Wavelet Transform
WVD	Wigner-Ville Distribution
PWVD	Pseudo-Wigner-Ville-Distribution
AD	Affine-Distribution
CD	Cohen-Distribution
EMD	Empirical Mode Decomposition
IMF	Intrinsic Mode Functions
EEMD	Ensemble Empirical Mode Decomposition
HHT	Hilbert-Huang Transform
MPC	Model Predictive Control
DoF	Degree of Freedom
MBC	Multi-Blade Coordinate
RCA	Rainflow Counting Algorithm
LIB	Lithium-Ion Battery
DoD	Depth-of-Discharge
EoC	End-of-Charge
EoL	End-of-Life
CC-CV	Constant Current - Constant Voltage
DC	Direct Current
SEI	Solid-Electrolyte Interphase
NSGA-II	Non-dominated Sorting Genetic Algorithm II
SoH	State-of-Health
DI	Degradaion index
EIS	Electrochemical Impedance Spectroscopy
EV	Electric Vehicles
HEV	Hybrid Electric Vehicles
OCV	Open Circuit Voltage
SoC	State-of-Charge
ICA	Incremental Capacity Analysis
SoF	State-of-Function
DBN	Dynamic Bayesian Network
LQR	Linear-Quadratic Regulator
IPC	Individual Pitch Controller

1 Introduction

Generation of electrical energy using alternative energy sources at the beginning of the nineteenth century becomes not a question of a choice but rather a requirement due to a number of factors. Among the factors which have high impact on rapid development of energy conversion systems based on use of renewable resources, the following factors can be stated: i) high population expansion, ii) depletion of fossil fuels (oil and gas), and iii) negative environmental impacts of conventional energy sources. Along with high demands on electrical energy generation in addition to growing water and food demands, the sustainability of provided solutions for electricity generation becomes more important taking in consideration social and economical issues: conservation of available natural resources along with social benefits (protection of overall population health, systems harmless to an environment). Precedence of economical issues over sustainability issues is still conspicuous as the cost-effective solutions in general sacrifice sustainability for the sake of economical benefits [KK13]. This all implies that the trade-off between aforementioned goals need to be found. If a variety of renewable resources as wind, solar, geothermal, biomass, and hydro energy conversion systems are analyzed in context of the ratio between installment/operation costs, efficiency, availability, and sustainability some differences are visible. For instance, installment costs of WT system are lower than installment costs for solar, geothermal, and biomass energy systems, but Operation and Maintenance (O&M) costs for onshore as well as offshore wind energy systems are higher [KK13]. Moreover, availability of particular renewable energy supplies is different over the year at different sites (different wind speeds or intensity of light/heat emission from the sun, and similar).

The idea of wind energy exploitation dates back thousand years ago serving wind energy as the oldest energy resource the mankind ever used; at that time, for grinding cereals and propulsion of sailing vessels [KZ11]. Despite some similarities in principal design, an inceptive windmills used at that time are even not comparable with wind energy conversion systems known nowadays. Enormous advances and continuous improvements of WT systems especially concerning Wind Turbine (WT) design and maintenance strategies during and after oil crisis in seventieths enforced accelerated development and improvement of WT systems. As a result of such continuous improvement of WT systems, numerous different designs are developed. Most common WT design up to 2015 is horizontal axis rotor implementation consisting of various number of rotor blades. Beside horizontal axis rotor implementation, vertical and up-stream axis converters are used. The discussion following in Chapter 2 does not focus on a particular WT design but discusses wind turbine systems in general framework pointing out still existing shortcomings and not solved issues. Among advantages to be emphasized regardless of WT design, the following ones can be singled out: i) existence of wind potential in a large number of countries, what is not the case with oil, ii) environment-friendly solution, iii) relatively low

cost of investment, iv) possibility for installment in rural areas (still limited by site specific wind characteristics), and v) generally less area taken for WT installment (providing the possibility for multipurpose use of area). Conversely, from disadvantages to be mentioned are: i) closely approaching but still not cost competitive with conventional energy sources, ii) intermittent wind supply availability (concerning in general terms), iii) if installed at remote sites or offshore, additional costs for WT connection to a grid [SB14]. Some requirements set on WT systems have gained special attention in recent years: i) an achievement of system's longevity through mitigated impacts on the aging processes of WT systems and ii) adapted control of wind turbine systems according to the current aging/deterioration level of system's components. For these purposes, continuous monitoring of WT system component aging/deterioration state is necessary.

1.1 Problem statement and motivation

Although WT systems experienced a major technology breakthrough in the last decades, especially in WT size increase (increasing simultaneously the capability of WT to harvest more energy), there are still a number of shortcomings to be overcome. Among them, necessary improvements primarily belong to application of advanced control strategies and Structural Health Monitoring (SHM) of particular system components (affecting implicitly overall system). Due to unavoidable system weakening and consequent decrease of system's reliability followed by ultimate loss of functionality, monitoring of deterioration level through accumulated damage or similar indicators in the system is indispensable. For estimation of deterioration level, not only fault detection, localization, and quantification (as depicted in Figure 1.1) are concerned, but also an estimation of the point in time at which failure occurs is taken in consideration. The occurrence of fault is reflected in the deviation of at least one system variable from predefined/expected value [HNNM13]. According to this, fault initiation and propagation are closely related to system's aging and overall damage accumulation, but the functionality of system, even disrupted, exist. The system is still functional (is capable to perform predefined functionalities) and the impact of fault occurrence on the system performance is tolerable. It is worth to emphasize that, although the system with faults is not the system without functionality, the fault occurrence/propagation inevitably leads to a loss of functionality and, without an exception, occurs under the influence of applied loads. In these terms, loss of functionality is understood as a *failure*, whereas the system is not capable to perform predefined functionalities [PFC89]. Additionally, the term *system reliability* can be used in a similar manner. As that, system reliability is defined as "the ability of an item to perform its required function under given conditions for a given time interval" [IEE90], or "the probability that an item will perform a required function without failure under stated conditions for a stated period of time" [OK12].

However, the decision about appropriate actions to be performed according to detected fault belongs also to SHM tasks. In dependence on the fault type and assigned fault criticality, aforementioned actions may include corrective maintenance whereas it is aimed to restore the system state to an undamaged state, or emergency maintenance whereas it is aimed to prevent failures with catastrophic consequences. Regardless of corrective or emergency maintenance introduced above, both approaches take in consideration the decision made at the point of fault detection but not before the fault is detected. Completely different approach is preventive maintenance whereas the decision about an action to be carried out is required before the failure happens. It may be preestablished maintenance interval, elapsed predefined service time, or similar [KHV09]. More advanced approaches that have taken more attention in recent years, concerns condition-based and reliability-based maintenance. Taking in consideration condition-based maintenance, the decision to conduct maintenance action is based on the continuous system state observation/inspection, and as such is typically system specific. Herein, the decision to pursue the maintenance action is conditioned by fulfillment of predefined condition(s), like exceedance of system's variable predefined limit, high vibration index, too high or too low temperature (beyond acceptable boundaries), or similar [ZTBF11] [GMPP12] [ZDEA15]. Reliability-based maintenance, as opposed to condition-based maintenance, involves not only an observation of current system states but additionally also previous system states targeting to gather the probability of failure [LCC+14]. In accordance with this, an estimation of system reliability as well as prediction of system health state are issues to be solved in order to make the decision on whether the maintenance action should be performed or postponed [FBB12]. System health state prediction and the estimation of deterioration level of system components require both: continuous structural health monitoring as well as the establishment of lifetime models. Beside the definition of SHM introduced above, there are numerous other definitions introduced in literature [LLEB09] [SFH+04]. However, most of them are nearly identical. For instance, Laveuve et al. [LLEB09] denote SHM concept as a concept

"... for the continuous or at least frequent acquisition, processing and interpretation of physical quantities related to the condition and loading of structures with the objective of detecting existing damage as well as assessing future behavior of the structure based on its history, current condition and expected future loading including environmental conditions".

Sohn et al. [SFH+04] discuss SHM in terms of statistical pattern recognition problem. The authors represent structural health monitoring process as a statistical pattern recognition problem whereas four successive steps are identified targeting to solve SHM tasks successfully. In these terms, the first step is to clarify and gain an awareness about the data acquirement limitations, operational and environmental conditions, as well as failure criterion. Moreover, consideration of the

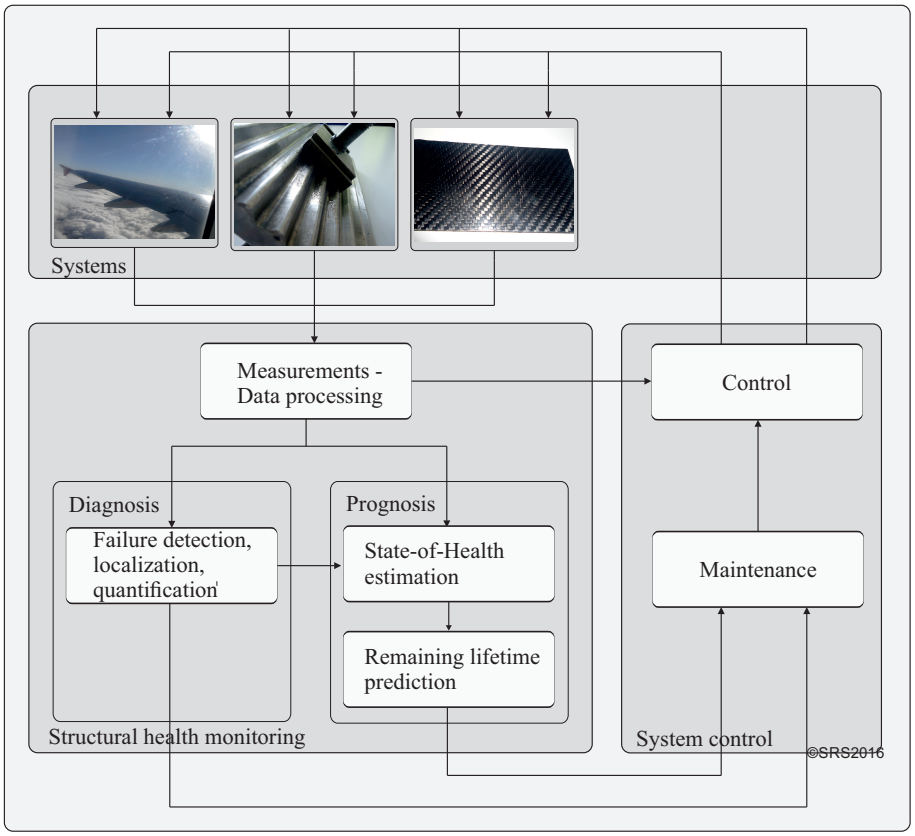

Figure 1.1: Concept of structural health monitoring [BS16]

economic feasibility of SHM implementation should not be neglected. Regarding to Sohn et al. [SFH+04], the second step involves data acquisition and measurement chain deployment. This belongs to the selection of sensor types, the number of sensors, and include decisions related to optimal localization of sensors and associated hardware/software modules to be used. In some cases, the data from different sensors are preprocessed (whitened, filtered, normalized, or similar) and fused to get unambiguous and more accurate deterioration analysis. The third step involves features extraction and selection. As the fourth step, statistical indicators of feature change are calculated as the damaged/undamaged state of a particular system can be seen from the deviation in statistical indicators. Farrar et al. [FL07] have pointed out the aggravating circumstances for efficient damage prediction. As that, the authors [FL07] note that additional improvements are necessary in the following fields: i) measurement chain and processing techniques of sensor data, ii) feature extraction/selection algorithms, iii) prediction models establishment and validation, and iv) the analysis of model reliability and uncertainty.

Remaining Useful Lifetime (RUL) prediction may be seen as quantitative indicator of a system's deterioration level. According to Banjevic [Ban09], remaining useful lifetime is defined as the difference between the moment in time at which the failure

occurs and elapsed time within which the system have been operational. By denoting T as the moment of failure occurrence and t as supposed survival time, mathematical expression for remaining useful lifetime calculation takes the following form: $R_t = T - t$ (defined for $T > t$). Supposed survival time t is herein threated as an unknown variable whose accurate estimation is of high importance. According to the author [Ban09], an assignment of reliability function to remaining useful lifetime gives an opportunity to calculate supposed survival time using probability theory. For this purposes, the probability of failure is defined as

$$P_t(x) = P(R_t > x) = P(T - t > x | T > t), \tag{1.1}$$

where T denotes moment of failure occurrence, t supposed survival time, and P_t assigned reliability function [Ban09]. Probability of failure denotes the probability that the system survives until time point x and provides at the same time all necessary information to estimate remaining useful lifetime (as well as used/consumed lifetime). However, the estimation and prediction of remaining lifetime belongs to SHM tasks but is simultaneously the most challenging tasks. In practical applications, sensor measurements are indispensable to detect fault as well as to predict failure occurrence. As depicted in Figure 1.1, sensor measurements and suitable data processing techniques are a prerequisite for diagnosis and prognosis. Remarkable advantage, especially concerning reliability-based SHM, is the possibility to forecast the fault/failure occurrence. Aggravating factors and major challenges faced herein are related to the prognostic models that have to be capable to describe a relationship between applied load to the system and system's (health) state. In some practical cases, system's health state is discussed in terms of accumulated damage. Therefore, challenges in prognosis are of major concern in this thesis with special emphasis on reliability-based SHM and system reliability decrease over service lifetime. Different approaches regarding to RUL prediction are detailed in the following chapters.

1.2 Scope of research and objectives

With respect to introduced SHM definitions in Chapter 1.1, the advantages of SHM integration may be stated as: i) an avoidance of system premature breakdowns, ii) reduction of system downtimes, iii) reduction of operation and maintenance costs, iv) an improvement of system safety with respect to an avoidance of catastrophic consequences (human lives as well as high economic loses), v) an improvement of system's design, as well as vi) an extension of system's lifetime (remaining useful lifetime) [GYR+14] [GP15] [TSD15] [MMT15] [HHC+09] [LC10]. Advanced sensing methods and data analysis techniques along with powerful computational efficiency contribute to the reduction of time necessary for sensor data analysis, consequently also to faster and more efficient fault detection and diagnosis [CRB14]. Hence, the

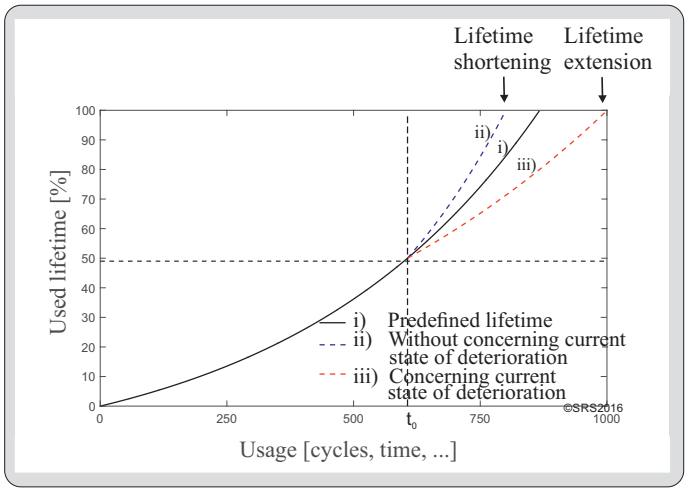

Figure 1.2: Impact of reliability-oriented system usage [BS16]

development of advanced sensing methods as well as data analysis techniques is prerequisite for efficient failure prognostic through remaining useful lifetime estimation. An improvements concerning sensing system and data analysis are still possible in the field of online (real-time) data analysis, sensor data reduction (algorithms and approaches), and nondestructive SHM sensing techniques. The disadvantage worth to be mentioned, lies in an additional costs associated with SHM integration. However, these costs are less in comparison with O&M costs, approximated to be 20% to 25% of overall costs of wind turbine system, concerning condition- or reliability-based operation and maintenance [VDB15]. With condition- or reliability-based O&M, unnecessary maintenance or replacement actions are reduced, number and duration of system downtimes can be minimized, and number of unnecessary operator inspections, especially at remote sites, are decreased [VDB15]. Preliminary analysis shows promising potential of Condition-based Structural Health Monitoring (CSHM) and Reliability-based Structural Health Monitoring (RSHM) in terms of returning the initial investments in a long term framework, but additional improvements in this field are necessary [VDB15].

Certain economical profit, justifying in part the resources invested in SHM, is achieved through remaining useful lifetime extension of the system. However, remaining useful lifetime extension is conditioned by advanced SHM systems (capable to detect fault occurrence efficiently) as well as by precise prognostic approaches (capable to predict remaining useful lifetime accurately). As already noted, the deterioration and damage accumulation within system is closely related to operating conditions to whom the system is subjected. If operating conditions are regarded as an environmental operating conditions, such as temperature, wind speed, wind direction, humidity, and similar (in case of wind turbine systems), they cannot be largely affected by a human factor. Contrary, some process or system parameters

are undoubtedly controllable/adaptable to the specific system states. If deterioration level (either aging process or accumulated damage) is taken into consideration, the problem boils down to the discussion whether it is possible to mitigate system deterioration (aging process, accumulated damage) through adapted control strategy [SZKP12]. The concept of adapted control strategy to current state of deterioration is depicted in Figure 1.2. Herein, exponential relationship between used (consumed) lifetime and the deterioration indicator (days, lifecycles, accumulated damage in the system, service hours, driven kilometers, or similar parameters related to a particular system) is visualized. System behavior exhibited under three different control strategies is depicted in Figure 1.2: i) belongs to a system with no unexpected or sudden changes of system's reliability, which is rather theoretical, in practice often unattainable case (predefined system's lifetime is in this case achieved), ii) shows a system with a control strategy whereas system's actual deterioration state is not considered even it contributes to the decrease of system's reliability, and iii) considers a system whereas system's actual deterioration state is integrated into control strategy. Deterioration process is rarely when ever pure exponential, but such representation is used only to clarify the concept in general. If sudden (not predicted, not expected) failure occurs or damage accumulates within system, it is reflected simultaneously in shortening of remaining useful lifetime. If such failure/change in accumulated damage is not compensated through control strategy, a part of system's lifetime is irretrievably lost. Contrary, if control strategy is adapted targeting to mitigate deterioration/accumulated damage, remaining useful lifetime of a system can be extended in comparison with predefined remaining useful lifetime. Prerequisite for application of such concept is to obtain an information about current system's health state (system reliability). Application of aforementioned concept is of main concern in this thesis and is detailed in the following chapters with special emphasis on different approaches to RUL prediction and accompanying lifetime prediction models.

1.3 Thesis outline

The thesis consist of six chapters. Some parts of this thesis are published/submitted as journal papers ([BS17], [BNS], [BS], [BS16]) or presented/accepted in international conferences ([BRS16], [BBS15], [BMS15], [BNRS15], [BS15b], [BRS14]).

Whilst the introductory part defines main challenges identified within SHM and gives an overall overview of the thesis, thesis objectives, and the scope of thesis, second chapter provides detailed insight into WT reliability, sensing techniques applicable to different WT components, and accompanying signal-based techniques based on preliminary literature review [BS16]. Hence, state-of-the-art of different approaches towards lifetime modeling is given. Additionally, the development of control strategies which can provide extended lifetime of a system component and

overall system is discussed. In this chapter, lifetime modeling as well as control strategies are considered in general terms without referring to an individual system or system's component.

The third chapter introduces fatigue load evaluation and remaining useful lifetime estimation of WT systems [BNRS15]. The analysis is done by concerning WT simulation model developed by National Renewable Energy Laboratory (NREL). Structural loads of WT blades are examined using blade flap-wise bending moments. Remaining useful lifetime is calculated using Palmgren-Miner damage accumulation rule within utilization of online rainflow counting algorithm for load levels estimation [BNS]. In addition, an application of adapted reliability-oriented control strategy is illustrated on an example of WT simulation model.

In the fourth chapter the experimental setup of the tribological system for purpose of wear examination of metallic plates is presented. Acoustic Emission (AE) and hydraulic pressure measurements along with accompanying signal processing techniques are used to establish the lifetime models [BS15b] [BRS14] [BBS15]. In addition, three different newly developed lifetime models used for purpose of useful (consumed) or remaining lifetime estimation are proposed. Models optimization is based on original or modified, depending on certain model, Non-dominated Sorting Genetic Algorithm II (NSGA-II). Obtained results as well as the efficiency of particular models are illustrated and discussed at the end of Chapter 4.

The fifth chapter is related to the RUL estimation of Lithium-Ion Batteries (LIB) based on experimental results [BMS15]. As such, experimental setup for purpose of LIB aging process examination is introduced. Relevant system variables are measured and unaccessible states are estimated based on measured variables. Firstly, system variables are correlated to the deterioration level of LIB indirectly, whereas additional intermittent variables are calculated. Along with indirect estimation of LIB degradation level, the possibility for direct correlation of AE measurements to the deterioration level of LIB based on experimental results is examined [BS]. Lithium-ion battery lifetime model based on AE measurements is developed and the results are discussed.

The thesis closes with conclusion, final remarks, and outlook. The problems not solved in this thesis but identified for future work are pointed out.

2 Structural health monitoring: State-of-the-art with special focus to lifetime modeling, diagnosis, and prognosis

Mitigation of WT system reliability decrease, remaining useful lifetime prediction, and implementation of adapted control strategies concerning the deterioration state of the system are identified as existing challenges in SHM in the first chapter. Chapter 2 includes the discussion about current state-of-the-art of research fields related to aforementioned challenges as they are an integral part of structural health monitoring.

Beside the discussion about some aspects of WT system reliability analysis at the beginning of Chapter 2, main focus is given to literature review of sensing methods as well as accompanying signal processing techniques with special emphasis to wind turbine blades, gearboxes, and bearings, as well as to an estimation of remaining useful lifetime or similar aging indicators. Hence, existing approaches towards RUL prognosis/estimation known in literature, as well as control strategies capable to take into account current system or system components deterioration state are detailed. For these purposes, Safety and Reliability Control Engineering (SRCE) concept, firstly introduced in [RS97] and [RS96], is detailed. Some parts of Chapter 2 are published in [BBS15], [BMS15], [BS], and [BS16].

2.1 Wind turbine systems as example for SHM research focused to diagnosis and prognosis

The deployment of structural health monitoring system requires the knowledge about operating conditions of the system, so that the equipment of SHM system can be adequately protected. Concerning WT systems, operating conditions belong primarily to intermittent fluctuating loads to whom WT are exposed and to the contradictory requirements set on WT system: i) the lowest possible energy production costs, ii) as long as possible service lifetime, and iii) the maintenance actions performed at the proper time, neither too early nor too late [YTC+14]. However, WT system operates in a harsh environment whereas aerodynamic factors such as wind speed, wind direction, and similar, as well as hydrodynamic factors in case of offshore WT systems have to be considered. Moreover, climate factors such as salinity, humidity, temperature, and others cannot be neglected.

Under aforementioned conditions, particular components are more subjected to the deterioration than the others; not all components are equally susceptible to the fault or failure occurrence. Moreover, not only extreme cases (fault or failure occurrence) have to be considered in reliability analysis but also some intermediate system or

component states leading to a fault or failure. Therefore, system and system components deterioration is herein considered in terms of an aging process occurred within structure (the damage accumulated in WT system, or the growth of degradation mechanisms such as corrosion, wear, fatigue, and similar). All of these effects are closely related to system's reliability and availability decrease. System's availability is defined as a timespan in which the system is operable and able to withstand aforementioned effects concerning overall service lifetime [IEE90].

To determine the reliability of a system and/or component, statistical indicators related to failure occurrence, as well as accumulated damage occurred over system service lifetime due to material and component aging are analyzed. Reliability-related indicators most often used in reliability analysis are: i) failure rate, ii) mean time between failures (MTBF), iii) mean downtime (MDT), iv) mean time to failure (MTTF), v) mean time to repair (MTTR), and vi) availability. Above stated indicators are defined as: i) a number of failures in considered timespan, ii) mean length of timespan between subsequent failures (for repairable components), iii) average time within which the device is not functional (often overlapped with MTTR), iv) a ratio between elapsed service lifetime and the number of fault occurrences, v) average time necessary for system/component repairment, and vi) a ratio between MTBF and sum of MTBF and MDT, respectively [OK12].

Statistical analysis of reliability indicators is basically supposed to be carried out to identify the most critical components of WT system whose inspection and monitoring gains high attention in nowadays WT systems. Intuitively, critical components cause the most economical losses due to necessity for frequent maintenance and/or replacement actions. Reliability analysis presented here is based on a number of reports and reliability databases targeting to identify the components which are the most susceptible to faults and consequently failures. Even the databases have been created, an open access to benchmark data sets is often not provided. Therefore, reliability analysis in this thesis is limited to a number of reports and conference as well as journal publications, most of them showing obtained results on graphs or charts. For purpose of gaining the knowledge about WT system reliability, an analysis of different statistical indicators such as: mean time between failures, mean time to repair, total number of failures over the year, system availability, frequency of system downtimes, and similar is carried out. Stated reliability indicators are, as expected, closely related to failure occurrence. Hence, the decision about maintenance and replacement actions is influenced by the knowledge about reliability indicators.

Conversely, some databases contain the records related to a particular component or even material (for instance: fatigue analysis of composite structures, which is not directly correlated to system reliability but can be seen as an indirect reliability indicator). Some databases contain only statistical data on failures but do not include failure classification in terms of failure criticality, failure type, or cause of failure

Database/Programme/Project	Area	Content	Year
Continuous Reliability Enhancement for Wind (CREW) Database [HOB13]	USA	Operational availability, capacity factor, mean time between failures, mean downtimes, power curve analysis, component level based records	1970s - ...
Scientific Measurement and Evaluation Programme (WMEP) [FHT11]	Germany	Mean time to repair, mean time between failures (reciprocal of failure rate), mean downtimes, WT availability	1989 - 2006
Offshore Scientific Measurement and Evaluation Programme (OWMEP) [FPKL12]		Follow up of WMEP, reliability indicators of offshore WT systems	2007 - 2011
Dutch Offshore Wind Energy Converter (DOWEC) Programme [VBB03] [PMTP13]	Netherlands	Offshore WT systems, maintenance actions, downtimes and failure statistics	1999 - 2003
Reliability Focused Research on Optimizing Wind Energy Systems Design, Operation and Maintenance (RELIAWIND) Project [WHH+11]	EU	Component level oriented, introduction of the ideas towards reliability database unification	2008 - 2011
Landwirtschaftskammer (LWK) Database [TVBS06]	Germany	Statistical data of system failures, production data	1993 - 2006
Technical Research Center of Finland [She13]	Finland	Failure data, downtimes, production data, not component level based	1992 - ...
WindStats Newsletter	Denmark	Failure data, component level based, not the cause is specified	1987 - ...
WindStats Newsletter	Germany	Failure data, component level based, not the cause is specified	1987 - ...
Vindstat (Elforsk) [PAOS10]	Sweden	Specification of failure type and cause, statistical data of occurred downtimes but not component level based	2005 - ...

Table 2.1: Reliability databases and reports (based on [BBS15])

determination. This being the case, it is questionable whether such databases can be considered as reliability databases as they do not contain enough information for feasible reliability analysis. In Table 2.1, some WT reliability databases together with corresponding projects related to WT reliability analysis are listed. The database created under particular programmes and initiatives contain the records mostly collected and imported either by end-user or through Supervisory Control and Data Acquisition (SCADA) systems [YJ11] [HOB13]. At first glance, Table 2.1 reveals that each database refers to a particular site, particular wind turbine design or component, as well as to a different timespan in which the data have been collected.

Even though the databases are related to the different WT designs, sites, and considered timespan, reliability indicators contained in a particular database also vary. By comparing different databases, the problem of database unification and standardization is conspicuous and has in turn a consequence that the comparison between different reliability databases is hardly possible. Apart from evident lack of unified reliability databases concerning [SMM12] [SMM13] [Val15] [FHT11] [HOB13] [FPKL12] [VBB03] [TVBS06], some general conclusions and trends are noticeable.

In a study of Hines et al. [HOB13], rotor blades, generator, control system, and

Database	Area	Focus	Year
Department of Energy/Montana State University (DOE/MSU) [SMM12] [SMM13]	USA	Tensile and compressive fatigue tests revealing stress-strain behavior of composites, detailed test reports including exact test parameters, geometry of specimens nearly the same	2010 - ...
Fatigue of Composites for Wind Turbines (FACT) [Val15]	EU	Fatigue tensile tests under different conditions revealing stress-strain behavior of composites, not easy to extract exact test conditions from the database; afterwards integrated in OptiDat database	1994 - 1995
OptiDat Database [Val15]	EU	Stress-strain behavior of composites, geometry of specimens as well as manufacture process varies	2002 - 2006

Table 2.2: Fatigue tests on composite materials: Database overview (based on [BBS15])

gearboxes are identified as a components with the highest number of fault/failure related events per year (including failure occurrence, maintenance or replacement actions, and downtime events). Similarly, Faulstich et al. [FHT11] have found annual failure rate of electrical system, electronic control, and sensors as the highest one among all WT components (0.25 to 0.57). Even annual failure rate of gearboxes and rotor blades is lower (0.11), caused system downtime per failure in this case is the highest among all WT components [FHT11]. In a report of DOWEC [VBB03], rotor blades, control system, and gearboxes are stated as the components with the highest failure rate per year whereas they cause of 85% of overall downtimes. According to LWK Database [TVBS06], electrical elements, electric control, and rotor blades are found in the first three groups with highest annual failure rate. Summarized from WindStats Newsletter (Germany and Denmark), control, electrical system, yaw system, and blades are revealed as the components with highest mechanical failure rates. Along with listed databases there are additional reports covering an area of Denmark and Sweden [TGW+13] [RB07] with consistent results taking in consideration previously listed databases. The analysis summarized from all above mentioned reports and databases is in general consistent, with some slight variations caused probably by different environmental and site conditions, as well as different wind turbine designs. Additionally, through OWMEP and RELIAWIND projects some steps towards reliability database standardization and unification have taken according to [FPKL12] [WHH+11].

In addition, there are a few databases focusing on examination of composite materials and on the effect of different composite designs on fatigue behavior. Fatigue tests carried out under different test conditions and different materials are of high importance for gaining the knowledge about individual characteristics of composite materials as well as the most efficient manufacture process with respect to those characteristics [Val15]. As such, fatigue tests and their analysis is closely related to the State-of-Health monitoring and lifetime prediction, primarily of WT blades. Un-

like to the most of reliability databases listed in Table 2.1, an access to the databases listed in Table 2.2 is provided for public.

Notwithstanding the fact that the results from reliability databases and corresponding reports are hardly comparable, a detailed insight into reports reveals that electrical systems including power modules, WT blades, gearboxes, and bearings are the most susceptible components to the failure occurrence and aging effects due to applied loads. Therefore, special attention in this thesis is given to continuous monitoring of WT blades (composites), bearings, and gearboxes (metallic structures).

2.2 Structural health monitoring of wind turbine systems

An adequate structural health monitoring method applied to a particular component along with the choice of suitable system parameters to be monitored serve as a prerequisite for fault detection, fault diagnosis, as well as failure prediction. Appropriate and carefully selected sensing method is supposed to contribute to the prevention of ambiguous results regarding fault detection and diagnosis, consequently to more accurate prediction of failure occurrence. At this point it is worth to emphasize that sensing methods are not seen exclusively as a sensor selection task. Moreover, sensing method(s) include sensor location selection, the choice of suitable signal processing technique, as well as the selection of data acquisition and data transmission elements [Rum11].

2.2.1 Sensing methods

The number of reviews on SHM methods applicable to WT system components gives an insight into existing SHM approaches: sensing methods as well as signal processing techniques [HHC+09] [GMPP12] [YTC+14] [TWTE13] [LLWY09] [ABBW07]. However, it is still questionable if the reviews are exhaustive (even if they can be) concerning rapid technology development and fast changes in a manufacture process as well as used materials. Moreover, some of aforementioned listed reviews have focus on a particular group of SHM methods or on the methods applicable to a specific WT component. For instance, nondestructive SHM methods are reviewed in [YZZA14], [LMIC14], [HTPC14b], [ZCAA15], while the SHM methods discussed in general framework in the greater or lesser extent are given in [GMPP12] and [ABBW07]. Similarly, Tchakoua et al. [TWTE13] concern SHM methods classification not only in destructive and nondestructive methods, but additionally in intrusive and nonintrusive methods. Some of reviews, such as [HHC+09] and [YTC+14], discuss in detail accompanying benefits of SHM integration into the system along with SHM methods and signal processing techniques.

The state-of-the-art of SHM sensing methods and accompanying signal processing techniques given in this thesis tends to bring in a conjunction previous and recently developed methods (up to 2016) used for structural health monitoring of wind turbine blades, gearboxes, and bearings. As that, analysis done herein can be seen as a review of reviews about SHM of WT blades, gearboxes, and bearings with special emphasis on existing shortcomings, the possibilities for further improvements, and utilization of SHM sensor data for RUL prediction.

2.2.1.1 Acoustic emission measurements

The transient elastic waves generated as a consequence of rapid energy release due to present material deformation are defined in [Sta] as acoustic emission. An application of AE is nowadays found in different application fields, such as in the SHM of gearboxes and bearings [LLWY09], bridges [TSC15], or planetary gearboxes [LLZH14] due to AE nondestructive nature and unneeded additional excitation source for wave generation (passive method) [PN13]. Still dominant and the most explored application field of AE, despite its application in other fields, is an inspection of composite structures. Taking in consideration composite materials, elastic waves are typically generated due to micro structural material changes like fiber breakage, debonding, crack initiation, matrix cracking, or delamination [SCBH13].

Conventional sensors used for acoustic emission measurements are surface-mounted piezoceramic sensors. Concerning low amplitude range as well as high-frequency bandwidth of acoustic emission signal, high requirements are set on measurement chain. An amplification of low amplitude signal, usually by 100 to 1000 times whereby also existing noise is amplified, and noise-elimination using some filtering method (as usual bandpass filter limiting the frequency bandwidth beyond several kHz and 1 MHz) is necessary [GO08]. High frequency bandwidth in which AE signal is located requires consequently high sampling rates if the raw signal is intended to be captured. Thus, fast I/O throughput, such as FPGAs or CPU arrays, as well as A/D converters working in high-frequency bandwidth is needed. Nevertheless, not always there is a necessity for raw signal capturing. Targeting to reduce amount of data but to retain the information contained in AE signal, amplitude peaks, event counts, rise time, signal energy content, and similar can be utilized.

Sometimes, AE method is combined with vibration method to obtain fault signatures of gearboxes and bearings [SVLP+13]. As that, Soua et al. [SVLP+13] outline different results obtained using AE- and vibration-based monitoring method with respect to different operating conditions, sensor type choice, and damage size. According to [SVLP+13], vibration monitoring method shows particularly poor results concerning fault detection in gearboxes and bearings in their initiation phase, what is not the case with AE-based monitoring. Al-Ghamd et al. [AGM06] applied AE and vibration method to detect the faults in bearings with special emphasize to

individual differences between aforementioned methods, this time not used in a conjunction but standalone. Similarly as reported in [SVLP+13], good fault detectability in their initiation phase based on AE is outlined. Additionally, satisfying results in fault criticality determination based on AE method, which is hardly achievable using vibration method, are outlined. In a similar way, Tandon et al. [TC99] investigate time- and frequency-domain analysis of AE and vibration signals and outline the possibility for fault localization using vibration method, whilst the localization is not possible using AE method. Different pattern recognition algorithms and features used for fault detection in composites are examined by Gutkin et al. [GGV+11]. The authors compare competitive neural network, k-means, and self-organizing map combined with k-means algorithms along with five different features extracted from AE signal. The most efficient algorithm, reported in [GGV+11], is self-organizing map combined with k-means algorithm and time-frequency-based signal signatures.

2.2.1.2 Structural monitoring using guided waves - Lamb waves

Specific group of ultrasound waves guided along structure boundaries and propagating parallel to the solid structure, so called lamb waves whose frequency bandwidth lies between 0.5 and 4 MHz, are used for fatigue damage as well as crack growth monitoring in composites [HSW15] [HSL+15]. Unlike AE method whereas the waves are not generated by external source, SHM aided using lamb waves require external source for wave generation. In accordance with this, lamb waves are generated and sensed using piezoelectric tentacles, comb transducers, wedges, fiber optic, electromagnetic, acoustic, or piezoelectric transducers. Traditional actuators and sensors used for lamb waves generation and sensing require coupling media between actuators/sensors and the surface to be monitored. Thus, coupling media has to be properly chosen to avoid undesirable effects of couplings [MKM+15]. Even better solution is to avoid coupling media completely and use noncontact methods for lamb wave generation and sensing. For these purposes, mainly laser-based devices are used.

Leong et al. [LSLS05] propose the use of piezoceramic actuator to generate lamb waves and laser vibrometer to capture their responses. High level of noise as well as high level of signal attenuation is observed, but the detection of cracks in aluminum plate equal or above 6 mm is possible. As reported in [LSLS05], the costs of such system are relatively high and additional research, especially regarding improvements in signal processing methods as well as sensitivity to damage, is necessary. Similarly, Gaul et al. [GPHJ03] discussed utilization of lamb wave SHM in automated procedure for detection as well as localization of notches and discontinuities in isotropic plates. For purpose of lamb wave analysis in this case, captured signal is transformed from time-domain to time-frequency domain using Short Time Fourier Transform (STFT) and further into "slowness-frequency domain" [GPHJ03]. Such signal transformation makes the signal invariant to the distance between the source

and receiver enabling unequivocal estimation of notch/discontinuity in the plate. Even research here is related to notches and discontinuities localization in isotopic plates, the authors [GPHJ03] point out possibility for application of such approach to cracks and anomalies detection and localization in composites.

However, the method is characterized by high sensitivity to the anomalies of small sizes, being at the same time capable to estimate the damage location. Limitation factors for lamb wave utilization in SHM are a priori required knowledge about healthy state of the structure which is used as a reference. Moreover, the features of reflected wave to be used for damage detection and diagnosis have to be known in advance [RC07].

2.2.1.3 Ultrasound measurements

Ultrasonic SHM method utilizes elastic waves generation and accompanying analysis of ultrasonic responses to detect anomalies within structures. As ultrasound waves lie in high-frequency range, namely 20 kHz to several GHz, they are not audible for humans. Depending on frequency bandwidth and propagation characteristics, ultrasound waves are differentiated into bulk, acoustic, or lamb waves (Section 2.2.1.2). For ultrasound monitoring purposes, generated ultrasound waves are injected into the structure, whilst the reflection of ultrasound waves is tracked using ultrasound receivers. As that, the method is classified as an active SHM method due to the necessity for external ultrasound excitation source as well as ultrasound receiver.

Noncontact SHM of WT rotor blades using laser vibrometers is proposed by Park et al. [PAS14] and Sohn et al. [SDY$^+$11]. Herein, ultrasonic imaging is applied to visualize the damage. Laser vibrometers utilize Doppler effect principle to analyze optical signals with respect to oscillation frequency and phase difference. Hence, the authors point out existing challenges in in-situ application of laser imaging method. Even in-situ application of ultrasound SHM method still faces many challenges, some steps ahead are already done, as outlined by Ye et al. [YNB$^+$14].

Conversely, acoustic-laser vibrometers use acoustic source as an external excitation source and scanning laser vibrometers to measure structural vibration signatures. The parameters of interest are identified as dwell time, sound level, and laser signal along with its incidence level [CHB15]. The tests done with acoustic-laser vibrometers and reported in [CHB15] are conducted under laboratory conditions whereas the major concern is given to the testing of different operating conditions, specimen geometries, and measurement chain in general.

In a similar way, Scheerer et al. [SCR$^+$12] combines acoustic emission and ultrasound monitoring method not only to detect but also to localize damaged areas. The system consists of a number of sensors and actuators whereas they all are activated alternately; while one sensor/actuator combination is activated others are deactivated. The authors noted very good results with respect to damage localization and

crack length estimation by intermittent activation of all possible sensor/actuator combinations.

2.2.1.4 Strain measurements

Shape deformation or changes in length under the influence of applied loads, mainly compressive or tensile stress, is quantitatively described through strain measurements. Proportional relationship between applied stress and measured strain gives possibility to analyze accumulated loads. Subsequently, calculation of accumulated damage in the system providing the possibility for remaining useful lifetime prediction can be carried out [YGS13].

The number and type of sensors to be used for strain monitoring, as well as adequate sensor positioning is primarily conditioned by the component itself (WT supporting structures, rotor blades, and similar) and the size of inspecting area to be covered. Aggravating circumstance in strain condition monitoring is necessity for a priori knowledge of maximum strain level and expected hot spots (whereas the strain is most conspicuous), and a high number of sensors to cover broad inspection area [SCBH13]. Even the deformation is detected, maximum stress level has to be known to predict the failure based on strain measurements. Similarly, an expected hot spots are required for suitable sensor positioning taking into consideration strain measurement exclusively at one point with one sensor. As outlined in [CLB08], blade roots and blade bonded/welded joints are critical hot spots, whereas the strain is dominant.

Traditional electrical strain gauges are utilized in measurement of blade flap-wise or side-to-side bending moments, as well as blade deflection. Electrical strain gauges work on principle of electrical parameters measurements: resistance, conductance, or inductance depending on sensor type. Recently, fiber optical sensors have displaced traditional electrical gauges to a great extent. Unlike traditional electrical gauges whereas electrical parameters are correlated to the strain, fiber optical sensors correlate either light intensity, light phase, or wavelength change to the strain [Pie14].

Fibre Bragg Gratings use the principle of exactly predefined propagation and reflection of light wave along the grating; propagating only the waves of well defined light wavelengths while reflecting all others. Along with strain measurements, specific FBG sensors are able to measure temperature, pressure, or displacement in dependence of application. Moreover, optical Fibre Bragg Gratings (FBGs) are seen as sensors especially adapted to WT blade monitoring primarily due to their insusceptibility to electro-magnetic interference and long distance signal transmission under negligible signal attenuation [KSH12]. The specific wavelength, on which basis each

particular FBG sensor is differentiated, as well as their small dimension enable multiplexing of up to 100 FBG sensors on one transmission line and embedding in composite structure (smart structures) [KSH12].

Moreover, piezoelectric-based polymer nanofibers and piezoresistive-based nanofibers embedded in composite structures are capable of strain and stress monitoring [SSW+15]. The manufacture and embedding of nanofibers is quite expensive, but their resistance to errors, simplicity of handling and shipping, as well as potential shown in signal amplification, justify an effort planned to be invested in further method development. As a newly developed method, a lot of research is still necessary to make the technology commercially acceptable.

2.2.1.5 Vibration measurements

Changes in stiffness or damping, occurred mainly due to the mechanical disturbances, unbalanced rotating parts, or the damage present in the system, are reflected in system's vibrational characteristics. Vibration method serve as a typical monitoring of WT rotating parts (bearings, gearboxes), but is also applicable to the composite materials and supporting structures of WT systems, as well as to WT shafts [MMR06] [SL14]. Anomalies present in rotating parts of WT systems are reflected in amplitude and/or frequency changes of vibrational signal. The change in frequency is mostly correlated to the cause of the damage, whilst the change in amplitude of vibrational signal is related to the damage criticality [GP15]. Thus, vibration measurements can be used for SHM of composites, bearings, and gearboxes, whence the information about the damage is extracted from vibration characteristics.

The sensors utilized for vibration monitoring are laser vibrometers, accelerometers, velometers, and inductive velocity transducers. Sensor selection depends on inspecting structure and frequency bandwidth of interest [FQ11]. Concerning damage detection methods, Fan et al. [FQ11] divide vibration-based approaches into mode shape based, curvature shape based, frequency-based, and combined shape- and frequency-based approaches. Moreover, Figueiredo et al. [DCA+14] propose usage of machine learning techniques, namely nonlinear Neural Networks, Auto-Associative Neural Network, and Radial Basis Function Network, for WT blade damage detection.

Safizadeh et al. [SL14] discuss damage detection in bearings using fusion of sensor data acquired from accelerometer and load cell. The authors [SL14] use signal signatures in both time and frequency domain. Principal Component Analysis (PCA) is applied to reduce the number of features along with K-Nearest Neighbor classifier to differentiate various anomalies within bearings. Regardless of applied approach, often used signatures extracted from vibration signal and used for damage detection are time-, frequency-, and time-frequency-based signatures capable to correlate

damage severity and damage type to the measurements (such as damage index, strain energy, mode shape index, and similar).

2.2.1.6 Eddy current thermography

In the presence of deterioration, certain structures and materials exhibit the phenomenon of conductivity variation. As that, the measure of conductivity variation can be used for damage detection as well as damage quantification using eddy-current-based monitoring methods. The limitation of aforementioned methods is their applicability exclusively on conductive and nonmagnetic materials. Nondestructive but not in-situ applicable conventional eddy current thermography uses induced high-frequency eddy currents whose densities vary between damaged and undamaged areas [KHK13]. Variation of eddy current densities has as a consequence nonuniform heating of damaged and undamaged areas. Eddy current thermography thus utilizes heating effect to detect structural or material anomalies by capturing temperature changes using infrared cameras or similar sensors. Targeting to detect anomalies, an application of suitable image processing technique on captured infrared thermal image is required to reveal deterioration related image signatures [HTPC14a].

The improvements introduced over the last decades in eddy current thermography basically involve changes related to: i) an excitation source (if measurement chain is concerned), and ii) the development of enhanced image processing techniques, whence a variety of features are extracted, analyzed, and used for deterioration detection [LMIC14]. For instance, eddy current pulsed thermography, eddy current pulsed phased thermography, and eddy current lock-in thermography are all related to inceptive eddy current thermography, but vary in excitation source as well as in parameters to be concerned for image analysis [HTPC14b]. As that, eddy current pulsed thermography uses not only information about conductivity change but additionally also the information about magnetic field intensity variation. Eddy current pulsed phased thermography introduces thermal waves of different frequencies into inspected structure and performs superposition of frequency-domain responses to obtain the information about deterioration in a structure [LMIC14].

Although the conductivity of composite materials is not high, the application of eddy current SHM method on composite materials shows satisfying results in delamination, matrix cracking, or fiber breakage detection, but also in production quality testing by fiber distribution and orientation, or fiber density examination [KHK13] [HTPC14a]. Moreover, application of eddy current inspecting methods is also seen in crack and corrosion detection in metallic structures [HTPC14b].

2.2.1.7 Thermographic measurements

Structural health monitoring based on thermographic measurements uses similar principles as eddy current thermography. Monitoring of temperature change for purpose of deterioration detection in composites structures, bonded joints at the blade roots, and similar structures can be implemented as a passive or as an active method. Whilst passive method compares the ambient temperature with the temperature of inspecting structure, active method examine the change of temperature under applied stress. For these purposes, external excitation source like flash lamps or other heating sources are needed to introduce the thermal energy into the structure [PHK+10]. The distribution of thermal energy is not uniform, what especially belongs to the areas in the vicinity of the damage. This phenomena are thus utilized to detect anomalies, both internal and external, present within the structure.

According to Yang et al. [YS13], the application of thermal imaging for the detection of delamination, matrix cracking, debonding, as well as fiber pulling out occurred within composite structures in their early stage shows satisfying results. The limitation to be concerned is its dependence on ambient temperature. In addition, thermal imaging is used with great success for the analysis of fatigue aging, but there are still difficulties in the application of thermal imaging within in-situ WT systems [CT12].

2.2.1.8 Radioscopy/Radiography testing

An X-ray scanning method relies on a phenomenon of nonuniform absorption of X-rays in damaged areas. As nondestructive method, radiography testing traditionally uses thermionic electron beam on one side to generate X-rays through the component being monitored, and radiography film on the other side as X-ray detector [HFU08]. Additionally, flat panels, CMOS cameras or line detectors can also serve as X-ray detectors. However, the choice of X-ray detector to be used is basically conditioned by X-ray source type [PGH+15].

Two-dimensional imaging along with accompanying image processing technique is utilized to inspect the component and to detect anomalies in a structure. Most often application of X-ray scanning regarding to WT systems is found in SHM of WT rotor blades, whereas in-situ implementation is not possible. In addition, X-ray scanning is usually used for quality testing of production process. The method is capable to detect and localize damages like delamination, debonding, and matrix cracking in composite structures, but requires both external X-ray sources and X-ray detectors [HFU08]. Moreover, the method is often applied for solder joints inspection of electronic components.

Recent improvements in the development of X-ray sources lead to the displacement, still not completely but to a large extent, of conventional thermionic electron beams

by nanotube-based beams [PCMC15]. Thermionic electron beams are characterized by slow response, high size, low photon flux, and the simplicity of their manufacture, while nanotube-based beams offer highly controllable photon flux, lower size in comparison with thermionic electron beams, pulsed high-frequency X-ray generation, but have also higher costs. As outlined by Parmee et al. [PCMC15], further research is unavoidable to make the technology commercially viable, even the use of carbon nanotubes for X-rays generation show encouraging results.

Similarly, Hofmann et al. [HNS+15] outline recent development in X-ray detectors manufacture. The authors propose use of multi-line detectors to achieve higher frame rates, wider imaging field, better image quality, as well as faster image capturing in comparison with flat panels. Advances in X-ray sources and detectors development lead to the displacement of traditional two-dimensional imaging by computed tomography (3D X-ray digital imaging) intending to make the X-ray method in-situ applicable [PCMC15] [HNS+15]. Apart from Computed Tomography (CT) utilization in medical diagnostics, application of CT in SHM field has experienced rapid growth in recent years as it offers possibility not only to detect damage but also to determine damage criticality; gives an information about the depth and volume of damage.

2.2.1.9 Visual inspection

The damages that are visible to the naked eye, such as cracks and scratches, are detectable by visual inspection. Although any component can be visually monitored, it is indisputable that visually noticed damage overcomes microscopic scale; at the time when the damage becomes evident, the damage had already grown to a large extent. Performed without aided equipment and often subjectively judged by humans, visual inspection is not considered as a reliable monitoring method. Thus, the method is rarely applied standalone and serves more often as a proof of detected damage. Concerning WT rotor blades, vision system can be installed on mobile platforms including remote control of camera positions. Images captured through vision system are analyzed with respect to a shape recognition. Once the shape is recognized, an analysis whether the shape conforms to the shape of an expected damage have to be carried out as a subsequent step [KKJ+13].

2.2.1.10 Oil analysis

An analysis of lubrication or hydraulic oils is noted as an inceptive technique applicable primarily to SHM of bearings and gearboxes [GMPP12]. The detection and analysis of ferromagnetic as well as nonferromagnetic wear particles, present in lubrication or hydraulic oils, are utilized to detect deterioration of bearings and gearboxes. Wear particles herein are analyzed with regards to particle size, type,

SHM method	Advantages	Disadvantages	Online applicability
Acoustic emission measurements [LLWY09] [TSC15] [SCBH13] [SVLP+13] [GGV+11] [AGM06] [TC99]	- Continuous monitoring during system loading - High-sensitivity - No need for additional excitation source	- High requirements on measurement chain - Damage localization still not possible - No physical relation between acoustic emission and correlated damage - As often applied in noisy operating environments, the discrimination of AE signal difficult due to signal weakness	Yes
Structural monitoring using guided waves - Lamb waves [HSW15] [HSL+15] [MKM+15] [LSLS05]	- High signal attenuation in high-frequency range - Damage localization	- Active nondestructive technique - Coupling between transducers and inspecting surface - Laser based lamb waves generation and sensing as noncontact solution	Yes
Ultrasound measurements [YNB+14] [PAS14] [SDY+11] [CHB15] [SCR+12]	- Detection of extremely small anomalies in material - Imaging of the size, shape, and orientation of anomalies - Damage localization - High potential of noncontact optical and sound excitation sources	- Additional excitation source necessary, inspected surface have to be accessible for the transducer - Time-consuming technique	Yes
Strain measurements [YGS13] [Pie14] [CLB08] [KSH12] [SCBH13] [SSW+15]	- Possible in-situ structural continuous monitoring - Tremendous potential of optical sensors - Embedding in composite structures - Suitable for component lifetime prediction	- The knowledge about component hot spots in advance necessary - Necessity for a huge number of sensors due to the fact that one sensor measures strain only at one point	Yes
Vibration measurements [MMR06] [SL14] [FQ11] [GP15] [DCA+14]	- Nondestructive technique - Indication of both the location and the severity of damage	- Difficult distinction of vibration signatures originating from normal usage and changes resulting from damage occurrence - Unsatisfactory results in detection of failures in gearboxes/bearings in early initiation phase	No
Eddy current thermography [LMIC14] [KHK13] [HTPC14a]	- High accuracy of internal damage detection - High accuracy of damage localization - Detection of the defect depth	- Time-consuming processing - In its original form, not applicable as in-service inspection method - Advances recently introduced show potential for in-situ application, but further research still necessary	No

Table 2.3: Structural health monitoring techniques applicable to wind turbine system components I [BS16]

SHM method	Advantages	Disadvantages	Online applicability
Thermographic measurements [YS13] [PHK+10] [CT12]	- Useful in fatigue testing - Simplicity of application - Short inspection interval (time consumption relatively low)	- High sensitivity to temperature variations - Limited application to in-situ WT systems - Requirement on external excitation source in active thermal imaging method	No
Radioscopy/ Radiography testing [PCMC15] [PGH+15] [HFU08] [HNS+15]	- Detection of internal damages - Mostly used in blade production quality testing - High accuracy concerning damage localization	- Requirement on X-ray source and X-ray detector - Long exposure time - Not applicable to continuous in-service monitoring	No
Visual inspection [KKJ+13]	- Used as supplement to other monitoring techniques - Possibility to detect external damages such as cracks and scratches	- Accuracy low - Rarely used standalone - High computational requirements for image processing	Yes
Oil analysis [GMPP12] [HMS+06] [MPBS15]	- Applicable as online and offline SHM - Direct determination of health state	- High cost technique - Mainly applicable offline due to high costs of online implementation - Online implementation sets requirements on closed oil system of bearings or gearboxes	Yes
Shock pulse method [YKZ+14] [ZZYX08] [TYR07] [MPBS15]	- Low cost technique - Accurate detection as well as localization of failure occurrence in bearings and gearboxes - Often used combined with vibration technique	- Low sensitivity to loading profile change - Not useful in terms of fatigue analysis	No

Table 2.4: Structural health monitoring techniques applicable to wind turbine system components II [BS16]

and particle number along with oil temperature, targeting not only to detect the damage but also to examine deterioration criticality [HMS+06]. Main advantage of oil analysis, according to Marquez et al. [GMPP12], is the possibility for direct determination of deterioration states. As oil analysis requires relatively expensive equipment such as spectrometers, analyzers, or scanning electron microscopes, the method itself is considered as relatively expensive and time consuming [MPBS15]. Hence, oil analysis is mainly applied offline as a result of high cost of in-situ application and the requirement for closed oil system to enable in-situ oil analysis.

2.2.1.11 Shock pulse method

Shock pulse method (SPM) is recognized as a method suitable for bearings and gearboxes monitoring. Mechanical contact between bearing ball and damaged area or between bearing balls placed next to each other generates high-frequency shock vibration pulse waves whose signal signatures are used for analysis. As that, the damage detection, severity estimation, as well as damage localization in bearings along with gathering an information about thickness of lubrication oil is performed using SPM [YKZ+14]. Shock pulse sensors used to capture generated waves are mounted on the bearing housing.

Possible approach towards damage detection and damage criticality estimation based on SPM is the calculation of shock pulse normalized single value. Shock pulse normalized single value is afterwards directly correlated to the health state of bearings. By utilization of shock pulse normalized single value in analysis, an application of conventional spectral analysis methods is avoided [YKZ+14]. Even conventional spectral analysis methods are avoided in this case, the direct signal demodulation entailed within normalized shock pulse value calculation can lead to incorrect estimation of normalized shock pulse single value [ZZYX08]. In accordance with this, Zhen et al. [ZZYX08] introduce signal preprocessing using "wavelet transform based on lifting scheme" taking in consideration normalization factors.

Moreover, Yang et al. [YKZ+14] propose frequency spectrum analysis of shock pulse wave to detect as well as localize damage. Similarly, stator current, vibration, and acoustic emission measurements are compared with SPM in [TYR07]. With respect to obtained parameters change due to damage propagation, AE peak amplitude and shock pulse value are reported as parameters with the largest increase. Accordingly, the authors [TYR07] state acoustic emission as the most accurate method whereas SPM is placed directly after AE with respect to accuracy of damage detection.

2.2.2 Signal processing techniques

Unequivocal correlation of signal signatures contained in measured signal to occurred faults or failure typically requires signal transformation in appropriate form as well as appropriate signal preprocessing, such as cleansing, denoising, removing out-of-range or impossible values, etc. Signal processing methods applied to measured signals targeting to extract signal signatures capable to reveal anomalies in the system are divided in time-, frequency-, and time-frequency-domain based methods.

2.2.2.1 Time- and frequency-domain analysis

Time-domain-based signal analysis belongs to signal analysis in its original form. Signal transformation is not carried out but only appropriate preprocessing of measured signal. Signal processing in time domain is discussed in terms of statistical

	Acoustic emission	Guided waves	Ultrasound measurements	Strain measurements	Vibration analysis	Eddy current testing	Thermography	Radiography	Visual inspection	Oil analysis	Shock pulse method
Low complexity					x	x	x	x	x		x
In-service monitoring possible	x	x	x	x					x	x	
Time consuming	x	x	x			x		x			
High costs		x	x	x						*x	

* high costs belong to a high cost of an equipment: spectrometers, analyzers, SEM

Table 2.5: Overview of monitoring techniques [BS16]

as well as modal analysis. Statistical signal signatures to be calculated, such as mean value, root mean square value, standard deviation, kurtosis, skewness, and crest factor, are well known and are in a number of contributions [SL14] [LHZ09a] [XXS+09] defined as

$$s_1 = \sum_{i=1}^{n} \frac{x_i}{n},$$

$$s_2 = \sqrt{\frac{\sum_{i=1}^{n} {x_i}^2}{n}},$$

$$s_3 = \sqrt{\frac{n \cdot \sum_{i=1}^{n} {x_i}^2 - (\sum_{i=1}^{n} x_i)^2}{n \cdot (n-1)}},$$

$$s_4 = \frac{n}{(n-1)(n-2)} \sum_{i=1}^{n} \left(\frac{x_i - s_1}{s_2}\right)^3,$$

$$s_5 = \frac{n \cdot (n+1)}{(n-1)(n-2)(n-3)} \sum_{i=1}^{n} \left(\frac{x_i - s_1}{s_2}\right)^4 - \frac{3 \cdot (n-1)^2}{(n-2)(n-3)},$$

$$s_6 = \frac{max(x)}{s_2},$$

$$s_7 = \frac{max|x|}{(\frac{1}{n} \sum_{i=1}^{n} |x_i|^{1/2})^2}.$$

Time-domain signal analysis in terms of modal analysis includes the calculation of specific signal features such as peak amplitude, arrival time, count, duration, etc [GGV+11]. Although time-domain-based signal analysis methods worth for one of the simpler methods, difficulties in application are noticeable in the selection of time-domain variables suitable for detection of particular fault or failure.

Transformation of signal in frequency-domain using Fast Fourier Transform (FFT)

reveals information about the frequency spectrum contained in signal. Signal transformation using FFT reveals the frequency spectrum of the signal, but the time scale of signal becomes unknown; information about the instant at which particular frequency appears is lost. Fast Fourier Transform is thus unsuitable for analysis of non-stationary signals.

2.2.2.2 Time-frequency-domain analysis

Conversely to frequency-domain analysis where frequency spectrum of signal is revealed but not also the timespan in which particular frequency appear, time-frequency-domain analysis considers transformation of signal in frequency domain without loosing an information about the timespan in which referred frequencies appear. For those purposes, signal processing methods like Short Time Fourier Transform (STFT), Continuous Wavelet Transform (CWT), Discrete Wavelet Transform (DWT), Wigner-Ville Distribution (WVD), and similar are applied.

2.2.2.2.1 Short Time Fourier and Discrete/Continuous Wavelet Transform

Short Time Fourier Transform uses a window-dependent time-frequency content of signal where time and frequency resolutions are causally dependent; better frequency resolution means at the same time poor time resolution, and vice versa. Concerning aforementioned shortcoming of STFT, CWT and DWT are developed targeting to overcome the problem of dependency between time and frequency resolutions by using multiple scaled and shifted window function, so-called mother wavelet. Shifting and multiple scaling of mother wavelet provide adjustable time-frequency resolution contrary to STFT whereas one constant, neither scaled nor shifted window function, is used. Due to adjustable time-frequency resolution CWT and DWT are suitable for an analysis of non-stationary signals what is not the case with STFT. An example of CWT application in fault and failure detection and classification is found in vibration signal analysis from bearings and gearboxes [SWZ+10] [ZAB+16] [RRT10]. As outlined in [SWZ+10], aggravating circumstances in fault and failure detection based on vibration signal in inceptive phase are: i) overwhelming of vibration signal by noise as well as ii) superposition of vibration signals on signals originating from other sources. Concerning this, the authors of [SWZ+10] propose utilization of advanced filtering technique, so-called Morlet wavelet-based filtering, for noise removal and transient events detection. According to [SWZ+10], good results are obtained with respect to both aforementioned goals. Moreover, not exclusively CWT coefficients can be used for fault and failure detection/classification but also its variance [ZAB+16]. For instance, Ziaja et al. [ZAB+16] discuss wavelet-based variance analysis in terms of signal self-similarity determination and utilization

of machine learning algorithms within neural networks targeting to detect anomalies in vibration signals. Introduced tests include simulated data, data originating from laboratory test rig, as well as industrial data from WT system. Judging on the reported results, aforementioned approach for bearing fault detection is shown as a successful. Hence, statistical variables such as "standard deviation, kurtosis, variance, and fourth central moment of CWT coefficients of synchronized vibration signals" [RRT10] captured from two different test rigs are applicable in fault detection of bearings and gearboxes. The following can be given as a conclusion of [RRT10]: i) fourth central moment of CWT coefficients of synchronized vibration signals is identified as a feature capable to reveal anomalies in both bearings and gearboxes vibrational signals, ii) standard deviation and variance of synchronized vibration signals are the features better suitable for anomalies detection in bearings than in gearboxes, and iii) kurtosis of synchronized vibration signals is feature suitable for anomalies detection of gearboxes.

2.2.2.2.2 Wigner-Ville Distribution

Conversely to STFT, CWT, and DWT, Wigner-Ville Distribution (WVD) belongs to a bilinear time-frequency signal transformation whereas utilization of window function in its original form is avoided. As such, WVD represents the signal energy distribution in the time-frequency-domain obtained by FFT calculation of signal's ambiguity function - auto-correlation function. If a signal is composed of more than one signal component, an application of WVD is aggravated as the sum of WVDs of individual signal components differs from WVD of overall signal. Due to this fact, cross terms originating from quadratic form of WVD cannot be neglected [PSS99]. From other point of view, existence of cross terms limits an application of WVD in real application. Therefore, some modifications of WVD are introduced targeting to overcome cross terms such as Pseudo-Wigner-Ville-Distribution (PWVD), Affine-Distribution (AD), Cohen-Distribution (CD), and others. For instance, AD considers scaling and shifting of WVD achieved by adding a kernel function in WVD term whereas behavior similar to these of CWT is exhibited [PSS99].

2.2.2.2.3 Empirical Mode Decomposition

Empirical Mode Decomposition (EMD) is a self-adaptive technique applicable to non-stationary signals which decomposes a signal into empirical modes. Spline interpolation is used for signal decomposition in Intrinsic Mode Functions (IMFs), whereas each empirical mode relates to an oscillation mode present in a signal. Intrinsic mode functions are defined as functions with zero mean value, the same number of zero-crossings, and the same number of maximum values or number of maximum values differing by one. Within IMFs, signals are represented as a linear superposition of IMFs. This technique is especially applicable to signals overwhelmed by noise; shows good results with respect to noise removal. Contrary, EMD

Method	Application	Characteristics
Statistical analysis/ Modal analysis	- WT rotor blades (AE/ultrasound waveform) - Bearings/gearboxes/drive train (along with FFT or similar method)	- Analysis of signal in time-domain - Simplicity of application - Rarely applied standalone but rather in combination with some other method such as FFT
FFT	- WT rotor blades - Bearings/gearboxes/drive train - Nacelle - Generator	- Reveals frequency spectrum of signal - Lack of an information about the time - Not suitable for an analysis of non-stationary signals
STFT	- WT rotor blades - Bearings/gearboxes/drive train - Nacelle - Generator	- Reveals window-dependent time-frequency content of signal - Fixed time-frequency resolution due to fixed window function obtained - Information about the time is preserved - Suitable for an analysis of non-stationary signals
CWT/ DWT	- WT rotor blades - Bearings/gearboxes/drive train - Nacelle - Generator	- Reveals window-dependent time-frequency content of signal using wavelet functions - Conversely to STFT, time-frequency resolution adaptable through a number of CWT scales or DWT levels - Suitable for an analysis of non-stationary signals - Commonly used signal processing methods
WVD	- WT rotor blades - Bearings/gearboxes/drive train - Nacelle	- Reveals time-frequency content of signal which is not window dependent - Computes FFT of auto correlation function of signal - Introduces cross terms in case of signal consisting of two or more signal components (aggravated application) - High computational requirements - Suitable for an analysis of non-stationary signals
EMD	- WT rotor blades - Bearings/gearboxes/drive train - Nacelle	- Self-adaptive technique for decomposition of non-stationary signals - Signal decomposed in so-called empirical modes - Especially useful for signal noise removal - High computational requirements
HHT	- WT rotor blades - Bearings/gearboxes/drive train - Nacelle	- Adaptive technique providing better time-frequency resolution in comparison with CWT - Requires signal decomposition in empirical modes - Suitable for an analysis of non-stationary signals - High computational requirements

Table 2.6: Signal processing methods [BS16]

gives poor results with respect to fault detection if applied in its original form as empirical modes are often overlapped [DZ14]. Some improvements introduced in EMD aim to overcome the problem of overlapping empirical modes. These improvements are introduced in bivariate EMD, orthogonal EMD, or ensemble EMD implementation [LLHZ13] [LHZ09b]. Ensemble EMD as such uses uniformly distributed white noise superposed to a signal which is afterwards decomposed in IMFs. White noise superposed to a signal and providing uniform distribution of signal scales is reflected also in output signal, but it can be removed by ensemble mean calculation [LHZ09b]. Targeting to mitigate an effect of superposed noise to the signal, Jiang et al. [JLL13] utilize EEMD with multiwavelet packet. Two or even more wavelet functions are introduced and used for signal prefiltering. Weak signal signatures are in turn revealed and provide better accuracy in fault detection in comparison with EEMD. Application of such approach is shown on an example of vibration signal of rotating machinery [JLL13]. Furthermore, EMD is used in Hilbert-Huang Transform (HHT).

2.2.2.2.4 Hilbert-Huang Transform

Hilbert-Huang Transform is characterized with an adaptive time-frequency resolution [QTW03]. The calculation of HHT is roughly divided in two parts: i) firstly, EMD is applied to decompose a signal in IMFs, and ii) afterwards, Hilbert transform is applied to each particular IMF revealing thereby the frequency and amplitude spectrum of IMFs. Change in HHT amplitude and/or frequency spectrum is an indication of fault occurrence but can also be used for damage severity and damage quantification determination [EBT12].

From mentioned signal processing methods (Table 2.6), "it can be concluded that not any signal processing method is applicable to any signal. The analysis of signals characterized by transient events, non-stationary signals, as well as signals covered by noise are basically analyzed in time-frequency-domain as transient events and non-stationary signatures are hardly revealed in time-domain. Analysis of signals covered by noise requires the application of filtering techniques to consider the useful parts of the signal. Signal processing methods to be applied are closely related to the sensing technique. The nature of the measured signal has to be taken in consideration to realize efficient and accurate failure detection and diagnosis" [BS16].

2.3 Remaining useful lifetime prognostics of wind turbine components

Beside the requirement for trade off between efficient energy production and fail-safe operation of wind turbine systems, an achievement of as long as possible service lifetime or at least predefined service lifetime plays an equally important role. As shortly introduced in Chapter 1, by adapting the control strategy targeting to take

in consideration the knowledge about current State-of-Health of the system, either predefined or extended system's lifetime can be attained. The estimation and continuous monitoring of current State-of-Health (in appropriate form) is thus prerequisite for an achievement of predefined or extended system's lifetime. For these purposes, remaining useful lifetime estimation is discussed in detail in this chapter.

2.3.1 Remaining useful lifetime determination

Remaining useful lifetime prediction and reliability estimation becomes mandatory in technical systems in the 21th century, as such also in wind turbine systems. Instead of the term *remaining useful lifetime*, some additional terms are used in some technical fields to express the aging of system (for instance: fatigue life, crack growth or crack propagation rate, corrosion rate, wear rate, and similar), but they all refer to the same phenomena [BS15a] [XWWH15]. According to existing literature up to 2015, the approaches used for remaining lifetime estimation are roughly grouped in model-based, data-based, and physics-based approaches. Nevertheless, some authors extend this classification so as the approaches are grouped in: i) physics-based, ii) data-based, iii) experimental-based, and iv) combined data-based and physics-based approaches [AL14].

According to Ahmadzadeh et al. [AL14], physics-based approaches require accurate theoretical models whereas the correlation between input signal (excitation) and output signal (response to an excitation) is known. As the physical relations lies behind the model, changes in the feature values obtained from such models reflect the changes of model parameters. These changes can be correlated to a physical phenomena like wear, corrosion, crack growth, or similar. Some limitations of the physics-based approach is a requirement for physical model development which is not always easy to establish. Consequently, this limits model applicability exclusively to a particular component for which the model is made. Along with mathematical description of degradation phenomena, cumulative damage models as well as hazard rate models belong to this group.

Data-based models rely on the data captured from the structural health monitoring system and represent basically the trend of degradation [AL14]. Unlike physics-based models, the models arising out from data-based approaches do not require the knowledge about the physics of degradation phenomena but also do not have physical representation. As the approach rely in fact on the data captured through SHM system, RUL prediction is highly dependent on quality and quantity of data, as well as on the presence of noise in data. For instance, the models that belong to this group are Artificial Neural Network (ANN) models, Hidden Markov Models (HMMs), Hazard Rate Models (HRMs), as well as Proportional Hazard Rate Models (PHRMs).

Experimental-based approaches (also stated as experience-based approaches in [AL14]) use stochastic as well as probabilistic models to examine degradation present in the system. Prerequisites for an establishment of such models are the data captured during experiments and the knowledge gained by experience [AL14]. Such an approach is necessary especially for some prototype products whereas the relations between load and some additional system variables are not known but are of high importance. As an example may be mentioned the model developed by Sutrisno et al [SOVP12], whereas experimental data sets from the number of bearings are used to train and evaluate three prognostic algorithms; namely "Moving Average Spectral Kurtosis and Bayesian Monte Carlo", "Soft Computing Model with Support Vector Regressors", and "Vibration Frequency Signature Anomaly Detection and Survival Time Ratio" [SOVP12]. The authors have reported satisfying results in RUL prediction despite a presence of uncertainties.

Combination of different approaches may contribute to overcoming the shortcomings of individual groups and therefore are supposed to gain better results according to RUL prediction. As that, this group of approaches is stated as combined data-based and physics-based approaches in [AL14].

Similarly, Chen and Pecht [CP12] group a variety of RUL prediction algorithms in model-based and data-driven algorithms. According to [CP12], data-driven approaches use the data captured through SHM to establish necessary relations and models, while model-based approaches tend to establish mathematical models using experimental or empirical knowledge of the process. Data-driven algorithms according to the authors include statistical as well as probability theory targeting to predict RUL, what is consistent with description given in [AL14]. In addition, Cheng and Pecht [CP09] discuss a Physics of Failure (PoF) approach along with model- and data-based approaches. Physics of failure is understood as an approach which comprises the knowledge about load profile, failure mechanisms, material properties, as well as component geometry. Failure mechanisms are herein discussed in terms of different ways in which the component fails [CP09]. According to this, PoF provides the possibility to calculate the damage growth occurred and propagated under specific conditions, either environmental or operating, as well as to estimate RUL concerning specific failure mechanisms and loading profiles. A priori knowledge about failure mechanisms and their mutual interactions required within PoF makes its application difficult. Thus, standalone application of PoF is rarely used but more often in addition to an another approach. For instance, PoF is used in combination with data-driven approach which is used to detect and identify failure mechanisms in [CP09].

Without losing generality and according to aforementioned reviews [CP09] [SWHZ11] [AL14] [SOVP12] [BRS14], it could be concluded that the authors often resort to combine different approaches targeting to determine RUL. A number of application examples follow in Chapter 2.3.2.

2.3.2 Overview of existing lifetime models

Among initially established analytical damage accumulation lifetime models, it is worth to mention an Arrhenius model [Arr89] [Lai84]. Even established in 1889, the model is widely used in its modified form to describe the effect of temperature on service lifetime of electrical components. Model application is found in nonmechanical systems whereas rate of chemical processes and their dependence on temperature is modeled. Parameter to be optimized concerning Arrhenius model is activation energy reflecting the minimum energy required to contribute to the processes related to failure mechanisms [Arr89]. Shortly after the model is developed, an extension of Arrhenius model is introduced.

An extension of Arrhenius model is done in such a way that the model includes additional input (stress) and two additional model parameters. Such model is known as Eyring model and establishes the relation between voltage/temperature and service lifetime of electrical component. Similarly as Arrhenius model, Eyring model is applicable to the constant amplitude stress [GLE41]. Simoni et al. [SMML93] also introduce the relation between thermal and electrical stress. As a result, the model especially applicable to insulation materials is developed. In addition, cracks in metals are concerned in Coffin-Manson's model [SMML93], whereas the temperature effects are considered in terms of their effect on crack growth. As outlined above, aforementioned models are applicable exclusively in the case of constant amplitude loading.

As the loading is often neither known nor constant, some models concerning time-varying loading profiles are deployed. The Palmgren-Miner model is one of inceptive models which consider time-varying loading profile [Pal24] [Min45]. The Palmgren-Miner model uses S-N relation (nominal stress amplitude versus number of cycles before failure occurrence relation) to describe accumulated damage within material. The model do not take in consideration the stresses (loading profile) under a certain level. These stress levels are thereby not considered as contributors to the damage growth. Aforementioned level under which the damage growth is neglected is known as endurance limit. Therefore, system loading with amplitudes found under the endurance limit provide theoretically infinite lifetime. According to the Palmgren-Miner model, damage increment (d_i) is defined as the ratio of current number of cycles (n_i) and the maximum number of cycles to failure under constant stress (N_i). Accumulated damage (D_k) is consequently defined as a sum of damage increments [Pal24] [Min45]. The analytical expression of the Palmgren-Miner model is given as

$$D_k = \sum_{i=1}^{k} d_i = \sum_{i=1}^{k} \frac{n_i}{N_i}. \tag{2.1}$$

Because of neglected loading profiles under the endurance limit, predefined sequence of loading profiles, as well as linear relationship between loading profiles and accumu-

lated damage, Palmgren-Miner model do not reflect the situation in practice. In addition, the endurance limit does not always exist. Thus, Henry [Hen55], Marco and Starkley [MS45], and Subramanyan and Srivatsavan [Sub76] have introduced some modifications in Palmgren-Miner model intending to include nonlinearities present in practice. Therefore, Henry [Hen55] introduces the change of endurance limit in terms that endurance limit becomes dependent on accumulated damage. Within increased damage, the endurance limit is also increased according to [Hen55]. Marco and Starkley [MS45] introduce nonlinearities into the model by including power rule between current number of cycles and the maximum number of cycles to failure. Submayan and Srivatsavan [Sub76] include variable amplitude loading by representing variable amplitude loading as a set of isodamage lines. Regardless of introduced modifications, aforementioned models are neither capable to consider stochastical nature of damage accumulation nor stochastical aging of materials.

Initial attempts to describe damage accumulation using stochastical hypotheses are seen in works of Parzen [Par59] and Bogdanoff [Bog78a] [Bog78b]. Stochastical hypothesis are closely related to probability theory considering in turn the load and/or damage as a random variable and process. Thus, Parzen [Par59] uses renewal theory (field of probability theory) to describe stochastical damage accumulation process, whilst Bogdanoff consider damage accumulation process as a discrete Markov process [Bog78a] [Bog78b]. Herein, accumulated damage is assigned to an individual load cycle. Hence, Kutt and Bieniek [KB88] study fatigue of metals by applying stress of varying amplitudes. The results obtained from tests are integrated in nonlinear stochastic model of fatigue aging of metals taking in consideration high-to-low and low-to-high changes of stress levels. Such changes in loading profile can also be considered in terms of the change in sequence of stress levels.

Apart from cumulative damage models which consider stress-strain and temperature relations, Liao [Lia14] uses data-driven approach to estimate RUL of bearings. The model established by Liao [Lia14] is based on aging-related features obtained using genetic algorithm. Vibration measurements captured from experimental tests on bearings are analyzed concerning advanced feature recognition techniques, where obtained features are analyzed in terms of their applicability for prognosis. It is shown [Lia14] that not all features extracted from vibration measurements are capable to describe gradual degradation of bearings. Consequently, not all features can be used for prognostics purposes. After the features are selected, the RUL is estimated using Bayesian update method under an assumption of deterioration growth in form of Paris' law. Paris' law is traditionally used for crack growth modeling but is applied with success also in this case. Two shortcomings appeared herein are. i) the estimation of suitable threshold limit as well as ii) physical correlation of discovered features to the failure.

Similarly, Coble et al. [CH09] utilize the genetic algorithms and a number of measured parameters to find out a single parameter, so called prognostic parameter,

to be used within prognostics. According to [CH09], the monotonicity (number of parameter increase/decrease), the prognosability (spread of prognostic value within a group of systems), and the trendability (the same trend for a group of systems) are used as a measure of prognostic parameter suitability. The sum of monotonicity, prognosability, and trendability with assigned weights serve as an objective function to be minimized in genetic algorithm. For purposes of RUL prediction based on aforementioned prognostic parameter, the General Path Model, originally proposed by [LM93] having in its basis linear regression model, is employed.

Data-driven prognosis outlined by Bechhoefer [Bec12] includes Kalman Filter and Extended Kalman Filter for RUL determination of gearboxes. The signatures of vibration measurements from gearboxes are extracted and correlated to current deterioration level. Obtained signatures are considered as input into lifetime model. The model consists of two Kalman filters. The first Kalman filter calculates the velocity of change of deterioration indicator, whilst the second filter (Extended Kalman Filter) is used to estimate crack growth which is modeled by Paris' law. The determination of threshold at which the system becomes nonfunctional is seen as a high challenge and weakness of the model.

Hence, Lall et al. [LZD15] investigate remaining useful lifetime of Light Emitting Diodes (LEDs) encapsulated in package. The luminous flux degradation and color shift are found as the most important contributors to failure occurrence. Moreover, it is shown that the material used for package production has high impact on failure growth. As that, formerly used epoxy is displaced by silicon material, as the epoxy yellow over time reducing thereby luminous flux. At the same time, the color shift distance becomes higher. To determine remaining useful lifetime, an Unscented Kalman Filter (UKF) and the fourth order dynamic transfer function is used. An estimator is established using measurements of luminous flux and color shift distance. Prognosis of future deterioration levels using designed estimator, consequently also RUL defined as the time necessary for a significant color shift, becomes possible.

The model proposed by Lorton et al. [LFG13] involves prognosis of deterioration level of a pneumatic valve. The procedure towards deterioration estimation consists of two successive steps. In the first step, the model includes RUL distribution calculation which is followed by degradation modeling in the second step. The degradation is modeled as Markov process. Special emphasis here is given to an optimization of maintenance actions.

By comparing different stochastical approaches with deterministic approaches, it can be stated that stochastical approaches provide in general better prognostic accuracy but also have higher model complexity and computational requirements in comparison with deterministic approaches. A trade-off between available prognostic models concerning all their strengths, weaknesses, and personal needs is usually conditioned by limitations of particular model, ability to measure or estimate degradation parameters along with capability of their integration into the model, as well as possibilities for model validation.

2.4 A short look to other application fields

The higher the number of wind turbines integrated into wind farm is, the more pronounced is the problem of ensuring the stability of grid. To reduce grid power gradients, an integration of different storage devices to compensate a lack of wind abundance in some periods is proposed as a solution [ZWH+15]. Even more, the aging of storage devices has to be examined to provide optimal WT operation with respect to generated power and aging rate of Lithium-Ion Battery (LIB) [SSST13] [KCA13] [ZZC+13].

2.4.1 Remaining useful lifetime determination of LIB

An integration of LIBs as energy storage devices in WT conversion systems is shown on an example of smart Carbon-Fiber-Reinforced-Polymers (CFRP) in [LNW+15]. Here, LIBs serve as energy storage elements in wind turbine systems, whilst the physical area to be occupied by LIBs is reduced. Inceptive research steps towards embedding of lithium-ion-based energy storage units in CFRP is carried out. The requirement set on embedded LIB-based energy sources is to retain the same electrochemical characteristics in comparison with conventional LIB pouch batteries or cells. Even some shortcomings regarding to fabrication and the design of embedded LIB-based storage units exist, the difference in electrochemical characteristics between embedded LIB-based energy storage units and conventional LIB cells with respect to service lifetime and capacity fade is small [LNW+15]. Taking in consideration aforementioned discussion, experimental tests done on conventional LIBs seems to be applicable also to embedded LIB-based storage devices introduced in [LNW+15].

2.4.1.1 Degradation mechanisms

Over the time, different LIB components such as electrolyte, separator, anode or cathode degrade under the influence of various loading profiles and operating conditions [WFS14]. Lithium-ion battery performance and electrochemical characteristics are as that highly dependent on external operating conditions (environmental: primarily temperature) as well as on internal operating conditions (actual State-of-Health and applied load). Internal and external loads with major impact on the LIB characteristics degradation are: i) the rate of charging and discharging currents over LIB lifetime and ii) the temperature, which induces thermo-mechanical effects in the LIB which are especially pronounced during LIB discharging [WWK+14]. In practice, LIB charge and discharge rate is often expressed through the C-rate. Using this terminology, battery with a nominal capacity of 3 Ah charged with 1C is fully charged in 3 hours, or the same battery charged with 0.5C is fully charged in

6 hours; it gives correlation between charging/discharging currents and the amount of LIB energy charge expressed through ampere-hours.

As a result of applied load in a form of LIB charging and discharging currents, some mechanical and electrochemical phenomena related to LIB degradation become conspicuous. Among these phenomena, the formation of Solid-Electrolyte Interphase (SEI) layer due to lithium-ion intercalation into anode (negative electrode) is stated as the aging mechanism mostly contributing to LIB degradation [PB13]. Those irreversible electrochemical reactions and loss of active materials, in this case intercalated lithium-ions, cause SEI layer growth. Accordingly, lifetime models developed by some authors [PB13] are able to describe SEI formation process quantitatively and to correlate SEI layer growth to LIB lifetime reduction (occurred under the degradation of anode).

The degradation mentioned above can be discussed in terms of capacity fade effect [AF13]. Capacity fade stands for an effect of decreased capability of LIB to store the same amount of energy compared with undamaged nonaged battery [AF13]. Simultaneously with SEI formation, the change of LIB internal resistance becomes conspicuous. Internal resistance of LIB as that increases with higher level of LIB degradation.

Beside SEI layer formation and growth, additional phenomena strongly contributing to LIB degradation is lithium plating/deposition, whereas the lithium dendrites are formed [AF13]. The phenomena is mainly occurred as a result of lithium intercalation under excessive charging due to high C-rates. Additionally, lithium plating can cause short circuits whereas the safety can be endangered taking in consideration the possibility for uncontrolled electrochemical reactions occurrence. Thus, lithium plating leads to the decreased diffusion rate of lithium-ions and ultimately to the End-of-Life.

The dependence of C-rate and LIB degradation is discussed in a number of contributions [WGS+14] [AF13]. According to [WGS+14], increased C-rate contributes to faster LIB degradation. The authors of [WGS+14] state that the LIB degradation occurs due to irreversible loss of active material in LIB leading consequently to LIB capacity fade. These statements are in compliance with previous discussion. The experimental results reported in [WGS+14] cover the testing of five different LIBs cycled under different C-rates. Post-mortem analysis herein is carried out using electron microscopy and X-ray imaging. The results show strong differences in LIBs aging in dependence on LIB C-rate.

As previously emphasized, aging mechanisms of the LIB are influenced not only by charging and discharging currents but also by temperature. Accordingly, different aging phenomena become noticeable in dependence on temperature range in which the LIB operates. As outlined by Waldmann et al. [WWK+14], post-mortem analysis carried out on LIBs with $Li_xNi_{1/3}Mn_{1/3}Co_{1/3}O_2/Li_yMN_2O_4$ cathode and graphite

anode shows different LIB behavior with respect to aging in temperature range bellow 25°C and above 25°C. As that, aging rate above 25°C increases almost linearly with temperature increase, whilst aging rate bellow 25°C decreases with temperature increase (again almost linearly). The same authors state lithium platting as the most pronounced aging mechanisms in temperature range bellow 25°C, while SEI formation takes precedence in temperature range above 25°C. This all proves the dependence of chemical reactions on temperature range in such a manner that the battery usage at higher temperatures is accompanied by faster electrochemical reactions accelerating thereby aging processes. Hence, the Depth-of-Discharge (DoD) as well as battery overcharging and undercharging also accelerate the LIB degradation.

An aging of LIB, even the LIB is not in use (not charged or discharged) but only stocked, is known in literature as calender aging. Targeting to understand calender aging phenomena, Eddahech et al. [EBV14] have examined the LIBs State-of-Health indicators related to calender aging. The tests are carried out on four different types of LIB differing in active material in cathode which have been stored under three different temperatures and three different states of charge: 30, 45, 60°C, and SoC of 30%, 65%, and 100%. By periodical Constant Current-Constant Voltage (CC-CV) charging and discharging of LIB with appropriate rest times after each particular charging or discharging cycle along with periodical check up of the battery State-of-Health (SoH) using Electrochemical Impedance Spectroscopy (EIS), the dependence between State-of-Charge (SoC) and the temperature, at which the LIB is stored, is revealed. As that, accelerated aging is manifested with either temperature or SoC increase.

Similarly, Stiaszny et al. [SZK+14] have performed different calender aging tests on two types of LIBs stored at temperature of 60°C and different SoCs (storage voltage of 4.0 and 4.2 V). The in-depth post-mortem analysis using EIS as well as physical/analytical analysis is carried out targeting to distinguish capacity fade occurred due to SEI layer formation/growth (loss of active material) and due to internal resistance increase. According to [SZK+14], the decrease of storage voltage of only 200 mV (4.0 V instead of 4.2 V) contributes to better results with respect to the LIB lifetime compared with the lifetime of LIB stored at lower voltage. The battery stored at 4.0 V shows decreased capacity fade rate and decreased rate of internal resistance as well as ohmic resistance growth, whilst the same effect is not noticeable in the LIB stored at 4.2 V.

2.4.1.2 Degradation indicators

As a measure of the LIB degradation level, different parameters such as SoH, State-of-Function (SoF), Degradation Index (DI), or RUL may be employed. The State-of-Health of LIB calculated based on capacity fade tracking is defined by a number

of authors [NMCH09] [MR05] as

$$\begin{aligned} SoH &= \frac{Q_{cmax}}{Q_n} \cdot 100\% \text{ or} \\ SoH &= \frac{C_{actual} - C_{threshold}}{C_{nonaged} - C_{threshold}}, \end{aligned} \tag{2.2}$$

where Q_{cmax}, Q_n, C_{actual}, $C_{threshold}$, and $C_{nonaged}$ denote current maximum LIB capacity, nominal LIB capacity, current LIB capacity, capacity of aged LIB (most often 80% of nominal capacity), and capacity of nonaged LIB, respectively. If the same parameter is calculated based on tracking of internal resistance increase, an analytical expression for SoH calculation is

$$SoH = 1 + \frac{R_{ref} - R_{actual}}{R_{ref}}, \tag{2.3}$$

where R_{ref} denotes internal resistance of nonaged battery and R_{actual} actual resistance estimated during operation time [RBSGD13]. Remaining useful or consumed lifetime estimation implies an analysis of life cycles of LIB, where the life cycle of LIB relates to the number of full charging/discharging cycles (if applicable using certain test setup) or threshold-crossings of LIB currents. In case of LIBs embedded in WT system, the life cycle definition based on counts of full charging/discharging cycles is not applicable as the loading profile required for smoothing of power delivered to the grid is neither identical at each point in time nor easy foreseeable. As a result, full charged or discharged state of LIB in this case is rarely occurred. State-of-Function describes not only the degradation level of LIB but also certain functionality parameters in a similar manner as SoH. By comprising SoC, SoH, T, and the history of charging/discharging loading, SoF describes LIB aging resulting from different aging effects (capacity fade, internal resistance increase, and similar) and gives the possibility for detailed tracking of LIB performance (for instance: LIB storage capability) [MR05].

Precise prediction of LIB remaining useful lifetime or similar indicator capable to describe current level of LIB aging (SoH, SoF, DI) is important not only for manufacture industry but also for end-users. The importance of degradation parameter prediction for manufacture industry is reflected primarily in the possibility to extend LIB lifetime, for which the prediction of degradation level is an inceptive step. Additionally, prediction of degradation level is important for end-users as the maintenance actions can be scheduled or postponed, avoiding simultaneously unnecessary expenses and efforts. In addition, premature failures can be avoided.

2.4.2 Overview of approaches for LIB lifetime modeling

In accordance with the discussion in Chapter 2.4.1.1, not directly measurable LIB parameters, namely actual capacity fade and internal resistance, are indicators of

LIB aging. Hence, the estimation of these immeasurable parameters is crucial for LIB degradation prediction. Different approaches towards degradation indicators estimation are developed through the years. Observed in general framework, the developed approaches imply the use of measurable system inputs to estimate immeasurable system outputs. Measurable system inputs highly affecting LIB aging process to be considered within LIB degradation parameters estimation are charging/discharging currents, terminal voltage, and temperature. Concerning aforementioned system inputs depicted in Figure 2.1 on the left side, any parameter shown on the right side can be treated as an output and act as indicator of LIB degradation: SoH, RUL, DI, or SoF. Accordingly, often used approaches towards degradation variable estimation are depicted in Figure 2.2 and detailed in this chapter.

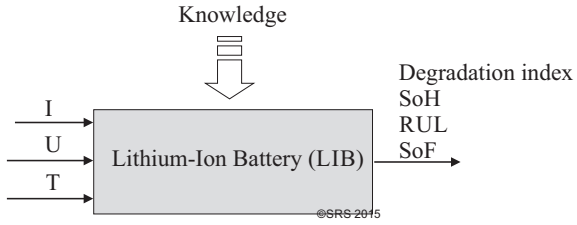

Figure 2.1: Damage indicators of LIB [BMS15]

Some of the developed approaches include the analysis of SoC-OCV (State-of-Charge - Open Circuit Voltage) curve to reveal aging level of LIB. In accordance with this, the relation between SoC and OCV in analytical form, as a look-up table, or similar is required. Therefore, the modeling of OCV as a function of SoC plays an important role in SoC estimation and subsequent SoH estimation.

An example of SoH estimation based on monitoring of changes in SoC-OCV curve is introduced in [WSP13] and [WSP14]. The main issue pointed out by Weng et al. [WSP13] is modeling of SoC-OCV curve and the calculation of so-called incremental capacity. As Incremental Capacity Analysis (ICA) considers the first derivation of charged capacity with respect to terminal voltage, accurate estimation of charged capacity as well as precise measurements of terminal voltage is necessary. Hence, terminal voltage after appropriate rest/relaxation time becomes equal to OCV. Different models proposed in [WSP13] are compared with respect to their complexity, effectiveness in SoH estimation, and sensitivity to measurement noise. Parametric models developed in [WSP13] are used along with Extended Kalman Filter (EKF) to estimate SoC. By differentiation of analytical SoC-OCV curve with respect to SoC, incremental capacity peaks become noticeable, each of them corresponding to a particular SoH. Similar models are introduced also in [WSP14] including the improvements related to the development of more efficient algorithms for model optimization, SoC estimation, and correlation of model parameters to LIB deterioration level. As depicted in Figure 2.2, measurements of LIB currents, temperature,

and terminal voltage measurements under the low charging rates are herein considered as inputs in the system, whereas SoC shows high dependency on temperature. Extended Kalman Filter is used to estimate SoC and subsequently ICA is used to estimate SoH. Moreover, identical OCV model is utilized in SoH estimation in combination with support vector regression in [WCP13]. Further, ICA associated with different charging/discharging rates is applied in [DL09] to identify relationship between OCV, SoC, and SoH of $LiFePO_4$ batteries. Herein, dynamic stress tests are carried out along with periodical reference performance tests targeting to detect drop in LIB rated capacity and changes in "peak power capability" [DL09]. Contrary to [WSP13], the peaks in incremental capacity curve are correlated not only to SoH but also to electrochemical processes occurred in LIB. Moreover, the dependence of incremental peaks on charging/discharging rate is inferred [DL09].

Similarly, Roscher et al. [RAB10] analyze the relation between changes in SoC-OCV curve and SoH. Electrochemical characteristics of LIB are modeled using electric-equivalent model consisting of ohmic resistance in series with a branch of parallel connected ohmic resistance and capacitor, and voltage source (serving as OCV). To estimate SoH, the authors compare OCV value calculated using LIB model and OCV value acquired through terminal voltage measurements. Relationship between SoC and OCV is modeled using polynomial functions and contains measured temperature as additional parameter ψ in the equation. As outlined in [RAB10], the higher the difference between OCV values is, the more aged the LIB is. Presented results with respect to a particular cell type are satisfying, but there are still unresolved issues related to not considered calender aging effects and the inability of model application to a variety of cell types due to unadjusted model parameters. Recently, more attention is attracted to the development of varying equivalent electric circuit models and model parameter optimization algorithms [HLP12].

Serrao et al. [SCGR05] carried out experimental LIB testing targeting to find the dependency of OCV/internal resistance on SoC and T as the RUL/SoH can be determined based on these parameters. The data gathered during experiments are used along with Thevenin model for RUL/SoH estimation enabling thereby the establishment of relations between OCV, SoC, DoD, temperature, and internal resistance, whereas OCV and internal resistance are represented as functions of SoC and temperature. State-of-Health according to [SCGR05] can be estimated using internal resistance values at certain values of SoC and T. After these relations are established, aging model is shown as damage accumulation rule. Main problem faced in such approach is the definition of individual life cycle. In [SCGR05], life cycle is defined as time period between two zero-crossings of the current. This means, with each full discharge of LIB an amount of lifetime is irreversibly lost. As the load applied to LIB is not always the same, life cycles are not identical. To overcome this problem, an observation of life cycles in terms of equivalent life cycle rather than individual life cycles facilitates the analysis. Moreover, consumed lifetime is expressed as the product of a number of life cycles at particular DoD and the nominal capacity.

Preliminary results according to authors give satisfying results according to RUL estimation, analogously also according to consumed lifetime of LIB.

Coulomb counting method in its original form considers SoC estimation by using the integration of measured charging/discharging currents. The losses resulting from inaccurate current measurements and self-discharging currents are here neglected. Therefore, Ng et al. [NMCH09] apply improvements in traditional coulomb counting method by recalibration of SoC at the moment of fully charged and fully discharged LIB using so-called operation efficiency parameter. Operation efficiency parameter is defined as the ratio of charge flowed into LIB during charging period and the charge flowed out of LIB during discharging period [NMCH09]. Taking into account mutual dependencies between SoC, SoH, and DoD, estimation of SoH based on SoC and operation efficiency monitoring is shown as adequate method for SoH estimation according to [NMCH09].

Conversely to LIB degradation model deployment based on tracking the changes in SoC-OCV curve, Remmlinger et al. [RBM+11] examine internal resistance increase by calculating the degradation index. Equivalent circuit model used for these purposes consists of time-varying model parameters changing with temperature, SoC, as well as SoH. As such, model parameters are correlated to LIB degradation and identified using linear least-square algorithm, terminal voltage, and current measurements, as depicted in Figure 2.2. The impact of temperature changes on internal resistance increase is not neglected but is carried out using the measurements of external temperature at specific temperature values. According to authors [RBM+11], the model for DI estimation presented in [RBM+11] has low complexity, gives satisfying results regarding DI estimation, but further improvements in the temperature measurements are necessary; the measurements of external temperature measurements has to be replaced by inner cell temperature measurements. Similar LIB model is used in [RBSGD13] whereas SoH is treated as an unknown parameter and represented as a function of internal resistance. The parameter is identified using nonlinear Kalman Filter, namely Central Difference Kalman Filter (CDKF), and current and temperature measurements.

Data-driven method for online SoH estimation based on Dynamic Bayesian Networks (DBNs) is stated in [HGM+14]. As noted in [HGM+14] and depicted in Figure 2.2, such a model requires terminal voltage measurements from LIB aging experiments for training. Proposed DBNs consider SoCs as hidden states and terminal voltage as observed state. Collected data sets are divided in K classes, each of them corresponding to a particular SoH state. Accordingly, K DBNs are trained and used for real-time SoH estimation. In accordance with the results presented in [HGM+14], introduced model enables real-time SoH estimation but requires the data sets from aging experiments. The more data sets are available, the larger is the number of DBNs. As pointed out by authors, also current as well as temperature measurements can be considered as observed states in DBNs, but it is not applied in [HGM+14].

An achievement of trade-off between battery aging rate and energy costs is extremely important in the field of HEVs, as outlined by Moura et al. [MSF13] and Moura et al. [MFB+11]. Even the optimization of power flow in HEV in both aforementioned contributions has gained more attention in comparison with the modeling of LIB aging processes, developed LIB aging models and their utilization into the power flow optimization concept are of high relevance. The State-of-Health estimation in terms of SEI layer formation/growth as well as consequent internal resistance increase is considered in [MSF13]. By integrating electrochemical SEI layer formation/growth models in Markov chain with absorbing states model, SoH estimation of battery pack becomes possible. Electrochemical model proposed here tends to explain diffusion and intercalation of lithium-ions at the SEI layer by using mathematical expressions for intercalation currents. As depicted in Figure 2.2, input variables to this model are current, voltage, and temperature, whereas increase of internal resistance is used to calculate SoH. Similar approach is applied in [MFB+11].

Furthermore, monitoring of side-reaction current density along with "the two step Recursive Least Squares version of Retrospective-Cost Subsystem Identification" algorithm is used to estimate SoH in [ZESD13]. Side-reaction current density is indicator of the rate of lithium-ion consumption, which is highly dependent on measured terminal voltage and charging/discharging currents. The rate of lithium-ion consumption is in turn related to LIB capacity fade and consequently to SoH. Electrochemical model of LIB is utilized to model nonlinear LIB intercalation process whereas SEI film growth is represented through additional unknown system. Under the assumption of accurate SoC estimation, the algorithm is proved as effective according to [ZESD13]. Further research is still required to reduce sensitivity to the model errors as well as to the errors in SoC estimation.

Goebel et al. [GSS+08] discuss different prognostic models with respect to accuracy, uncertainty, and complexity. As that, LIB-related data sets are used within linear regression, Gaussian process regression, and particle filter model to predict RUL. As a conclusion, the authors report improvements in prediction accuracy and uncertainty by adaptive models able to learn nonlinear dynamics over service time. According to this, particle filter model has better accuracy but has also higher complexity and computational effort in comparison with two other models.

Remaining useful lifetime estimation of LIB is also illustrated in the work of Raghavan et al. [RF15]. The authors, unlike most of previous RUL models which assume only one failure mechanism contributing to the failure, propose multi-modal framework and particle filter in RUL estimation of LIB. The "Akaike Information Criterion" [RF15] herein provides the possibility to determine number of failure mechanisms, which are afterwards integrated in particle filter model. Depicted results show high congruency between estimated and experimentally obtained remaining useful lifetime.

Meissner et al. in [MR03] discuss SoH in terms of SoF by representing SoF as a function of SoC, SoH, and T. Proposed approach for SoC estimation is the tracking

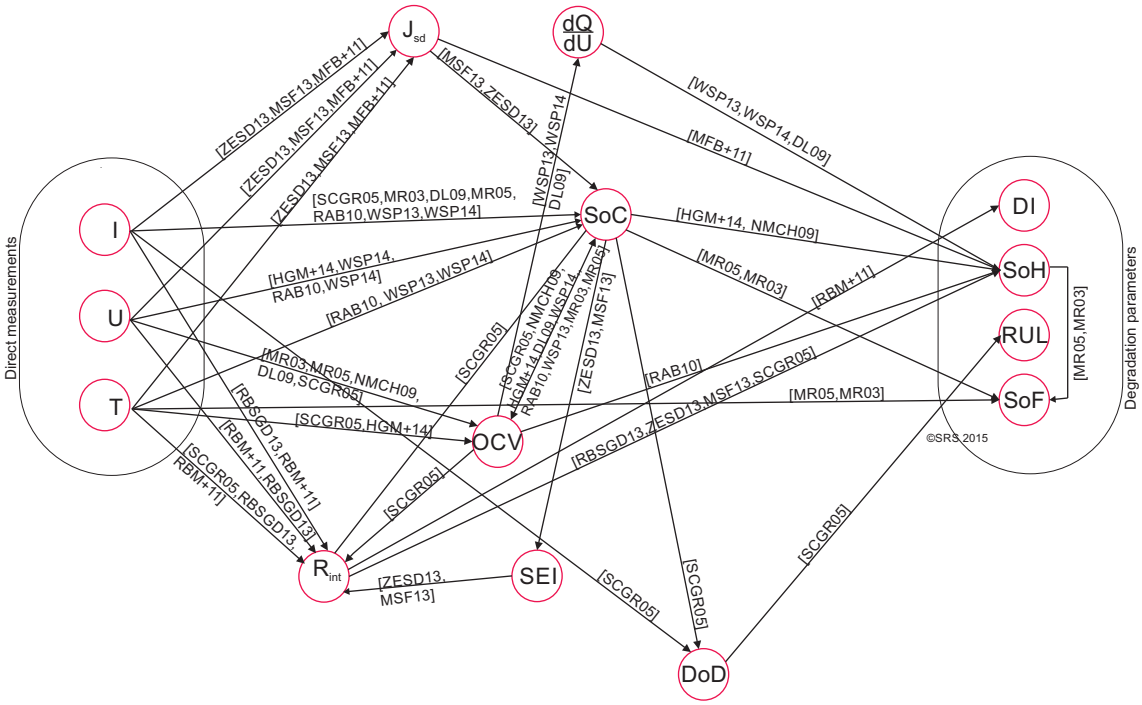

Figure 2.2: Survey on relationships between LIB parameters and degradation characteristics based on available literature up to 2015 (based on [BMS15])

I	Charging/discharging currents	U	Voltage
T	Temperature	OCV	Open Circuit Voltage
Q	Charged capacity	SoC	State-of-Charge
SEI	Solid-Electrolyte Interphase	DoD	Depth-of-Discharge
SoH	State-of-Health	RUL	Remaining Useful Lifetime
SoF	State-of-Function	J_{sd}	Side reaction current density
R_{int}	Internal resistance	DI	Degradation index

of changes in OCV curve. As already emphasized, State-of-Health is capable to describe actual level of degradation but as a standalone parameter reveals a little bit or nothing about the current LIB performance. This belongs to power output capability as well as power flow optimization in case of more than one storage elements in the system with respect to the achievement of efficient LIB functionality and the lowest possible LIB degradation. However, LIB performance tracking is especially necessary in WT systems where charging/discharging of LIB occurs irregularly and under different current rates due to stochastic nature of WT load. Moreover, in these systems the capability of LIB to deliver required amount of power plays an important role. Similar approach is discussed in [MR05] with special emphasis on SoC, SoH, SoF estimation according to known load and operation history.

The relations between measurable parameters of LIB, intermediate parameters aiding immeasurable degradation parameters estimation, and the degradation param-

eters itself are depicted in Figure 2.2. At first glance, the dependence of OCV on SoC and terminal voltage is noticeable, as detailed in the discussion above. Terminal voltage is in some contributions assumed to be equal to OCV under an assumption that the LIB is charged under low current rates or is measured after appropriate rest period. Further, the dependence of SoC on charging/discharging currents, temperature, terminal voltage is evident in Figure 2.2. The calculation or estimation of intermediate parameters related to LIB degradation and degradation parameters itself in most cases, requires either the use of suitable electrical or electrochemical LIB models along with appropriate algorithms for LIB model parameters determination or the utilization of machine learning algorithms. Common to all these approaches is the necessity for accurate current, terminal voltage, and temperature measurements.

Targeting to avoid the need for current, terminal voltage, and temperature measurements, structural health monitoring of the LIB based on Acoustic Emission measurements is examined. The main challenge herein is to elaborate the possibility for direct measurement of LIB degradation level, without necessity for the information about operation variables (such as current, terminal voltage, and temperature). Accordingly, an indirect correlation of operation variables to the degradation level of LIB may be avoided. As a result, inaccuracies in degradation level estimation resulting from inaccuracies present in LIB model or accompanying optimization/identification algorithms may be avoided by measurements of variables which can be directly correlated to LIB degradation.

2.5 Reliability-oriented control strategy of WT systems

The application of reliability-oriented control strategy in terms of service lifetime extension is briefly introduced in Chapter 1. Detailed, and not only a superficial insight at reliability-oriented control strategy including concrete steps towards implementation of the same follows in this chapter.

Recognized challenges within reliability-oriented control strategy implementation can be summarized as: i) continuous monitoring of particular, system specific parameters, ii) correlation of measured data to the State-of-Health which basically requires an establishment of lifetime models, and iii) an integration of lifetime models into control loop. The focus here is given to an implementation of the control loop, whereas the knowledge about State-of-Health is concerned. For these purposes, Safety and Reliability Control Engineering (SRCE) concept, firstly introduced by Rakowsky and Söffker [RS97] [RS96], is elaborated in general terms without emphasizing particular application fields.

2.5.1 Safety and Reliability Control Engineering (SRCE) concept

Main issues to be solved to make SRCE concept implementation possible may be stated as: i) gaining the knowledge about system's reliability in the given moment, and ii) statement about how long will the system be reliable under predefined operating conditions. According to these statements, the maintenance actions can be optimized in terms of their scheduling, minimizing thereby operation and maintenance costs.

Unlike traditional reliability theory introduced for instance by Banjevic [Ban09] (detailed in Chapter 1), reliability in SRCE concept is considered as the parameter highly dependent on applied loads. From the other point of view, applied loads can be influenced by operating conditions. Thus, the relationship between applied loads and their impact on system reliability has to be examined in the initial step of SRCE concept realization. Accordingly, the State-of-Health of system should not only be determined but also continuously monitored and updated. In the case of fault occurrence, the fault has to be evaluated especially with respect to fault criticality and its consequent effect on system's reliability. Moreover, it is supposed to avoid or postpone the failure by integration of continuous State-of-Health monitoring into the system, leading in turn to an achievement of predefined service lifetime and its extension. Herein, remaining useful lifetime is usually considered as a measure of system's reliability.

Important advantage of an awareness about system's reliability is seen especially in the systems where neither immediate maintenance is possible nor repairment or reconfiguration action. Within the SRCE concept, overall system reliability is considered rather than reliability of individual components. Thus, there is usually a need to make conclusions about overall system reliability on the basis of the reliability of individual system components.

Along with gathering the information about system's reliability and under an assumption of known previous and estimated future loading profiles, the prediction of system's reliability is possible. As far as previous loading profiles are known and loading profiles in the future can be estimated, the prediction of system's reliability is carried out using suitable lifetime models. The utilization of lifetime models in prognosis enables the correlation of given loading profiles to system's State-of-Health. Safety and Reliability Control Engineering concept as such unifies three closely related areas depicted in Figure 2.3: continuous structural health monitoring, diagnosis, and prognosis. Accordingly, listed three fields can be clearly differentiated and assigned to an individual units of SRCE concept, defining at the same time their mutual interrelations.

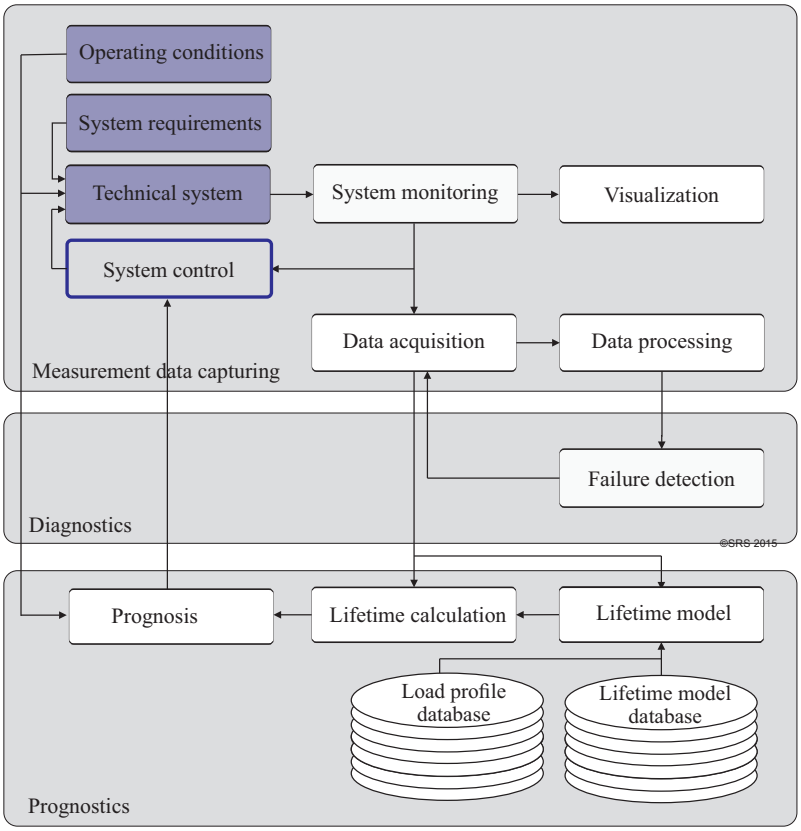

Figure 2.3: Safety and Reliability Control Engineering Concept (based on [RS97], [RS96], and [BS16])

2.5.2 Modular approach towards SRCE implementation

Discussing above mentioned realization tasks in terms of modular interpretation and structured approach, it becomes noticeable that the tasks can be arranged in a number of SRCE units or modules. In this sense, each module has clearly assigned tasks as well as predefined interrelations to other modules. According to [RS97] [RS96], SRCE concept implementation can be organized as three-modular concept.

The information about operating conditions is passed to the first module which includes structural health monitoring (comprising sensing system, accompanying acquisition modules, and signal processing techniques) and the control loop, where additional input into controller module is the information about system's reliability (predicted remaining useful lifetime, consumed lifetime, damage accumulated in the system, and similar).

The second module uses measurements provided by structural health monitoring system, incorporated in the first module, to detect and diagnose the faults. Hence, an information about eventual fault occurrence along with fault criticality estimation

is passed to the third module and utilized in update of remaining useful lifetime estimation.

Lifetime model establishing a relationship between applied loads, operating conditions, and previous health states is entailed in prediction of current State-of-Health. As previously mentioned, degradation variable used in SRCE concept is often remaining useful lifetime. The establishment of relationship between loading profiles, operating conditions, and system deterioration is up to now the most challenging task in realization of SRCE concept, and therefore is discussed in detail through all the subsequent chapters concerning particular systems, materials, and components. For purpose of SRCE concept realization, lifetime model to be used can be chosen from lifetime model database and made adaptive (if necessary).

2.6 Summary and conclusions

The state-of-the-art of research areas related to an implementation of reliability-oriented control strategy is discussed in detail in Chapter 2.5.1. Special emphasis is given to pointing out the main shortcomings as well as still existing challenges in particular fields. Concerning the discussion in this chapter, following research areas are closely related to SRCE concept and its implementation/application:

- structural health monitoring: sensing methods, signal processing techniques, failure detection, and failure criticality estimation,
- establishment of lifetime models and remaining lifetime prediction using established lifetime models, and
- deployment of control strategy capable to integrate system's State-of-Health for purpose of service lifetime extension.

By identification of still existing challenges in SHM, it can be concluded that the improvements of sensing methods as well as signal processing techniques, especially with regards to the reduction of computational complexity and real-time implementation, are still possible. Furthermore, the implementation of real-time signal processing techniques requires not only the examination of hardware capabilities (the development of FPGA-based modules or similar hardware units) but also the development of various algorithms for efficient feature selection and extraction. According to the discussion about lifetime models establishment in this chapter, the approaches proposed for RUL estimation can be grouped in

- model-based approaches including cumulative damage models,
- data-driven approaches including statistical models and the models relied on probability theory, such as regression-based models, Brownian motion (Wiener process), Gamma process, Markovian-based models, filtering-based models, ANN, HMMs, HRMs, PHRMs, and

- physics-based approaches which rely on modeling of physics of failures.

The approaches are discussed in terms of RUL estimation accuracy, model complexity, and assumptions lying behind the model. As that, the approaches which take in consideration probability theory (thereby also stochastic nature of deterioration process) show in general better results concerning RUL prediction accuracy but do not have analytical representation of dependencies between applied loads and deterioration growth. The lack of analytical relationships between applied loads and RUL is noticeable.

The ensuing conclusion is that the implementation of SRCE concept along with the development of appropriate lifetime models, in this case related to WT system components, has to be developed and analyzed. In accordance with this, the goals of the thesis are defined as

- implementation of SRCE concept on an example of wind turbine system, whereas the simulation model of WT is used,
- development of lifetime models using experimental data from tribological system and analytical representation of dependencies between accumulated damage and degradation level, and
- development of lifetime model using experimental data from LIB system.

3 Lifetime modeling and reliability-oriented control strategy on example of WT system

Wind turbine system is subjected to intermittent fluctuating load and is exposed to a harsh environment where not only environmental conditions (temperature, humidity, salinity, icing, and similar) but also complex operating conditions (instantaneously changing and hardly predictable wind speed, wind direction, and wind share) have strong impact on system's performance. Above mentioned impacts lead to ultimate WT failure; herein being understood as a complete loss of system's functionality. These impacts are especially pronounced in offshore WT systems where some additional effects, mainly captured by underwater measurements, have to be considered (for instance: sea currents). The discussion herein is carried out with special emphasize on the effects leading to damage initialization and propagation as well as cost-oriented justification of damage initialization and propagation tracking over entire lifespan of WT.

As may be concluded from Chapter 2, rotating parts of WT systems, in the first line bearings/gearboxes, drivetrain system, and rotor blades are the components with highest susceptibility to structural loads. Taking in consideration an examination of different material characteristics, it becomes noticeable that different materials exhibit different behavior with respect to material fatigue resistance, strength, or material deterioration. These changes in material characteristics in turn cause decreased component/system reliability. To gain the knowledge about the impact of operating conditions on accumulated damage in components, to detect system's state which differs from an initial undamaged state, and to become able to predict remaining lifetime, continuous monitoring of system State-of-Health is necessary. Concerning above statements, suitable material selection alongside integrated SHM in WT systems may contribute to extended service lifetime of WT, more precise State-of-Health estimation, and more accurate RUL prediction. An examination of structural loads affecting aging processes of wind turbine systems/components and contributing to lifetime shortening are of a high importance for the development of reliability-oriented control strategy.

By considering the objectives to be included in control strategy development, the contradiction between requirements related to efficient operation with respect to energy production costs and those related to service lifetime and maintenance becomes noticeable. These challenges have to be overcome. To integrate the knowledge about RUL of WT in control strategy, an identification of structural loads in WT system is necessary as it is the precondition for accumulated damage calculation (and subsequently for lifetime prognosis). As depicted in Figure 3.1 on the right side, structural load examination may concern any of listed output variables: flap- and edge-wise bending moments of wind turbine rotor blades, drive train torsional torque, tower fore-aft deflection, and tower side-to-side deflection.

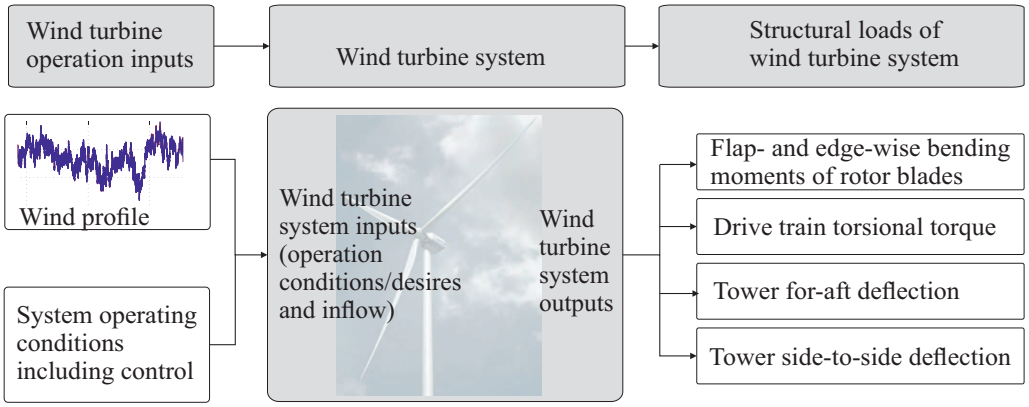

Figure 3.1: Qualitative relations of structural loads (right side) to operating conditions (left side) [BS16]

Simulation model of WT system, based on which adapted control strategy, fatigue evaluation model, and control strategy are implemented, are discussed in detail in Chapters 3.1.1, 3.1.2, and 3.2. Reliability-oriented control strategy requires information about remaining useful lifetime. Remaining useful lifetime prediction model introduced in these terms uses structural loads of WT as input into the model. In this particular case, accumulated damage in WT is obtained from the information about structural loads and afterwards correlated to remaining useful lifetime. As previously stated, structural loads are reflected in top-tower side-to-side tower bending moment, rotor blade flap-wise bending moments, and top-tower fore-aft bending moment. Flap-wise bending moments of wind turbine blades are used to calculate accumulated damage and to predict RUL of wind turbine in this specific case.

It is important to emphasize that some parts discussed in this chapter are published/submitted/prepared in/for international journals/conferences ([BNRS15], [NBS16], and [BNS]).

3.1 Remaining useful lifetime estimation

3.1.1 Simulation model of wind turbine

The wind turbine model used in scope of this thesis is developed by National Renewable Energy Laboratory (NREL). Due to high number of Degrees of Freedom (DoF), it is possible to consider different control objectives by enabling or disabling the Degrees of Freedom relevant for predefined control objectives. Such a wind turbine model is in general represented by a nonlinear equation of motion expressed as

$$\mathbf{M}(\underline{\mathbf{q}}, \underline{\mathbf{u}}, t)\underline{\ddot{\mathbf{q}}} + f(\underline{\mathbf{q}}, \underline{\dot{\mathbf{q}}}, \underline{\mathbf{u}}, \underline{\mathbf{u_d}}, t) = 0, \tag{3.1}$$

whereas $\mathbf{M}$ denotes the mass matrix, f is a nonlinear function relating input variables to DoFs, and $\underline{\mathbf{u}}$ denotes control inputs, which can either be individual blade pitch or generator torque. Here, $\underline{\mathbf{u_d}}$ denotes unknown disturbance which is in this case unknown wind speed variation about its mean value, whilst $\underline{\mathbf{q}}$, $\underline{\dot{\mathbf{q}}}$, $\underline{\ddot{\mathbf{q}}}$ denote the DoF displacements, its corresponding velocities, and accelerations, respectively. Vector $\underline{\mathbf{q}}$ defines enabled Degrees of Freedom in accordance with considered control objectives and as such is not arbitrarily chosen. In this particular case, vector $\underline{\mathbf{q}}$ is expressed as

$$\underline{\mathbf{q}} = \begin{bmatrix} \tau_f \\ \Psi \\ \zeta_1 \\ \zeta_2 \\ \zeta_3 \end{bmatrix}, \tag{3.2}$$

whereas τ_f is denoted as the fore-aft deflection mode, Ψ is DoF related to a variable generator speed mode, and ζ_1, ζ_2, and ζ_3 are Degrees of Freedom related to individual blade flap-wise bending modes.

Further, nonlinear WT model is linearized around the operating points targeting to enable the use of linear control design tools. Linearization is carried out using FAST linearization tool provided by NREL. Under an assumption that the controllers are designed for predefined nearly constant wind profiles, operating points at which the linearization is done differs. In this thesis, five nearly constant wind profiles are taken in consideration. For predefined wind profiles of 14 m/s, 16 m/s, 18 m/s, 20 m/s, and 22 m/s and desired rotor rotational speed of 20 rpm, corresponding pitch angles used for model linearization equals to 12.69, 16.435, 19.585, 22.289, and 24.685 deg, respectively.

The model obtained after linearization is a periodic model due to presence of unbalanced load distribution. To take in consideration periodicity caused by fluctuating wind speed, wind shear, tower shadow deflection, and yaw misalignment, Multi-Blade Coordinate (MBC) transformation converting the DoF coordinates from a rotating reference frame to a non-rotating reference frame is used. The detail insight into MBC transformation is given by NREL and is therefore beyond the scope of the thesis. However, further details about MBC transformation can be found in [Bir10]. State space model of WT in non-rotating reference frame after MBC transformation is done, takes the following form

$$\begin{aligned} \dot{\mathbf{x}} &= \mathbf{A}\mathbf{x} + \mathbf{B}\mathbf{u} + \mathbf{B_d}\mathbf{u_d}, \\ \mathbf{y} &= \mathbf{C}\mathbf{x} + \mathbf{D}\mathbf{u} + \mathbf{D_d}\mathbf{u_d}, \end{aligned} \tag{3.3}$$

where $\mathbf{A}$, $\mathbf{B}$, $\mathbf{C}$, and $\mathbf{D}$ denote system matrix, control input matrix, control output matrix, and transmission matrix, respectively. Matrices $\mathbf{B_d}$ and $\mathbf{D_d}$ are disturbance

Description	Value
Rating	1.5 MW
Rotor orientation	Upwind
Nacelle mass	51.170 T
Hub mass	15.148 T
Rated rotor speed	20 rpm
Tower height	82.39 m
Gearbox ratio	87.965
Rotor diameter	35 m
Blade pitch angle	$0 \sim 90$ deg
Cut-in, Rated, Cut-out wind speed	4 m/s, 12 m/s, 24 m/s

Table 3.1: Wind turbine configuration

input and transmission matrices, respectively. As noted above, $\mathbf{u_d}$ corresponds to the variation of wind speed where vector

$$\mathbf{u} = \begin{bmatrix} \Delta\beta_1 \\ \Delta\beta_2 \\ \Delta\beta_3 \end{bmatrix}, \tag{3.4}$$

represents control inputs. The system state vector $\mathbf{x}$ is defined as

$$\mathbf{x} = \begin{bmatrix} \Delta\underline{q} \\ \Delta\underline{\dot{q}} \end{bmatrix}, \tag{3.5}$$

while output vector $\mathbf{y}$ represents output measurements. Here, $\Delta\underline{\mathbf{q}}$ is defined as

$$\Delta\underline{\mathbf{q}} = \underline{\mathbf{q}} - \underline{\mathbf{q_{op}}}, \tag{3.6}$$

where $\underline{\mathbf{q}}_{\mathbf{op}}$ relates to steady state for enabled DOFs.

The model given by Equation 3.3 is used for purpose of control design, where blade flap-wise bending moments are used to calculate accumulated damage in rotor blades.

Complete analysis and implementation of control strategy with respect to accumulated damage at rotor blades is carried out for a three-bladed upwind WindPACT 1.5 MW with characteristics listed in Table 3.1. Wind turbine simulation model in general framework is illustrated in Figure 3.2.

3.1.2 Structural fatigue loads and RUL modeling

As outlined in Chapter 2, an implementation of reliability-oriented control strategy requires the knowledge about actual deterioration level present in the system. Not

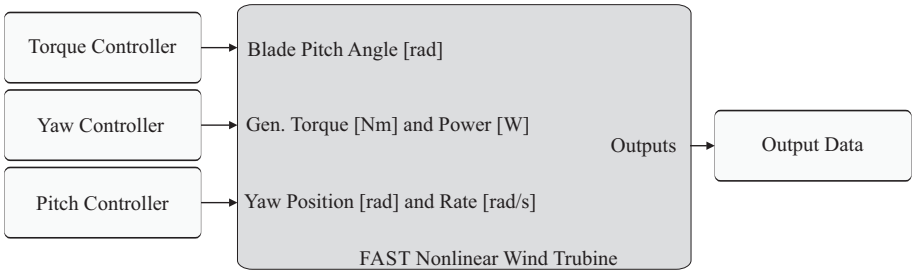

Figure 3.2: National Renewable Energy Laboratory (NREL) wind turbine simulation model

only the estimation of actual deterioration level is utilized in reliability-oriented control strategy but also the prediction of degradation growth over the time. However, prediction and estimation of aforementioned deterioration indicators imply the use of lifetime models through which the relations between operating conditions and the deterioration growth are established. According to discussion from Chapter 2.3.2, the Palmgren-Miner fatigue damage accumulation rule is capable of describing accumulated damage in WT system. Here, the Palmgren-Miner rule is applied to rotor blade flap-wise bending moments to calculate overall damage accumulated over time, as noted in Chapter 3.1.1.

Representation of fatigue load as a function of load amplitude against frequency of occurrence, reducing at the same time the spectrum of varying load, is inevitable for an application of the Palmgren-Miner rule. Represented in this way, load amplitude corresponds to the equivalent half or full life cycle. A number of counting method algorithms are known, such as level crossing or peak counting, simple range counting, rainflow counting algorithm, and others. Here, Rainflow Counting Algorithm (RCA) is used to obtain relationship between load amplitude and frequency of occurrence.

Rainflow Counting Algorithm in its original form is offline algorithm without capability to recognize different load amplitudes and corresponding half or full life cycles in real-time. Conversely, real-time calculation concerning wind turbine simulation model and associated reliability-oriented control strategy is necessary. The controller designed to support reliability-oriented usage of the system has to take into account actual value of accumulated damage as additional input into controller to generate controller outputs which are compliant with actual value of accumulated damage. Due to this, RCA implementation used along with WT simulation model has to be modified targeting to enable online calculation.

An example of RCA online implementation is introduced in [MJ12]. Online RCA implementation involves recursive counting of equivalent half and full cycles. The equivalent half or full life cycle is defined based on two minimum or maximum crossings of input values so that the equivalent half or full cycle is processed at the time at which it occurs. In contrast to offline RCA implementation, the knowledge about

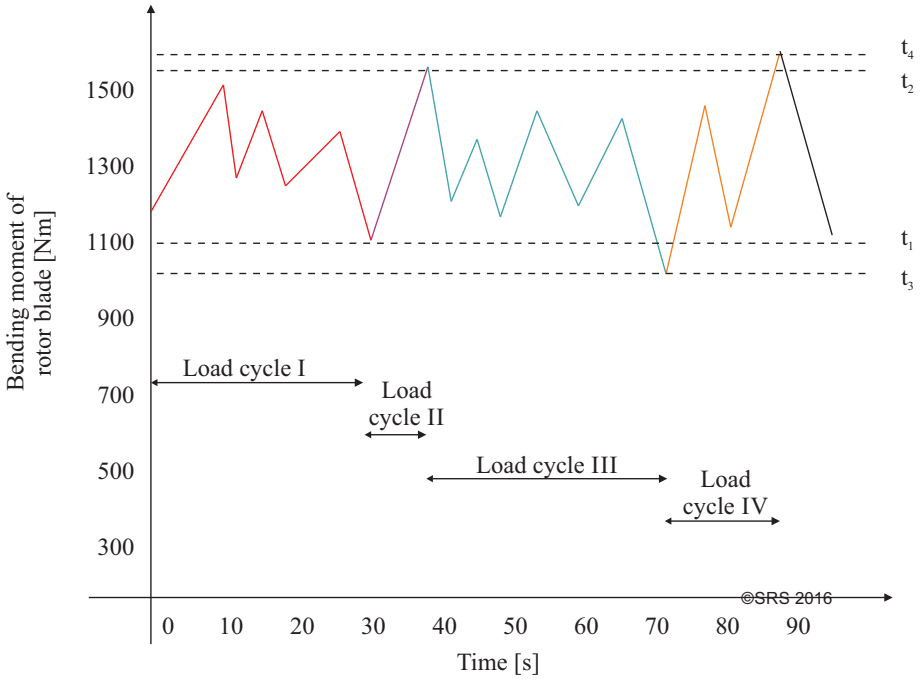

Figure 3.3: Online implementation of RCA - Load cycles determination [BNS]

complete load history is not required as the peaks are processed at the moment of occurrence, but additional uncertainty is introduced within online RCA calculation. In Figure 3.3, different life cycles are depicted in different colors. As may be noticed here, life cycle is defined at the time point of crossing extremal values t_1, t_2, t_3, and t_4. Although online implementation reduces memory requirements, it is still necessary to store the values that belong to one load cycle (as they are recursively calculated).

Additionally, the Wöhler equation is used to describe the degradation of materials and machine components. The Wöhler equation is formulated as

$$K = s^m N, \tag{3.7}$$

where K and m are material specific parameters, N is a number of cycles remained until failure occurrence under a given stress amplitude s. Parameter m is known as Wöhler coefficient. The values of the Wöhler coefficient relevant for WT systems is a coefficient referring to steel-made and CFRP-made components; the Wöhler coefficient is equal to 3 for steel-made components and 10 for CFRP-made components. Depending on above stated relations, the damage accumulated in the system can be calculated using the Palmgren-Miner equation as

$$D_k = \sum_{i=1}^{k} d_i = \sum_{i=1}^{k} \frac{n_i}{N_i} = \sum_{i=1}^{k} \frac{n_i \cdot s_i^m}{K}, \tag{3.8}$$

where s_i denotes stress range corresponding to i_{th} life cycle, N_i corresponds to the number of life cycles endurable until failure under stress level s_i, and k denotes the total number of life cycles.

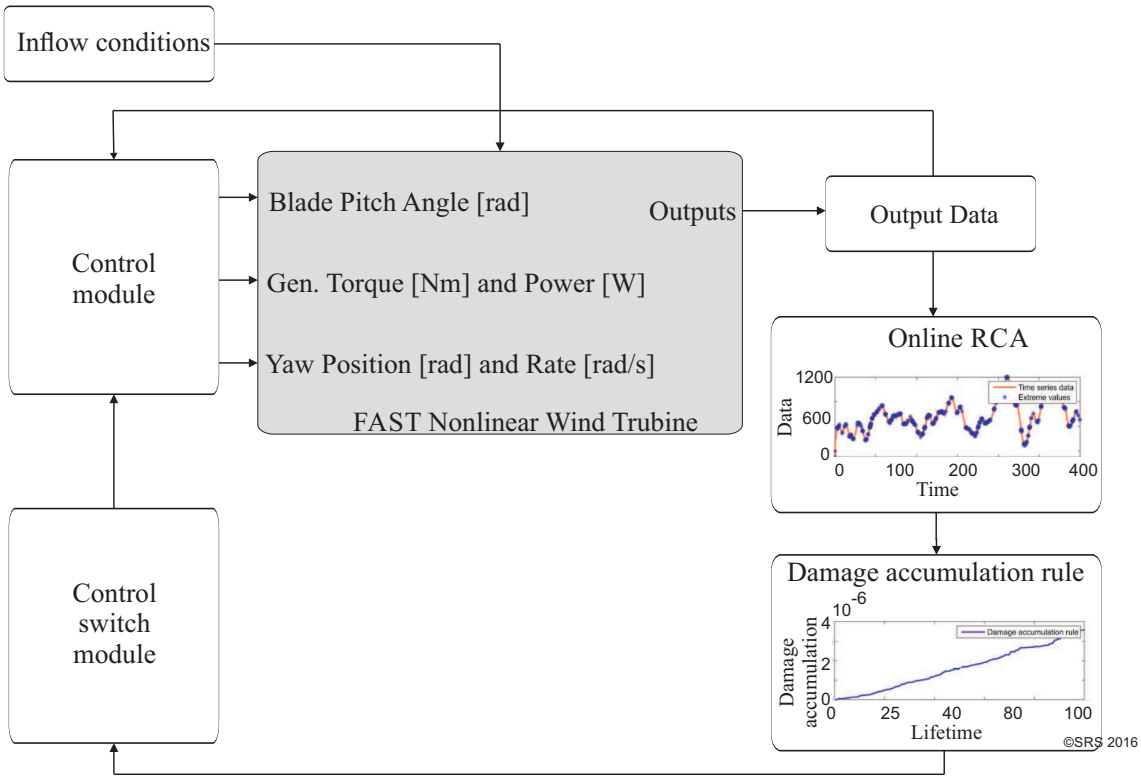

Figure 3.4: Fatigue load calculation with integrated online RCA and proposed control strategy (based on [BNS], [NBS16], and [BNRS15])

It is worth to emphasize that not run-to-failure data is used for RUL calculation in this thesis. Only representative time-series data of flap-wise bending moments of rotor blades corresponding to 600 s of simulation time are selected. This means that accumulated damage obtained in this way is not equal to unity, but damage increments up to the predefined failure, which is D=1, are extrapolated using representative data set. Load cycles are understood as individual load units.

By an application of RCA, the constant amplitude equivalent load, resulting in identical fatigue damage as is caused by a varying amplitude load over corresponding

number of life cycles, can be found. Relation for constant amplitude Equivalent Fatigue Load (EFL) calculation according to Equation 3.8 is given as

$$EFL = \left(\sum_{i=1}^{k} \frac{s_i^m}{N_i} \right)^{\frac{1}{m}}. \tag{3.9}$$

The End-of-Lifetime is considered as the moment in time at which D_k equals to unity, $D_k = 1$. Mathematical expression for End-of-Lifetime calculation is given as

$$T_f = T_k \cdot D_k^{-1}. \tag{3.10}$$

Here, T_f denotes the time to failure and T_k the time to accumulate the damage D_k. Under assumption that wind turbine service lifetime is known in advance (for instance: predefined by a manufacturer), remaining useful lifetime can be calculated from Equation 3.10. Pursuant to above detailed damage accumulation calculation, the control scheme involves, beside certainly controlled operating parameters such as generator torque and generator speed, also an information about the accumulated damage (Figure 3.4).

3.2 Reliability-oriented control strategy concerning simulation model of WT

Some aspects outlined in this chapter have also been discussed in [BNS] and [NBS16]. According to predefined nearly constant wind profiles, explained in detail in Chapter 3.1.1, induced structural load (consequently also accumulated damage on rotor blades) are different. In accordance to this, control strategy has to be capable to ensure structural load mitigation along with retaining the objectives related to power generation.

Targeting to reduce structural loads, five different controllers are designed. Adaptive control strategy consisting of five different Multi-Input Multiple-Output (MIMO) controllers each of them providing different level of structural loads reduction are designed. These five controllers provide in turn reduction of structural loads to a lesser or greater extent in dependence of current health state of wind turbine rotor blades (here: accumulated damage in rotor blades). It means that the controllers introduced here have varying control parameters. Such control strategy provides adaptive control of structural loads along with maintained power generation (as close as possible to desired values), but only in discrete steps. This means that with different number of controllers and varying control parameters there are the same number of predefined levels of structural loads reduction (in this case: five different levels) [NBS16]. The controller providing the lowest impact on structural load reduction is hereinafter stated as Controller #1, whilst Controller #5 is recognized as a controller providing the highest impact on structural load reduction.

Generator power and rotor speed are controlled using baseline PI controller which is not further elaborated in this thesis. Targeting to reduce structural loads, Linear-Quadratic Regulator-based (LQR-based) Individual Pitch Controllers (IPC) are designed [NBS16]. Structural load reduction using LQR-based IPC controllers is ensured through the calculation of corrective values of individual pitch angles. The signals generated from LQR-based IPC controllers are superposed to the signals generated by baseline PI controller. Objective function to be minimized and is used to design the controllers takes the following form

$$\mathbf{J} = \int_0^t \left(\mathbf{x}^T \mathbf{Q} \mathbf{x} + \mathbf{u}^T \mathbf{R} \mathbf{u} \right) dt, \tag{3.11}$$

where $\mathbf{Q}$ and $\mathbf{R}$ are state and control weighting matrices, respectively. The trade off between power generation and structural load mitigation is ensured by adjustment of $\mathbf{Q}$ matrix whilst $\mathbf{R}$ matrix is used to penalize the control efforts. Beside measured or estimated system variables, estimated damage increments or accumulated damage are inputs into control module as shown in Figure 3.4.

3.3 Simulation results

Simulation results obtained under usage of proposed control strategy with respect to structural load reduction and different inflow conditions are depicted in Figures 3.5, 3.6, 3.7, and 3.8. The results obtained using control strategy which concerns fatigue damage evaluation, controller selection based on current value of accumulated damage, and step-based inflow condition (wind speed) are depicted in Figures 3.5 and 3.6. Similarly, the results obtained using wind profile which is more close to real inflow conditions are depicted in Figures 3.7 and 3.8.

In the upper diagrams of aforementioned four figures, wind speed at hub height is depicted and serves as stochastic disturbance to WT model. The model variables used to validate developed controller strategy and illustrated in Figures 3.5, 3.6, 3.7, and 3.8 are generator power, rotor rotational speed, high-speed shaft torque, and variables related to structural loads (tower fore-aft bending moment, blade #1 flapwise bending moment, and tower side-side bending moment). The controller module consisting of five different LQR-based IPC controllers concern the reduction of flapwise bending moments on rotor blades, whilst tower fore-aft and side-side bending moments are not taken in consideration in controller design procedure. In addition, accumulated damage in the system, based on which the controller is selected, is depicted in Figures 3.5 and 3.7 in the lower diagrams. It is important to note that obtained value of accumulated damage (in this case $1.5 \cdot 10^{-6}$) corresponds to the damage accumulated up to 600 s (which is simulation time). As predefined service

lifetime of WT is much larger, the value accumulated in considered timespan is not equal to unity. Due to this, predefined WT service lifetime is taken in consideration to extrapolate representative data set of 600 s to overall service lifetime of WT.

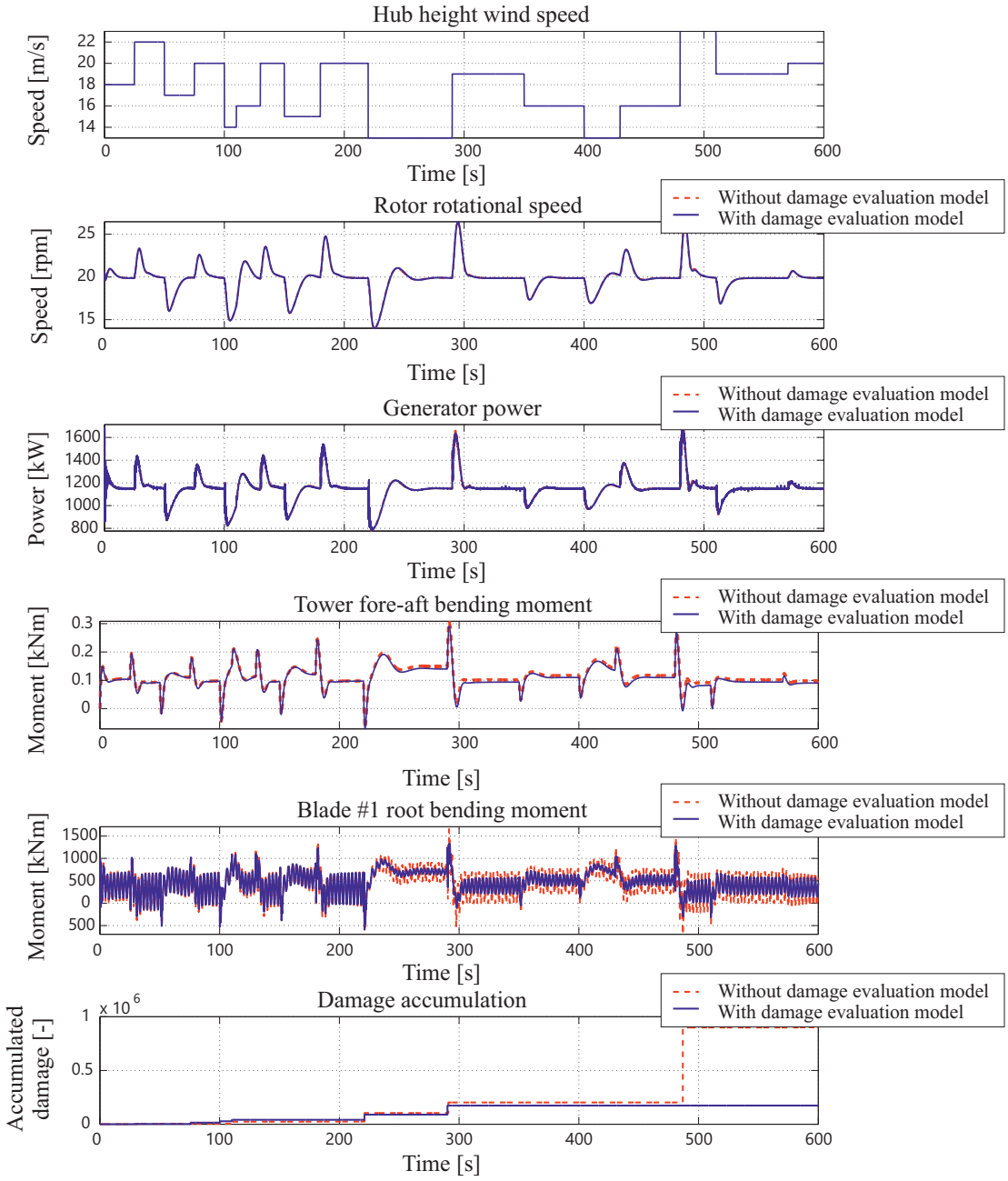

Figure 3.5: Simulation results concerning controller selection using the information about accumulated damage and step-based loading profile - Part I (based on [NBS16] and [BNS])

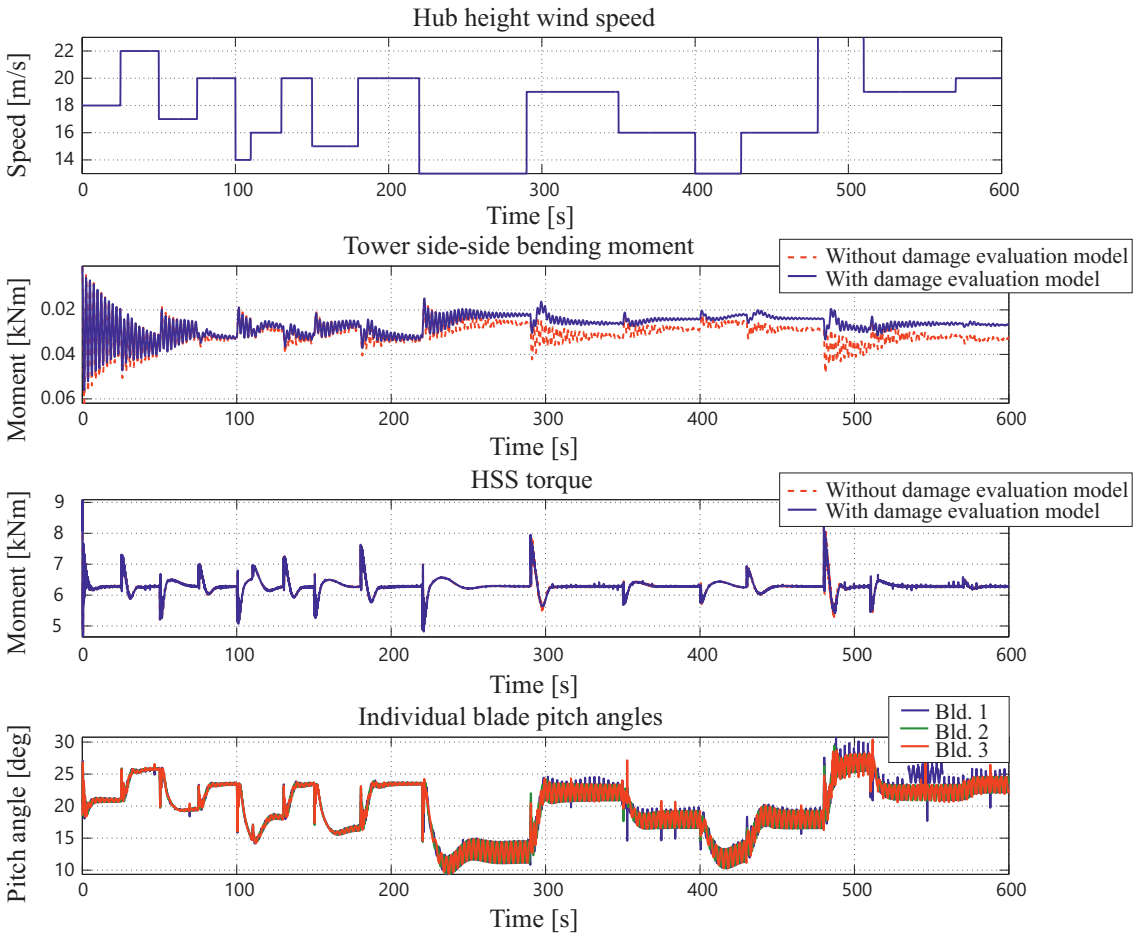

Figure 3.6: Simulation results concerning controller selection using the information about accumulated damage and step-based loading profile - Part II (based on [NBS16] and [BNS])

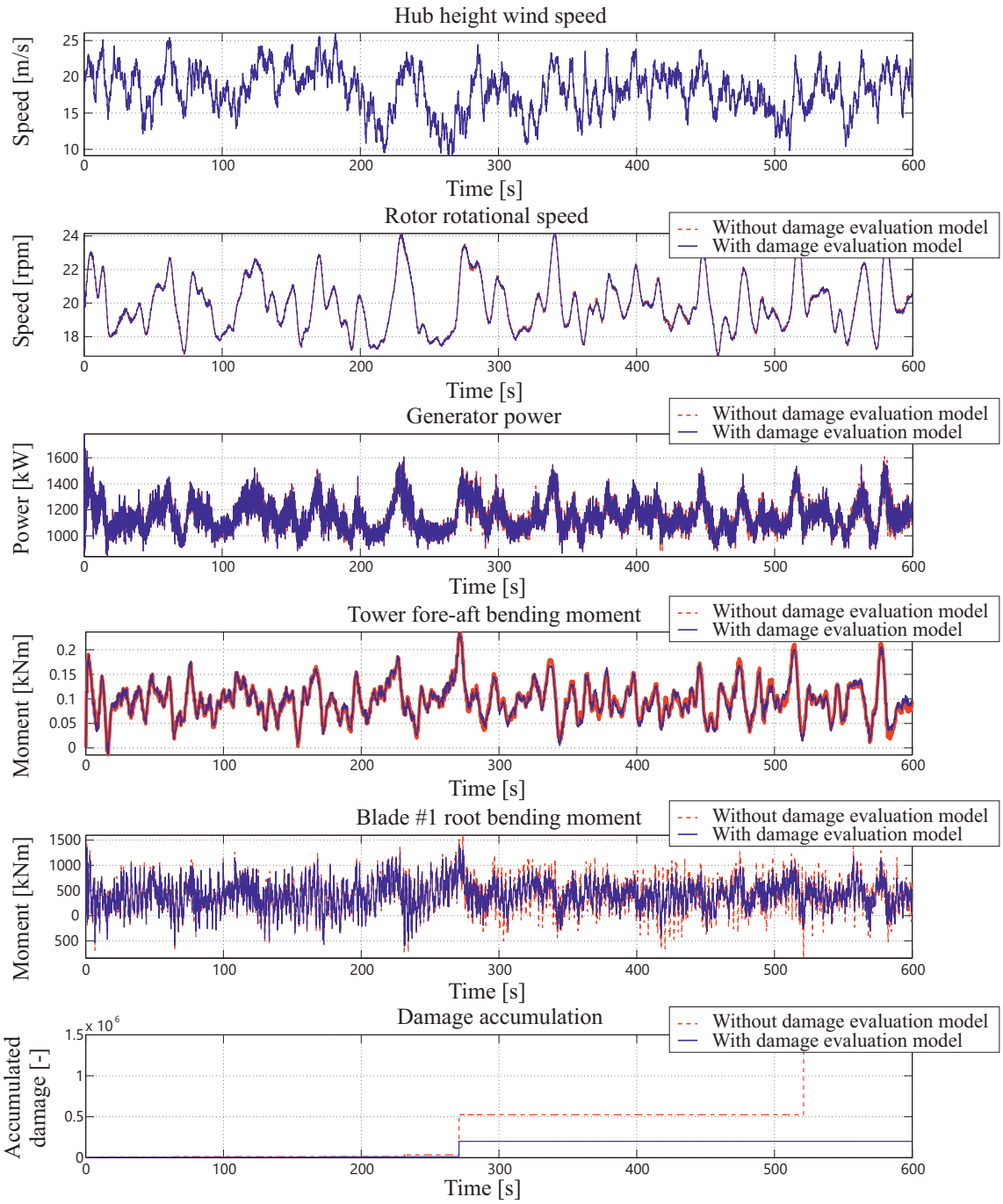

Figure 3.7: Simulation results concerning controller selection using the information about accumulated damage and loading profile generated by NREL - Part I (based on [NBS16] and [BNS])

The performance of designed control strategy can be evaluated using the analysis of dependencies between generated power and blade root bending moments or High

Speed Shaft (HSS) torque. The dependence between generated power and blade root bending moment for both loading profiles are depicted in Figures 3.9 and 3.11.

Additionally, the dependence between generated power and HSS torque are depicted in Figures 3.10 and 3.12. According to the results, high impact on flap-wise rotor bending moment is noticeable in both cases, whilst the impact on HSS torque is almost negligible. The most values in aforementioned figures are concentrated around the mean value of root blade bending moment or HSS torque.

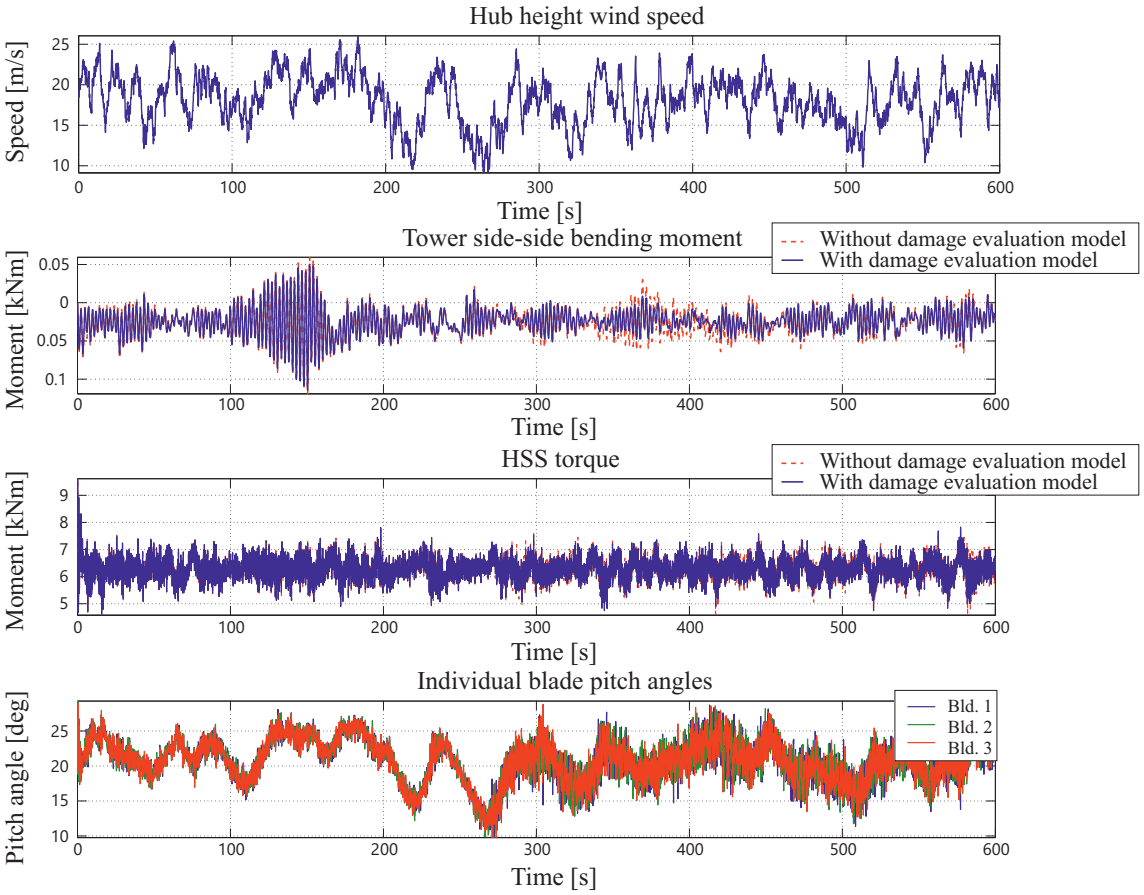

Figure 3.8: Simulation results concerning controller selection using the information about accumulated damage and loading profile generated by NREL - Part II (based on [NBS16] and [BNS])

3.4 Discussion of results

According to simulation results, the reduction of flap-wise bending moments of rotor blades in accordance with actual value of damage accumulation is clearly seen from the fifth diagram in Figures 3.5 and 3.7. The first apparent change in flap-wise rotor

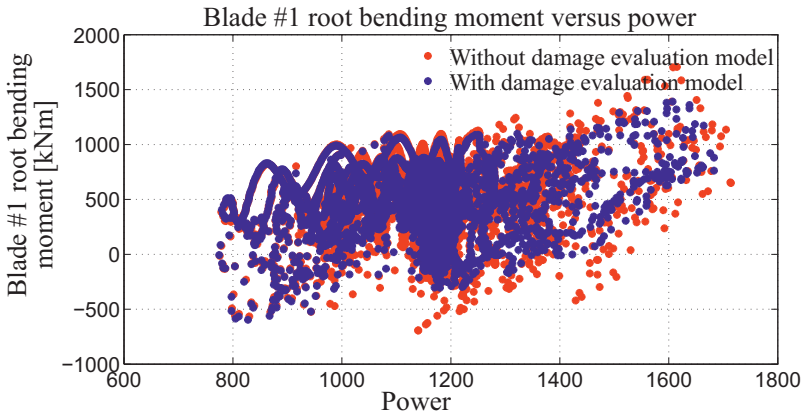

Figure 3.9: Dependence between rotor bending moment and generated power concerning step-based loading profile

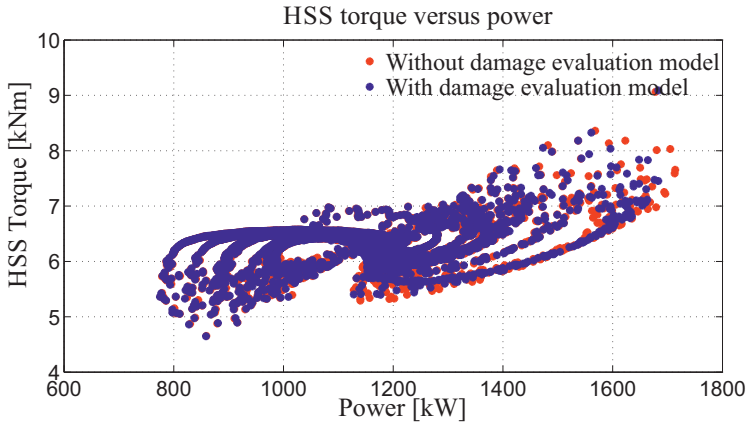

Figure 3.10: Dependence between HSS torque and generated power concerning step-based loading profile

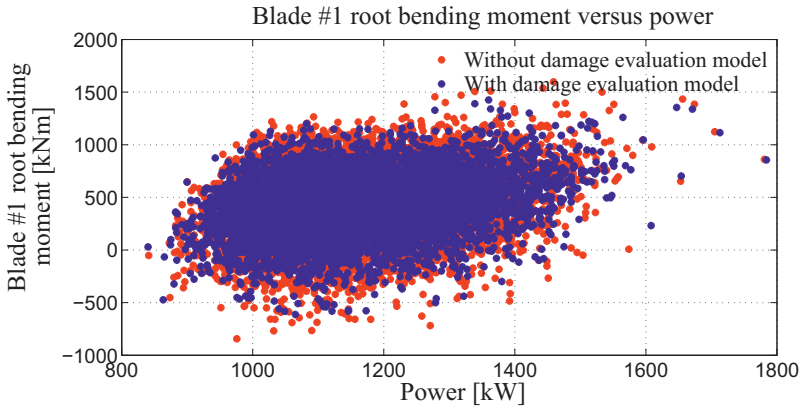

Figure 3.11: Dependence between rotor bending moment and generated power concerning loading profile generated by NREL [BNS]

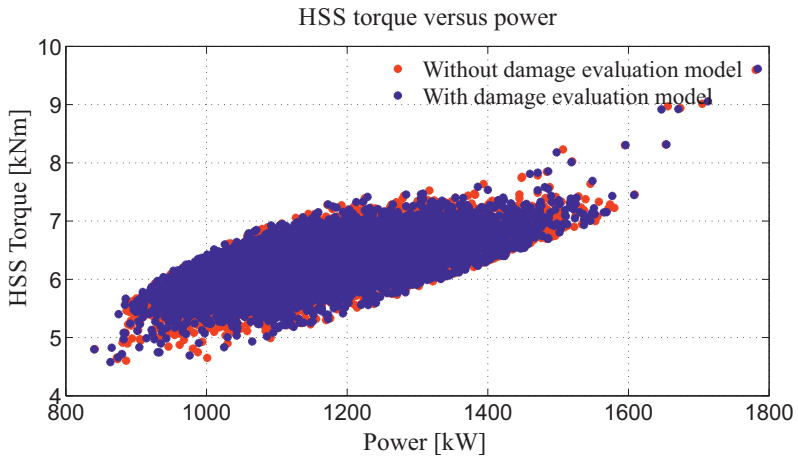

Figure 3.12: Dependence between HSS torque and generated power concerning loading profile generated by NREL [BNS]

bending moment of Blade #1 in comparison with control strategy which does not concern structural load reduction occurs at about 220 s in Figure 3.5. At this point, accumulated damage becomes higher so that the controller providing higher level of structural load reduction is selected. At about 290 s, further change of damage accumulation is noticeable causing the selection of the controller with higher level of structural load reduction. Reduction of bending moments of rotor blades is thus much more pronounced after 290 s. According to Figure 3.7, the change becomes noticeable at about 270 s as the damage accumulated up to this point in time causes the selection of a controller with higher level of structural loads reduction. As may be concluded, the controller with the highest level of flap-wise rotor blade bending moment reduction is selected shortly before the end of system's lifetime is reached. Consequently, selection of controllers is carried out in a successive manner. This means, once the controller with higher structural load reduction is selected, the controller with lower level of structural loads reduction cannot be selected. With such an approach, a monotonic increase of accumulated damage due to damage propagation and growth over the time is taken in consideration.

The effect of adapted control strategy on generator power as well as rotor rotational speed is not significant according to Figures 3.5 and 3.7. This means that the controller objectives related to desired power generation are met. Even though the power generation is slightly sacrified, the deviation between desired and obtained power generation is acceptable. It is important to note that the controller with smallest impact on structural load reduction (Controller #1) gives lower deviation between desired and actual power generation. The reason not to use the controller with the highest level of structural load reduction over the whole service lifetime lies in the requirement to minimize the sacrifice of power generation. Due to this, a trade off between power generation and structural load reduction is necessary.

Moreover, tower fore-aft and side-to-side bending moments are also affected. As the controller is not designed to take tower fore-aft and side-to-side bending moments in consideration, the changes noticeable in these cases are a consequence of the change in control strategy, but occurs occasionally.

An assumption lying behind accumulated damage calculation is that the damage between two subsequent half or full load cycles is held constant. Consideration of constant damage between two half or full load cycles is rather theoretical and is rarely met case in practice, as it means that the damage during some time periods do not appear. As such, the development of additional fatigue damage evaluation models targeting to obtain more accurate prediction of remaining/consumed lifetime can be considered in the future. Additionally, integration of further improvements into control strategy are still possible, especially concerning possibilities to affect/reduce top-tower fore-aft and top-tower side-to-side tower structural loads along with reduction of rotor blade structural loads.

Accurate estimation of consumed and/or remaining useful lifetime, as may be concluded, is of high importance to design the control strategy whereas desired actions of the system are compliant with current system's deterioration. From the other point of view, not only the damage occurred in WT rotor blades has to be considered for these purposes, but also the damage noticeable in any other wind turbine component (electric/electronic modules, generator, drive train, storage devices, and others). Due to this, the modeling of consumed/remaining useful lifetime of a system where sliding motion between metallic components is performed as well as RUL modeling of lithium-ion batteries are taken as examples in this thesis. Both the aforementioned RUL approaches are discussed in the scope of this thesis as they can be considered as a components of wind turbine system.

The results presented in Chapter 3 prove the efficiency of proposed controller strategy in accordance to predefined control goals. The trade off between energy production and wind turbine reliability is ensured, whilst slight sacrifice on power production is acceptable.

4 Lifetime modeling considering a tribological system: establishing a new approach

Wear examination of metallic materials on example of a tribological system with special emphasis to diagnosis and prognosis is discussed in Chapter 4. Wear examination implies the development of different lifetime modeling approaches/lifetime models capable to describe complex relationships between system usage (operating conditions) and gradual system degradation. An understanding of wear mechanisms and modes occurred in metallic structures may be useful for diagnosis and prognosis purposes as they highly affect the aging process of metallic structures (wear formation and growth). Most common failure mechanisms and modes occurred in tribological system are detailed at the beginning of Chapter 4. The knowledge about underlying degradation processes may be integrated in lifetime models to provide better model efficiency.

Three different new lifetime modeling approaches/models based on measurements originating from experimental tests conducted under different operating conditions are proposed in Chapter 4. Whilst the first proposed model is a parametric model which does not rely on the knowledge about actual State-of-Health to estimate remaining (consumed) lifetime, the second and the third proposed models consider the knowledge about system's actual State-of-Health to obtain an information about remaining or consumed lifetime. A number of lifetime models are imported into lifetime model database where the knowledge about current SoH is used to select appropriate model among a number of lifetime models from the database. Each of these models thus correspond to a particular State-of-Health.

Due to requirement on experimental data sets for lifetime model establishment and optimization, experimental setup of tribological system is concerned. Experimental data sets relates to different experimental test runs and are used not only for new lifetime models development but also for estimation of State-of-Health of tribological system. Here, acoustic emission as well as hydraulic pressure are continuously monitored and discussed in terms of measurements utilization for prognosis and diagnosis purposes (for instance: estimation of system's current deterioration level). In addition, accompanying signal processing techniques as well as feature selection/extraction are discussed in Chapter 4. As developed lifetime model, establishing complex relation between system deterioration (damage increments or damage accumulation) and consumed (remaining) lifetime, are dependent on the nature of operation variables measured from the system, experimental setup as well as operation variables used for lifetime model development are introduced directly after failure mechanisms and modes are discussed.

The features extracted from AE measurements are chosen as model input in all three cases. Model parameters optimization for each particular model is carried out by an application of Non-dominated Sorting Genetic Algorithm (NSGA-II); in its modified

form for parametric model, and in its original form for other two proposed models. Advantages, disadvantages, and possibilities of all three approaches are discussed. It is worth to emphasize that some parts of this chapter are published/submitted in international journals/conferences ([BS17], [BRS16], [BBS15], [BS15b], [BRS14]).

4.1 Failure mechanisms and modes of metallic structures

Technical systems are subjected to different operating conditions as well as loading profiles of different character and intensity. Due to this, different aging processes become noticeable. Aging related processes occurred in metallic structures are know as wear. According to [Sta06], wear is defined as a progressive loss of material due to a mechanical contact between two or more solid bodies. In this context, wear can be discussed in terms of wear mechanisms and wear modes. Using such terminology, wear mechanisms can be classified in mechanical, thermal and chemical wear mechanisms. Wear mechanisms can further be divided into different wear modes.

Mechanical wear mechanisms belong to the welding and bonding, crack initiation, fracturing, and plastic deformations of material (here: metallic structure). "Mechanical wear mechanism describes the welding and bonding of material, crack initiation, plastic deformations, and fracturing. Wear modes recognized within mechanical wear mechanism are adhesive (material displacements, occurrence of debris), abrasive (scraping of particles of higher strength along solid surface), and erosive (impact of strange particles into solid surface) wear modes. Hence, the chemical wear mechanism relates to the layer formation and growth between moving surfaces (corrosive wear mode, surface fatigue). Finally, thermal wear mechanism correlates to the material deformations resulting from the temperature rise appeared due to mutual surface motion." [BBS15]. Among all listed wear modes, adhesive wear, abrasive wear, and surface fatigue are stated in the literature as wear modes mostly contributing to system's aging [Sly02].

Over the time and almost always variable operating conditions applied to a system, aging processes become noticeable and raise to a lesser or greater extent in accordance with applied load. By considering metallic structures (here: tribological systems), different wear modes become noticeable such as adhesive wear at the beginning, abrasive wear, surface fatigue, fretting, and erosive wear at the End-of-Lifetime (EoL). It is worth to emphasize that different wear modes are usually overlapped: they appear simultaneously and there are no clearly defined moment in time at which one wear mode is displaced with another one. In this chapter, the intension is to examine whether it is possible to track the growth of wear in tribological system without special emphasize on a particular wear mode: wear modes are

rather considered in general framework with an aim to predict useful/remaining lifetime. For this purpose, parametric lifetime model as well as lifetime models which integrate the knowledge about current State-of-Health are introduced in 4.2.

4.2 Lifetime models establishment and optimization based on AE measurements

4.2.1 Lifetime models introduction

Highly varying character of load applied to the system, including mechanical, thermal, chemical, environmental, and/or electrical load, has necessitated the development of lifetime models to go in several directions. The models established here are not pure mathematical models but include in its basis mathematical description of relationships between damage occurred in the system and consumed (or remaining) service lifetime.

Each of three models are introduced in detail in Chapters 4.2.1.1, 4.2.1.2, and 4.2.1.3 and are hereinafter referred as *Model Type I*, *Model Type II*, and *Model Type III*. Obtained results using particular model are firstly discussed separately, whereas absolute and End-of-lifetime (EoL) prediction error are calculated and graphically illustrated. In addition, all three models are compared and analyzed in terms of Root Squared Error (RSE) and Mean Squared Error (MSE) calculation at the end of Chapter 4. The data from tribological system is used to optimize model parameters, giving at the same time high attention to practical application of the models.

4.2.1.1 Model Type I

Lifetime model introduced in 4.2.1.1 is a parametric model taking in consideration previous values of consumed lifetime and current as well as previous values of accumulated damage increments as model inputs. Mathematical formulation of parametric lifetime model, including previous and current values of accumulated damage increments at discrete moments along with all previously estimated values of consumed lifetime as model inputs, is reasonable concerning progressive character of damage. The damage increments accumulated over time show monotonic increase as the aging process is irreversible process; once the system reaches certain deterioration level it is hardly possible to revert lifetime without replacement of system's component(s). Lifetime model establishment is here discussed in terms of tracking damage increments and their accumulation over time. By labeling accumulated damage increments as DA and by observing DA at discrete moments, accumulated damage increment observed at discrete moment n can be denoted as

DA_n. Accordingly, the incomes of consumed lifetime values are here denoted as LT_n. The equation establishing relationship between accumulated damage increments and consumed lifetime is stated as

$$LT_n = \sum_{k=1}^{n} a_{n-k} \cdot DA_{n-k} + \sum_{k=1}^{n-1} b_{n-k} \cdot LT_{n-k}, \tag{4.1}$$

whereas a_k and b_k are unknown model parameters which have to be identified using appropriate optimization procedure. Using proposed parametric model, the calculation of consumed (and remaining) lifetime becomes possible. At first glance, it is evident that the system is closer to its End-of-Lifetime with each received income. The End-of-Lifetime is defined as the moment in time at which accumulated damage exceeds predefined limit, in this case $D_{max} = 1$.

Moreover, it is noticeable that the linear relationship between a_k and b_k parameters exist and can be calculated as

$$\begin{aligned} a_n &= \frac{LT_n - SA_{n-1} - b_n \cdot lt_{n-1} - SB_{n-2}}{DA_n} \text{ and} \\ b_n &= \frac{LT_n - a_n \cdot DA_{n-1} - SA_{n-1} - SB_{n-2}}{LT_{n-1}}, \end{aligned} \tag{4.2}$$

whereas SA_{n-1} and SB_{n-2} are denoted as

$$\begin{aligned} SA_{n-1} &= \sum_{k=1}^{n-1} a_{n-k-1} \cdot DA_{n-k-1} \text{ and} \\ SB_{n-2} &= \sum_{k=1}^{n-2} b_{n-k-1} \cdot LT_{n-k-1}. \end{aligned} \tag{4.3}$$

The linear relationship between a_k and b_k parameters is integrated in optimization algorithm, so that a_k (or b_k) parameters are randomly chosen while b_k (or a_k) parameters are calculated using available experimental data sets, and vice versa. Model parameters optimization is thereby simplified to the selection of those set of a_k and b_k parameters best fitting experimental data sets. This is nothing else but minimizing the function which represents the deviation between the results obtained using proposed lifetime model and experimental data sets.

4.2.1.2 Model Type II

Contrary to *Model Type I* which takes previous values of consumed lifetime as well as previous and actual values of accumulated damage, *Model Type II* takes neither all previous values of consumed lifetime nor all previous values of damage increments or accumulated damage increments. Conversely, the output of *Model Type II* is highly

dependent on the knowledge about current State-of-Health which is used within a state machine approach to establish relationship between damage increments and consumed lifetime.

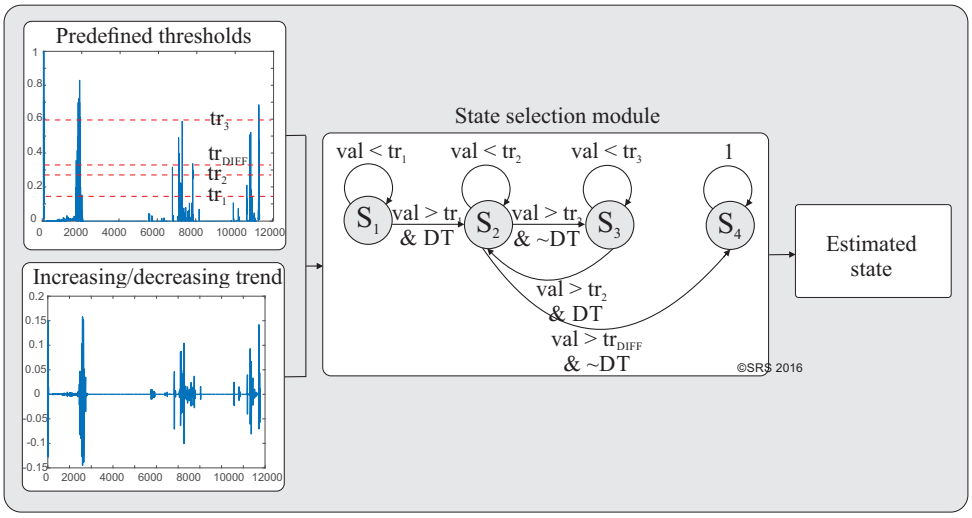

Figure 4.1: Machine state selection based on exceedance of predefined thresholds and increasing/decreasing trend of model input [BS17]

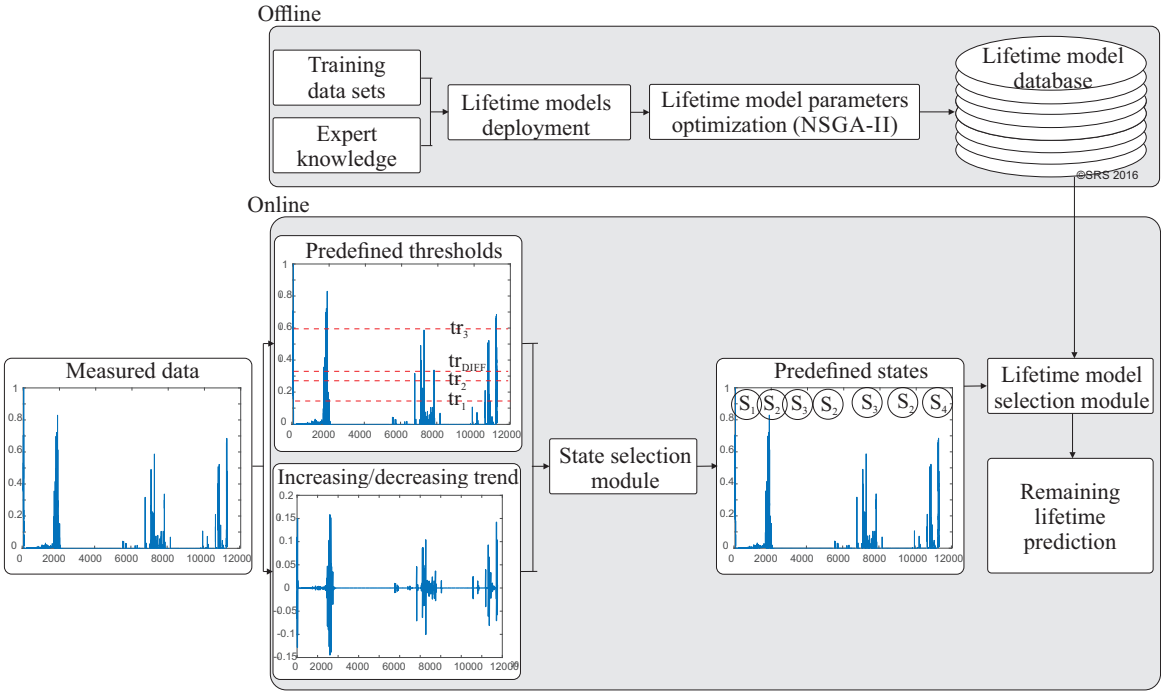

Figure 4.2: Remaining useful lifetime modeling using lifetime model selection based on actual State-of-Health [BS17]

Using state machine, it is possible to select an appropriate model from lifetime model database, but the transitions between machine states are done in accordance to current State-of-Health. This means consequently that different health states are modeled by different lifetime models (here: mathematical equations with different model parameters). State machine utilized in *Model Type II* has four states, whereas transitions between particular states are defined according to predefined thresholds of damage increments and decreasing or increasing trend of monitored system variable. The states are defined as follows: i) state S_1 is defined as the state with high changes in the system at the beginning of service lifetime (initial use of the system), ii) states S_2 and S_3 are the states with small and high changes in the system, respectively and are successively occurred between first use of the system and loss of functionality, and iii) state S_4 is a state close to system's loss of functionality [BS17].

Predefined thresholds are stated as tr_1, tr_2, tr_3, and tr_{DIFF} in Figures 4.1 and 4.2. It is of high importance to note that the thresholds in this case are fixed and are not concerned during model parameters optimization procedure. According to Figure 4.1, thresholds as well as determined decreasing/increasing trend of monitored variables are necessary to recognize actual machine state and to select mathematical model accompanied to a particular machine state.

The initial state of state machine is defined as S_1 (Figure 4.1). Only possible transition from state S_1 is to state S_2 and occurs when threshold tr_1 is exceeded and decreasing trend of model input variable is detected. Possible transitions from state S_2 are to states S_3 or S_4. If threshold tr_2 is exceeded and increasing trend is detected, the transition from state S_2 to state S_3 occurs. Otherwise, with exceeding the threshold tr_{DIFF} and detecting increasing trend of model input variable, machine state from state S_2 is changed to S_4. Only possible transition from state S_3 is to state S_2 in case that threshold tr_2 is exceeded and decreasing trend is detected. Once state S_4 is reached, further state transitions are not possible and state S_4 is not changed.

Mathematical expressions integrated in *Model Type II* which correspond to certain machine state are given in Table 4.1. As may be noticeable, mathematical expressions describing all four machine states are identical, but model parameters are not identical. Even identical functional form is used to model relation between system's deterioration level and consumed lifetime, high changes in the output of the model are noticeable by varying mathematical model parameters; often also by variation of model parameters to a lower extent. Consequently, it may be concluded that model parameters for each particular machine state have to be optimized. According to Table 4.1, parameters to be optimized are a_{x0}-a_{x8}, where x denotes a particular machine state. Concerning four different machine states, 36 model parameters have to be optimized, or otherwise noted: 9 parameters per machine state.

STATE 1	$LT = a_{10} + \frac{a_{11}}{1+e^{a_{12}(F_1-a_{13})}} + \frac{a_{14}}{1+e^{a_{15}(F_1-a_{16})}} + \frac{a_{17}}{1+e^{a_{18}F_1}}$
STATE 2	$LT = a_{20} + \frac{a_{21}}{1+e^{a_{22}(F_1-a_{23})}} + \frac{a_{24}}{1+e^{a_{25}(F_1-a_{26})}} + \frac{a_{27}}{1+e^{a_{28}F_1}}$
STATE 3	$LT = a_{30} + \frac{a_{31}}{1+e^{a_{32}(F_1-a_{33})}} + \frac{a_{34}}{1+e^{a_{35}(F_1-a_{36})}} + \frac{a_{37}}{1+e^{a_{38}F_1}}$
STATE 4	$LT = a_{40} + \frac{a_{41}}{1+e^{a_{42}(F_1-a_{43})}} + \frac{a_{44}}{1+e^{a_{45}(F_1-a_{46})}} + \frac{a_{47}}{1+e^{a_{48}F_1}}$

Table 4.1: Mathematical formulations of lifetime models for *Model Type II* (based on [BS17] and [WSP14])

The consumed lifetime in equations from Table 4.1 is denoted as LT, whereas extracted features from measured system variables are denoted as F_1 and are correlated to the damage occurred in system. Model parameters optimization considering estimation of optimal a_{x0}-a_{x8} parameters is required. Features denoted as F_1 are discussed in detail in Chapter 4.2.3.2.

4.2.1.3 Model Type III

Contrary to the state-machine-based lifetime model introduced in Chapter 4.2.1.2, *Model Type III* considers optimization of damage thresholds instead of state machine to recognize different deterioration levels. This implies that *Model Type III* also utilizes different lifetime models accompanied to different degradation levels.

Selection of particular model in this case is conditioned solely on accumulated damage threshold exceedance, endeavoring to select suitable lifetime model in accordance with current health state of the system. Conversely to *Model Type II* where thresholds are fixed and not concerned in optimization procedure, thresholds used within *Model Type III* are neither fixed nor excluded from optimization procedure. This means that thresholds along with particular model parameters are simultaneously optimized targeting to find model parameters and the thresholds which fit experimental data to the highest extent.

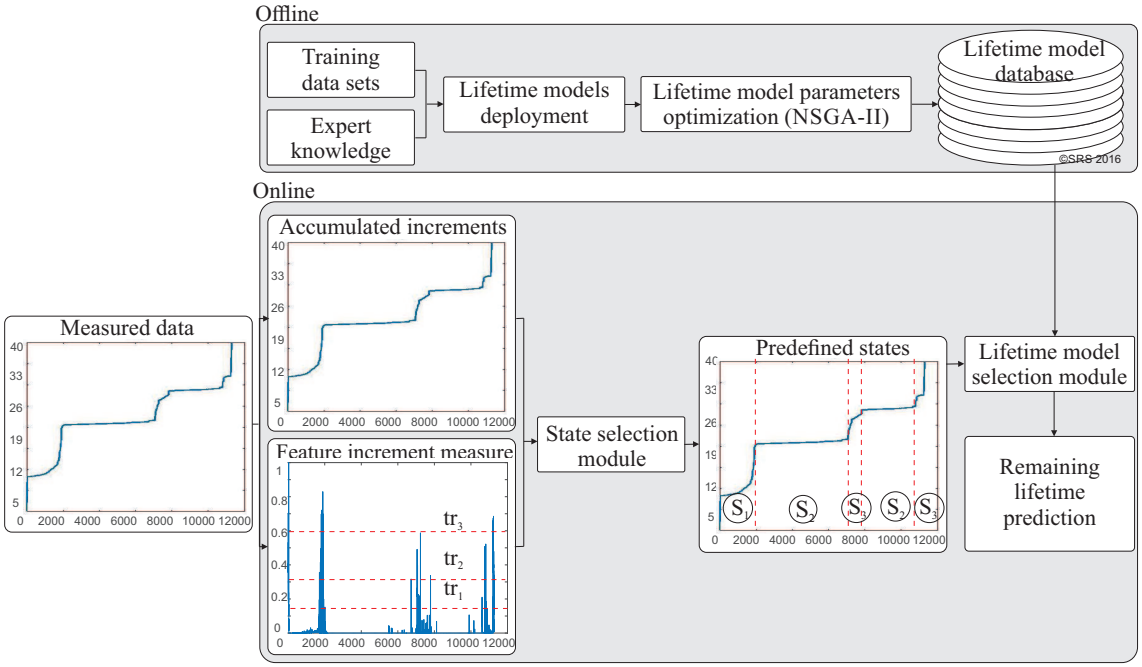

Figure 4.3: Concept of State-of-Health-based lifetime modeling by tracking predefined thresholds exceedance [BS17]

WITHOUT SIGNIFICANT CHANGE	$LT = b_{10} + \frac{b_{11}}{1+e^{b_{12}(F_2-b_{13})}} + b_{14}F_2 + b_{15}F_2^{b_{16}} + \frac{b_{17}}{1+e^{b_{18}F_2}}$
NOTICEABLE, BUT NOT SIGNIFICANT CHANGE	$LT = b_{20} + \frac{b_{21}}{1+e^{b_{22}(F_2-b_{23})}} + \frac{b_{24}}{1+e^{b_{25}(F_2-b_{26})}} + b_{27}e^{b_{28}(1-F_2)}$
SIGNIFICANT CHANGE	$LT = b_{30} + \frac{b_{31}}{1+e^{b_{32}(F_2-b_{33})}} + \frac{b_{34}}{1+e^{b_{35}(F_2-b_{36})}} + \frac{b_{37}}{1+e^{b_{38}F_2}}$

Table 4.2: Mathematical formulations of lifetime models for *Model Type III* (based on [BS17])

Three different deterioration levels (here: states) corresponding to aforementioned thresholds are concerned. These three states are hereinafter denoted as the states with: i) no significant change in lifetime consumption, ii) noticeable, but still not significant change in lifetime consumption, and iii) significant change in lifetime consumption. For each deterioration state, particular lifetime model from lifetime

model database is selected. As may be noticed from Figure 4.3, the thresholds are considered as an integral part of *Model Type III*.

Mathematical expressions used to model different states are given in Table 4.2. Parameters to be optimized concerning *Model Type III* are parameters related to mathematical equations given in Table 4.2 (b_{x0}-b_{x8}) and parameters related to deterioration level thresholds (b_{x9}-b_{x12}). Consumed lifetime in above stated mathematical equations is denoted as LT, whilst F_2 denotes extracted feature to be used for model establishment. Features denoted as F_2 are discussed in detail in Chapter 4.2.3.3. Thresholds are depicted in Figure 4.3 as tr_1, tr_2, tr_3, and tr_{DIFF}. Contrary to *Model Type II* where identical functional form is used to model relationship between current deterioration level and consumed lifetime, here different functional forms in dependence of current deterioration level are used.

4.2.2 Experimental setup

An examination of friction and the effects of operating conditions on growth and propagation of phenomena resulting from friction are major fields of tribology. Moreover, not only mechanical processes are areas of interest in tribology but also chemical, thermal, and allied processes, identifying thereby tribology as an interdisciplinary science.

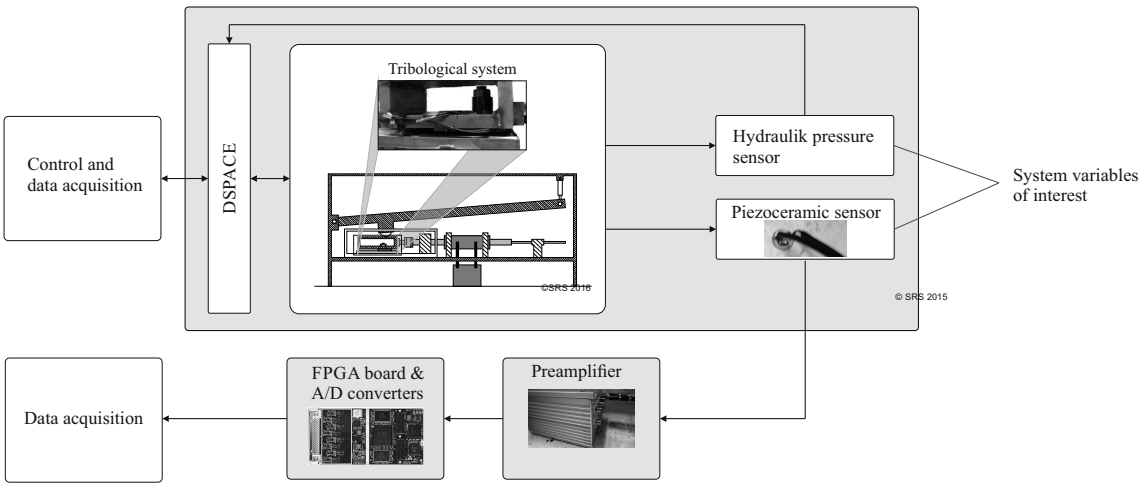

Figure 4.4: Tribological system, Chair of Dynamics and Control, SRS, U DuE (based on [BRS16], [SRS+13], and [BS15b])

By describing mutual dependencies between operating conditions (such as lubrication, temperature, material characteristics, and others) and the rate of wear propagation, it would be possible to affect wear growth rate through changing operating conditions. Main challenges related to tribology are reduction of wear growth and

mitigation of wear propagation rate. Different processes, hereinafter noted as wear or wear-related processes, occur between two interacting bodies due to their relative motion, such as sliding or rolling.

Test bench facility at the Chair of Dynamics and Control, U DuE, is used to conduct the analysis of deterioration processes occurred in metallic structures with respect to their sliding motion along with the examination of effects of operating conditions on wear. As depicted in sketch in Figure 4.4, the system consists of two metallic plates (contact partners) of different sizes sliding against each. The ratio between surface areas of used plates is 1:5, whereas the plate with larger surface area is fixed and performs no motion. Conversely, the plate with smaller surface area is driven by a hydraulic cylinder and performs linear motion. Additionally, normal force is applied to accelerate tribological effects. Programmable motion of plate as well as operating conditions such as lubrication or temperature are controlled, so that surface changes under certain operating conditions can be monitored. After particular number of cycles, cracks formed on the plates propagates over time to a large extent causing further movement of the plates impossible.

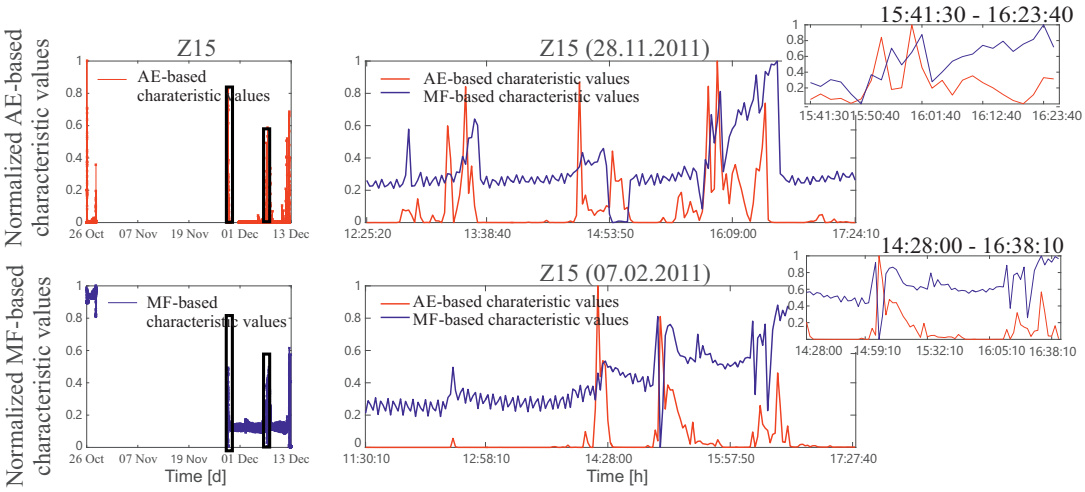

Figure 4.5: Comparison of AE and hydraulic data (Z15): complete measurements captured over service time (left side) and detail insight into the data (right side) [BRS16]

For purpose of SHM, test bench is equipped with a number of sensors. Among all measurements captured by sensors, AE and hydraulic pressure measurements are variables of high interest for the diagnosis and prognosis. Piezoelectric sensor is glued to the plate with smaller surface area and is capable to capture transient high-frequency elastic waves traveling within metallic structure. Localized high-frequency elastic waves are generated due to the existence of cracks and local displacements and enable in turn monitoring of surface changes in metallic structure. Signal analysis and signal signatures selection in case of AE measurements is performed on a huge amount of data. Acoustic Emission signal filtering and feature

selection/extraction capable to reveal the damage occurred in the system and its accumulation over time usually require signal transformation in frequency- or time-frequency domain (STFT, or DWT/CWT-based signal transformation). As such, Short Time Fourier Transform is applied to gather the information about energy of AE signal. Characteristic values obtained using STFT belong to considered cycle; only one characteristic value per cycle (forward and backward movements of plate in duration of 40 s) is calculated [SRS+13].

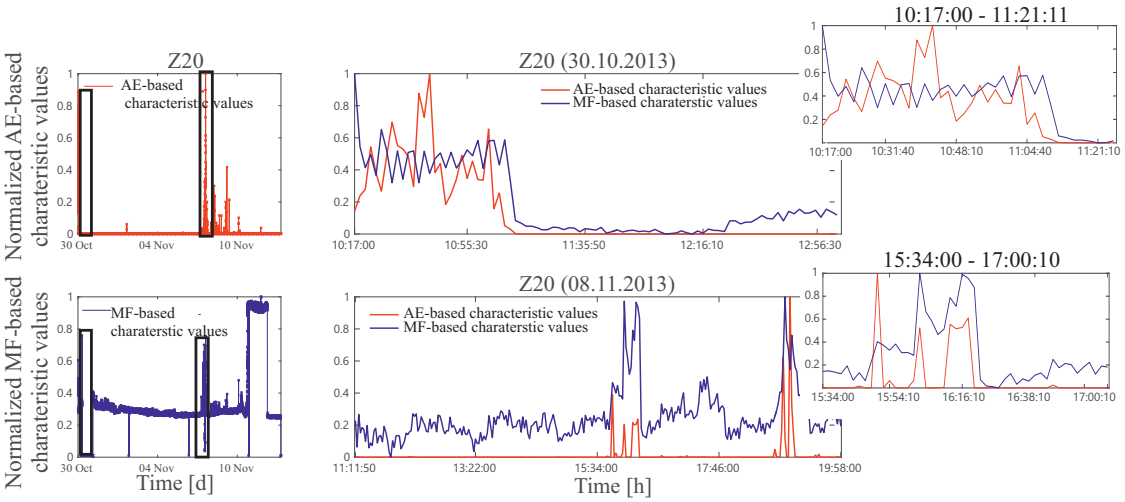

Figure 4.6: Comparison of AE and hydraulic data (Z20): complete measurements captured over service time (left side) and detail insight into the data (right side) [BRS16]

For signal filtering and damage-related feature selection from hydraulic pressure measurements, macro-data filtering is applied [SRS+13]. By an application of macro-data filtering, the characteristic values for all considered load cycles are generated. The calculation of characteristic values considers calculation of arithmetic mean of individual cycle by using sliding-window function (as a first step) and the calculation of arithmetic mean of means (as the second step). The value generated this way is considered as characteristic value of certain load cycle and is explained in detail in [SRS+13]. Similarly as in case of AE-based features, characteristic values obtained from hydraulic pressure measurements are also cycle-wise features, which means that one characteristic value per cycle is obtained. To prove whether both of these features, namely characteristic values of energy of AE signal and characteristic values of load cycles calculated based on hydraulic pressure measurements, may be utilized for diagnosis and prognosis purposes in a similar way, the direct comparison of obtained features is carried out.

Normalized characteristic values of AE- as well as hydraulic-pressure-based features relating to different test runs (here: Z22, Z21, Z15, and Z20) are depicted on the same time scale in Figures 4.5, 4.6, 4.7, and 4.8. Complete measurements captured

over service lifetime are depicted on the left side, whilst the detailed insight into the data is given on the right side of aforementioned figures. According to this, also a timespan in which particular experimental test is conducted can be identified.

At first glance, particular effects occurred in the system can be perceived by both measuring methods nearly at the same time. This fact is simultaneously good indicator that both gathered features can be used in similar manner to perform the optimization of lifetime model parameters. In this thesis only AE measurements are used, but proposed methods and model parameters can also be optimized using hydraulic pressure measurements in the same way. Not all data sets have to be used for model training for each particular model proposed in previous chapter.

In some particular cases, only two data sets are used for model training, but it is stressed individually which data set is used as training/test data set for each particular model. Data sets used for model optimization or validation are depicted in Figure 4.9, whereas Z16 and Z24 are for all models considered as test datasets, and Z20, Z15, Z21, as well as Z22 as training data sets. In addition, lifetime model parameters optimization under variation of training and test data sets is performed.

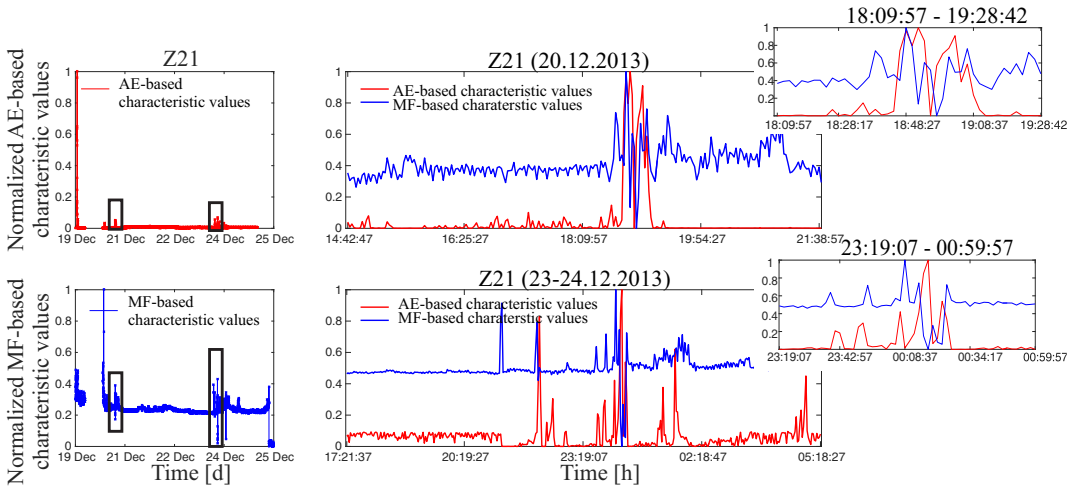

Figure 4.7: Comparison of AE and hydraulic data (Z21): complete measurements captured over service time (left side) and detail insight into the data (right side) [BRS16]

Whilst some models described in previous section consider characteristic values calculated based on AE measurements as model input, the other ones consider accumulated sum of damage increments as model input. As such, AE-based characteristic values correspond to damage increments. For each model, it is detailed individually whether characteristic values itself or their accumulated values are used as model input.

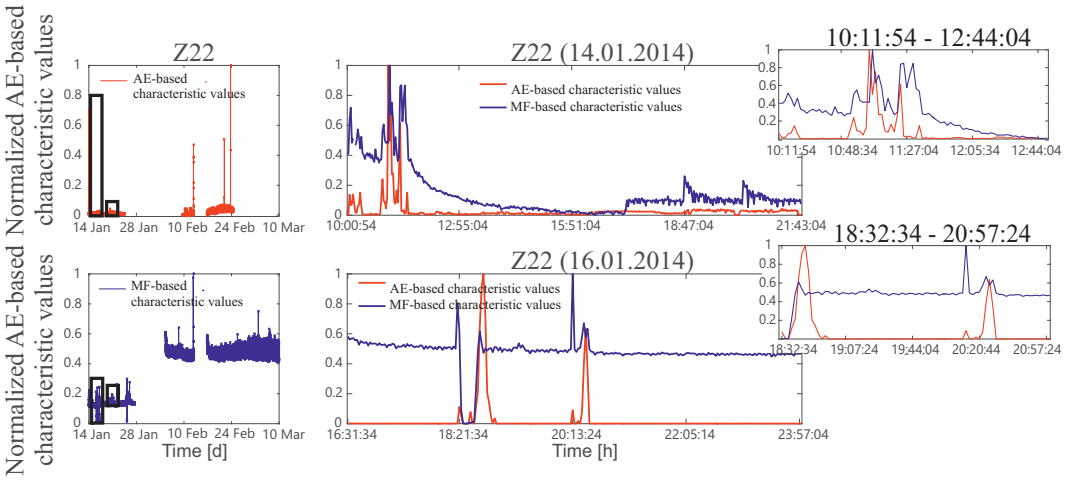

Figure 4.8: Comparison of AE and hydraulic data (Z22): complete measurements captured over service time (left side) and detail insight into the data (right side) [BRS16]

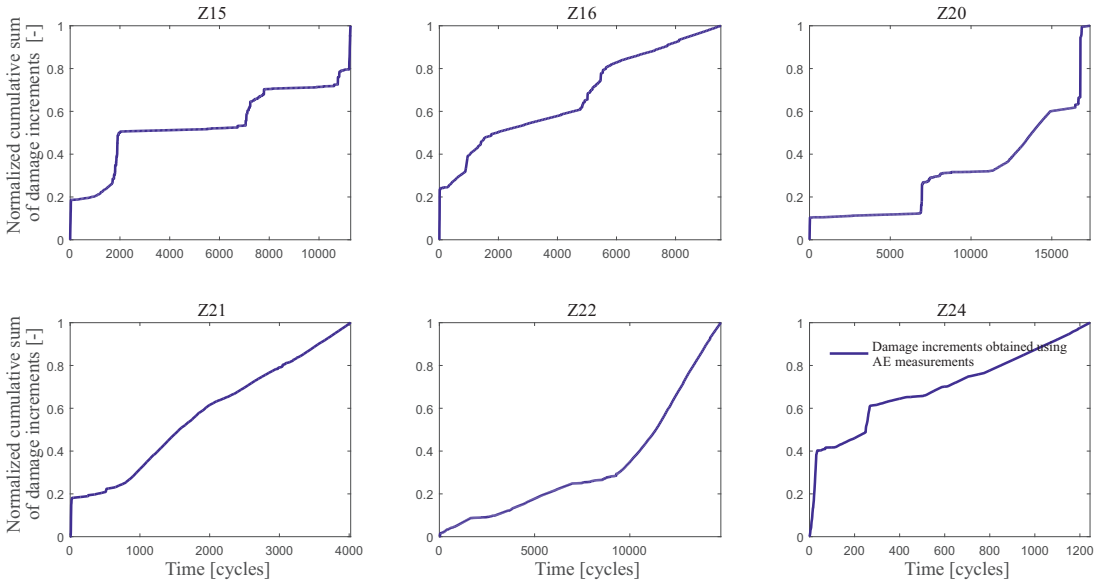

Figure 4.9: Normalized cumulative sum of damage increments obtained using AE measurements

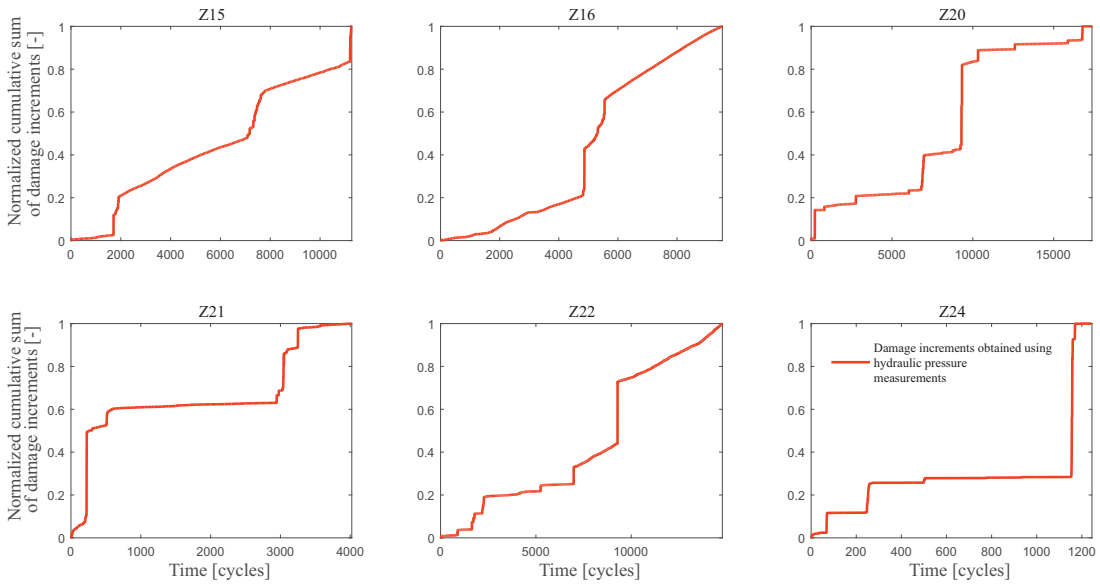

Figure 4.10: Normalized cumulative sum of damage increments obtained using hydraulic pressure measurements

4.2.3 Lifetime models optimization

4.2.3.1 Model Type I

Optimization algorithm used to find optimal set of (a_k, b_k) parameters of *Model Type I* has in its basis Non-dominated Sorting Genetic Algorithm II. In this case, NSGA-II is not used in its original form proposed by Song [Son14] but is modified targeting to include linear relationship between model parameters into optimization algorithm. Complete optimization algorithm is depicted in Figure 4.11, whilst the modification of NSGA-II belonging to the inclusion of model parameters calculation in algorithm itself is depicted in Figure 4.12.

If a_k (or b_k) parameters are randomly selected, there would be theoretically a countless number of sets of (a_k, b_k) parameters which can be utilized into the model. By usage of randomly selected sets of (a_k, b_k) parameters, obtained results do not match to a high extent to experimental data sets used for model validation. Contrary to countless number of randomly chosen a_k and b_k parameters, the number of experimental data sets is finite and limited.

Beside model parameters optimization, an examination of the dependency of the number of training data sets on prediction accuracy obtained using *Model Type I* is discussed as integral part of model establishment and validation. The discussion about the dependency of model accuracy on the number of training data sets is carried out in Chapter 4.2.4.

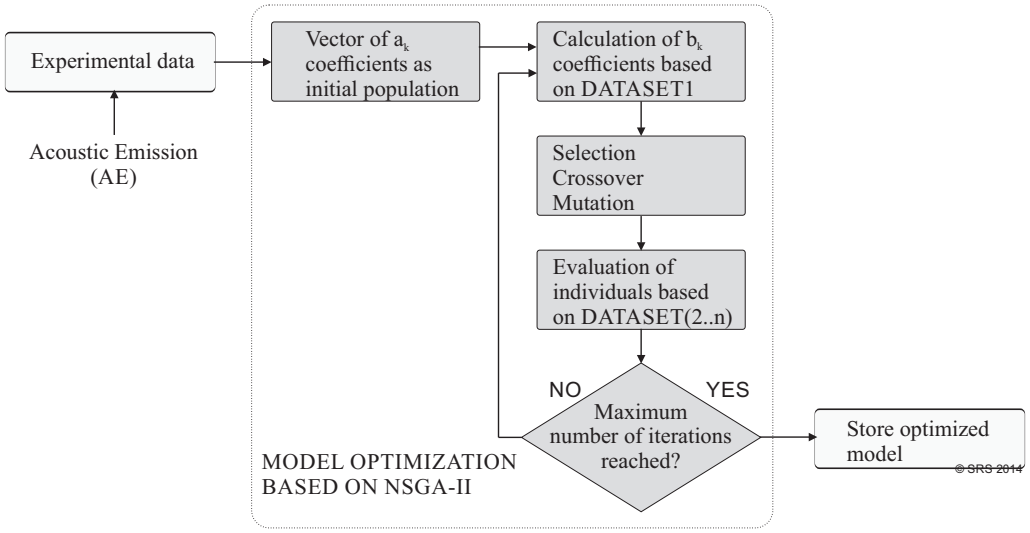

Figure 4.11: Optimization algorithm (based on [BS15b] and [BRS14])

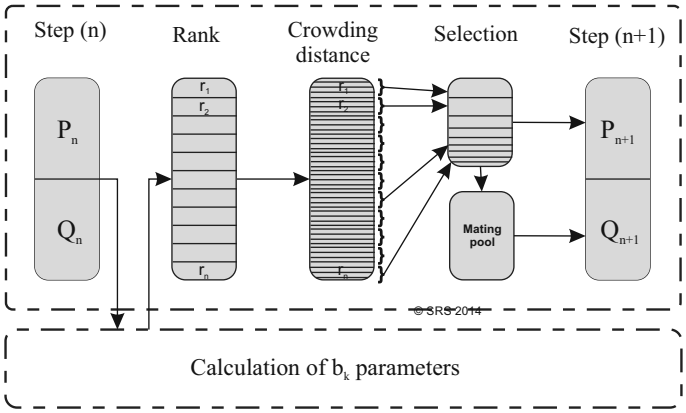

Figure 4.12: Modification introduced in NSGA-II

Accordingly, two different cases are studied concerning *Model Type I*. Firstly, the data used for model training includes two data sets of cumulative sum of damage increments (accumulated damage), whereas two additional data sets are used as test data sets. Secondly, the data used for model training is extended to four data sets, whereas two additional data sets are used as test data sets which are not used in training phase. Once the model parameters are optimized, these two cases are studied with respect to model prediction accuracy. Here, it is assumed that only a number of incomes of accumulated damage and predicted lifetime up to the certain time point are available (correlating to a part of monitored data). In such case the system is monitored up to time point T_N, but thereafter model input income correlated to damage increment remains either constant or as assumed up to the considered moment in time. Such an assumption does not reflect the situation in

practice as the damage increments vary with the time. The accuracy of prediction done in this manner, even though previously stated assumption lies behind, is analyzed to reveal whether obtained results may be satisfying with respect to prediction error. Prediction error has to be close to zero as the estimated and real values of accumulated damage in this case are almost identical.

Concretely, data sets Z15, Z20, Z21, and Z22 are stated as training data, whereas Z24 and Z16 are stated as test data sets which are not used during model optimization procedure. Additionally, different groups of four training data sets are utilized into model parameters optimization targeting to reveal dependencies of model prediction accuracy on different training data sets. Most of the data sets depicted in Figures 4.11 and 4.12 originate from test runs conducted under different operating conditions. As may be noticeable from Figures 4.11 and 4.12, the data sets are normalized to make the comparison of different data sets as well as model parameters optimization possible.

The effectiveness of optimization algorithm is firstly examined using two training data sets (here: Z20 and Z21) to explore whether the algorithm provides acceptable results with respect to prediction error. The arithmetic mean of Z20 and Z21 is calculated and used for b_k parameters calculation, whereas a_k parameters are randomly chosen as they represent a population generated using NSGA-II. The model established this way is validated using Z16 and Z24.

Afterwards, model parameters are optimized using four data sets, namely Z20, Z21, Z15, and Z22. Results obtained using two and four data sets for model parameters optimization are compared. For purposes of model parameters optimization, the arithmetic mean of Z20, Z21, Z15, and Z22 is calculated and used in a similar manner for b_k parameters calculation. The model validation is done using Z16 and Z24. Both models are compared with respect to prediction error, also in the case when not all measurement incomes are available. In addition, different groups of four data sets are selected and used to optimize model parameters.

4.2.3.2 Model Type II

Model parameters to be optimized with regards to *Model Type II* are a_{x0}-a_{x8}, where x denotes particular machine state. As previously emphasized, for four considered machine states total number of parameters to be optimized is 36. Characteristic values of AE-based features related to energy of AE signal are considered as input into *Model Type II*. As that, characteristic values of AE energy correspond to F_1 in equations from Table 4.1. However, indication of machine state change requires an information about last occurred damage increment, so that decreasing or increasing trend of AE-based feature can be recognized. It is important to note that this requirement is not identical as the requirement on the knowledge about all previous values of accumulated damage and consumed lifetime, as it is the case for *Model*

Type I. Thresholds tr_1, tr_2, tr_3, and tr_{DIFF} are in this case fixed and set to 0.4, 0.2, 0.1, and 0.2, respectively. Threshold tr_{DIFF} set to 0.2 indicates that the minimum change of 0.2 in input signal is required to consider state change. The data sets chosen as training data sets are, similarly as in previous case, Z21, Z22, Z15, and Z20. Data sets used as test data sets are Z16 and Z24. Data sets used for detailed model validation for all three models are identical, so that the comparison of results concerning these three models is possible. Identically as for *Model Type I*, different groups of four data sets are selected and used to optimize model parameters. In these terms, the comparison of the dependency between training data sets and prediction error obtained using *Model Type I* and *Model Type II* is possible. However, the dependency of different number of data sets used for model training on prediction accuracy, as it is done for *Model Type I*, is not examined.

	a_{x0}	a_{x1}	a_{x2}	a_{x3}	a_{x4}	a_{x5}	a_{x6}	a_{x7}	a_{x8}
STATE 1	-0.122	0.247	-0.202	0.143	0.023	0.06	-0.310	-0.018	0.084
STATE 2	0.173	-0.178	0.365	-0.200	-0.039	-0.034	0.05	-0.16	0.315
STATE 3	0.075	0.21	0.263	0.113	-0.113	0.333	-0.122	-0.055	0.085
STATE 4	-0.084	0.298	-0.168	-0.103	-0.285	-0.384	0.014	0.155	-0.414

Table 4.3: Optimized parameters of *Model Type II* (based on [BS17])

Similarly as for *Model Type I*, the discussion about prediction accuracy under an assumption that only a part of AE measurements (actually their corresponding features) are available is presented in Chapter 4.2.4.2. Accordingly, timespan T_N up to which the incomes are available is varied by 10% of all available incomes, denoted as I_N, and discussed in terms of available incomes rather than correlated time scale framework. Damage increments after T_N are assumed as constant.

Model parameters optimization of *Model Type II* is done using NSGA-II, but in this case NSGA-II implementation in its original form is used. Optimized values of previously listed parameters in Table 4.1 are listed in Table 4.3.

4.2.3.3 Model Type III

Not characteristic values of AE-based features related to energy of AE signal but cumulative sum of characteristic values of AE-based features is considered as input into *Model Type III*. This feature correspond to F_2 in equations given in Table 4.2. Data sets used for model training are identical as for *Model Type I* and *Model Type II* (Z20, Z15, Z22, and Z21). The same test data sets (Z16 and Z24) are considered for detailed comparison of obtained results between all three proposed models. Moreover, different groups of four data sets are selected and used to optimize model parameters (here: identical groups of four data sets as are used within *Model Type I* and *Model Type II*). In these terms, the comparison of the dependency

between training data sets and prediction error obtained using all three proposed models is possible.

Conversely to *Model Type II* where thresholds are fixed, the thresholds integrated in *Model Type III* are concerned for optimization. As that, the thresholds are considered as integral part of *Model Type III*.

	b_{x0}	b_{x1}	b_{x2}	b_{x3}	b_{x4}	b_{x5}	b_{x6}
WITHOUT SIGNIFICANT CHANGE	-176 10e-5	3 10e-5	92 10e-5	103 10e-5	4 10e-5	67 10e-5	-207 10e-5
NOTICEABLE, BUT NOT SIGNIFICANT CHANGE	12 10e-5	-57 10e-5	165 10e-5	-170 10e-5	71 10e-5	166 10e-5	75 10e-5
SIGNIFICANT CHANGE	85 10e-5	100 10e-5	-253 10e-5	-208 10e-5	-236 10e-5	-254 10e-5	255 10e-5

Table 4.4: Optimized parameters of *Model Type III* - Part I (based on [BS17])

	b_{x7}	b_{x8}	tr_1	tr_2	tr_3	T_{DIFF}
WITHOUT SIGNIFICANT CHANGE	248 10e-5	-162 10e-5				
NOTICEABLE, BUT NOT SIGNIFICANT CHANGE	142 10e-5	-301 10e-5	0.5988	0.6931	0.5903	0.9094
SIGNIFICANT CHANGE	-300 10e-5	-108 10e-5				

Table 4.5: Optimized parameters of *Model Type III* - Part II (based on [BS17])

According to Table 4.2, among model parameters to be optimized are found thresholds tr_1, tr_2, tr_3, and t_{DIFF} and they are integrated into optimization procedure. Model parameters stated as b_{x9}, b_{x10}, b_{x11}, and b_{x12} are in Table 4.2 listed as thresholds tr_1, tr_2, tr_3, and tr_{DIFF}, respectively. As such, it is possible to differentiate model parameters related to mathematical equations and those ones related to the thresholds. This gives in total 31 model parameters, where 24 of them belong to the parameters of mathematical equations accompanied to a particular deterioration level and 4 of them belong to the thresholds.

It is important to state that the threshold tr_{DIFF} is used to indicate whether deterioration level has even been changed. As previously stated, deterioration levels are recognized as different states: i) the state without significant change in lifetime

consumption, ii) the state with noticeable, but not significant change in lifetime consumption, iii) and the state with significant change in lifetime consumption.

According to values of optimized model parameters for *Model Type III* listed in Tables 4.4 and 4.5, it may be noticed that optimized value of threshold tr_{DIFF} is set to 0.9094 (where $tr_{DIFF} = 1$ is maximum allowed value due to normalized input values to 1). This means that the change of deterioration level is prevented and input/output relation is mostly modeled using only one mathematical equation from Table 4.2. For optimization purposes, thresholds tr_1, tr_2, tr_3 have to be given in ascending or descending order. Thresholds given in such order prevent optimization algorithm to be stacked in local minimum.

4.2.4 Experimental results

The results obtained using three proposed modeling approaches are discussed in terms of tracking: i) absolute error between estimated and experimental data sets, and ii) prognostic error under the assumption that not all measured model input incomes (extracted features) are available. Modeling approaches are at first discussed individually. At last, all three models are compared using Root Squared Error (RSE) and Mean Squared Error (MSE) measures. The dependence of model accuracy on the number of data sets used for model training is discussed in detail only for *Model Type I*, whilst the dependence of model accuracy on different groups of data sets used for model training is given for all three models. Advantages and disadvantages of each particular modeling approach is given at the end of Chapter 4.

4.2.4.1 Model Type I

The results obtained using NSGA-II based optimization algorithm and two data sets as training data sets (Z20 and Z21) are depicted in Figure 4.13.

In the upper diagram, training data sets Z20 and Z21 with accompanying estimated lifetime are depicted, whilst model validation using Z24 and Z16 is illustrated in the lower diagram. By analyzing the discrepancy between estimated and experimental training data sets (Z20 and Z21), high congruency between estimated and experimental data sets is noticeable providing low prediction error. As both data sets are used in training phase, such a low prediction error is also expected. By model validation using Z24 as well as Z16, prediction error is far beyond acceptable limits.

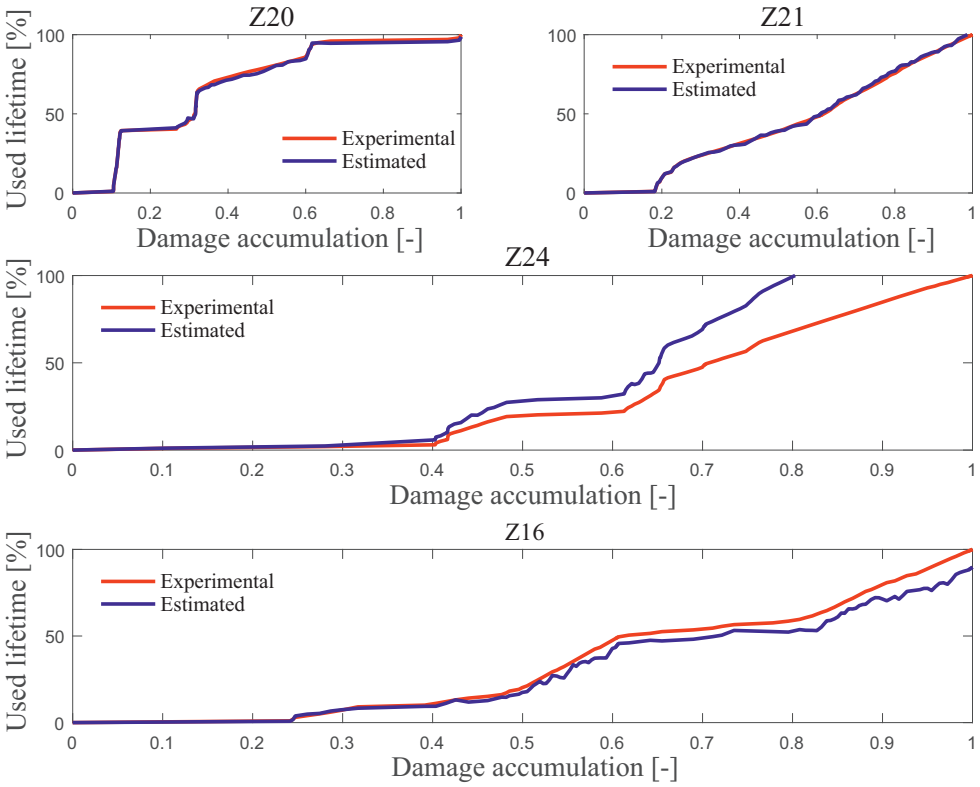

Figure 4.13: Model parameters optimization using Z20 and Z21 - *Model Type I* (based on [BS15b] and [BRS14])

Identical optimization procedure is applied to extended number of training data sets, namely Z20, Z21, Z15, Z22, and the results are illustrated in Figure 4.14. In the upper diagrams, the data sets used in model training phase with their accompanying estimated results (estimated/predicted lifetime) are depicted. Similar to previously discussed case, the discrepancy between estimated and experimental lifetime is here low providing prediction error which tends to zero. In the diagram bellow, the results of model validation using Z24 and Z16 are shown. Unlike the previous case, the discrepancy between estimated and experimental data sets, corresponding to prediction error, is close to zero. It can be stated that the more data sets are available for model optimization, the more precise is the prediction. Otherwise noted, the model becomes capable to capture the changes in the system over time. Model accuracy is thus significantly dependent on the number of data sets used in training phase.

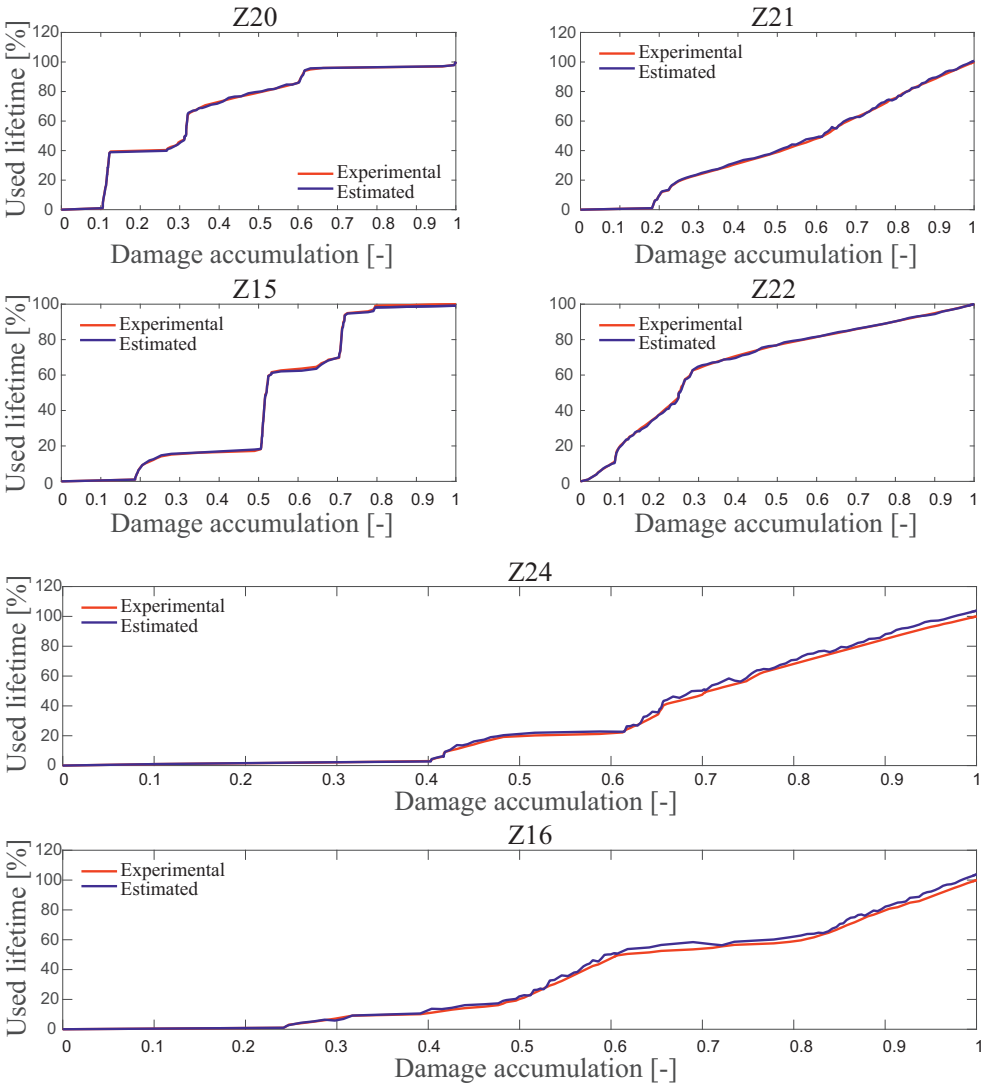

Figure 4.14: Model parameters optimization using Z20, Z21, Z15, and Z22 - *Model Type I* (based on [BS15b] and [BRS14])

The difference between aforementioned cases is clearly seen from the analysis of prediction errors. For these purposes, absolute deviation between estimated and experimental data sets is depicted in Figure 4.15. The maximum error obtained in the first case is 46.1504, whereas the same error is drastically decreased by increasing the number of data sets used in training phase, namely to 3.1136.

Notwithstanding the number of used data sets, it is often the case in practice that only a part of monitored data are available (for instance: when SHM is done in-situ or when diagnosis/prognosis models and algorithms have to cope with the data captured/monitored in real-time). Due to this, a number of assumptions have to be taken into account which may significantly aggravate lifetime prediction.

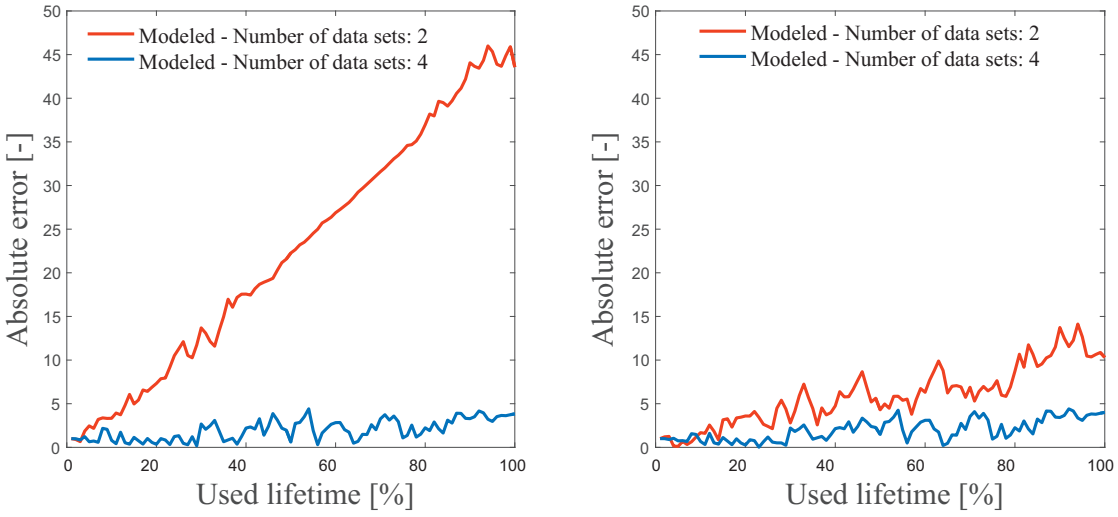

Figure 4.15: Absolute error - *Model Type I*

If the system is monitored up to the certain moment in time, the measurements only up to this moment are available, but thereafter the expected but still not captured data have to be assumed. Herein, an assumption considers that those incomes are held constant, as shown in Figures 4.16 and 4.17 for Z24 and Z16 test data sets. Assumed moments in time up to which the system is monitored are related to the time moments in which 10%, 20%, 30%, 40%, 50%, 60%, 70%, 80%, and 90% of all available incomes are available. Prediction of consumed lifetime obtained under the assumption that damage increments gathered after above mentioned time moments are constant, is shown in Figures 4.16 and 4.17.

According to presented results, it is shown that the closer the system is to its End-of-Lifetime, the prediction becomes more accurate. These results can be justified by a fact that a lesser timespan has to be estimated in such a case and the error occurred at the beginning, when only less number of available incomes are present, is not propagated and accumulated over time. For instance, if 50% of the lifetime has already passed, then the rest of 50% has to be estimated. Correspondingly, if 90% of the lifetime has passed, the rest of only 10% has to be estimated. In Figures 4.16 and 4.17, experimental as well as estimated results determined using two or four data sets and different number of available incomes are shown.

In addition, the prediction of End-of-Lifetime referring to above listed points in time are in detail depicted in Figure 4.18 and listed in Table 4.6. In Figure 4.18, an area around the End-of-Lifetime is zoomed targeting to provide the possibility for detailed analysis of discrepancies between expected (experimental) and estimated lifetime as well as its dependencies on the number of available incomes. As may be seen, the model trained using two training data sets exhibits higher prediction error in comparison with the model trained using four training data sets. Fur-

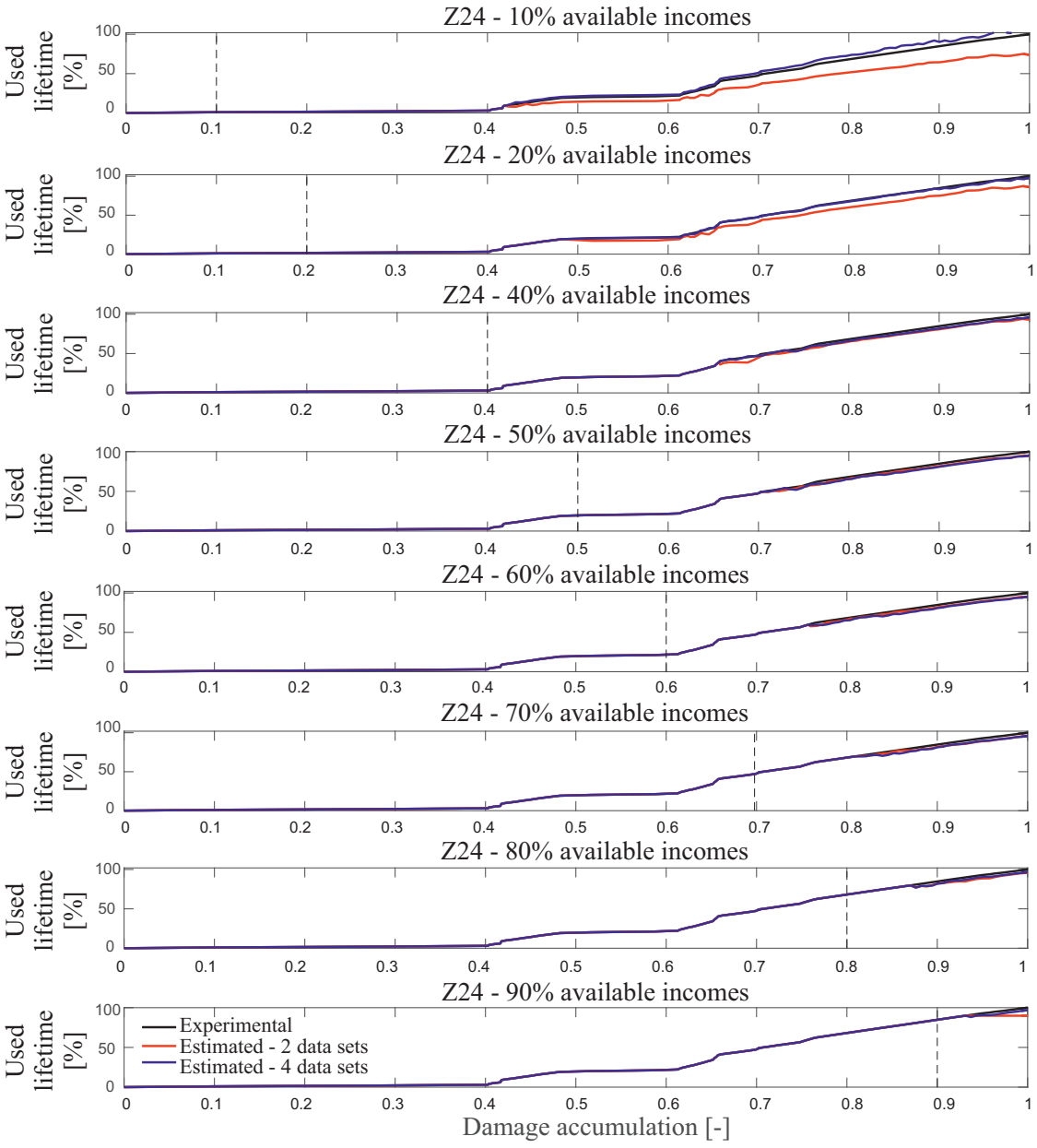

Figure 4.16: Prognosis of lifetime concerning varying number of incomes for Z24 - *Model Type I* (based on [BS15b])

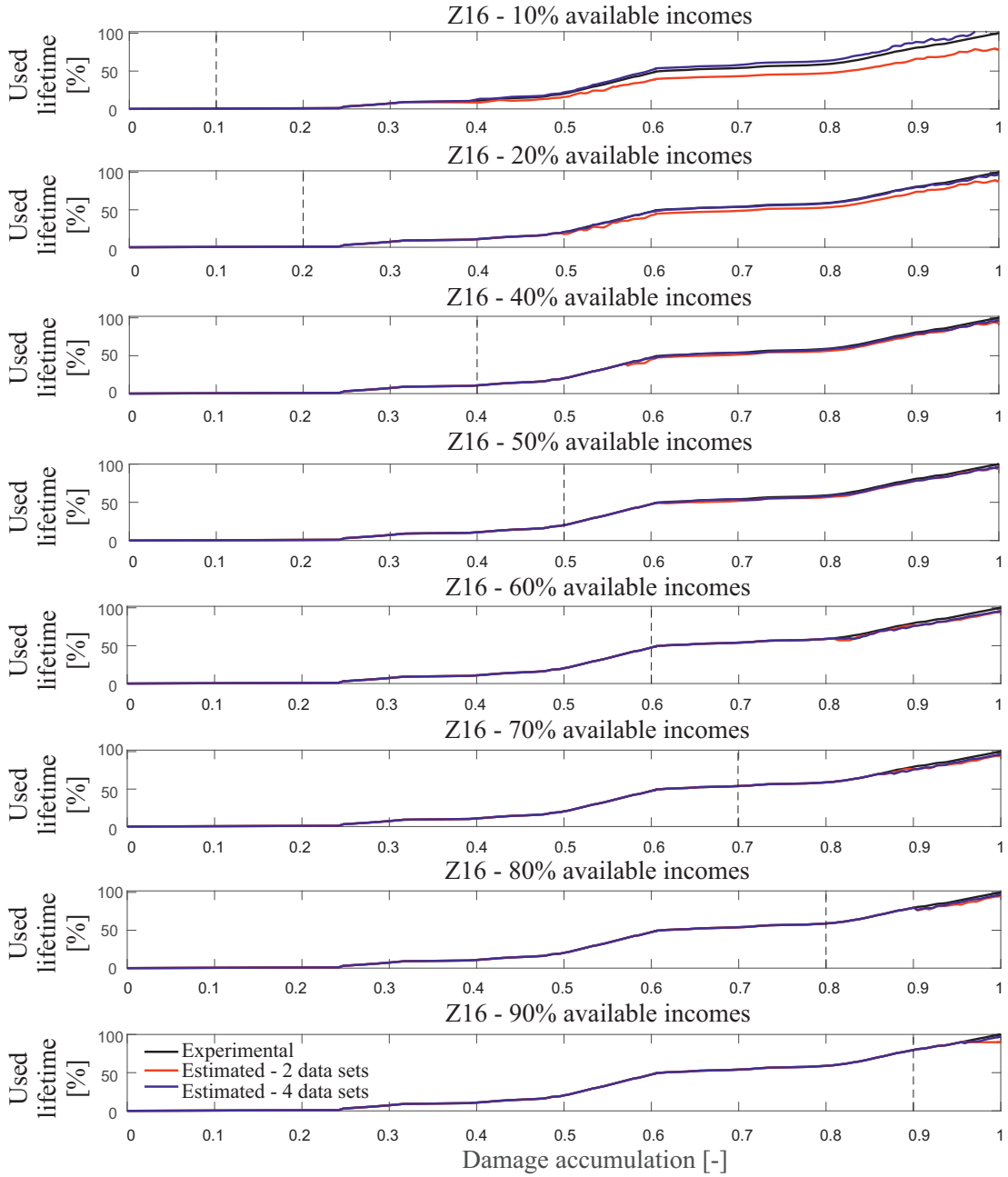

Figure 4.17: Prognosis of lifetime concerning varying number of incomes for Z16 - *Model Type I*

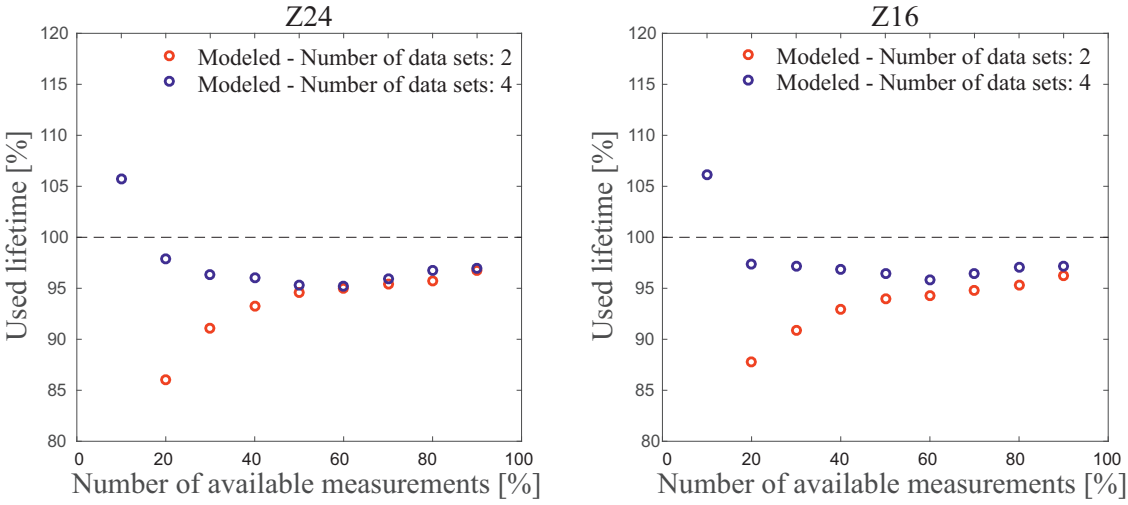

Figure 4.18: Prediction of End-of-Lifetime concerning different number of available incomes - *Model Type I* (based on [BS15b])

I_N	End-of-Lifetime Two data sets*	End-of-lifetime Four data sets*	ABS(error) Two data sets*	ABS(error) Four data sets*
10	73.7942/77.9185	105.7259/106.1183	26.2058/22.0815	5.7259/ 6.1183
20	85.9867/87.8158	97.8816/97.4123	14.0133/12.1842	2.1184/ 2.5877
30	91.0870/90.8732	96.3549/97.1289	8.9130/9.1268	3.64516/ 2.8711
40	93.2166/92.9847	96.0823/96.8704	6.7834/7.0153	3.9177/ 3.1296
50	94.5576/93.9307	95.2869/96.4087	5.4424/6.0693	4.7131/ 3.5913
60	94.9681/94.3074	95.2484/95.8420	5.0319/5.6926	4.7516/ 4.1580
70	95.4058/94.8123	95.9532/96.4219	4.5942/5.1877	4.0468/ 3.5781
80	95.7393/95.2922	96.7421/97.0402	4.2607/4.7078	3.2579/ 2.9598
90	96.7169/96.2472	96.9264/97.1807	3.2831/3.7528	3.0736/ 2.8193

* First values in cells correspond to the results related to Z24, whereas second values correspond to the results related to Z16.

Table 4.6: *Model Type I*: End-of-Lifetime prediction error in dependence of available number of incomes (based on [BS15b])

ther, EoL prediction error is in general higher with a lower number of available incomes. For instance, if the point in time at which the number of measured incomes reach 10% of all available incomes along with the model trained using two and four training data sets is considered, prediction error is 26.2058/22.0815 (ca. 25% of lifetime) and 5.7259/6.1183 (ca. 6% of lifetime) for both test data sets, respectively. End-of-Lifetime prediction error obtained using the model trained with two and four training data sets along with considered time point at which the number of measured incomes reach 80% of all available incomes is 3.2579/2.9598 (ca. 3% of lifetime), respectively. End-of-Lifetime prediction error obtained for 80% of all available incomes along with prediction error obtained for 90% of available incomes is the lowest EoL prediction error achieved using *Model Type I*. This shows only that the value of damage increment captured at the moment when 80% of available incomes is reached, is close to real (experimental) value of damage increment.

The trend of error change is clearly pointed out in Table 4.6. At first glance, it becomes noticeable that the trend of error change is not monotonic as the deviation between assumed and real (experimental) values of damage increments captured at certain time moments vary (and do not exhibit monotonic behavior). However, prediction results obtained in both of cases follow similar pattern.

4.2.4.2 Model Type II

The results obtained using *Model Type II*, model parameters optimization using NSGA-II in its original form, and four data sets as training data sets are depicted in Figure 4.19. In the upper diagrams in Figure 4.19, the data sets used for model training (Z15, Z20, Z21, and Z22) along with accompanied estimated lifetime are depicted. In the lower diagrams, data sets used for model validation along with their accompanied estimated lifetime are shown. Identical as for *Model Type I*, the discrepancy between estimated and experimental data sets concerning training data sets is low, but the same is valid also for validation data sets which are not used in training phase. This proves that lifetime modeling using proposed model gives satisfying results with respect to prediction error.

The discrepancy between estimated and experimental data sets is clearly visible in Figure 4.20, where absolute error between experimental and estimated lifetime is depicted. Maximum error obtained for test data set Z24 is 1.5, whereas absolute error for test data set Z16 equals to 1.05. As may be noticeable from Figure 4.20, there is no visible pattern or trend of change of prediction error, but absolute values obtained for *Model Type II* are much lower in comparison with the results obtained for *Model Type I*. Maximum value of absolute error in this case is 1.5, whereas absolute error concerning *Model Type I* equals 47.

The results obtained under an assumption that only a part of measured data (extracted features) are available, are depicted in Figures 4.21 and 4.22. Damage increments after predefined number of considered incomes is reached, are held constant.

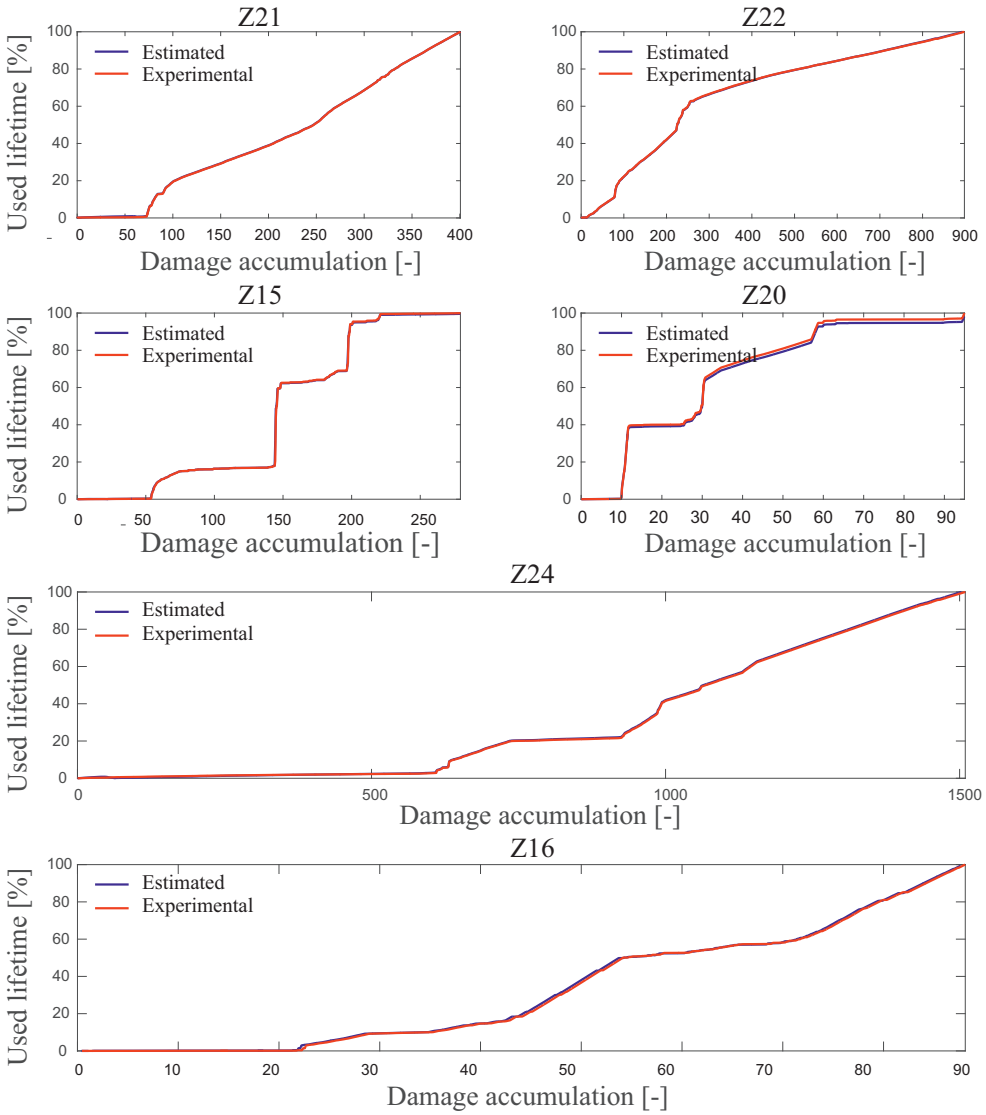

Figure 4.19: Model parameters optimization using Z20, Z21, Z15, and Z22 - *Model Type II* (based on [BS17])

Even this case is rarely occurred in practice, model evaluation and examination of model applicability for prognosis purposes on such a way is still possible.

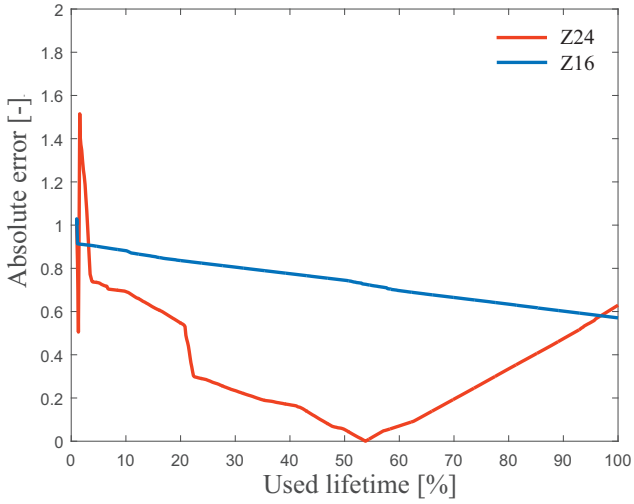

Figure 4.20: Absolute error - *Model Type II*

It may be noticeable that even in case when only 10% of all available incomes are available, prediction error is not too high but rather negligible. It may be concluded that the number of available incomes has no significant impact on prognostic error. This can be justified by the fact that active machine state at inspected moment in time is simultaneously real machine state of upcoming incomes. In addition, some machine states (as for instance 3 and 4) are similar and therefore can be modeled by similar mathematical equation. Under assumption that damage increments are constant, machine state would also be constant and probably wrongly determined. Error occurred in machine state recognition may be compensated through the model (in most of cases, according to Figures 4.21 and 4.22). Exactly this case can be clearly seen in Figure 4.21 in the second diagram for 20% of available incomes. The deviation between estimated and experimental lifetime is mainly caused by wrong determination of machine state which has to be compensated by proposed model.

As prediction error is not clearly seen from Figures 4.21 and 4.22, the detail insight into End-of-Lifetime prediction error is given in Figure 4.23. The End-of-Lifetime prediction error obtained using *Model Type II* is close to zero as predicted/estimated End-of-Lifetime is equal or close to experimental End-of-Lifetime (here: 100%). The trend of error change in dependence on the number of available incomes does not change monotonically, and has sudden increase in some cases (for instance: 20% of available incomes for Z24, as previously stated). Minimum End-of-Lifetime prediction error according to Table 4.7 is obtained for 40% of available incomes for Z24 but is in general much smaller in comparison with the one obtained using *Model Type I*. The deviation between experimental and estimated EoL lifetime is thus low.

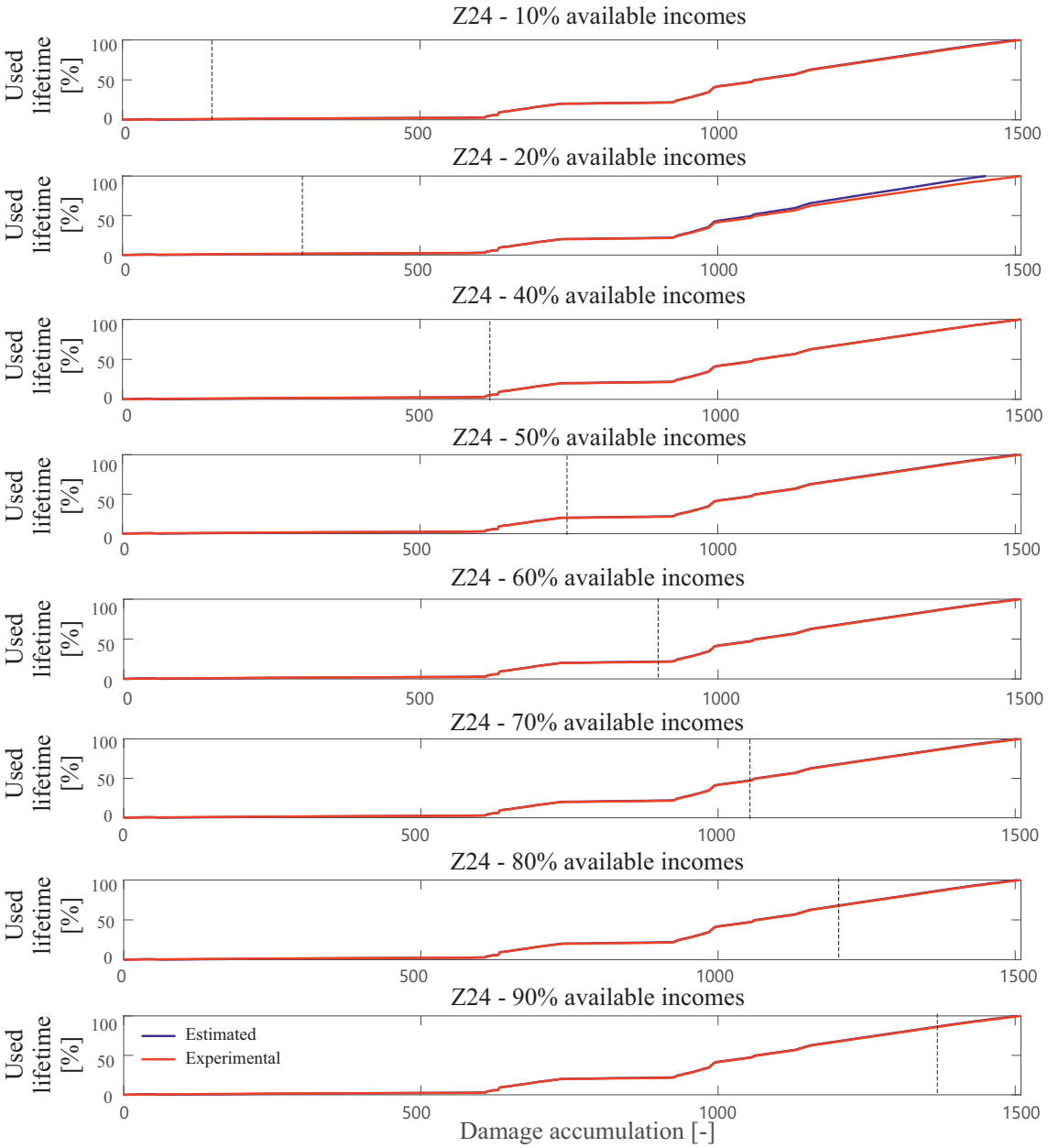

Figure 4.21: Prognosis of lifetime concerning varying number of incomes for Z24 - *Model Type II* (based on [BS17])

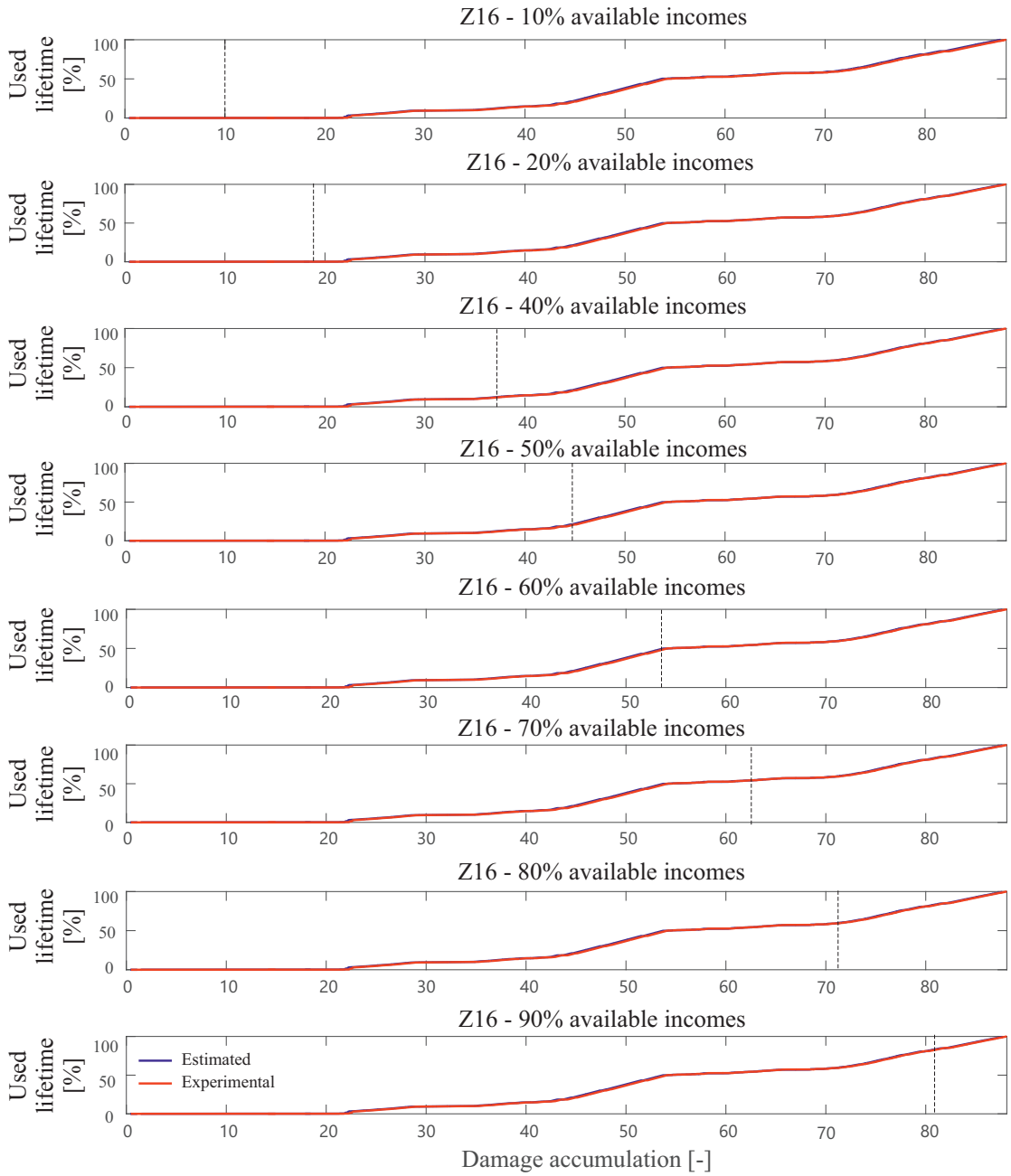

Figure 4.22: Prognosis of lifetime concerning varying number of incomes for Z16 - *Model Type II* (based on [BS17])

I_N	End-of-Lifetime Z24	End-of-lifetime Z16	ABS(error) Z24	ABS(error) Z16
10	100.79	100.25	0.78979	0.24685
20	106.03	99.407	6.0316	0.59333
30	100.25	99.405	0.25166	0.59515
40	100.07	99.405	0.074142	0.59514
50	100.67	99.405	0.67466	0.5948
60	100.41	99.424	0.41302	0.57567
70	100.61	99.43	0.61177	0.57023
80	100.61	99.428	0.61376	0.57249
90	100.62	99.429	0.61962	0.57103

Table 4.7: *Model Type II*: Prediction error in dependence of available number of incomes (based on [BS17])

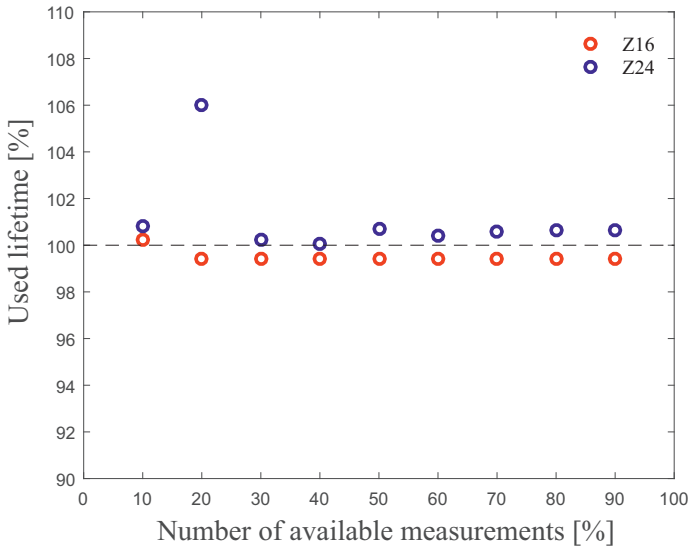

Figure 4.23: Prediction of End-of-Lifetime concerning different number of available incomes - *Model Type II*

4.2.4.3 Model Type III

Conversely to *Model Type II* where AE-based damage increments are used as input into the model, input into model *Model Type III* is cumulative sum of damage increments (AE-energy related characteristic values). The same experimental training data sets as for *Model Type I* and *Model Type II* are used to optimize model parameters, namely Z21, Z22, Z15, and Z20. Test data sets used for *Model Type III* parameters optimization are Z16 and Z24. Multi-objective optimization of model

parameters is carried out using Non-dominated Sorting Genetic Algorithm II in its original form. Principally, objectives integrated in NSGA-II are deviations between particular estimated and experimental data sets. Results obtained using *Model Type III* are depicted in Figure 4.24.

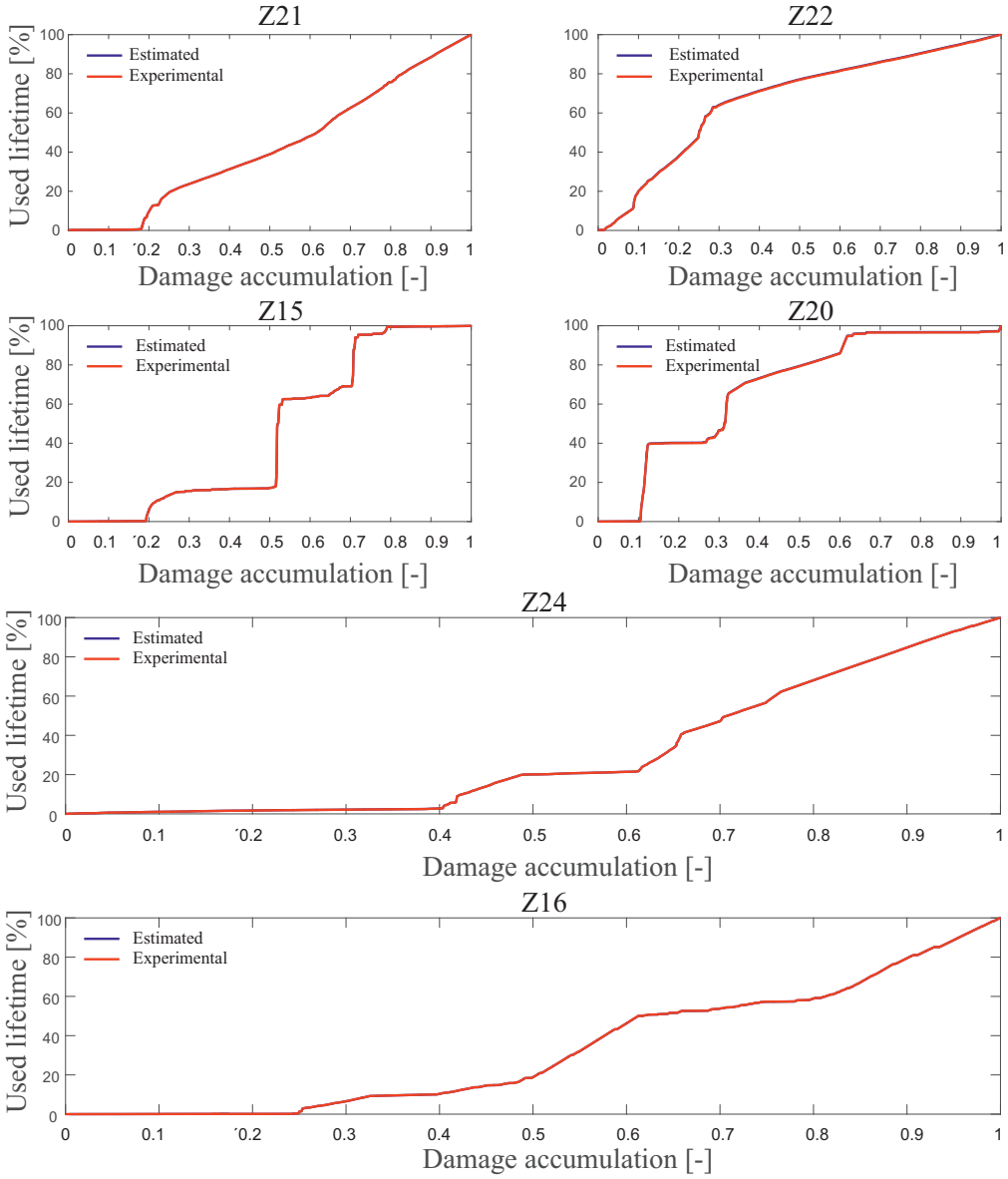

Figure 4.24: Model parameters optimization using Z20, Z21, Z15, and Z22 - *Model Type III* (based on [BS17])

In the upper four diagrams of Figure 4.24, training data sets and their associated estimated values are depicted. In the lower two diagrams of Figure 4.24, test data sets along with their accompanying estimated lifetime are visualized. Results obtained

using *Model Type III* show low discrepancy and satisfying degree of congruency between estimated and experimental data sets. Estimation error for both evaluation data sets is close to zero and can in turn be considered as negligible.

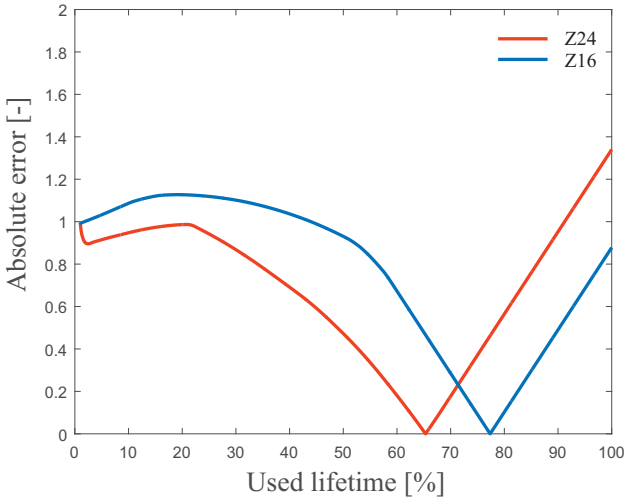

Figure 4.25: Absolute error - *Model Type III*

Absolute errors for both validation data sets are depicted in Figure 4.25. It is noticeable that maximum obtained absolute error using Z24 amount to ca. 1.3 occurred at the End-of-Lifetime (100% of lifetime). Absolute error concerning Z16 is less and amounts nearly to 1.8 at 20% of lifetime. In comparison with the same results obtained using *Model Type I*, much better congruency between estimated and experimental data sets is achieved. Conversely, slightly better results are achieved using *Model Type III* in comparison with the results obtained using *Model Type II*.

Identically as for *Model Type I* and *Model Type II*, the assumption that only a part of data are available is taken in consideration. Number of available incomes is varied by 10% of all available incomes and the results are depicted in Figures 4.27 and 4.28 concerning Z24 and Z16, respectively. According to the results illustrated in aforementioned figures, not significant impact of the number of available incomes to prediction error is noticeable. As that, high dependency of model accuracy to the number of available incomes is noticeable only by using *Model Type I*, whereas nearly the same results are obtained by using *Model Type II* and *Model Type III*.

End-of-Lifetime prognostic error is compliant with the results depicted in Figures 4.27 and 4.28. According to Figure 4.26 and Table 4.8, the trend of prognostic error here does not have monotonic character. Minimum prognostic error of End-of-Lifetime is obtained for 60% of all available incomes and test data set Z24 according to Table 4.8, and maximum for 30% of all available incomes and test data set Z16. Mean value of prognostic error is close to 1, what means that the estimated and experimental values match to a high extent.

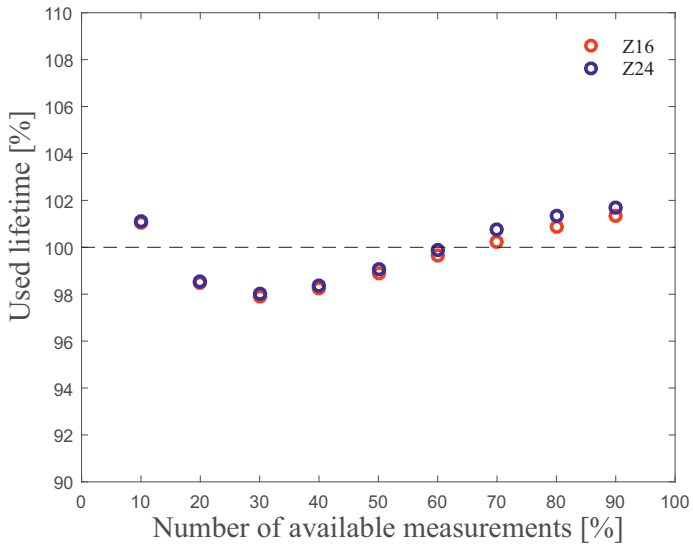

Figure 4.26: Prediction of End-of-Lifetime concerning different number of available incomes - *Model Type III*

I_N	End-of-Lifetime Z24	End-of-lifetime Z16	ABS(error) Z24	ABS(error) Z16
10	101.09	101.03	1.0868	1.0263
20	98.539	98.477	1.4615	1.5226
30	98.041	97.93	1.9589	2.0702
40	98.37	98.235	1.63	1.7653
50	99.052	98.914	0.94763	1.0865
60	99.911	99.639	0.089367	0.3607
70	100.75	100.26	0.74546	0.2602
80	101.34	100.88	1.3401	0.87785
90	101.7	101.37	1.7007	1.369

Table 4.8: *Model Type III*: Prediction error in dependence of available number of incomes

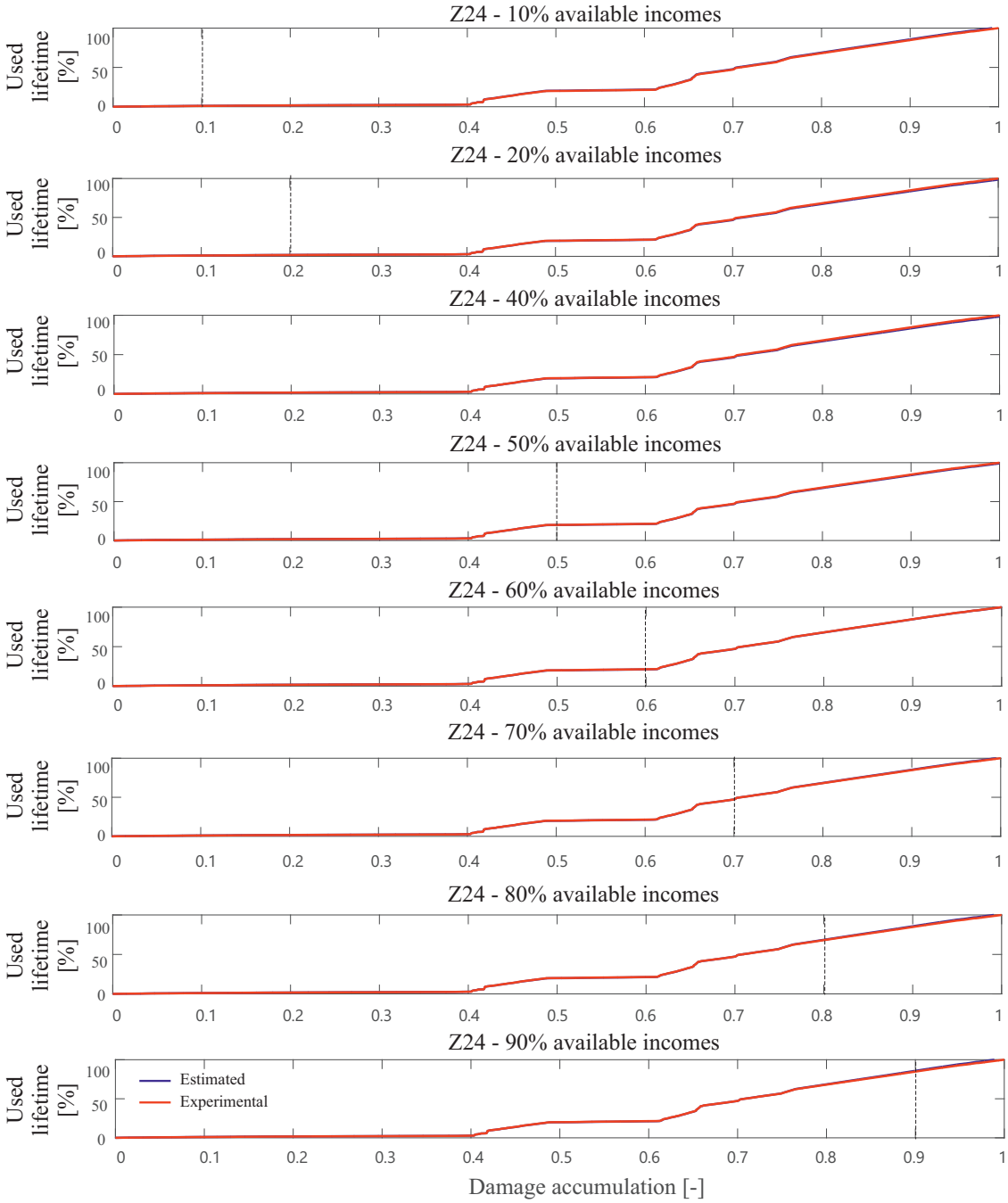

Figure 4.27: Prognosis of lifetime concerning varying number of incomes for Z24 - *Model Type III* (based on [BS17])

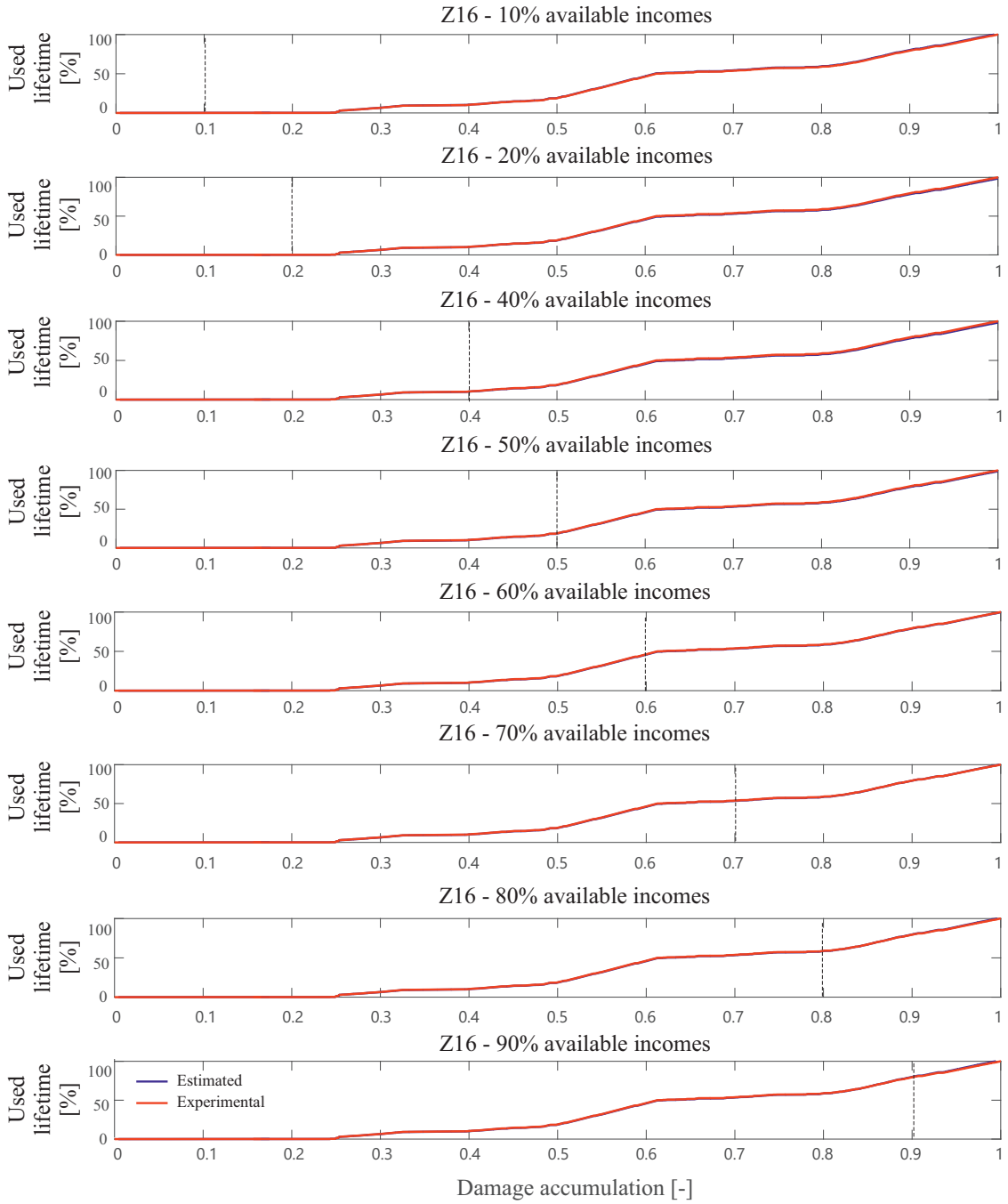

Figure 4.28: Prognosis of lifetime concerning varying number of incomes for Z16 - *Model Type III* (based on [BS17])

4.3 Discussion of obtained results

In Chapter 4, the deterioration processes related to metallic structures are discussed in terms of their initiation and propagation. With an intension to describe damage propagation of real time stressed tribological systems, AE and hydraulic pressure measurements are analyzed. Acoustic Emission measurements are utilized in the development of three different lifetime models, namely *Model Type I*, *Model Type II*, and *Model Type III*.

Along with calculation of absolute errors for each individual model presented in previous chapters, Root Squared Error (RSE) and Mean Squared Error (MSE) are calculated targeting to compare all three proposed models. These parameters (RSE and MSE) can be used as performance criterion revealing at the same time the accuracy of prediction obtained using particular model. Root Squared Error and Mean Squared Error are defined as

$$\begin{aligned} RSE &= \sqrt{\sum_{n=1}^{n} (estimated \quad value - experimental \quad value)^2} \text{ and} \\ MSE &= \sum_{n=1}^{n} \frac{(estimated \quad value - experimental \quad value)^2}{n}, \end{aligned} \tag{4.4}$$

respectively.

According to Table 4.9, a small difference in performance between *Model Type II* and *Model Type III* is noticeable, whilst the performance of *Model Type I* differs significantly from the performance of *Model Type II* and *Model Type III*. The results concerning *Model Type I*, *Model Type II*, and *Model Type III* presented in Table 4.9 belong to the models trained using four training data sets (Z15, Z20, Z21, and Z22). Taking in consideration obtained results, it may be concluded that *Model Type II* and *Model Type III* output slightly better results in comparison with *Model Type I*. Calculated values of MSE for *Model Type II* and *Model Type III* are close to zero. Such values of MSE correspond to a small prediction error and prove the capability of these two models to predict accurately consumed lifetime. Value of MSE concerning *Model Type I* is slightly higher, but still acceptable. Root squared error can be understood as a metrics similar to absolute error. As such, RSE gives a measure of the error accumulated over service lifetime.

Along with calculation of RSE and MSE, the dependency of used training/test data sets on prediction accuracy under the assumption that only a part of data is available for all three model is examined. The data sets used for model parameters optimization and model evaluation are given in Table 4.10. Model parameters obtained after model parameters optimization using different data sets for training and evaluation differ, but the deviation between estimated and experimental End-of-Lifetime is not high. For *Model Type I* the deviation between estimated and

	RSE - Z24	RSE - Z16	MSE - Z24	MSE - Z16
Model Type I	6296.5	6413.2	6.8996	6.6507
Model Type II	101.53	67.255	0.21109	0.092629
Model Type III	119.18	86.639	0.29087	0.15372

Table 4.9: RSE and MSE measures obtained using three different lifetime models and test data sets Z16 and Z24 (based on [BS17])

Data set Test run	Z15	Z16	Z21	Z22	Z24	Z20
1	Training	Test	Training	Training	Test	Training
2	Test	Test	Training	Training	Training	Training
3	Training	Training	Test	Test	Training	Training
4	Test	Training	Training	Test	Training	Training
5	Test	Training	Training	Training	Test	Training
6	Training	Training	Test	Training	Training	Test

TABLE 4.10: Selection of different groups of available data sets for model parameter optimization (based on [BS17])

experimental End-of-Lifetime regardless to used training/test data sets and number of available incomes equals to +/-10% of lifetime, whereas the deviation for *Model Type II* and *Model Type III* are +/-6% and +/-3% of lifetime, respectively. According to Figure 4.29, the lowest prediction error regardless of data sets used for training/test data sets are obtained for *Model Type III*.

The models exhibit different sensitivity to prediction error occurred at the beginning of service lifetime. Concerning *Model Type I*, prediction error once occurred is propagated and accumulated over whole operation period as the model is not capable to compensate the error. As that, resulting prediction error of *Model Type I* at the End-of-Lifetime is higher as it occurs earlier. Contrary, accumulation and propagation of error concerning *Model Type II* and *Model Type III* is not pronounced to that extent to which it is pronounced in *Model Type I*.

All three models have different characteristics concerning model complexity, model requirements, and model limitations. Common to all models is the requirement on suitable model parameters optimization algorithm. For model parameters optimization, experimental data sets are necessary. The data sets have to be enough diverse to reflect different operating conditions and varying behavior of the system with respect to different operating conditions. The number of model parameters for three proposed lifetime models differs and are closely related to model complexity. As that, *Model Type II* and *Model Type III* have much smaller number of model parameters in comparison with *Model Type I* and are therefore recognized as less complex in comparison to *Model Type I*. Further, *Model Type II* has a limitation

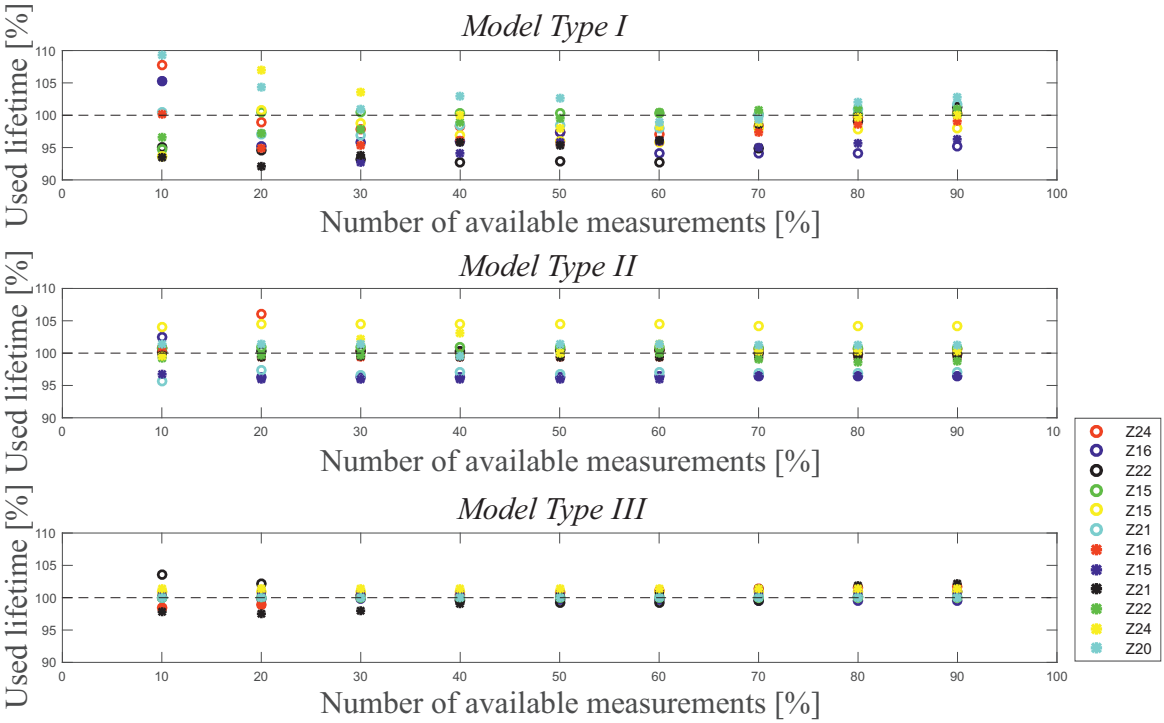

Figure 4.29: Examination of the dependency of training data sets on prediction accuracy (based on [BS17])

primarily reflected in its susceptibility to false determination of machine states (as discussed previously), whilst *Model Type I* has limitation related to a high number of model parameters. Due to this, *Model Type III* may be recognized as the least restrictive model of all proposed models.

According to presented results, all three lifetime models proposed in Chapter 4 are capable to predict End-of-Lifetime of considered tribological system with negligible error. Introduced models are thus capable to capture stochastically occurred changes in metallic structures often ensued under different operating conditions.

5 Diagnosis and prognosis of LIB based on experimental results

Lithium-Ion Batteries (LIBs) have shown enormous potential as energy storage devices primarily in transportation industry as well as solar and wind turbine conversion systems. Utilization of LIB in Electric Vehicles (EV)/Hybrid Electric Vehicles (HEV) and energy conversion systems can be justified by LIBs high energy density along with low weight and small size [SSST13] [STRC11]. The main problems are related to monitoring of State-of-Health of LIB batteries and to control of power flow between grid and storage elements, providing thereby efficient and optimized, with respect to LIB degradation, operation. The problem of LIB aging is even more pronounced for LIBs which are an integral part of wind turbine systems. Concerning intermittent and stochastic charging and discharging current profiles conditioned by intermittent and stochastic energy production as well as changeable grid requirements, modeling of LIB aging processes and optimization of LIB operation are necessary. In addition, Serrao et al. [SZK+14] state 20 years as a desired lifetime for LIBs integrated in WT system; much longer LIB lifetime than is desired for electric or hybrid electric vehicles.

According to the discussion in Chapter 2, measurable variables of lithium-ion batteries are charging/discharging currents, terminal voltage, and environmental temperature. Complexity of establishing a relation between aforementioned directly measurable system variables and degradation indicators (such as SoH, RUL, SoF, or degradation index) are detailed in Chapter 2. Taking in consideration the discussion from Chapter 2, the determination of degradation indicators requires the calculation or estimation of certain intermittent variables, whereas no direct correlation between measured variables and degradation parameters exist (Figure 5.1).

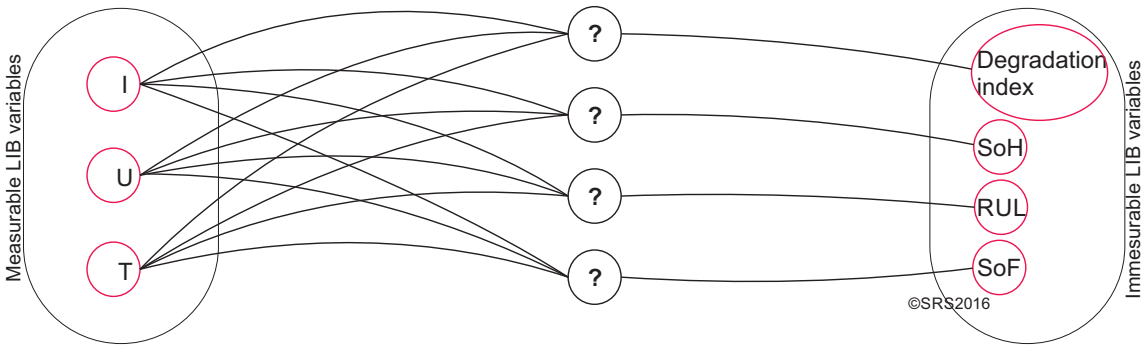

Figure 5.1: Indirect correlation of measurable (left side) and immeasurable degradation related (right side) LIB variables

The main idea introduced in Chapter 5 is to prove whether some directly measurable

system variables can be correlated to LIB degradation measures without calculation of intermittent variables, as depicted in Figure 5.2.

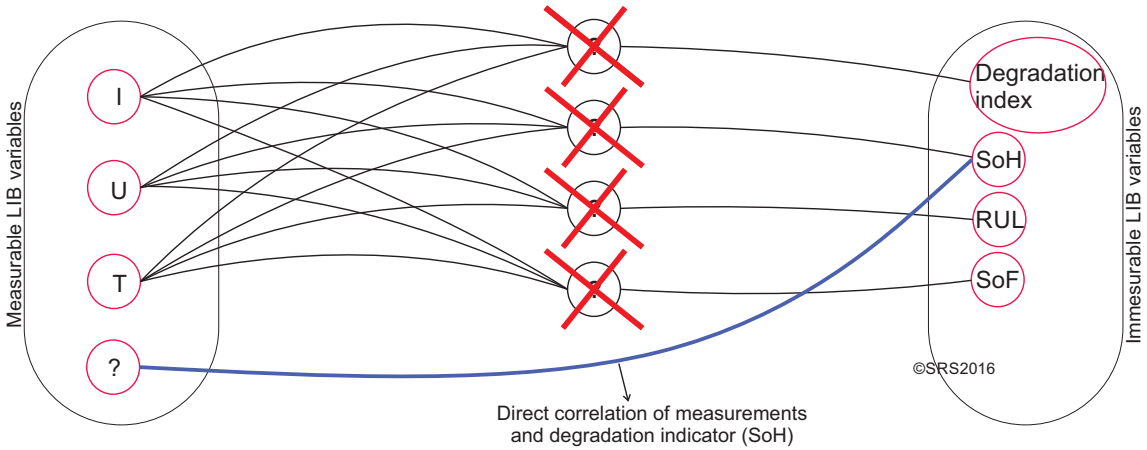

Figure 5.2: Problem statement: Direct correlation of measurable and immeasurable (degradation related) LIB variables [BS]

With respect to applicability of the tests carried out on conventional LIBs to an embedded LIB solutions mentioned above and predefined goals, a number of experimental tests are conducted with an intention to find direct correlation between measured variables and degradation indicators. According to aforementioned identified problems, the data captured during LIB aging tests are used for purpose of damage indicators identification and LIB lifetime modeling. Along with the measurements of terminal voltage, charging/discharging currents, and temperature, experimental setup includes measurements of AE signal whereas AE signal is correlated to LIB aging. Special attention is given to direct estimation of State-of-Health based exclusively on AE measurements, without the necessity for estimation of additional, mainly indirectly accessible, LIB parameters. Concerning this, lifetime modeling according to AE measurements is of main concern in Chapter 5. Some parts of this chapter are published in [BMS15] and [BS]. Inceptive steps towards LIB aging examination using AE measurements are done in [SB] and are partially used in this chapter.

5.1 Estimation of LIB damage indicators by means of AE measurements

Battery management systems, nowadays integrated in most commercial applications, have to provide both safe operation of LIB/system and optimized LIB performance with respects to the desired energy supplies and LIB aging. Targeting to meet aforementioned goals, the determination of SoH of LIB in a timely manner and under

varying operating conditions (hardly predictable charging/discharging profiles) is an inceptive step towards establishment of reliability-oriented operation of lithium-ion-based energy storage systems. Experiments conducted at University of Duisburg-Essen, Chair of Dynamics and Control include an examination of Acoustic Emission measurements utilization in direct SoH estimation [BS].

5.1.1 Experimental setup

Several experiments are conducted on lithium-ion batteries. Battery cells selected for experiments have nominal capacity of 10 Ah, nominal voltage of 3.7 V, maximum charging/discharging rates of 20/30 A, and operate in a temperature range between -10°C and +55°C.

Aging tests performed here entail successive charging and discharging of LIB. Charging currents are provided from Direct Current (DC) electrical source, which is controlled remotely and connected over low impedance switch module to the LIB. Connection to control station is implemented using DSPACE board which transfers control and measured operating signals to/from the test bench. As depicted in Figure 5.3, LIB are discharged using electric load. Electric load can provide discharging currents in range between 10 mA and 50 A. Here, discharging current of 30 A is used. End-of-Charge (EoC) voltage is considered as 4.2 V, whereas Depth-of-Discharge (DoD) voltage is considered as 2.7 V. The same operating conditions, namely charging/discharging currents, temperature range, and EoC and DoD voltages, are applied in all conducted experiments. Operating variables which are continuously monitored are charging/discharging currents as well as environmental temperature. In addition, measurements of elastic acoustic emission waves are utilized for purpose of continuous direct SoH monitoring. Measurement chain is similar to the one used for AE-based monitoring of tribological system [Det11].

The End-of-Life (EoL), as stated in Chapter 2, is defined as capacity decrease of 20%. Capacity decrease of 20% corresponds to the change of nominal capacity from 100% to 80%.

5.1.2 Testing procedure

As charging/discharging of LIB is long lasting process, the experiments have to be conducted under automated control and supervision of the tests. It is of high importance to emphasize that automated supervision sets at the same time high requirements on safety issues. Testing procedure implemented here includes basis tests, SoC-OCV tests, and CC-CV (Constant Current - Constant Voltage) tests, as illustrated in Figure 5.4. Such testing procedure is conducted to obtain the information about SoH indirectly. To estimate SoH indirectly, measurements from

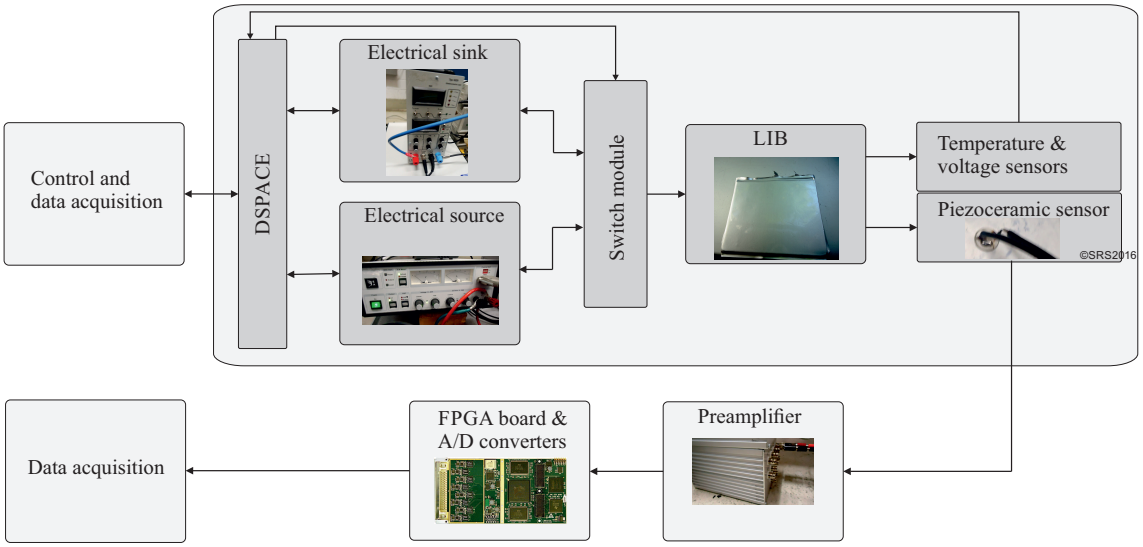

Figure 5.3: Test bench facility for LIB examination, Chair of Dynamics and Control, SRS, U DuE (based on [SB] and [BS])

basis tests as well as SoC-OCV tests can be used. State-of-Health estimated in such a manner is further used only to determine the point in time up to which the system is functional, and to compare whether the discrepancy between SoH obtained using AE-based measurements and the one obtained using indirect approach is low. Conversely to a number of existing indirect approaches towards SoH estimation, the SoH estimation using AE measurements is examined in terms of direct correlation of AE measurements to SoH. Under this assumption, AE-based measurements can be used as input into remaining useful lifetime model of LIB.

Basis test considers the analysis of voltage response of LIB under high-frequent discharging of LIB [Det11] [WZX09] [VPB07]. As previously discussed in Chapter 2, tracking of changes in ohmic and polarization resistance, as well as in LIB capacitance can be utilized for indirect SoH estimation.

The dependence of OCV on current charge amount (SoC) over time is not constant (as explained in detail in Chapter 2). This implies that SoH estimation by tracking changes in SoC-OCV curve is possible. The tests stated as SoC-OCV tests aim to determine SoC-OCV curve, which is understood as a prerequisite for SoH estimation. During SoC-OCV tests, fully charged battery is discharged with 3C over time period of 60 s, after which the LIB is in an idle mode in duration of 20 min. The battery is discharged in this manner until it reaches Depth-of-Discharge of 2.7 V.

Beside basis and SoC-OCV tests, accelerated aging of LIB is provided by CC-CV (Constant Current - Constant Voltage) tests. Successive charging and discharging of LIB is performed with charging and discharging rates of 2C and 3C, respectively. Contrary to basis tests where the LIB is charged up to End-of-Charge (4.2 V), the

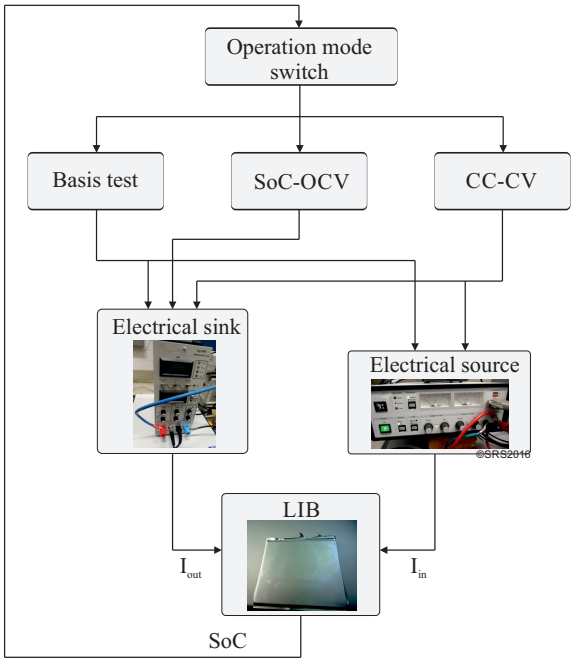

Figure 5.4: Testing procedure for LIB aging examination [BS]

charging of LIB during CC-CV tests is done until SoC reaches 4.3 V. Overcharging of LIB occurred in this case contributes to accelerated LIB aging. The value of DoD in comparison with basis tests is not changed (DoD = 2.7 V).

In this particular case, one aging cycle test consist of one basis test, one SoC-OCV test, and eleven CC-CV tests. Complete testing procedure is repeated up to the EoL of LIB.

5.2 Experimental results

The measurements of terminal voltage including basis tests, SoC-OCV tests, as well as CC-CV tests originating from three different tests, namely B8, B10, and B11, conducted under identical operating conditions are depicted in Figure 5.5.

At first glance, the changes in measurements of terminal voltage over time are noticeable. These changes are related primarily to a shorter time period in which SoC-OCV tests as well as CC-CV tests are performed. Otherwise noted, charging and discharging processes of LIB become faster as the LIB approaches to the EoL (for instance: SoC-OCV tests pointed out as red marked areas in Figure 5.5). This implies that aforementioned changes are closely related to LIB aging and as such are consistent with the explanation given in Section 5.1.2. According to [MFB+11], the reason for faster charging and discharging processes lies primarily in a loss of active lithium-ions in LIB.

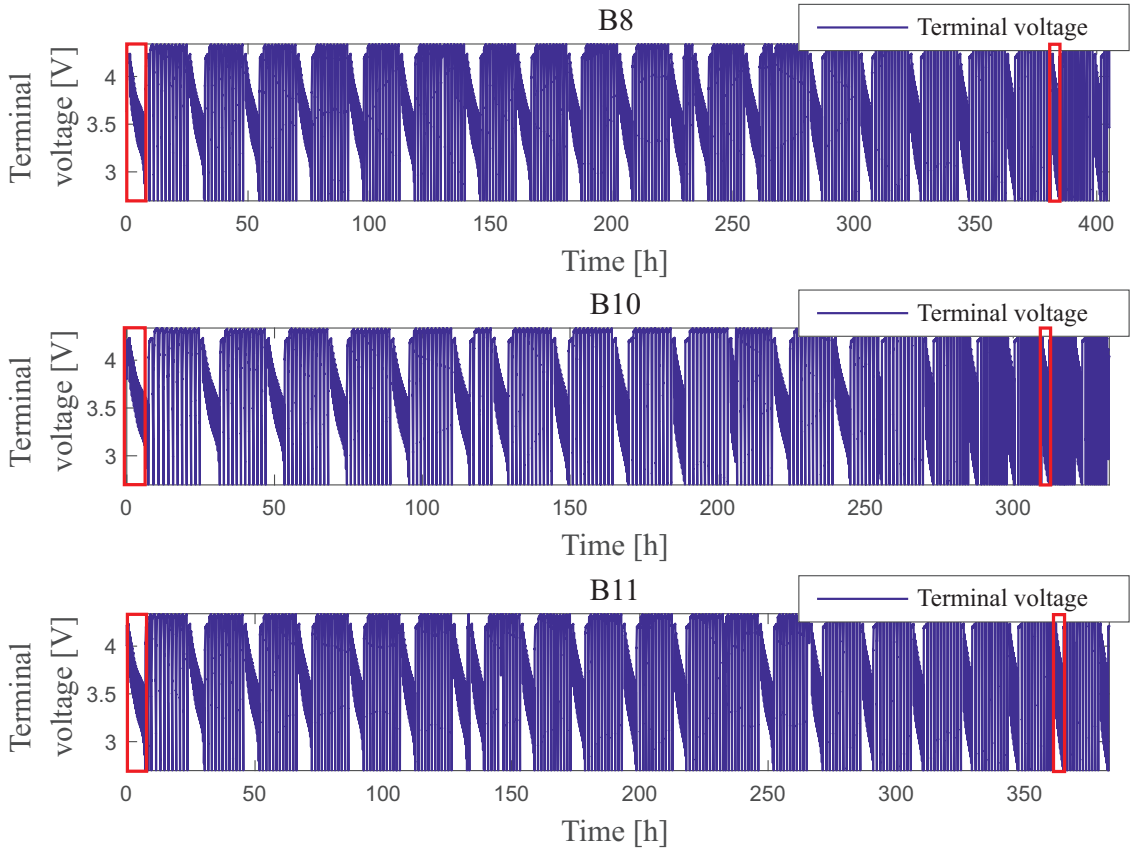

Figure 5.5: Terminal voltage measurements over complete testing procedure (B8, B10, B11)

Targeting to emphasize the change of charging profile of LIB at the beginning and at the end of life, more detailed illustration is given in Figure 5.6. According to Figure 5.6, it is clearly seen that the time period required to charge the LIB to EoC is shortened (at the beginning: $t_1 = 81.7373$ min and at the end: $t_2 = 66$ min). Moreover, it is noticeable that the voltage drop during basis tests becomes higher as the LIB is closer to its EoL.

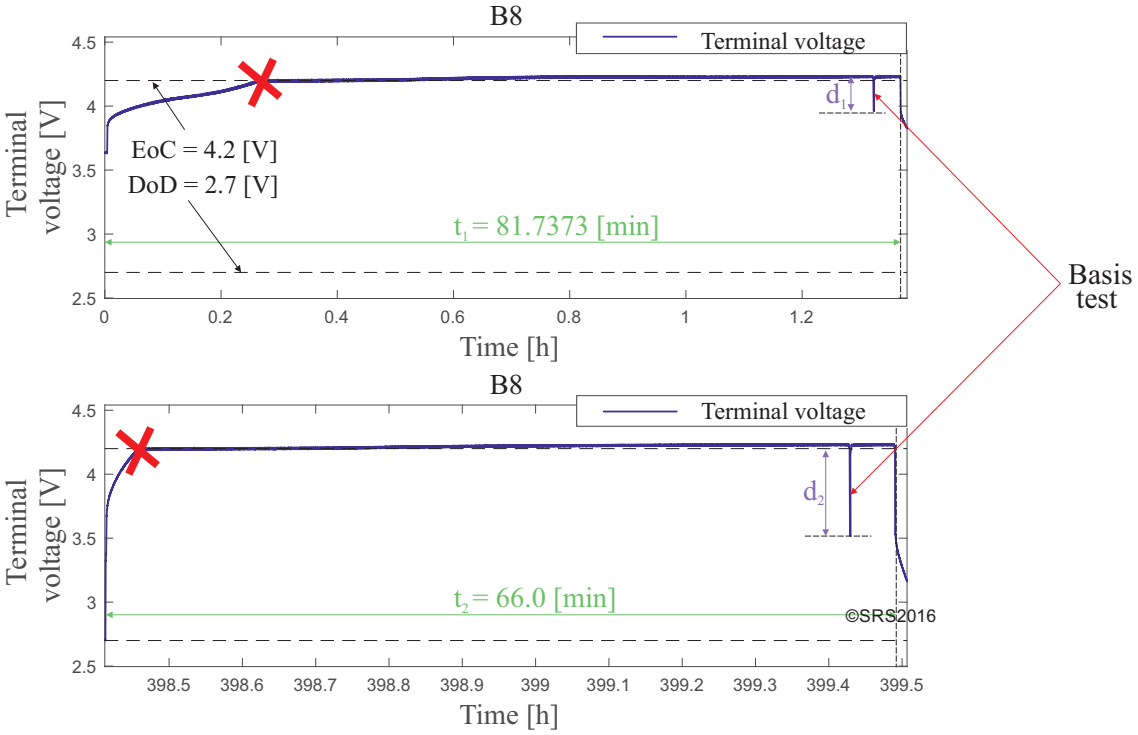

Figure 5.6: Detailed comparison of changes in charging profiles: The first test cycle (upper plot) and the last test cycle (lower plot)

Terminal voltage measurements and AE energy related to aging test named B8 are depicted on an identical time scale in Figure 5.7. Terminal voltage measurements are shown in the upper plot of Figure 5.7, whilst correlated AE measurements are shown in the lower plot. The measurements correspond to the first four complete aging cycles. Here, energy of AE signal is obtained by calculation of STFT of windowed AE measurements (in detail explained in Chapter 5.2.2). It is noticeable that the highest AE activity occurs during charging phase of LIB whereas charging current equals to 2C (20 A). Obtained AE energy is much lower during LIB discharging in comparison with AE energy obtained during charging phase. This means that almost no AE waves are emitted during discharging phase (where no charging current flows to the battery but only discharging current).

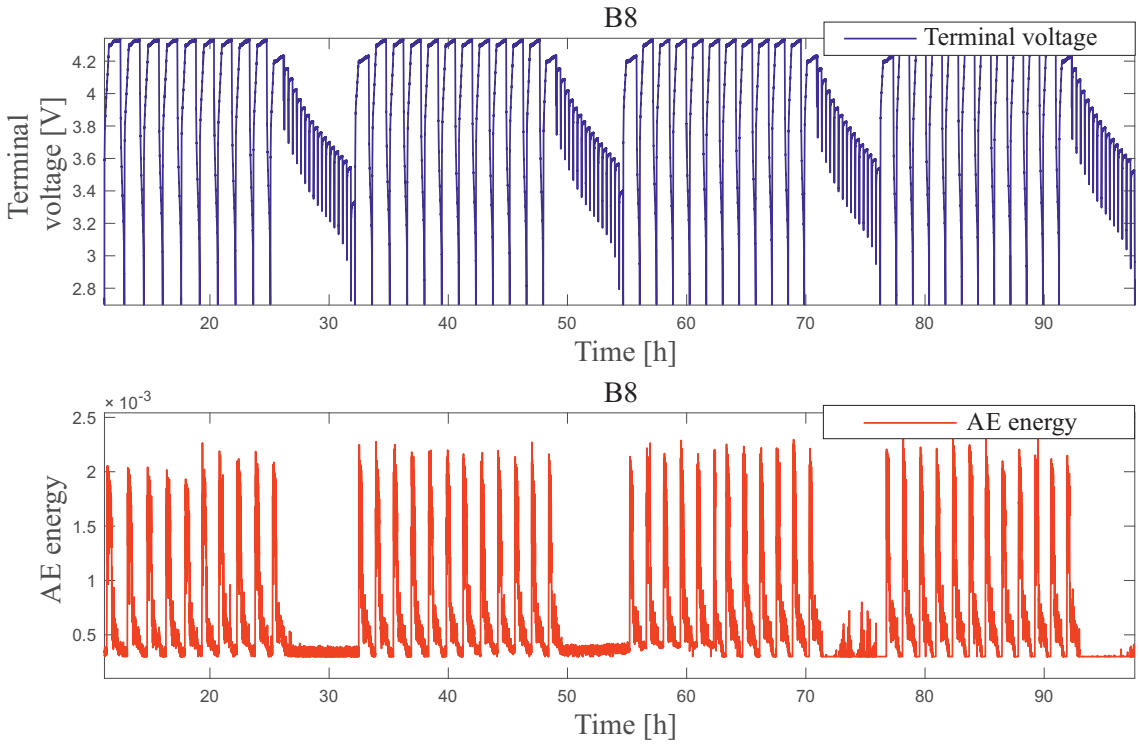

Figure 5.7: Terminal voltage measurements and corresponding AE energy (B8) [BS]

To reveal degradation related indicators from AE measurements, energy of acoustic emission signal occurred at the beginning of LIB lifetime is compared with the same one from the end of lifetime in Figure 5.8. Both signals are depicted on the same time scale. It is noticeable that the amplitude of AE energy decreases with the aging of the battery and is herein recognized as an aging indicator.

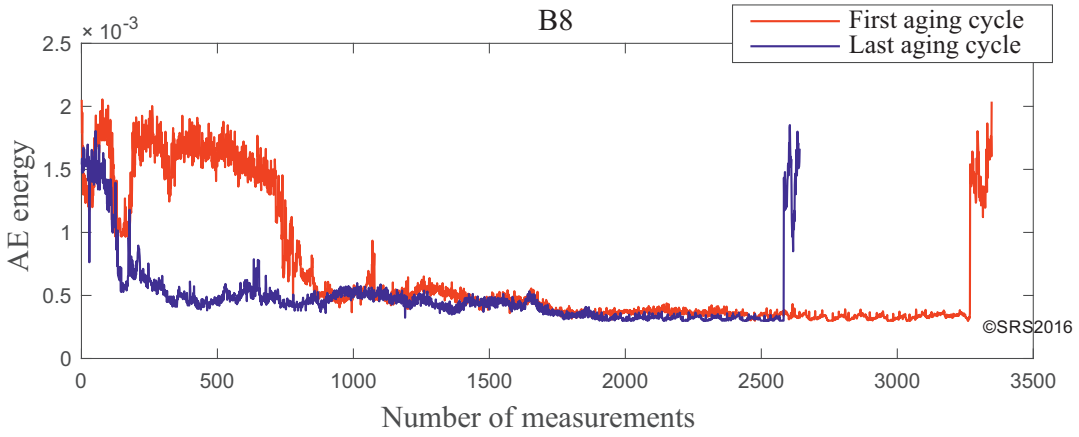

Figure 5.8: Energy of AE signal at the beginning and at the end of LIB lifetime (B8)

In addition, the analysis of frequency spectrum of AE energy signal is utilized to obtain features capable to describe LIB aging. Selection/extraction of time-frequency-based features is explained in detail in Chapter 5.2.2. These features are considered as input into the lifetime model. To establish the model for RUL estimation, the EoL has to be a priori defined. For these purposes, indirectly estimated capacity of LIB using calculation of internal ohmic and polarization resistance is used to obtain the information about the End-of-Life.

5.2.1 Estimation of SoH based on basis tests measurements

During basis test, LIB is charged with the current of 2C until End-of-Charge (equals to 4.2 V). Afterwards, the discharging procedure (energy withdrawal from LIB) is performed with the discharging current of 3C but only in duration of 500 ms (high-frequent discharging). The drop of terminal voltage at the moment at which the discharging current is fed to the battery becomes noticeable. In Figure 5.9, basis test measurements from four different experiments (B8, B9, B10, and B11) are depicted. Basis test measurements depicted in Figure 5.9 correspond to different aging cycles. These changes over time can be correlated to internal ohmic and polarization resistance as well as to polarization capacitance [WZX09] [VPB07].

To estimate internal ohmic resistance, polarization capacitance, and polarization resistance, the LIB is modeled by equivalent circuit model as proposed in [WZX09] and depicted in Figure 5.10 on the left side. Such model includes R_p, R_o, and C_p as model parameters whose changes over time reveal the information about SoH. Targeting to estimate R_p, R_o, and C_p, basis tests are conducted. The calculation of LIB model parameters concerning aforementioned approach is introduced in [VPB07]. Using well known relation between voltage and current along with determined values of U_o, U_1, U_2, and U_4, ohmic and polarization resistance as well as polarization capacitance according to [VPB07] can be calculated as

$$\begin{aligned} R_o &= \frac{U_1 - U_o}{I_{diss}}, \\ R_p &= \frac{U_2 - U_1}{I_{diss}}, \text{ and} \\ C_p &= \frac{\tau}{R_p}. \end{aligned} \tag{5.1}$$

Time constant τ is obtained from

$$\tau = -\Delta t \cdot ln(1 - \frac{U_4 - U_3}{U_o - U_3}). \tag{5.2}$$

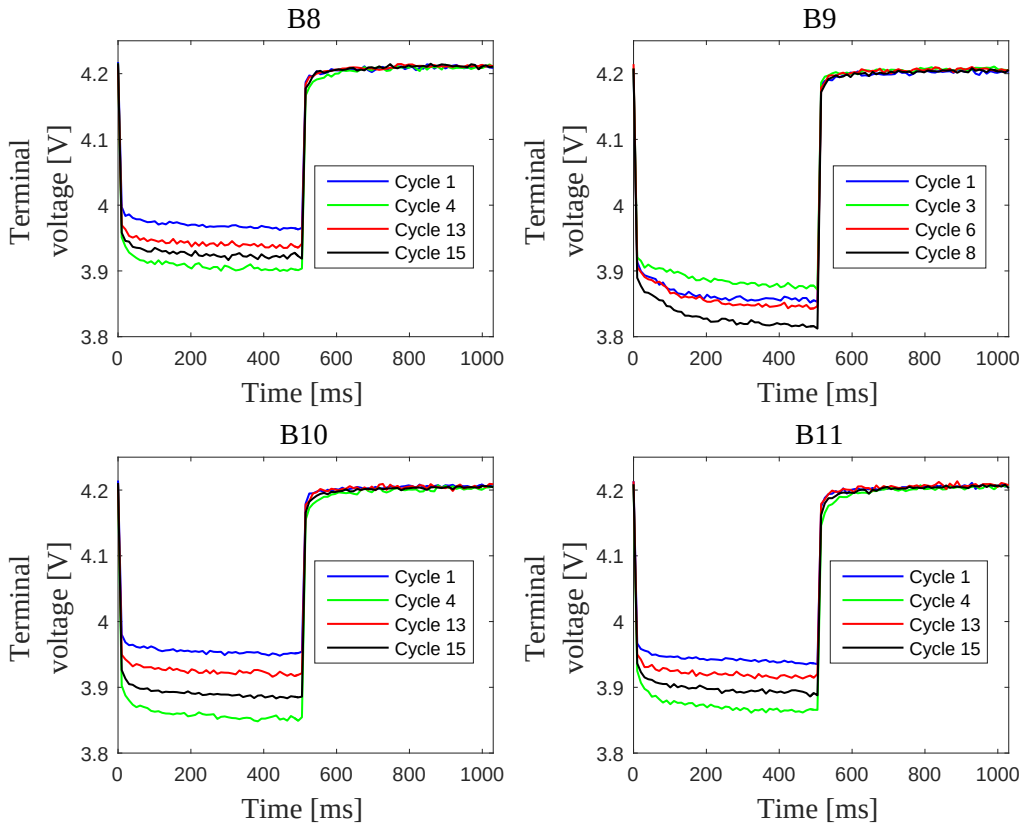

Figure 5.9: Drop of terminal voltage in dependence of considered aging cycle obtained from basis test measurements (B8, B9, B10, B11)

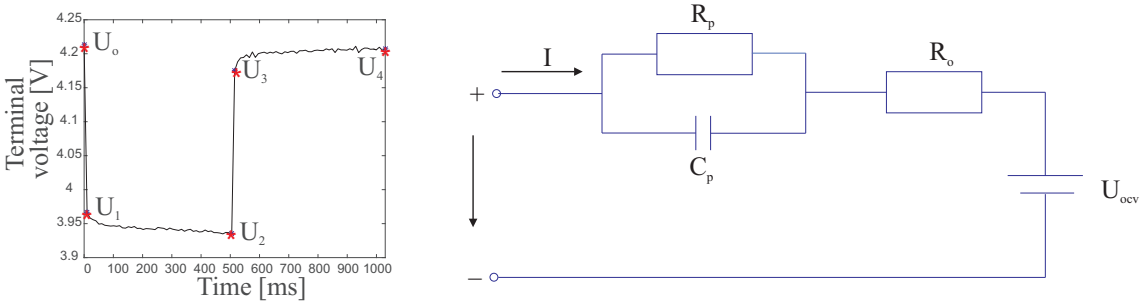

Figure 5.10: Equivalent circuit model for SoH estimation (right side) and model parameters calculation (left side) [WZX09]

Value of Δt in aforementioned equations equals to 500 ms, what is a timespan in which constant discharging current flows from the LIB (basis test).

Battery cell capacity C_t is calculated based on current integration during first discharging cycle of CC-CV tests. This means, fully charged LIB battery is discharged to DoD using constant discharging current (3C). Taking in consideration discharging current and timespan in which terminal voltage drops to DoD, it is possible to calculate LIB capacity as

$$C_{actual} = I_{dis} \cdot t, \tag{5.3}$$

where I_{dis} denotes discharging current and t considered timespan [SGT+01].

According to Figure 5.11 whereas LIB discharging under constant current for different CC-CV test cycles is shown, it becomes noticeable that the decrease of terminal voltage over time is not identical (for instance: at the beginning and at the end of lifetime).

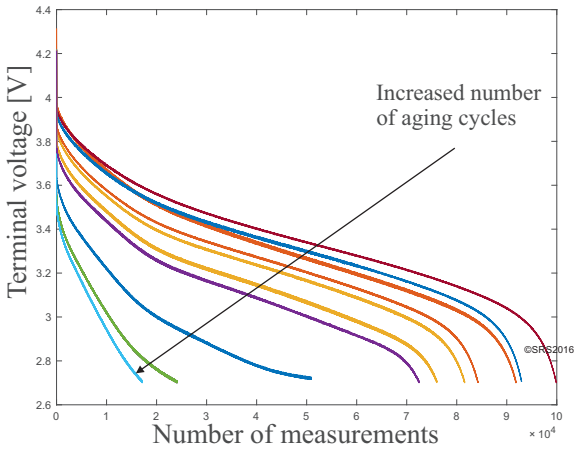

Figure 5.11: Capacity calculation using discharging current integration over the first CC-CV cycle (B8) [BS]

Obtained results using the procedure explained above are depicted in Figure 5.12. In upper plots, estimated ohmic and polarization resistances corresponding to certain CC-CV cycles are depicted. According to the results, the change of ohmic resistance over time is more pronounced in comparison with polarization resistance. Up to the certain point in time ohmic resistance increases, but afterwards sudden drop of ohmic resistance becomes noticeable (for instance: cycle 11 of B8, B10, or B11). Similar effect is noticeable also in LIB capacity, as depicted in Figure 5.12 in lower plot. The values obtained after aforementioned point in time are understood as outliers. The time point at which LIB capacity drops to 80% of nominal capacity is recognized as EoL.

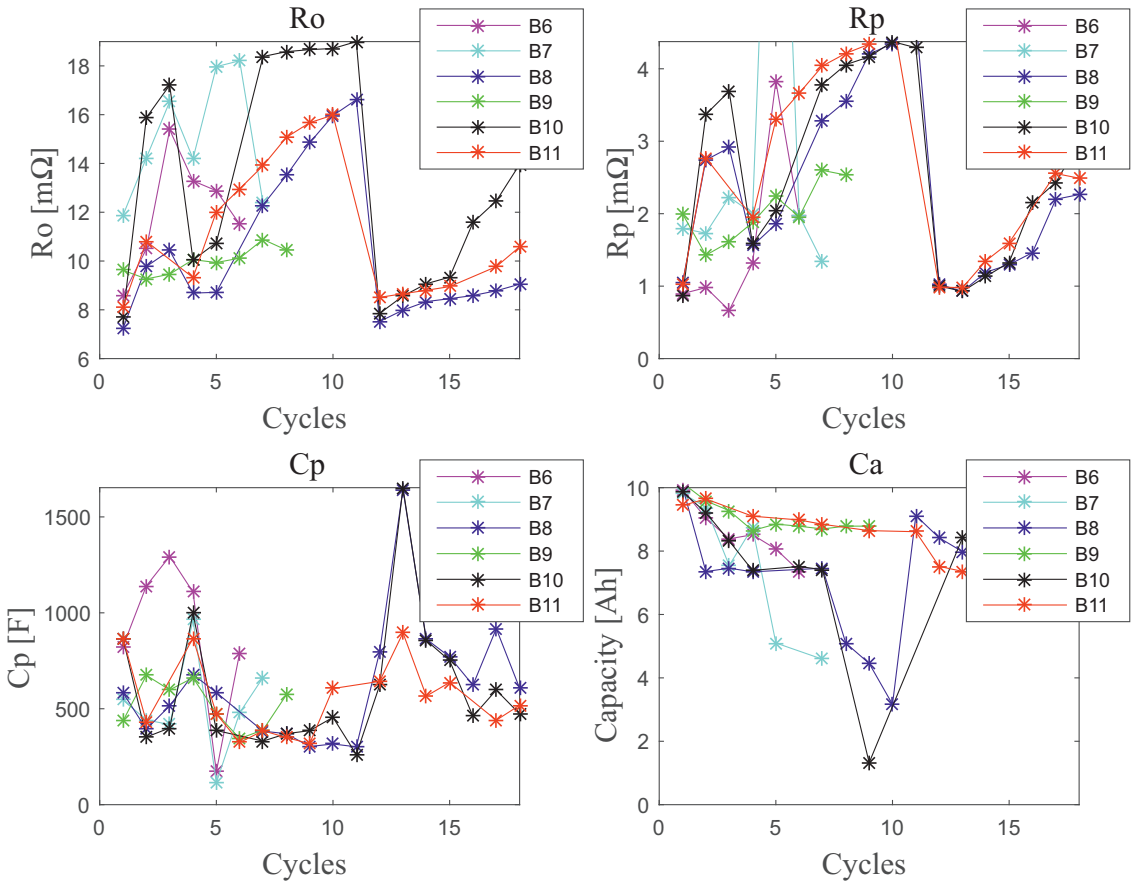

Figure 5.12: Estimated model parameters and LIB capacity over service lifetime

5.2.2 Estimation of RUL based on AE measurements

The knowledge about EoL obtained indirectly in Chapter 5.2.1 is utilized for lifetime model establishment using AE measurements. The information about EoL is necessary to select a part of AE measurements which have occurred before EoL, as no scientific proof for EoL definition based on AE measurements is found. The measurements obtained over complete testing period are given in appendix of this thesis. For purpose of RUL modeling, the data corresponding to indirectly obtained EoL are used, namely the first eight (8) cycles of B8 and B10, the first twelve (12) cycles of B11, the first four (4) cycles of B7, and complete measurements of B6 and B9.

The features to be used for RUL estimation are calculated from AE energy. The energy of AE signal corresponds to the power of STFT applied to the captured AE signal. Continuous Wavelet Transformation is further applied to AE energy signal, whereas the coefficients of CWT are calculated as

$$F_w(s,\tau) = \frac{1}{s^{1/2}} \int_{-\infty}^{+\infty} f(t) \cdot \psi^* \Big(\frac{t-\tau}{s} \Big) dt. \tag{5.4}$$

Here, s defines stretching and compressing factor of mother wavelet, τ denotes wavelet translation, and ψ^* denotes conjugate-complex value of mother wavelet [ZLC02].

According to Figure 5.7, the highest AE activity occur over LIB charging. Due to this, only charging cycles in which energy of AE exceeds predefined threshold is considered. Cumulative sum of CWT coefficients corresponding to aforementioned timespan is calculated and used as input in lifetime model, as depicted in Figure 5.13. Obtained results concerning CWT of energy of AE signal are depicted in Figure 5.14.

Remaining useful lifetime is modeled by mathematical equation expressed as

$$LT = m_1 + F_3 \cdot {m_2}^{m_3} + F_3^{m_4} + F_3^{m_5} + \frac{1}{1+e^{m_6}}, \tag{5.5}$$

whereas LT denotes consumed lifetime and F_3 calculated features. Model parameters which have to be optimized are denoted as $m_1 - m_6$. Such mathematical model establishes the relation between damage indicator (here: accumulated sum of CWT coefficients, as the higher values of CWT coefficients correspond to higher AE activity) and consumed lifetime. Almost linear relationship between consumed lifetime and damage measures is noticeable. High requirements here are set on experimental tests capable to reflect real situation where charging/discharging profile of LIB is not constant. Linear relationship here can be explained by accurately defined and controlled charging and discharging profile of LIB under constant temperature.

Non-dominated Genetic Algorithm II (NSGA-II) is used to optimize model parameters. Objective function used to optimize model parameters provides minimal deviation between experimental and estimated data sets. Mathematical formulation

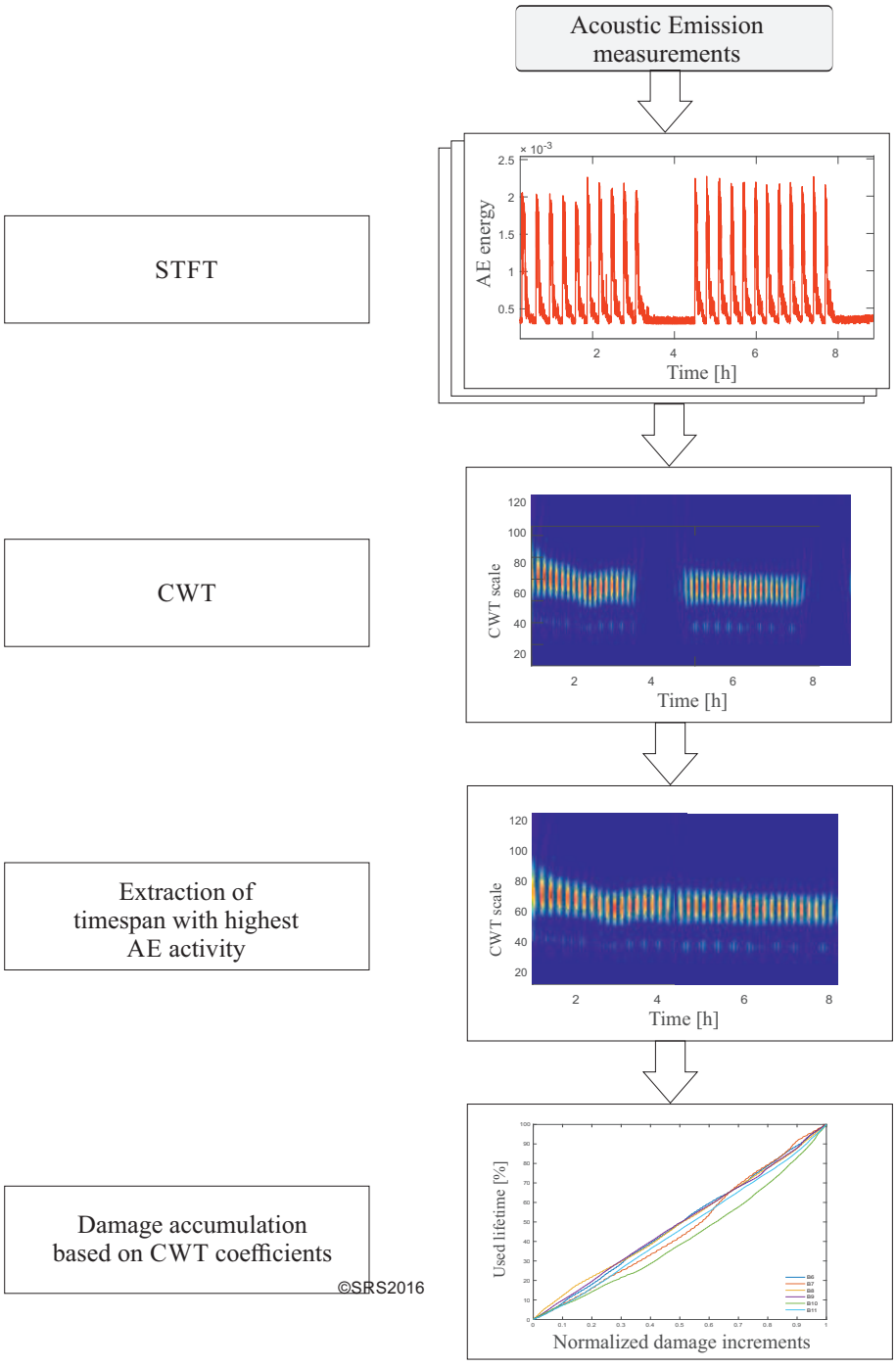

Figure 5.13: Feature selection from AE energy [BS]

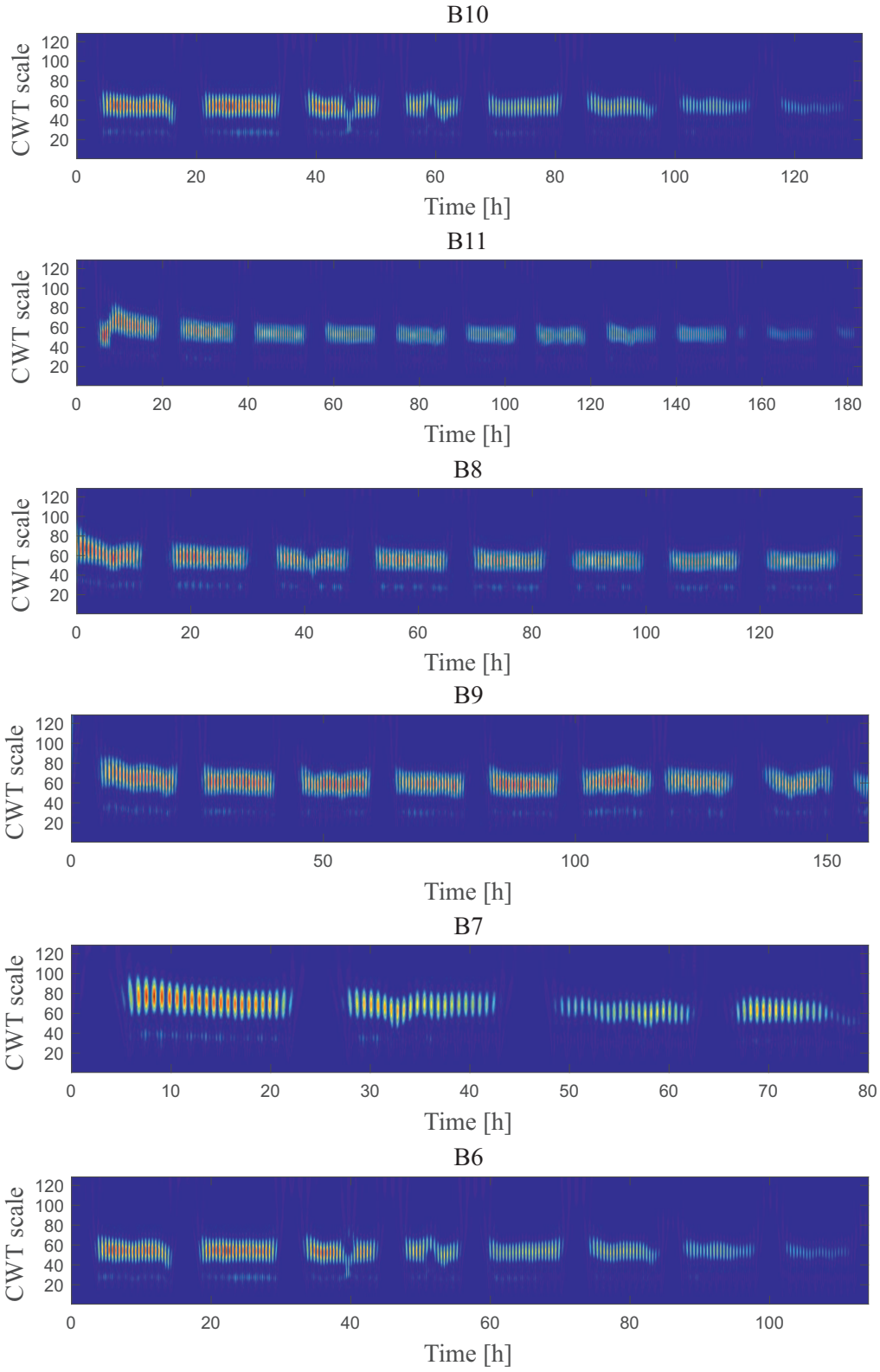

Figure 5.14: Analysis of frequency spectrum of energy of AE signal [BS]

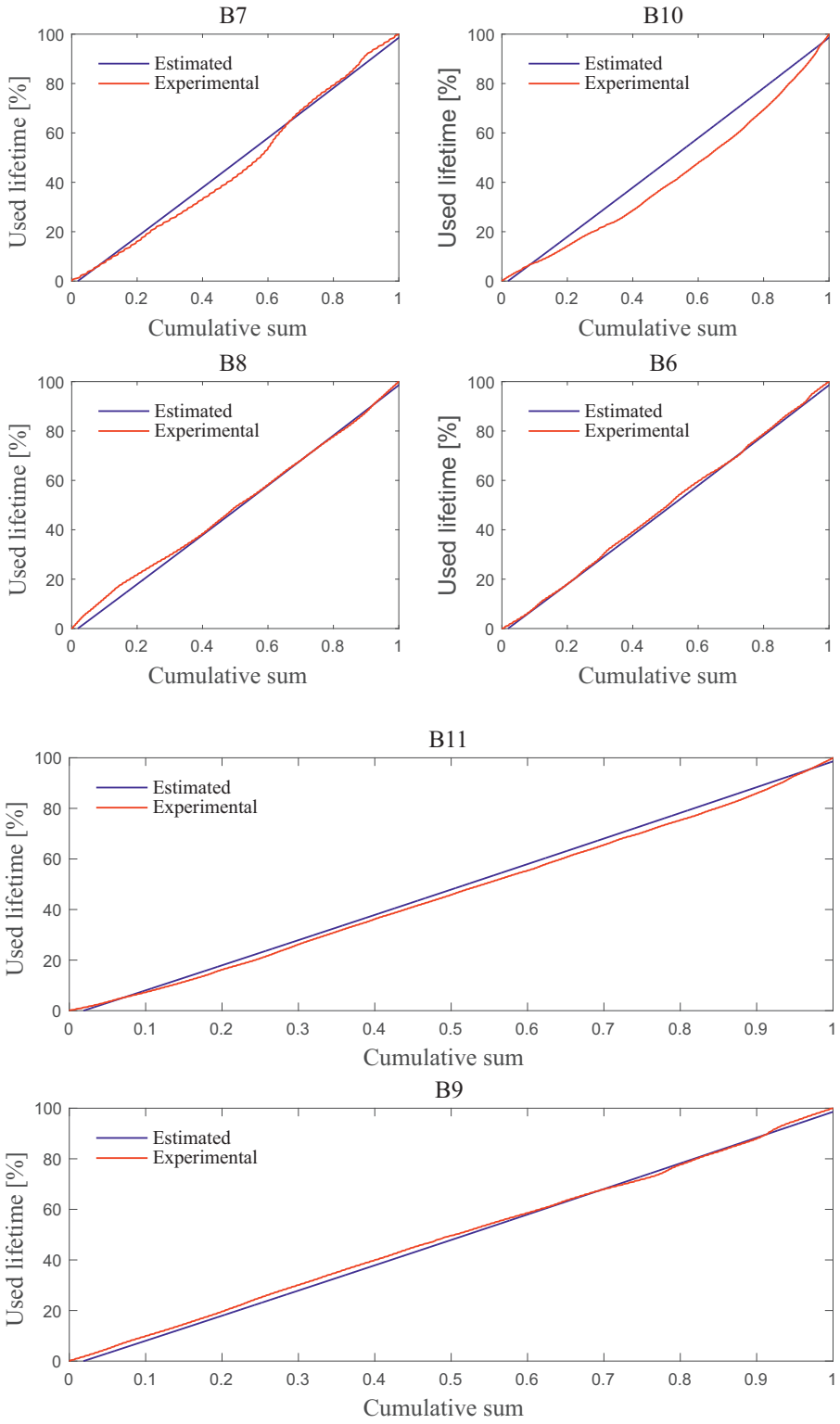

Figure 5.15: Estimation of consumed lifetime based on AE measurements [BS]

of objective function to be minimized is given as

$$objective\ function = min(abs\ (experimental\ data - estimated\ data)) \quad (5.6)$$

and denotes absolute deviation between experimental and estimated data sets. Values of model parameters after optimization are listed in Table 5.1. Experimental results obtained from B6, B7, B8 and B10 are used for model optimization, as depicted in upper plots of Figure 5.15. Experimental results obtained from B11 and B9 are used for model validation.

m_1	m_2	m_3	m_4	m_5	m_6
-3.4313	78.8112	1.0519	41.4297	13.4142	-33.9935

Table 5.1: Optimized model parameters

According to the results depicted in Figure 5.15, high discrepancy between estimated and experimental results is noticeable especially for two data sets which are used in model training phase, namely B10 and B8. Conversely to the results obtained for aforementioned two training data sets, high congruency between experimental and estimated data sets is obtained for both data sets used for model validation. It is worth to emphasize that the input into the model is normalized to one.

5.3 Discussion of results

An examination whether direct estimation of SoH and RUL using AE measurements is possible is concerned in this chapter. Concerning presented results, capability of AE measurements to reveal degradation indicator is shown. Firstly, energy of acoustic emission is calculated and compared with terminal voltage measurements. Obvious similarities are evident between both measurements with respect to amplitudes of AE energy and terminal voltage. Moreover, frequency spectrum of AE energy obtained by CWT calculation reveals decreased AE activity as the system approaches to EoL. Indirectly estimated capacity fade can therefore be correlated to decreased amplitudes of AE energy. Close to EoL, acoustic emission is not noticeable. Such direct estimation of SoH is especially useful if charging and discharging of LIB is not done in precisely arranged manner, what is almost always the case in practice. Indirect estimation of capacity fade is carried out using measurements of terminal voltage under LIB discharging with constant current, but this approach is possible only under controlled and precisely defined discharging profile of LIB.

Results obtained from AE measurements are utilized in RUL model, whereas features selected from AE energy are considered as input into the model.The model established as an example is expressed using arbitrarily chosen mathematical formulation whose parameters are optimized using NSGA-II. Presented results shows satisfying congruency between experimental and estimated results.

6 Conclusion, final remarks, and outlook

The research work presented in this thesis is closely related to finding solutions to existing problems in structural health monitoring of wind turbine systems. Subsequent to discussion about SHM related issues, identified unsolved problems in SHM field can be summarized as: i) accurate and efficient estimation/prediction of remaining useful lifetime of the system or system components and ii) integration of the knowledge about current health state of the system into control strategy. Due to this, the detection and severity estimation of occurred changes/anomalies in the system and modeling of damage propagation over time is an integral part of this research. High attention has been given to the development of modeling approaches for remaining useful and/or consumed lifetime prediction, whereas a few new models towards RUL estimation are presented. Moreover, the development of control strategy which integrates the knowledge about current SoH into control strategy is shown on an example of simulation model of wind turbine system. In this thesis, different RUL modeling approaches are developed concerning SHM data of different nature. For purpose of RUL model development, particular system components, namely elements with sliding or rolling motion of metallic bodies and storage elements, are discussed separately.

Overall conclusion and key results obtained during research are pointed out in Chapter 6.1. Similarly, further steps in this research field and some suggestions related to the future work are given in Chapter 6.2.

6.1 Conclusion

Integration of control strategy which includes the knowledge about current state of health based on simulation model of wind turbine developed by NREL has been presented in Chapter 3. According to the results, variable level of structural loads reduction on wind turbine blades corresponding to different system's health state is achieved. Structural loads reduction in this case is obtained using a number of controllers with variable controller parameters, whose selection is carried out based on damage accumulation thresholds exceedance. Slight impact on power generation using controllers providing higher level of structural load reduction are noticeable, but the deviation between desired and generated power is still found in acceptable limits. Especially high challenge in implementation of such controller strategy has been the development of remaining useful lifetime model which is capable to process changes in the system at the point in time at which the change occurs. For these purposes, Palmgren-Miner rule with online-based Rainflow Counting Algorithm is utilized, but some shortcomings related to delayed detection of life cycles are identified. As that, additional improvement in lifetime modeling concerning information about bending moments on rotor blades is possible.

Contrary to the results obtained using simulation setup, the SoH estimation and RUL modeling based on SHM data measured from different experimental test facilities, namely from tribological system as well as LIB experimental setup, are presented in Chapters 4 and 5.

Both experimental test rigs include the measurements of AE signal. According to the presented results, SoH estimation and remaining/consumed lifetime modeling based on energy of AE signal is possible. Features selected/extracted from measurements of AE are used as input into proposed lifetime models. Data analysis in both cases is performed in similar manner and relies on signal transformation in frequency domain with retained information about the time point at which specific event occurs. Such approach has been shown as efficient, but in some cases has also high computational requirements (for instance: in case of Continuous Wavelet Transformation). This becomes especially noticeable taking in consideration high frequency range in which AE occurs causing a huge number of gathered data from particular test rig.

Three developed lifetime models based on AE measurements have shown satisfying results with respect to system's consumed lifetime prediction. The first developed model is a sort of regression model which takes the knowledge about previous and current values of damage increments as well as previous values of consumed lifetime as model input. The second two models rely on the knowledge about SoH of the system to select appropriate model from lifetime model database. Each of these three models has its characteristics and limitations. The most pronounced limitation of the first model is a huge number of model parameters which have to be optimized and its incapability to compensate the error appeared in initial stages. Similarly, the most aggravating factor for application of the second and the third model lies in limited feasibility for a priori SoH estimation based on SHM data as well as in requirement for expert knowledge to optimize model parameters. However, even aforementioned limitations exist all of these three models, according to the results presented in Chapter 4, are capable to predict consumed/remaining lifetime with low prediction error.

The examination of capability of AE measurements to reveal gradual degradation of LIB is given in Chapter 5. Presented results illustrate the utilization of AE-based features to estimate RUL and SoH of LIB. Features selected from AE-energy signal are used as input into the model for remaining useful lifetime estimation. The experiments conducted for these purposes are carried out under precisely controlled operating conditions (constant charging and discharging currents as well as temperature). Such testing procedure do not reflect the situation from practice whereas LIB charging/discharging is rarely performed in such a manner. However, propose approach allows the estimation of SoH based on directly correlated parameters. Especially in inceptive phases of AE measurements utilization in battery management systems, it is of high importance to compare the results obtained from certainly measured system parameters which are indirectly correlated to SoH and AE measurements which are directly correlated to SoH.

6.2 Final remarks and outlook

Taking in consideration fatigue damage accumulation model integrated into controller design of WT system, it becomes noticeable that not only purely linear models, as it is Palmgren-Miner damage accumulation model, can be utilized in SRCE concept. Newly developed damage accumulation models have to be feasible to reveal and process damage increments at the moment of their occurrence, similarly as the model proposed in this thesis. Further improvements in SRCE concept implementation and application can be achieved through implementation of controller strategy which would not provide the reduction of structural loads only in predefined (discrete) levels.

Concerning high frequency of AE signal and consequent huge amount of captured AE data, improvements related to measurement chain are possible in terms of real-time signal processing, leading simultaneously to AE data reduction. From the other point of view, the improvements concerning proposed lifetime models are possible in terms of an avoidance of limitations assigned to each particular model (huge number of model parameters, incapability to compensate prediction error appeared in initial stages, feasibility for a priori SoH estimation).

An examination of AE measurements utilization in battery management systems can be extended to a variety of additional testing procedures. Gradual degradation process of lithium-ion batteries has to be analyzed during LIB operation under varying operating conditions, which can reflect real (often hardly predictable) charging/discharging profile of LIB. The examination of LIB aging under an assumption of varying operating conditions is not considered in presented work, but it can be considered for future work.

Bibliography

[ABBW07] Y. Amirat, M.E.H. Benbouzid, B. Bensaker, and R. Wamkeue. Condition monitoring and fault diagnosis in wind energy conversion systems: A review. In *IEEE International Conference on Electric Machines & Drives Conference, Antalya, Turkey*, volume 2, pages 1434–1439, 2007.

[AF13] V. Agubra and J. Fergus. Review - Lithium-ion battery anode aging mechanisms. *Journal of Materials*, 6(4):1310–1325, 2013.

[AGM06] A.M. Al-Ghamd and D. Mba. A comparative experimental study on the use of acoustic emission and vibration analysis for bearing defect identification and estimation of defect size. *Mechanical Systems and Signal Processing*, 20(7):1537–1571, 2006.

[AL14] F. Ahmadzadeh and J. Lundberg. Remaining useful life estimation: A review. *International Journal of System Assurance Engineering and Management*, 5(4):461–474, 2014.

[Arr89] S. Arrhenius. On the reaction rate of the inversion of non-refined sugar upon souring. *Zeitschrift für Physikalische Chemie*, 4:226–248, 1889.

[Ban09] D. Banjevic. Remaining useful life in theory and practice. *Metrika*, 69:337–349, 2009.

[BBS15] N. Beganovic, D. Baccar, and D. Söffker. Wear aging and related impact on system reliability. In *Chang, F.K.; Kopsaftopoulos, F. (Ed.). Structural Health Monitoring, Stanford, CA, USA*, pages 353–401, 2015.

[Bec12] E. Bechhoefer. Data-driven prognostics for rotating machinery. In *Kadry, S. (Ed.): Diagnostics and Prognostics of Engineering Systems: Methods and Techniques*, pages 1–13. Engineering Science Reference, Hershey, PA, USA, 2012.

[Bir10] G.S. Bir. Users guide to MBC3: Multi-blade coordinate transformation code for 3-bladed wind turbines. Technical report, National Renewable Energy Laboratory, Golden, CO, USA, 2010.

[BMS15] N. Beganovic, B. Moulik, and D. Söffker. LI-O battery aging process: A smart review with respect to the integration of aging into system's powermanagement. In *Proceedings of the ASME Dynamic Systems and Control Conference, Columbus, OH, USA*, pages 1–10, 2015.

[BNRS15] N. Beganovic, J.G. Njiri, S. Rothe, and D. Söffker. Application of diagnosis and prognosis to wind turbine system based on fatigue load. In *IEEE Conference on Prognostics and Health Management, Austin, TX, USA*, pages 1–6, 2015.

[BNS] N. Beganovic, J.G. Njiri, and D. Söffker. Reduction of structural loads in wind turbines through adapted control strategy concerning online fatigue damage evaluation model. *Journal of Wind Engineering & Industrial Aerodynamics*. Submitted.

[BNS17] N. Beganovic, J.G. Njiri, and D. Söffker. Wind turbine control strategy deployment concerning remaining useful lifetime prognostic model. Conference for Wind Power Drives, Aachen, Germany, 2017. Accepted.

[Bog78a] J.L. Bogdanoff. A new cumulative damage model: Part I. *Journal of Applied Mechanics*, 45(2):246–250, 1978.

[Bog78b] J.L. Bogdanoff. A new cumulative damage model: Part II. *Journal of Applied Mechanics*, 45(2):251–257, 1978.

[BRS14] N. Beganovic, S. Rothe, and D. Söffker. Establishing a wear-oriented deterioration model based on experimental data. In *Le Cam, Vincent and Mevel, Laurent and Schoefs, Franck. EWSHM - 7th European Workshop on Structural Health Monitoring, Nantes, France*, pages 1513–1520, 2014.

[BRS16] N. Beganovic, S. Rothe, and D. Söffker. Identification of diagnostic and prognostic features by means of AE and hydraulic pressure measurements. In *EWSHM - 8th European Workshop on Structural Health Monitoring, Bilbao, Spain*, pages 1–8, 2016.

[BS] N. Beganovic and D. Söffker. Remaining useful lifetime and State-of-Health estimation of LIB based on direct measurements. *Journal of Power Sources*. Submitted.

[BS15a] D. Baccar and D. Söffker. Wear detection by means of wavelet-based acoustic emission analysis. *Mechanical Systems and Signal Processing*, 60-61:198–207, 2015.

[BS15b] N. Beganovic and D. Söffker. Wear process lifetime prediction based on parametric model applied to experimental data. In *IEEE Conference on Prognostics and Health Management, Austin, TX, USA*, pages 1–6, 2015.

[BS16] N. Beganovic and D. Söffker. Structural health management utilization for lifetime prognosis and advanced control strategy deployment of wind turbines: An overview and outlook concerning actual methods, tools and obtained results. *Renewable & Sustainable Energy Reviews*, 64:68–83, 2016.

[BS17] N. Beganovic and D. Söffker. Remaining lifetime modeling using State-of-Health estimation. *Mechanical Systems and Signal Processing*, 92:107–123, 2017.

[CH09] J. Coble and J.W. Hines. Identifying optimal prognostic parameters from data: A genetic algorithms approach. In *Annual Conference of the Prognostics and Health Management Society, San Diego, CA, USA*, pages 1–11, 2009.

[CHB15] J.G. Chen, R.W. Haupt, and O. Buyukozturk. Operational and defect parameters concerning the acoustic-laser vibrometry method for FRP-reinforced concrete. *NDT & E International*, 71:43–53, 2015.

[CLB08] C.C. Ciang, J.R. Lee, and H.J. Bang. Structural health monitoring for a wind turbine system: A review of damage detection methods. *Measurement Science and Technology*, 19(12):1–20, 2008.

[CP09] S. Cheng and M. Pecht. A fusion prognostics method for remaining useful life prediction of electronic products. In *IEEE International Conference on Automation Science and Engineering, Bangalore, India*, pages 102–107, 2009.

[CP12] C. Chen and M. Pecht. Prognostics of lithium-ion batteries using model-based and data-driven methods. In *IEEE Conference on Prognostics and Health Management, Beijing, China*, pages 1–6, 2012.

[CRB14] X. Chen, H. Ren, and C. Bil. The influence of SHM techniques on scheduled maintenance of aircraft composite structures. In *14th AIAA Aviation Technology, Integration, and Operations Conference, Atlanta, GA, USA*, pages 2326–2335, 2014.

[CT12] L. Cheng and G.Y. Tian. Comparison of nondestructive testing methods on detection of delaminations in composites. *Journal of Sensors*, 2012:1–7, 2012.

[DCA+14] N. Dervilis, M. Choi, I. Antoniadou, K.M. Farinholt, S.G. Taylor, R.J. Barthorpe, G. Park, C.R. Farrar, and K. Worden. Machine learning applications for a wind turbine blade under continuous fatigue loading. *Key Engineering Materials*, 588:166–174, 2014.

[Det11] K.U. Dettmann. *Probabilistic-based method for realizing safe and reliable mechatronic systems.* PhD thesis, University of Duisburg-Essen, 2011.

[DL09] M. Dubarry and B.Y. Liaw. Identify capacity fading mechanism in a commercial $LiFePO_4$ cell. *Journal of Power Sources*, 194(1):541–549, 2009.

[DZ14] J. Dybała and R. Zimroz. Rolling bearing diagnosing method based on empirical mode decomposition of machine vibration signal. *Applied Acoustics*, 77:195–203, 2014.

[EBT12] R.A. Esmaeel, J. Briand, and F. Taheri. Computational simulation and experimental verification of a new vibration-based structural health monitoring approach using piezoelectric sensors. *Structural Health Monitoring*, 11(2):237–250, 2012.

[EBV14] A. Eddahech, O. Briat, and J.M. Vinassa. Determination of lithium-ion battery state-of-health based on constant-voltage charge phase. *Journal of Power Sources*, 258:218–227, 2014.

[FBB12] K. Fischer, F. Besnard, and L. Bertling. Reliability-centered maintenance for wind turbines based on statistical analysis and practical experience. *IEEE Transactions on Energy Conversion*, 27(1):184–195, 2012.

[FHT11] S. Faulstich, B. Hahn, and P.J. Tavner. Wind turbine downtime and its importance for offshore deployment. *Wind Energy*, 14(3):327–337, 2011.

[FL07] C.R. Farrar and N.A.J. Lieven. Damage prognosis: The future of structural health monitoring. *Philosophical Transactions of the Royal Society of London: Mathematical, Physical and Engineering Sciences*, 365(1851):623–632, 2007.

[FPKL12] S. Faulstich, S. Pfaffel, P. Kühn, and P. Lyding. Monitoring offshore wind energy use in Europe - Offshore WMEP. *Energy Procedia*, 24:322–327, 2012.

[FQ11] W. Fan and P. Qiao. Vibration-based damage identification methods: A review and comparative study. *Structural Health Monitoring*, 10(1):83–111, 2011.

[GGV+11] R. Gutkin, C.J. Green, S. Vangratanachai, S.T. Pinho, P. Robinson, and P.T. Curtis. On acoustic emission for failure investigation in CFRP: Pattern recognition and peak frequency analyses. *Mechanical Systems and Signal Processing*, 25(4):1393–1407, 2011.

[GLE41] S. Glasstone, K.J. Laidler, and H.E. Eyring. *The theory of rate processes.* McGraw Hill, New York, USA, 1941.

[GMPP12] M.F.P. García, T.A. Mark, P.J.M. Pinar, and M. Papaelias. Condition monitoring of wind turbines: Techniques and methods. *Renewable Energy*, 46:169–178, 2012.

[GO08] C.U. Grosse and M. Ohtsu. *Acoustic emission testing*. Springer Science & Business Media, Berlin, Germany, 2008.

[GP15] D. Goyal and B.S. Pabla. The vibration monitoring methods and signal processing techniques for structural health monitoring: A review. In *Kleiber, M. and Onate, E. (Ed.): Archives of Computational Methods in Engineering*, pages 1–10. Springer, Heidelberg, Germany, 2015.

[GPHJ03] L. Gaul, P. Pinto, S. Hurlebaus, and L.J. Jacobs. Localization and sizing of discontinuities using lamb waves. In *Chang, F.K. (Ed.). Structural Health Monitoring, Stanford, CA, USA*, pages 379–386, 2003.

[GSS+08] K. Goebel, B. Saha, A. Saxena, J.R. Celaya, and J.P. Christophersen. Prognostics in battery health management. *IEEE Instrumentation & Measurement Magazine*, 11(4):33–40, 2008.

[GYR+14] D.T. Griffith, N.C. Yoder, B. Resor, J. White, and J. Paquette. Structural health and prognostics management for the enhancement of offshore wind turbine operations and maintenance strategies. *Wind Energy*, 17(11):1737–1751, 2014.

[Hen55] D.L. Henry. A theory of fatigue-damage accumulation in steel. *Transactions of the ASME*, 77:913–918, 1955.

[HFU08] R. Hanke, T. Fuchs, and N. Uhlmann. X-ray based methods for non-destructive testing and material characterization. *Nuclear Instruments and Methods in Physics Research Section A: Accelerators, Spectrometers, Detectors and Associated Equipment*, 591(1):14–18, 2008.

[HGM+14] Z. He, M. Gao, G. Ma, Y. Liu, and S. Chen. Online state-of-health estimation of lithium-ion batteries using Dynamic Bayesian Networks. *Journal of Power Sources*, 267:576–583, 2014.

[HHC+09] Z. Hameed, Y.S. Hong, Y.M. Cho, S.H. Ahn, and C.K. Song. Condition monitoring and fault detection of wind turbines and related algorithms: A review. *Renewable and Sustainable Energy Reviews*, 13(1):1–39, 2009.

[HLP12] X. Hu, S. Li, and H. Peng. A comparative study of equivalent circuit models for Li-ion batteries. *Journal of Power Sources*, 198:359–367, 2012.

[HMS+06] R.W. Hyers, J.G. McGowan, K.L. Sullivan, J.F. Manwell, and B.C. Syrett. Condition monitoring and prognosis of utility scale wind turbines. *Energy Materials*, 1(3):187–203, 2006.

[HNNM13] F. Harrou, M.N. Nounou, H.N. Nounou, and M. Madakyaru. Statistical fault detection using PCA-based GLR hypothesis testing. *Journal of Loss Prevention in the Process Industries*, 26(1):129–139, 2013.

[HNS+15] T. Hofmann, F. Nachtrab, T. Schlechter, H. Neubauer, J. Mühlbauer, S. Schröpfer, J. Ernst, M. Firsching, T. Schweiger, M. Oberst, A. Meyer, and N. Uhlmann. Development of a fast multi-line X-ray CT detector for NDT. *Journal of Instrumentation*, 10(4):1–12, 2015.

[HOB13] V.A.P. Hines, A.B. Ogilvie, and C.R. Bond. Continuous reliability enhancement for wind (CREW) database: Wind plant reliability benchmark. Technical report, Sandia National Laboratories, Albuquerque, NM, USA, 2013.

[HSL+15] M. Hong, Z. Su, Y. Lu, H. Sohn, and X. Qing. Locating fatigue damage using temporal signal features of nonlinear lamb waves. *Mechanical Systems and Signal Processing*, 60:182–197, 2015.

[HSW15] C. Heinze, M. Sinapius, and P. Wierach. Lamb wave propagation in complex geometries - A minimal model approach. In *Proceedings of the 5th International Workshop on Aircraft System Technologies, Hamburg, Germany*, pages 383–390, 2015.

[HTPC14a] Y. He, G. Tian, M. Pan, and D. Chen. Impact evaluation in carbon fiber reinforced plastic (CFRP) laminates using eddy current pulsed thermography. *Composite Structures*, 109:1–7, 2014.

[HTPC14b] Y. He, G. Tian, M. Pan, and D. Chen. Non-destructive testing of low-energy impact in CFRP laminates and interior defects in honeycomb sandwich using scanning pulsed eddy current. *Composites Part B: Engineering*, 59:196–203, 2014.

[IEE90] IEEE. Standard computer dictionary: A compilation of IEEE standard computer glossaries. Institute of Electrical and Electronics Engineers, New York, 1990.

[JLL13] H. Jiang, C. Li, and H. Li. An improved EEMD with multiwavelet packet for rotating machinery multi-fault diagnosis. *Mechanical Systems and Signal Processing*, 36(2):225–239, 2013.

[KB88] T.V. Kutt and M.P. Bieniek. Cumulative damage and fatigue life prediction. *AIAA Journal*, 26:213–219, 1988.

[KCA13] E.M. Krieger, J. Cannarella, and C.B. Arnold. A comparison of lead-acid and lithium-based battery behavior and capacity fade in off-grid renewable charging applications. *Energy*, 60:492–500, 2013.

[KHK13] K. Koyama, H. Hoshikawa, and G. Kojima. Eddy current nondestructive testing for carbon fiber-reinforced composites. *Journal of Pressure Vessel Technology*, 135(4):1–6, 2013.

[KHV09] R. Kothamasu, S.H. Huang, and W.H. VerDuin. System health monitoring and prognostics - A review of current paradigms and practices. In *Ben-Daya, M. and Duffuaa, A.O. and Raouf, A. and Knezevic, J. (Ed.): Handbook of Maintenance Management and Engineering*, pages 337–362. Springer, Heidelberg, Germany, 2009.

[KK13] F. Kreith and S. Krumdieck. *Principles of sustainable energy systems*. CRC Press, Boca Raton, FL, USA, 2013.

[KKJ+13] D.Y. Kim, H.B. Kim, W.S. Jung, S. Lim, J.H. Hwang, and C.W. Park. Visual testing system for the damaged area detection of wind power plant blade. In *IEEE 44th International Symposium on Robotics, Seoul, Korea*, pages 1–5, 2013.

[KSH12] S. Käseberg, M.B. Schaller, and K. Holschemacher. CFRP systems with embedded FBG for structural monitoring and retrofitting. In *Le Cam, Vincent and Mevel, Laurent and Schoefs, Franck. EWSHM - 6th European Workshop on Structural Health Monitoring, Dresden, Germany*, volume 2, pages 1–9, 2012.

[KZ11] J.K. Kaldellis and D. Zafirakis. The wind energy (r)evolution: A short review of a long history. *Renewable Energy*, 36(7):1887–1901, 2011.

[Lai84] K.J. Laidler. The development of the Arrhenius equation. *Journal of Chemical Education*, 61(6):494–498, 1984.

[LC10] W. Lu and F. Chu. Condition monitoring and fault diagnosis of wind turbines. In *IEEE Conference on Prognostics and Health Management, Macao, China*, pages 1–11, 2010.

[LCC+14] J. Lin, L. Cheng, Y. Chang, K. Zhang, B. Shu, and G. Liu. Reliability based power systems planning and operation with wind power integration: A review to models, algorithms and applications. *Renewable and Sustainable Energy Reviews*, 31:921–934, 2014.

[LFG13] A. Lorton, M. Fouladirad, and A. Grall. Computation of remaining useful life on a physic-based model and impact of a prognosis on the maintenance process. *Proceedings of the Institution of Mechanical Engineers, Part O: Journal of Risk and Reliability*, 227(4):434–449, 2013.

[LHZ09a] Y. Lei, Z. He, and Y. Zi. Application of an intelligent classification method to mechanical fault diagnosis. *Expert Systems with Applications*, 36(6):9941–9948, 2009.

[LHZ09b] Y. Lei, Z. He, and Y. Zi. Application of the EEMD method to rotor fault diagnosis of rotating machinery. *Mechanical Systems and Signal Processing*, 23(4):1327–1338, 2009.

[Lia14] L. Liao. Discovering prognostic features using genetic programming in remaining useful life prediction. *IEEE Transactions on Industrial Electronics*, 61(5):2464–2472, 2014.

[LLEB09] D.M. Laveuve, M. Lehmann, K. Erdmann, and A. Bütter. SHM-reliability demands on the multidisciplinary challenge of structural health monitoring. In *NDT in Progress, 5th International Workshop of NDT Experts, Prague, Czech Republic*, pages 1–10, 2009.

[LLHZ13] Y. Lei, J. Lin, Z. He, and M.J. Zuo. A review on empirical mode decomposition in fault diagnosis of rotating machinery. *Mechanical Systems and Signal Processing*, 35(1):108–126, 2013.

[LLWY09] B. Lu, Y. Li, X. Wu, and Z. Yang. A review of recent advances in wind turbine condition monitoring and fault diagnosis. In *IEEE Conference on Power Electronics and Machines in Wind Applications, Lincoln, NE, USA*, pages 1–7, 2009.

[LLZH14] Y. Lei, J. Lin, M.J. Zuo, and Z. He. Condition monitoring and fault diagnosis of planetary gearboxes: A review. *Measurement*, 48:292–305, 2014.

[LM93] C.J. Lu and W.O. Meeker. Using degradation measures to estimate a time-to-failure distribution. *Technometrics*, 35(2):161–174, 1993.

[LMIC14] F. Lopez, X. Maldague, and C. Ibarra-Castanedo. Enhanced image processing for infrared non-destructive testing. *Opto-Electronics Review*, 22(4):245–251, 2014.

[LNW+15] P. Ladpli, R. Nardari, Y. Wang, P.A. Hernandez-Gallegos, R. Rewari, H.T. Kuo, F. Kopsaftpopulos, K.D. Kepler, H.A. Lopez, and F.K. Chang. Multifunctional energy storage composites for SHM distributed sensor networks. In *Chang, F.K.; Kopsaftopoulos, F. (Ed.). Structural Health Monitoring, Stanford, CA, USA*, pages 1–10, 2015.

[LSLS05] W.H. Leong, W.J. Staszewski, B.C. Lee, and F. Scarpa. Structural health monitoring using scanning laser vibrometry: III. Lamb waves for fatigue crack detection. *Smart Materials and Structures*, 14(6):1387–1395, 2005.

[LZD15] P. Lall, H. Zhang, and L. Davis. Prognostication of LED remaining useful life and color stability in the presence of contamination. In *IEEE*

Conference on Prognostics and Health Management, Austin, TX, USA, pages 1–8, 2015.

[MFB+11] S.J. Moura, J.C. Forman, S. Bashash, J.L. Stein, and H.K. Fathy. Optimal control of film growth in lithium-ion battery packs via relay switches. *IEEE Transactions on Industrial Electronics*, 58(8):3555–3566, 2011.

[Min45] M.A. Miner. Cumulative damage in fatigue. *Applied Mechanics*, 12:159–164, 1945.

[MJ12] M. Musallam and C.M. Johnson. An efficient implementation of the rainflow counting algorithm for life consumption estimation. *IEEE Transactions on Reliability*, 61(4):978–986, 2012.

[MKM+15] S.I. Mishra, A. Kumar, R.K. Mishra, S. Sharma, and S. Sashwat. Structural health monitoring and propagation of lamb waves to identification of crack. *Materials Today: Proceedings*, 2(4):1833–1840, 2015.

[MMR06] D. Montalvao, N.M.M. Maia, and A.R. Ribeiro. A review of vibration-based structural health monitoring with special emphasis on composite materials. *Shock and Vibration Digest*, 38(4):295–326, 2006.

[MMT15] A. May, D. McMillan, and S. Thöns. Economic analysis of condition monitoring systems for offshore wind turbine sub-systems. *IET Renewable Power Generation*, 9(8):900–907, 2015.

[MPBS15] A. Manwatkar, P.S. Phale, M.A. Bawase, and M.R. Saraf. Application of scanning electron microscopy used for oil analysis. In *SIAT Symposium on International Automotive Technology, Pune, India*, pages 1–8, 2015.

[MR03] E. Meissner and G. Richter. Battery monitoring and electrical energy management: Precondition for future vehicle electric power systems. *Journal of Power Sources*, 116(1-2):79–98., 2003.

[MR05] E. Meissner and G. Richter. The challenge to the automotive battery industry: The battery has to become an increasingly integrated component within the vehicle electric power system. *Journal of Power Sources*, 144(2):438–460, 2005.

[MS45] S.M. Marco and W.L. Starkley. A concept of fatigue damage. *Transactions of the ASME*, 76:627–632, 1945.

[MSF13] S.J. Moura, J.L. Stein, and H.K. Fathy. Battery-health conscious power management in plug-in hybrid electric vehicles via electrochemical modeling and stochastic control. *IEEE Transactions on Control Systems Technology*, 21(3):679–694, 2013.

[NBS16] J.G. Njiri, N. Beganovic, and D. Söffker. Integration of fatigue load-based prognostic model into wind turbine control strategy. *Journal of Dynamic Systems, Measurements, and Control*, 2016. Submitted.

[NMCH09] K.S. Ng, C.S. Moo, Y.P. Chen, and Y.C. Hsieh. Enhanced coulomb counting method for estimating state-of-charge and state-of-health of lithium-ion batteries. *Applied Energy*, 86(9):1506–1511, 2009.

[OK12] P. O'Connor and A. Kleyner. *Practical reliability engineering*. John Wiley & Sons, Sussex, WI, USA, 2012.

[Pal24] A. Palmgren. Die Lebensdauer von Kugellagern. *Zeitschrift des Vereines Deutscher Ingenieure*, 68(14):339–341, 1924.

[PAOS10] L. Pettersson, J.O. Andersson, C. Orbert, and S. Skagerman. RAMS-database for wind turbines: Pre-study. Technical report, Elforsk AB, Stockholm, Sweden, 2010.

[Par59] E. Parzen. On models for the probability of fatigue failure of a structure. Technical report, Applied Mathematics and Statistics Laboratory, Stanford University, CA, USA, 1959.

[PAS14] B. Park, Y.K. An, and H. Sohn. Visualization of hidden delamination and debonding in composites through noncontact laser ultrasonic scanning. *Composites Science and Technology*, 100:10–18, 2014.

[PB13] M.B. Pinson and M.Z. Bazant. Theory of SEI formation in rechargeable batteries: Capacity fade, accelerated aging and lifetime prediction. *Journal of the Electrochemical Society*, 160(2):243–250, 2013.

[PCMC15] R.J. Parmee, C.M. Collins, W.I. Milne, and M.T. Cole. X-ray generation using carbon nanotubes. *Nano Convergence*, 2(1):1–27, 2015.

[PFC89] R.J. Patton, P.M. Frank, and R.N. Clark. *Fault diagnosis in dynamic systems: Theory and application*. Prentice Hall, New Jersey, USA, 1989.

[PGH+15] A. Panna, A.A. Gomella, K.J. Harmon, P. Chen, H. Miao, E.E. Bennett, and H. Wen. Performance of low-cost X-ray area detectors with consumer digital cameras. *Journal of Instrumentation*, 10(5):1–10, 2015.

[PHK+10] M. Perterer, F. Höchtl, A. Kiefmann, H. Baier, and V. Senner. Ultrasonic and thermographic monitoring of impact induced damage of CFRP structures. In *SAMPA Conference, Society for the Advancement of Material and Process Engineering, Seattle, WA, USA*, 2010.

[Pie14] F. Pierre. The evolution of optical fiber sensors technologies during the 35 last years and their applications in structure health monitoring. In *Le Cam, Vincent and Mevel, Laurent and Schoefs, Franck. EWSHM - 7th European Workshop on Structural Health Monitoring, Nantes, France*, pages 914–929, 2014.

[PMTP13] J.M.P. Pérez, F.P.G. Márquez, A. Tobias, and M. Papaelias. Wind turbine reliabiliy analysis. *Renewable and Sustainable Energy Reviews*, 23:463–472, 2013.

[PN13] A. Purarjomandlangrudi and G. Nourbakhsh. Acoustic emission condition monitoring: An application for wind turbine fault detection. *International Journal of Research in Engineering and Technology*, 2(5):907–918, 2013.

[PSS99] W.H. Prosser, M.D. Seale, and B.T. Smith. Time-frequency analysis of the dispersion of Lamb modes. *The Journal of the Acoustical Society of America*, 105(5):2669–2676, 1999.

[QTW03] S.T. Quek, P.S. Tua, and Q. Wang. Detecting anomalies in beams and plate based on the Hilbert–Huang transform of real signals. *Smart Materials and Structures*, 12(3):447, 2003.

[RAB10] M.A. Roscher, J. Assfalg, and O.S. Bohlen. Detection of utilizable capacity deterioration in battery systems. *IEEE Transactions on Vehicular Technology*, 60(1):98–103, 2010.

[RB07] J. Ribrant and L. Bertling. Survey of failures in wind power systems with focus on Swedish wind power plants during 1997-2005. In *IEEE Power Engineering Society General Meeting, Tampa, FL, USA*, pages 1–8, 2007.

[RBM+11] J. Remmlinger, M. Buchholz, M. Meiler, P. Bernreuter, and K. Dietmayer. State-of-health monitoring of lithium-ion batteries in electric vehicles by on-board internal resistance estimation. *Journal of Power Sources*, 196(12):5357–5363, 2011.

[RBSGD13] J. Remmlinger, M. Buchholz, T. Soczka-Guth, and K. Dietmayer. On-board state-of-health monitoring of lithium-ion batteries using linear parameter-varying models. *Journal of Power Sources*, 239:689–695, 2013.

[RC07] A. Raghavan and C.E.S. Cesnik. Review of guided-wave structural health monitoring. *Shock and Vibration Digest*, 39(2):91–116, 2007.

[RF15] N. Raghavan and D.D. Frey. Remaining useful life estimation for systems subject to multiple degradation mechanisms. In *IEEE Conference on Prognostics and Health Management, Austin, TX, USA*, pages 1–8, 2015.

[RRT10] J. Rafiee, M.A. Rafiee, and P.W. Tse. Application of mother wavelet functions for automatic gear and bearing fault diagnosis. *Expert Systems with Applications*, 37(6):4568–4579, 2010.

[RS96] U.K. Rakowsky and D. Söffker. Verknüpfung von Methoden der Regelungstheorie und der technischen Zuverlässigkeit zur Modellierung dynamischer Systeme. *Jahrestagung der Gesellschaft für Mess - und Automatisierungstechnik, Baden-Baden*, pages 753–763, 1996.

[RS97] U.K. Rakowsky and D. Söffker. Real-time reliability evaluation of vibrating mechanical structures. *Proceedings of the 12th ASME Conference on Reliability, Stress Analysis and Failure Prevention, Virginia Beach, VA, USA, In: Pusey, H.C. (Ed.): A Critical Link: Diagnosis to Prognosis*, pages 625–636, 1997.

[Rum11] M.A. Rumsey. An evaluation of sensing technologies in a wind turbine blade: Some issues, challenges and lessons learned. In *SPIE Conference on Industrial and Commercial Applications of Smart Structures Technologies, International Society for Optics and Photonics, San Diego, CA, USA*, pages 1–8, 2011.

[SB] D. Söffker and D. Baccar. Classification approach for evaluation of usage independent degradation processes of Li-O cells using Acoustic Emission. *Journal of Power Sources*. In preparation.

[SB14] M.A. Sanz-Bobi. *Use, operation and maintenance of renewable energy systems: Experiences and future approaches*. Springer, Heidelberg, Germany, 2014.

[SBR14] D. Söffker, N. Beganovic, and S. Rothe. Von der Diagnose zur Prognose: Signal- und modellbasierte Methoden zur aktiven Anlagenüberwachung am Beispiel der Überwachung eines Verschleißprozesses. In *10. Aachener Kolloquium für Instandhaltung, Diagnose und Anlagenüberwachung (AKIDA), Aachen*, pages 293 – 303, 2014.

[SCBH13] P.J. Schubel, R.J. Crossley, E.K.G. Boateng, and J.R. Hutchinson. Review of structural health and cure monitoring techniques for large wind turbine blades. *Renewable Energy*, 51:113–123, 2013.

[SCGR05] L. Serrao, Z. Chehab, Y. Guezennee, and G. Rizzoni. An aging model of Ni-MH batteries for hybrid electric vehicles. In *IEEE Conference on Vehicle Power and Propulsion, Chicago, IL, USA*, pages 78–85, 2005.

[SCR+12] M. Scheerer, T. Cardone, A. Rapisarda, S. Ottaviano, and D. Francesconi. Online damage detection on metal and composite space structures by active and passive acoustic methods. In *Le Cam, Vincent and Mevel, Laurent and Schoefs, Franck. EWSHM - 6th European Workshop on Structural Health Monitoring, Dresden, Germany*, pages 1–9, 2012.

[SDY+11] H. Sohn, D. Dutta, J.Y. Yang, M. DeSimio, S. Olson, and E. Swenson. Automated detection of delamination and disbond from wavefield images obtained using a scanning laser vibrometer. *Smart Materials and Structures*, 20(4):1–10, 2011.

[SFH+04] H. Sohn, C.R. Farrar, F.M. Hemez, J.J. Czarnecki, D.D. Shunk, D.W. Stinemates, and B.R. Nadler. A review of structural health monitoring literature: 1996-2001. Technical report, Los Alamos National Laboratory Report, Los Alamos, NM, USA, 2004.

[SGT+01] H. Shimoda, B. Gao, X.P. Tang, A. Kleinhammes, L. Fleming, Y. Wu, and O. Zhou. Lithium intercalation into opened single-wall carbon nanotubes: Storage capacity and electronic properties. *Physical Review Letters*, 88(1):1–4, 2001.

[She13] S. Sheng. Report on wind turbine subsystem reliability - A survey of various databases. Technical report, National Renewable Energy Laboratory, Golden, CO, USA, 2013.

[SL14] M.S. Safizadeh and S.K. Latifi. Using multi-sensor data fusion for vibration fault diagnosis of rolling element bearings by accelerometer and load cell. *Information Fusion*, 18:1–8, 2014.

[Sly02] C. Sly. Tribologist attacks wear and friction from the inside. *Practical Failure Analysis*, 2:9–10, 2002.

[SMM12] D. Samborsky, J. Mandell, and D. Miller. The SNL/MSU/DOE fatigue of composite materials database: Recent trends. In *AIAA 53rd Conference on Structures, Structural Dynamics and Materials and AIAA/ASME/AHS 20th Conference on Adaptive Structures, Honolulu, HI, USA*, pages 1–13, 2012.

[SMM13] D. Samborsky, J. Mandell, and D. Miller. Creep/fatigue behavior of resin infused biaxial glass fabric laminates. In *AIAA SDM Conference, Wind Energy Session, Boston, MA, USA*, pages 1–15, 2013.

[SMML93] L. Simoni, G. Mazzanti, G.C. Montanari, and L. Lefebre. A general multi-stress life model for insulating materials with or without evidence for thresholds. *IEEE Transactions on Electrical Insulation*, 28:349–364, 1993.

[Son14] L. Song. A NSGA-II program in Matlab v1.4. http://www.mathworks.com/matlabcentral/fileexchange/31166-ngpm-a-nsga-ii-program-in-matlab-v1-4. Access date: 20.02.2014.

[SOVP12] E. Sutrisno, H. Oh, A.S.S. Vasan, and M. Pecht. Estimation of remaining useful life of ball bearings using data driven methodologies. In *IEEE Conference on Prognostics and Health Management, Denver, CO, USA*, pages 1–7, 2012.

[SRS+13] D. Söffker, S. Rothe, S. Schiffer, H. Aljoumaa, and D. Baccar. Smart, tough, and successful: Three innovative approaches for diagnosis and prognosis of technical systems. In *Chang, F.K. (Ed.). Structural Health Monitoring, Stanford, CA, USA*, pages 81–88, 2013.

[SSST13] M. Swierczynski, D.I. Stroe, A.I. Stan, and R. Teodorescu. The lifetime of the LiFePO 4/C battery energy storage system when used for smoothing of the wind power plant variations. In *IEEE 39th Annual Conference on Industrial Electronics Society, Vienna, Austria*, pages 6825–6830, 2013.

[SSW+15] P. Servati, S. Soltanian, L.Y. Wan, D. Badawy, Y. Li, K. Walus, D. Michelson, and F. Ko. Composite nanofibers for structural health monitoring. In *Chang, F.K.; Kopsaftopoulos, F. (Ed.). Structural Health Monitoring, Stanford, CA, USA*, pages 272–280, 2015.

[Sta] ASTM Standard. E1316, Standard terminology for nondestructive examinations. *American Society of Testing and Materials*, pages 675–720.

[Sta06] G.W. Stachowiak. *Wear - Materials, mechanisms and practice*. John Wiley & Sons, Sussex, WI, USA, 2006.

[STRC11] M. Swierczynski, R. Teodorescu, and P. Rodríguez-Cortés. Lifetime investigations of a lithium iron phosphate (LFP) battery system connected to a wind turbine for forecast improvement and output power gradient reduction. In *Proceedings of International Stationary Battery Conference, Orlando, USA*, pages 1–8, 2011.

[Sub76] S. Subramanyan. A cumulative rule based on the knee point of the S-N curve. *Journal of Engineering Materials and Technology*, 98:316–321, 1976.

[SVLP+13] S. Soua, P. Van Lieshout, A. Perera, T.H. Gan, and B. Bridge. Determination of the combined vibrational and acoustic emission signature of a wind turbine gearbox and generator shaft in service as a pre-requisite for effective condition monitoring. *Renewable Energy*, 51:175–181, 2013.

[SWHZ11] X.S. Si, W. Wang, C.H. Hu, and D.H. Zhou. Remaining useful life estimation - A review on the statistical data driven approaches. *European Journal of Operational Research*, 213(1):1–14, 2011.

[SWZ+10] W. Su, F. Wang, H. Zhu, Z. Zhang, and Z. Guo. Rolling element bearing faults diagnosis based on optimal morlet wavelet filter and autocorrelation enhancement. *Mechanical Systems and Signal Processing*, 24(5):1458–1472, 2010.

[SZK+14] B. Stiaszny, J.C. Ziegler, E.E. Krauß, J.P. Schmidt, and E. Ivers-Tiffée. Electrochemical characterization and post-mortem analysis of aged $LiMn_2O_4$-NMC/graphite lithium-ion batteries. Part I: Cycle aging. *Journal of Power Sources*, 251:439–450, 2014.

[SZKP12] B. Sun, S. Zeng, R. Kang, and M.G. Pecht. Benefits and challenges of system prognostics. *IEEE Transactions on Reliability*, 61(2):323–335, 2012.

[TC99] N. Tandon and A. Choudhury. A review of vibration and acoustic measurement methods for the detection of defects in rolling element bearings. *Tribology International*, 32(8):469–480, 1999.

[TGW+13] P.J. Tavner, D.M. Greenwood, M.W.G. Whittle, R. Gindele, S. Faulstich, and B. Hahn. Study of weather and location effects on wind turbine failure rates. *Wind Energy*, 16(2):175–187, 2013.

[TSC15] A.S. Tillmann, A.E. Schultz, and J.E. Campos. Protocols and criteria for acoustic emission monitoring of fracture-critical steel bridges. Technical report, University of Minnesota, Department of Civil, Environmental, and Geo- Engineering, MI, USA, 2015.

[TSD15] N. Talebi, M.A. Sadrnia, and A. Darabi. Fault detection of wind energy conversion systems using recurrent neural networks. *International Journal of Sustainable Energy*, 34(1):52–70, 2015.

[TVBS06] P.J. Tavnet, G.J.W. Van Bussel, and F. Spinato. Machine and converter reliabilities in wind turbines. In *IET 3rd International Conference on*

Power Electronics, Machines and Drives, Dublin, Ireland, pages 127–130, 2006.

[TWTE13] P. Tchakoua, R. Wamkeue, T.A. Tameghe, and G. Ekemb. A review of concepts and methods for wind turbines condition monitoring. In *IEEE World Congress on Computer and Information Technology, Sousse, Tunisia*, pages 1–9, 2013.

[TYR07] N. Tandon, G.S. Yadava, and K.M. Ramakrishna. A comparison of some condition monitoring techniques for the detection of defect in induction motor ball bearings. *Mechanical Systems and Signal Processing*, 21(1):244–256, 2007.

[Val15] K. Vallons. Databases for fatigue analysis in composite materials. In *Carvelli, V. and Lomov, S.V. (Ed.): Fatigue of Textile Composites*, pages 75–82. Woodhead Publishing Series in Composite Science and Engineering, Cambridge, MA, USA, 2015.

[VBB03] G.J.W. Van Bussel and W.A.A.M. Bierbooms. The DOWEC offshore reference wind farm: Analysis of transportation for operation and maintenance. *Wind Engineering*, 27(5):381–391, 2003.

[VDB15] J. Van Dam and L.J. Bond. Economics of online structural health monitoring of wind turbines: Cost benefit analysis. In *AIP 41st Annual Review of Progress in Quantitative Nondestructive Evaluation Conference, Boise, ID, USA*, volume 34, pages 899–908, 2015.

[VPB07] A. Vasebi, M. Partovibakhsh, and S.M.T. Bathaee. A novel combined battery model for state-of-charge estimation in lead-acid batteries based on extended Kalman filter for hybrid electric vehicle applications. *Journal of Power Sources*, 174(1):30–40, 2007.

[WBS16a] S.F. Wirtz, N. Beganovic, and D. Söffker. Experimental results of frequency-based classification of damages in composites. In *EWSHM - 8th European Workshop on Structural Health Monitoring, Bilbao, Spain*, pages 1–10, 2016.

[WBS16b] S.F. Wirtz, N. Beganovic, and D. Söffker. Investigation of damage detectability in composites using frequency-based classification of acoustic emission measurements. *Structural Health Monitoring*, 2016. Submitted.

[WBTS16a] S.F. Wirtz, N. Beganovic, P. Tenberge, and D. Söffker. Frequency-based damage detection of spur gear using wavelet analysis. In *EWSHM - 8th European Workshop on Structural Health Monitoring, Bilbao, Spain*, pages 1–10, 2016.

[WBTS16b] S.F. Wirtz, N. Beganovic, P. Tenberge, and D. Söffker. Gear transmission monitoring 4.0: What can be expected from upcoming diagnostic and prognostic systems. In *11. Aachener Kolloquium für Instandhaltung, Diagnose und Anlagenüberwachung (AKIDA), Aachen*, pages 1–14, 2016.

[WCP13] C. Weng, J. Cui, and H. Peng. On-board state of health monitoring of lithium-ion batteries using incremental capacity analysis with support vector regression. *Journal of Power Sources*, 235:36–44, 2013.

[WFS14] W. Waag, C. Fleischer, and D.U. Sauer. Critical review of the methods for monitoring of lithium-ion batteries in electric and hybrid vehicles. *Journal of Power Sources*, 258:321–339, 2014.

[WGS+14] T. Waldmann, S. Gorse, T. Samtleben, G. Schneider, V. Knoblauch, and M. Wohlfahrt-Mehrens. A mechanical aging mechanism in lithium-ion batteries. *Journal of the Electrochemical Society*, 161(10):1742–1747, 2014.

[WHH+11] M. Wilkinson, K. Harman, B. Hendriks, F. Spinato, T. van Delft, G.L. Garrad, and U.K. Thomas. Measuring wind turbine reliability, results of the RELIAWIND project. In *EWEA Conference, Brussels, Belgium*, pages 1–8, 2011.

[WSP13] C. Weng, J. Sun, and H. Peng. An open-circuit-voltage model of lithium-ion batteries for effective incremental capacity analysis. In *Proceedings of the ASME Dynamic Systems and Control Conference, Palo Alto, CA, USA*, pages 1–8, 2013.

[WSP14] C. Weng, J. Sun, and H. Peng. A unified open-circuit-voltage model of lithium-ion batteries for state-of-charge estimation and state-of-health monitoring. *Journal of Power Sources*, 258:228–237, 2014.

[WWK+14] T. Waldmann, M. Wilka, M. Kasper, M. Fleischhammer, and M. Wohlfahrt-Mehrens. Temperature dependent aging mechanisms in lithium-ion batteries - A post-mortem study. *Journal of Power Sources*, 262:129–135, 2014.

[WZX09] X. Wei, B. Zhu, and W. Xu. Internal resistance identification in vehicle power lithium-ion battery and application in lifetime evaluation. In *IEEE International Conference on Measuring Technology and Mechatronics Automation, Hunan, China*, volume 3, pages 388–392, 2009.

[XWWH15] C. Xie, Z. Wang, P. Wang, and H. Huang. Probability of corrosion failure analysis using an adaptive sampling approach. In *IEEE Conference*

on Prognostics and Health Management, Austin, TX, USA, pages 1–8, 2015.

[XXS+09] Z. Xu, J. Xuan, T. Shi, B. Wu, and Y. Hu. Application of a modified fuzzy ARTMAP with feature-weight learning for the fault diagnosis of bearing. *Expert Systems with Applications*, 36(6):9961–9968, 2009.

[YGS13] B. Yeter, Y. Garbatov, and C.G. Soares. Spectral fatigue assessment of an offshore wind turbine structure under wave and wind loading. *Developments in Maritime Transportation and Exploitation of Sea Resources*, pages 425–433, 2013.

[YJ11] W. Yang and J. Jiang. Wind turbine condition monitoring and reliability analysis by SCADA information. In *IEEE 2nd International Conference on Mechanic Automation and Control Engineering, Hohhot, China*, pages 1872–1875, 2011.

[YKZ+14] R. Yang, J. Kang, J. Zhao, J. Li, and H. Li. A case study of bearing condition monitoring using SPM. In *IEEE Conference on Prognostics and System Health Management, Hunan, China*, pages 695–698, 2014.

[YNB+14] G. Ye, B. Neal, A. Boot, V. Kappatos, C. Selcuk, and T.H. Gan. Development of an ultrasonic NDT system for automated in-situ inspection of wind turbine blades. In *Le Cam, Vincent and Mevel, Laurent and Schoefs, Franck. EWSHM - 7th European Workshop on Structural Health Monitoring, Nantes, France*, pages 826–833, 2014.

[YS13] B. Yang and D. Sun. Testing, inspecting and monitoring technologies for wind turbine blades: A survey. *Renewable and Sustainable Energy Reviews*, 22:515–526, 2013.

[YTC+14] W. Yang, P.J. Tavner, C.J. Crabtree, Y. Feng, and Y. Qiu. Wind turbine condition monitoring: Technical and commercial challenges. *Wind Energy*, 17(5):673–693, 2014.

[YZZA14] B. Yang, L. Zhang, W. Zhang, and Y. Ai. Non-destructive testing of wind turbine blades using an infrared thermography: A review. In *IEEE International Conference on Materials for Renewable Energy and Environment, Chengdu, China*, volume 1, pages 407–410, 2014.

[ZAB+16] A. Ziaja, I. Antoniadou, T. Barszcz, W.J. Staszewski, and K. Worden. Fault detection in rolling element bearings using wavelet-based variance analysis and novelty detection. *Journal of Vibration and Control*, 22(2):396–411, 2016.

[ZCAA15] A. Zaki, H.K. Chai, D.G. Aggelis, and N. Alver. Non-destructive evaluation for corrosion monitoring in concrete: A review and capability of acoustic emission technique. *Sensors*, 15(8):19069–19101, 2015.

[ZDEA15] T. Zhang, R. Dwight, and K. El-Akruti. Condition based maintenance and operation of wind turbines. In *Tse, W.T. and Mathew, J. and Wong, K. and Lam, R. and Ko, C.N. (Ed.): Engineering Asset Management-Systems, Professional Practices and Certification*, pages 1013–1025. Springer, Heidelberg, Germany, 2015.

[ZESD13] X. Zhou, T. Ersal, J.L. Stein, and S. Bernstein Dennis. Battery health diagnostics using retrospective-cost subsystem identification: Sensitivity to noise and initialization errors. In *Proceedings of the ASME Dynamic Systems and Control Conference, Palo Alto, CA, USA*, pages 1–10, 2013.

[ZLC02] H. Zheng, Z. Li, and X. Chen. Gear fault diagnosis based on continuous wavelet transform. *Mechanical Systems and Signal Processing*, 16(2):447–457, 2002.

[ZTBF11] T. Zhigang, J. Tongdan, W. Bairong, and D. Fangfang. Condition based maintenance optimization for wind power generation systems under continuous monitoring. *Renewable Energy*, 36(5):1502–1509, 2011.

[ZWH+15] H. Zhao, Q. Wu, S. Hu, H. Xu, and C.N. Rasmussen. Review of energy storage system for wind power integration support. *Applied Energy*, 137:545–553, 2015.

[ZZC+13] B. Zhao, X. Zhang, J. Chen, C. Wang, and L. Guo. Operation optimization of standalone microgrids considering lifetime characteristics of battery energy storage system. *IEEE Transactions on Sustainable Energy*, 4(4):934–943, 2013.

[ZZYX08] L. Zhen, H. Zhengjia, Z. Yanyang, and C. Xuefeng. Bearing condition monitoring based on shock pulse method and improved redundant lifting scheme. *Mathematics and Computers in Simulation*, 79(3):318–338, 2008.

Intermediate results presented/published in the following conferences/journals or prepared for submission to following journals are stated as an integral part of this thesis:

[BNS17] N. Beganovic, J.G. Njiri, and D. Söffker. Wind turbine control strategy deployment concerning remaining useful lifetime prognostic model. Conference for Wind Power Drives, Aachen, Germany, 2017. Accepted.

[BS] N. Beganovic and D. Söffker. Remaining useful lifetime and State-of-Health estimation of LIB based on direct measurements. *Journal of Power Sources*. Submitted.

[BS17] N. Beganovic and D. Söffker. Remaining lifetime modeling using State-of-Health estimation. *Mechanical Systems and Signal Processing*, 92:107-123, 2017.

[BNS] N. Beganovic, J.G. Njiri, and D. Söffker. Reduction of structural loads in wind turbines through adapted control strategy concerning online fatigue damage evaluation model. *Journal of Wind Engineering & Industrial Aerodynamics*. Submitted.

[BRS16] N. Beganovic, S. Rothe, and D. Söffker. Identification of diagnostic and prognostic features by means of AE and hydraulic pressure measurements. In *Proceedings of 8th European Workshop on Structural Health Monitoring, Bilbao, Spain*, pages 1-8, 2016.

[BS16] N. Beganovic and D. Söffker. Structural health management utilization for lifetime prognosis and advanced control strategy deployment of wind turbines: An overview and outlook concerning actual methods, tools and obtained results. *Renewable & Sustainable Energy Reviews*, 64:68-83, 2016.

[BBS15] N. Beganovic, D. Baccar, and D. Söffker. Wear aging and related impact on system reliability. In *Chang, F.K.; Kopsaftopoulos, F. (Ed.). Structural Health Monitoring, Stanford, CA, USA*, pages 353-401, 2015.

[BMS15] N. Beganovic, B. Moulik, and D. Söffker. LI-O battery aging process: A smart review with respect to the integration of aging into system's powermanagement. In *Proceedings of the ASME Dynamic Systems and Control Conference, Columbus, OH, USA*, pages 1-10, 2015.

[BNRS15] N. Beganovic, J.G. Njiri, S. Rothe, and D. Söffker. Application of diagnosis and prognosis to wind turbine system based on fatigue load. In *IEEE Conference on Prognostics and Health Management, Austin, TX, USA*, pages 1-6, 2015.

[BS15b] N. Beganovic and D. Söffker. Wear process lifetime prediction based on parametric model applied to experimental data. In *IEEE Conference on Prognostics and Health Management, Austin, TX, USA*, pages 1-6, 2015.

[BRS14] N. Beganovic, S. Rothe, and D. Söffker. Establishing a wear-oriented deterioration model based on experimental data. In *Le Cam, Vincent and Mevel, Laurent and Schoefs, Franck. Le Cam, Vincent and Mevel, Laurent and Schoefs, Franck. EWSHM - 7th European Workshop on Structural Health Monitoring, Nantes, France*, pages 1513-1520, 2014.

[WBS16b] S.F. Wirtz, N. Beganovic, and D. Söffker. Investigation of damage detectability in composites using frequency-based classification of acoustic emission measurements. *Structural Health Monitoring*, 2016. Submitted.

[WBTS16b] S.F. Wirtz, N. Beganovic, P. Tenberge, and D. Söffker. Gear transmission monitoring 4.0: What can be expected from upcoming diagnostic and prognostic systems. In *11. Aachener Kolloquium für Instandhaltung, Diagnose und Anlagenüberwachung (AKIDA), Aachen*, pages 1-14, 2016.

[NBS16] J.G. Njiri, N. Beganovic, and D. Söffker. Integration of fatigue load-based prognostic model into wind turbine control strategy. *Journal of Dynamic Systems, Measurements, and Control*, 2016. Submitted.

[WBS16a] S.F. Wirtz, N. Beganovic, and D. Söffker. Experimental results of frequency-based classification of damages in composites. In *Proceedings of 8th European Workshop on Structural Health Monitoring, Bilbao, Spain*, pages 1-10, 2016.

[WBTS16a] S.F. Wirtz, N. Beganovic, P. Tenberge, and D. Söffker. Frequency-based damage detection of spur gear using wavelet analysis. In *Proceedings of 8th European Workshop on Structural Health Monitoring, Bilbao, Spain*, pages 1-10, 2016.

[SBR14] D. Söffker, N. Beganovic, and S. Rothe. Von der Diagnose zur Prognose: Signal- und modellbasierte Methoden zur aktiven Anlagenüberwachung am Beispiel der Überwachung eines Verschleißprozesses. In *10. Aachener Kolloquium für Instandhaltung, Diagnose und Anlagenüberwachung (AKIDA), Aachen*, pages 293-303, 2014.

In the context of the research work at the Chair of Dynamics and Control the following student theses have been supervised by Nejra Beganovic, M.Sc. and Univ.-Prof. Dr.-Ing. Dirk Söffker:

2016 Cunha, Adauto Pereira Andrade: Realization of DWT on real-time signal processing FPGA-system for purpose of continuous structural health monitoring. Bachelor thesis. University of Duisburg-Essen, Chair of Dynamics and Control (SRS),

2016 Shen, Tong: Literature research: Remaing useful lifetime modeling of Li-x batteries. Bachelor thesis. University of Duisburg-Essen, Chair of Dynamics and Control (SRS),

2016 Yangmu, Wang: Literature research on lifetime models for composite material. Bachelor thesis. University of Duisburg-Essen, Chair of Dynamics and Control (SRS),

2015 Wirtz, Sebastian Felix: Qualification of AE measurements for damage classification in composites. Master thesis. University of Duisburg-Essen, Chair of Dynamics and Control (SRS), and

2014 Wei, Ka Ho: Seizmic Measurement Approaches used for Diagnostic and Prognostic. Bachelor thesis. University of Duisburg-Essen, Chair of Dynamics and Control (SRS).

Apendix

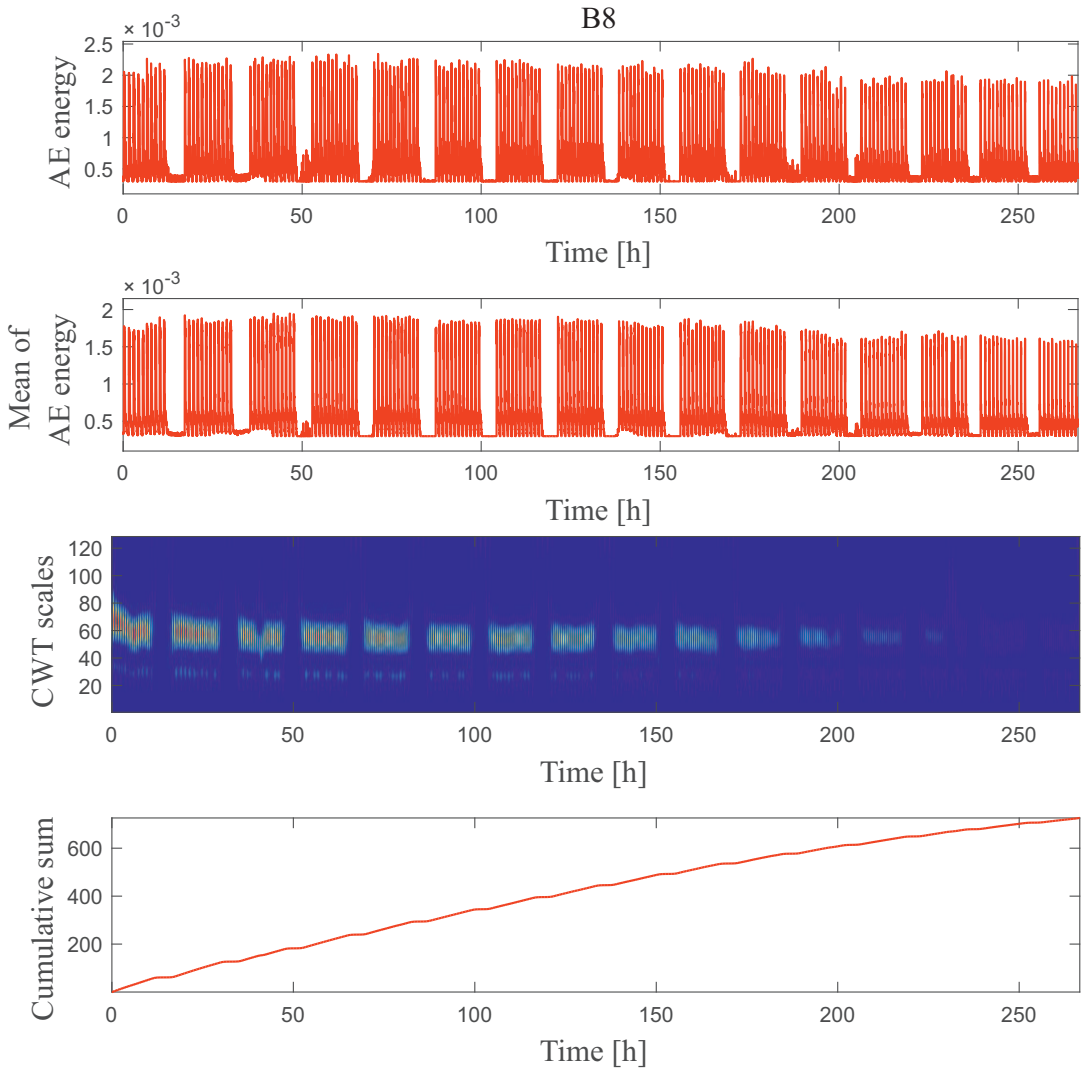

Figure A.1: Energy of AE signal during complete testing period with accompanying time-frequency-based features of B8

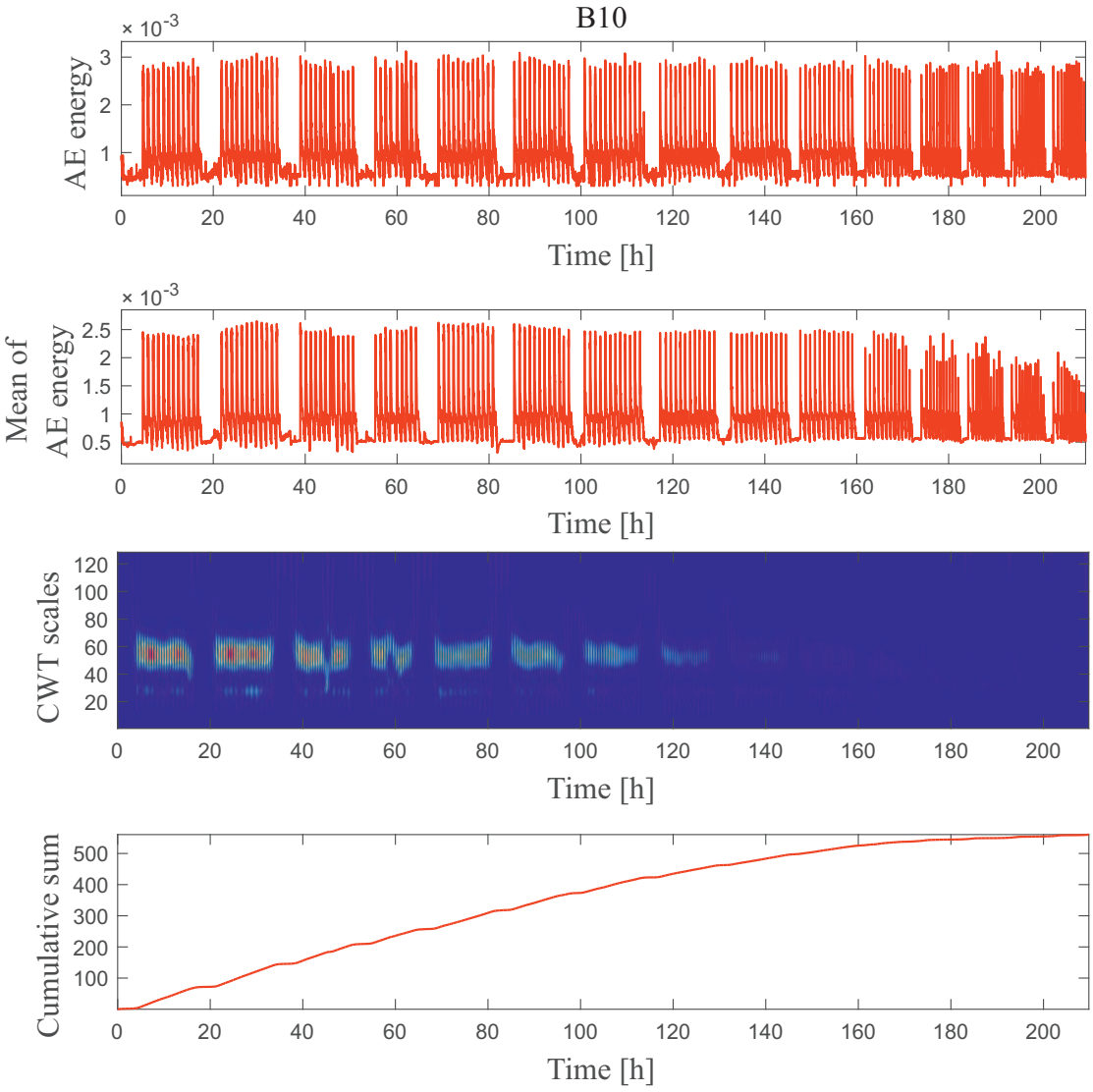

Figure A.2: Energy of AE signal during complete testing period with accompanying time-frequency-based features of B10

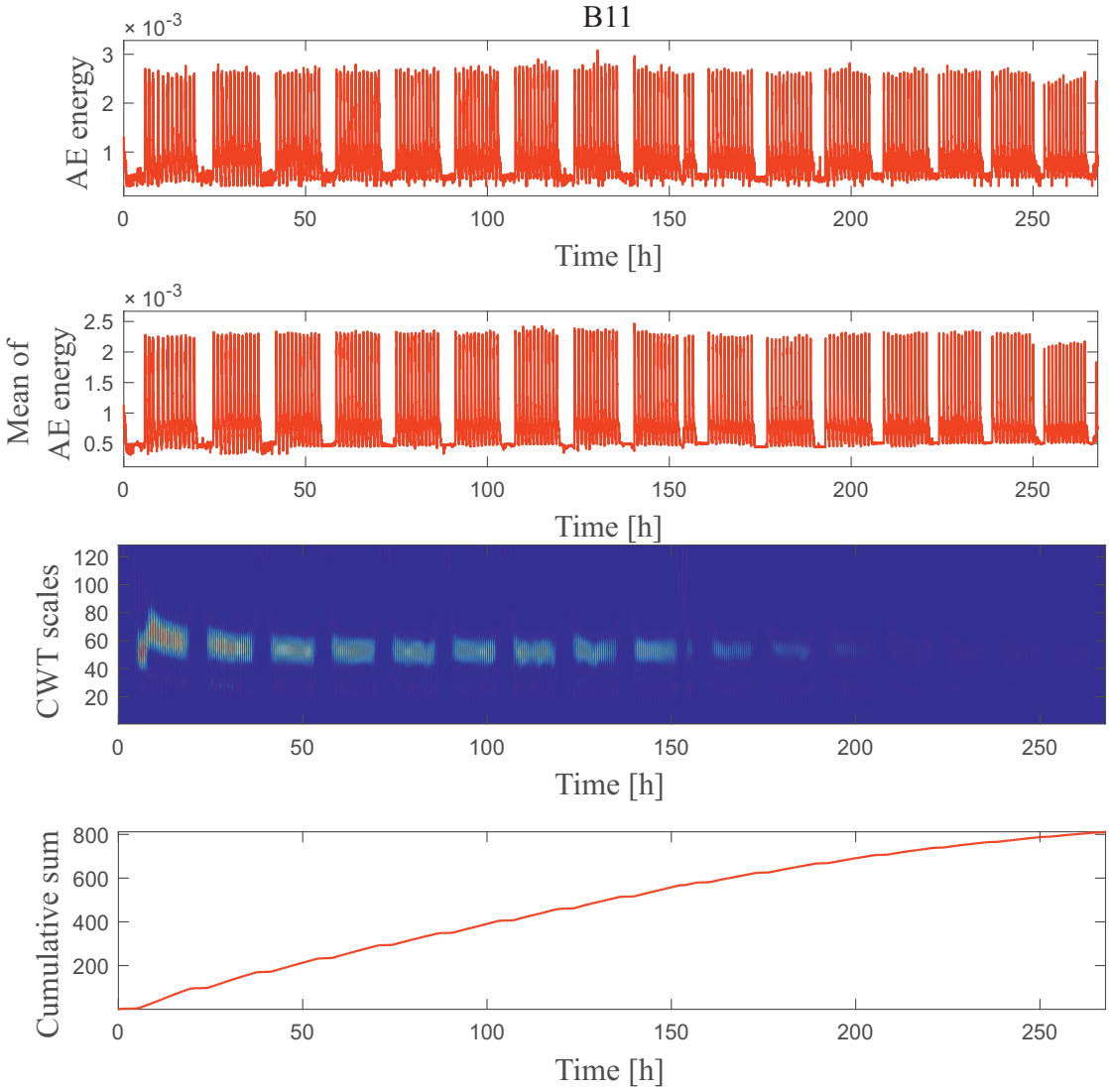

Figure A.3: Energy of AE signal during complete testing period with accompanying time-frequency-based features of B11

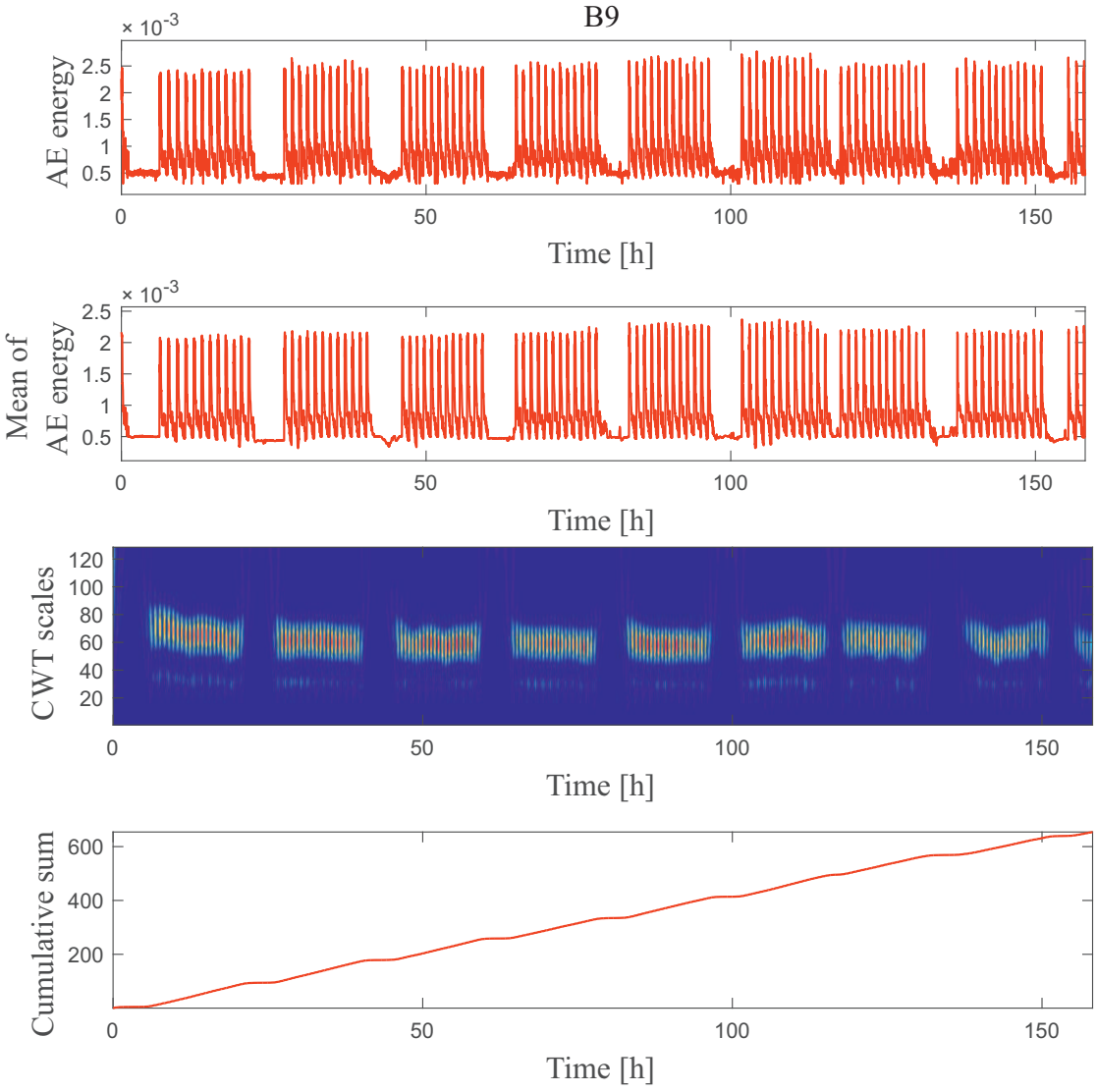

Figure A.4: Energy of AE signal during complete testing period with accompanying time-frequency-based features of B9

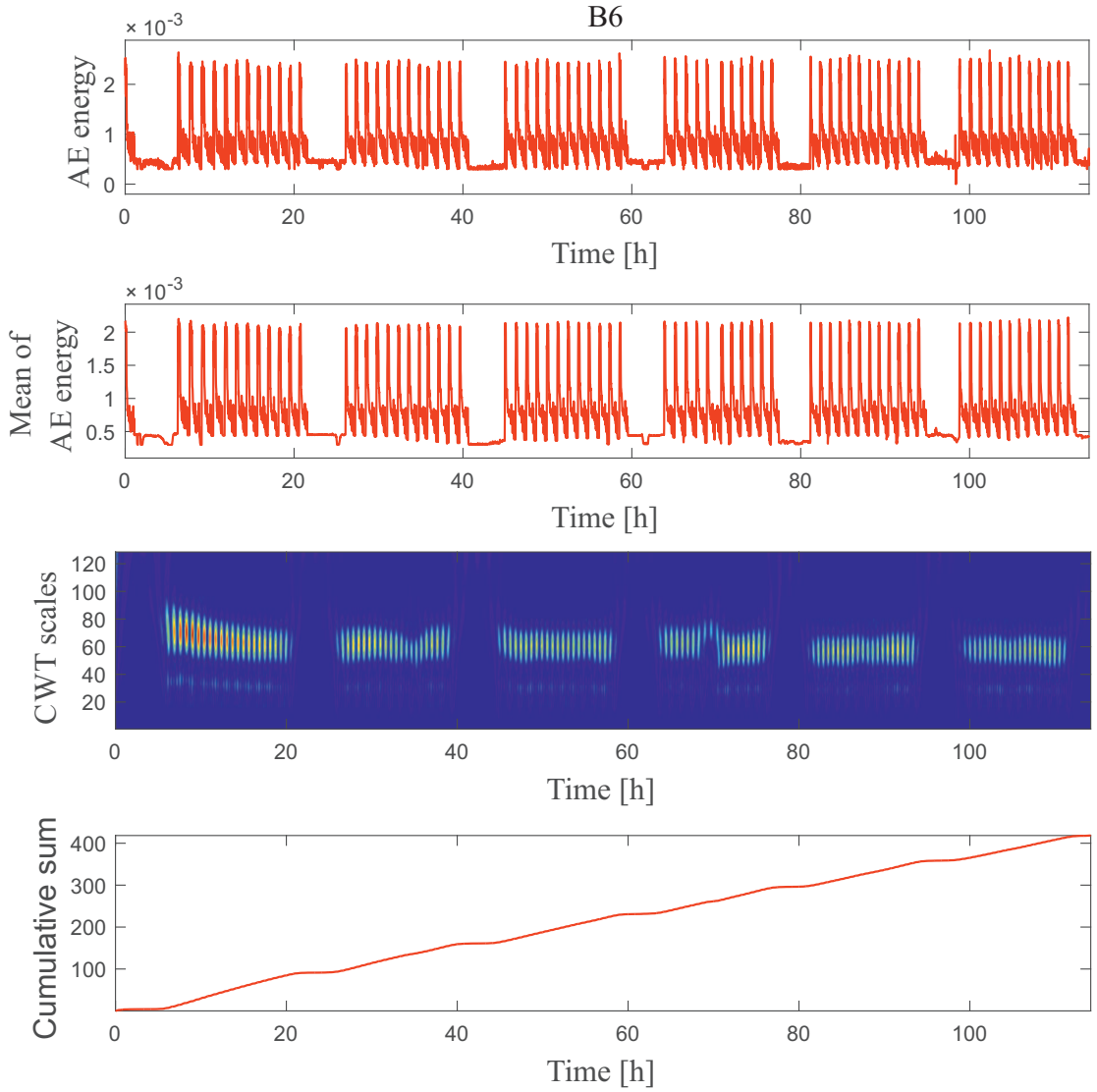

Figure A.5: Energy of AE signal during complete testing period with accompanying time-frequency-based features of B6

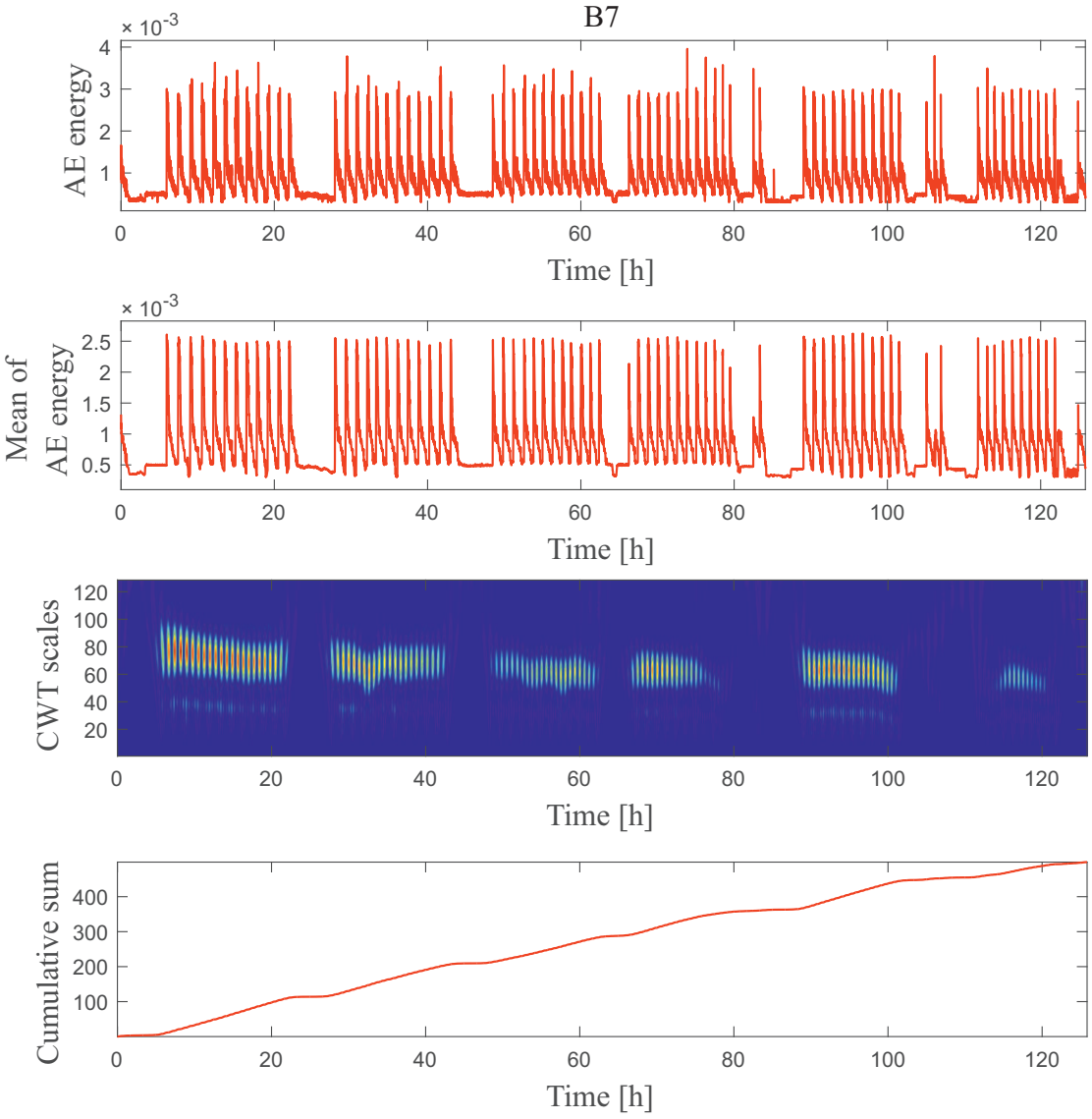

Figure A.6: Energy of AE signal during complete testing period with accompanying time-frequency-based features of B7